

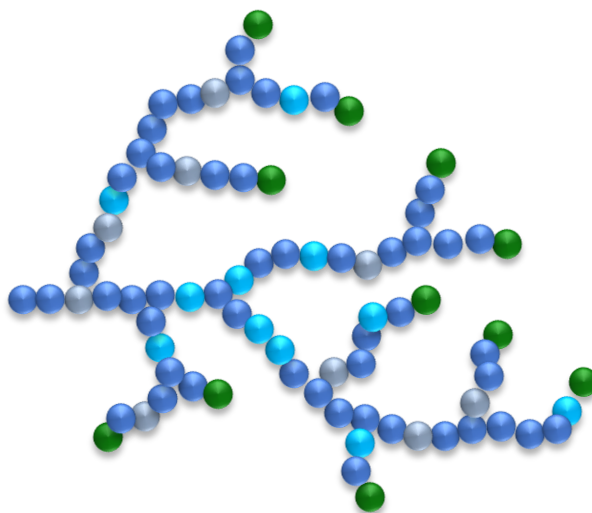


University of
Nottingham

UK | CHINA | MALAYSIA

Synthesis and Application of Novel Hyperbranched Polymers

Sophie Rebecca Goodwin, MSci



**Thesis submitted to the University of Nottingham
for the degree of Doctor of Engineering**


March 2021

"It always seems impossible until it's done."

Nelson Mandela

Declaration

Except where specific reference has been made to other sources, the work presented in this thesis is the original work of the author. It has not been submitted, in whole, or in part, for any other degree or professional qualification.

Signed.....  Date...29/03/2021....

Sophie Goodwin

Abstract

In this thesis, a novel control method for the chain transfer polymerisation of di-functional monomers is presented, in which macromers, produced *via* catalytic chain transfer polymerisation, undergo β -scission to act as stoichiometric transfer agents for di-acrylate, -methacrylate and -styrenyl monomers. This versatile macromer control method enables the facile synthesis of hyperbranched (HB) polymers, which may be tailored for use as coatings in a wide variety of industrial and biological applications through suitable choice of monomer and macromer. In particular, the use of lauryl methacrylate macromers to control the polymerisation of divinyl benzene (DVB) (8:2 v/v LMA:DVB), facilitated the solubilisation of the HB DVB in hydrocarbyl engine oil through the incorporation of LMA fragments in the HB DVB structure. This HB DVB/LMA polymer was then demonstrated to readily form robust, protective films between metal contact surfaces under a wide range of temperatures, rolling speeds and lubrication regimes, which reduced friction and wear between the surfaces. Additionally, this synthesis method was found to be easily scalable, with the polymers demonstrating no significant difference in performance when synthesised at either 1 or 50mL scales. Thus, these HB polymers showed great promise as oil additives for prolonging engine life and improving engine efficiency, while the macromer control method was proven to be industrially viable. Meanwhile, when compared to catalytic control methods, macromeric control was found to give improved control over the polymerisation of the bio-active monomer tricyclodecanedimethanol diacrylate (TCDMDA), with greater consistency of polymerisation rate and architecture, and improved levels of functionality achieved due to the increased level of compatibility between the hydrophobic TCDMDA monomer and the macromer control agent. When butyl methacrylate macromers were used in a 2:1 v/v TCDMDA:BMA ratio, this enabled the synthesis of up to 50 mL

of HB polymer which, when applied as a thin film coating to tissue culture plastic, was shown to support the growth of human pluripotent stem cells for up to 12 days. Finally, the use of thiolic control agents at high concentration (up to 65 mol%) was demonstrated to deliver improved yield of HB polymers, while enabling a similar ability to functionalise the HB polymers for a variety of applications, including as anti-fouling coatings and as a feedstock for two-photon polymerisation.

Acknowledgements

Foremost, I would like to express my sincere gratitude to my supervisor, Professor Derek Irvine, for all of his help, guidance and support throughout my PhD research and study.

I am also grateful to all of my colleagues at BP/Castrol, for their advice and support with my research. Special thanks to Dr Filip Sorin, Andrew Smith, Dr Lauren Cowie, Dr Ieuan Adams and Dr Laura Felisari.

I would also like to thank all the staff and researchers in the Centre for Doctoral Training in Carbon Capture and Storage and Cleaner Fossil Energies, particularly Professor Colin Snape and Diane Vincent, for their help and support with my CDT projects and funding.

I am grateful too, to the whole of B10/B10a and the wider “polymer group”, for providing lots of help, fun, and gossip over the last 4.5 years. You have all helped to make my time in the lab far more enjoyable than I ever expected it to be.

Finally, I am incredibly thankful to Lizzie, for putting up with and supporting me throughout the many stressful times, and to my family, without whom I would never have made it to this point. Thank you for all your love and support.

Contents

1	Chapter 1: Introduction	1
1.1	Background	1
1.2	Polymer Structures	2
1.3	Polymerisation Methods	4
1.3.1	Step Growth.....	5
1.3.2	Chain Growth	6
1.4	Free Radical Polymerisation.....	6
1.4.1	Limitations of FRP	10
1.5	Pseudo Living/Controlled Free Radical Polymerisations.....	11
1.6	Chain Transfer	12
1.6.1	Chain Transfer Agents	13
1.6.2	Thiol Chain Transfer Agents for FRP.....	14
1.6.3	Catalytic Chain Transfer Polymerisation (CCTP)	15
1.7	Hyperbranched Polymers	21
1.7.1	History of Hyperbranched Polymers.....	21
1.7.2	Synthesis of Hyperbranched Polymers	24
1.8	Polymer Characterisation	31
1.8.1	Gel Permeation Chromatography (GPC)/ Size Exclusion Chromatography (SEC)	31
1.8.2	Nuclear Magnetic Resonance (NMR)	34
1.8.3	Dielectric Materials, Properties and Analysis	35
1.9	Overview of this Thesis.....	40

1.10	Reference	42
2	Chapter 2: Experimental Methods	56
2.1	General Synthetic Procedure	56
2.1.1	Materials.....	56
2.1.2	Chain Transfer Polymerisation (CTP) of Mono- or Di- functional Monomers	56
2.1.3	Note on Gelation:	57
2.1.4	Gel Permeation Chromatography:	57
2.1.5	Nuclear Magnetic Resonance:	57
2.2	Experimental Methods for Chapter 3.....	58
2.2.1	Materials.....	58
2.2.2	Synthetic Procedures.....	58
2.2.3	Application Testing	60
2.2.4	Film Formation Data Analysis	65
2.2.5	Dielectric Monitoring – Cavity Perturbation	66
2.2.6	Liquid Handler System.....	66
2.3	Experimental Methods for Chapter 4.....	68
2.3.1	Materials.....	68
2.3.2	Synthetic Procedures.....	69
2.4	Experimental Methods for Chapter 5.....	75
2.4.1	Materials.....	75
2.4.2	Synthetic Procedures.....	75
2.5	References	77

3	Chapter 3: Synthesis and Testing of Novel, Low Viscosity Hyperbranched Lubricant Additives synthesised <i>via</i> Chain Transfer Polymerisation with Catalytic, Thiolic and Macromeric Control Agents	78
3.1	Introduction & Background.....	78
3.1.1	Overview of Lubricants	78
3.1.2	Hyperbranched (HB) Polymers as Lubricants	86
3.1.3	Styrene and Divinyl Benzene	90
3.1.4	Dielectric Monitoring for Batch Repeatability	92
3.1.5	Liquid Handler Screening	93
3.2	Aims and Objectives.....	94
3.3	Results and Discussion	96
3.3.1	Synthesis of Oil Soluble Hyperbranched Polymers	96
3.3.2	Application Testing of Controlled Morphology Hyperbranched Polymers104	
3.3.3	Synthesis Scale Up of HB Semi-Block Polymer	124
3.3.4	Further Application Testing of HB Semi-Block Polymer at Increased Scale.....	126
3.3.5	Using Thiol CTA to Develop Oil Soluble Polymers.....	140
3.3.6	Dielectric Monitoring for HB Polymer Quality Control.....	145
3.3.7	High Throughput Copolymer Viscosity Screening.....	153
3.4	Conclusions	157
3.4.1	Synthesis and Tribological Testing of HB DVB/LMA	157
3.4.2	Using Thiol CTAs to Synthesise Higher-Yielding Oil Soluble HB Polymers160	

3.4.3	Dielectric Monitoring of HBPs for Batch-to-Batch Reproducibility	160
3.4.4	Liquid Handler For Screening New Copolymers	161
3.5	Future Work	162
3.5.1	Synthesis and Tribological Testing of HB DVB/LMA	162
3.5.2	Using Thiol CTAs to Synthesise Higher-Yielding Oil Soluble HB Polymers	163
3.5.3	Dielectric Monitoring of HBPs for Batch-to-Batch Reproducibility	163
3.5.4	Liquid Handler For Screening New Copolymers	164
3.6	References	164
4	Chapter 4: Synthesis and Optimisation of Bio-Active Hyperbranched Polymers.....	174
4.1	Introduction	174
4.1.1	Biofilms and Anti-Fouling Surfaces	174
4.1.2	Stem Cells and Pro-Stem Cell Attachment Surfaces.....	177
4.1.3	Hit Polymers.....	180
4.1.4	Additive Manufacturing for Bio-Applications.....	182
4.2	Aims and Objectives.....	186
4.3	Results and Discussion	188
4.3.1	TCDMDA Homopolymers <i>Via</i> CCTP.....	188
4.3.2	TCDMDA Homopolymers <i>Via</i> Chain Transfer Polymerisation (CTP) with Thiol CTA	196

4.3.3	Preliminary Studies of HB Copolymers <i>via</i> Macromer Controlled CTP for Stem Cell Attachment	207
4.3.4	Solution Casting Pro-Attachment Polymers on Well Plates	211
4.3.5	Biological Testing – Stem Cell Attachment.....	220
4.4	Conclusions.....	221
4.4.1	Optimising TCDMDA Homopolymerisation for Anti-Bacterial- Attachment Applications:	221
4.4.2	Macromer Control of TCDMDA for Pro-Stem Cell Attachment Surfaces	222
4.5	Future Work	223
4.5.1	Optimising TCDMDA Homopolymerisation for Anti-Bacterial- Attachment Applications:	223
4.5.2	Macromer Control of TCDMDA for Pro-Stem Cell Attachment Surfaces	223
4.6	References.....	224
5	Chapter 5: Synthesis and Optimisation of Clean Burn & Anti-Biofilm Copolymers	235
5.1	Introduction	235
5.1.1	Soot Formation in Engines	235
5.1.2	Biofilms and Anti-Fouling Surfaces	238
5.2	Aims and Objectives.....	243
5.3	Results and Discussion	244
5.3.1	EGDMA/LMA Copolymers	244
5.3.2	DVB/DEGMA Copolymers	254

5.3.3	TCDMDA/LMA Copolymers.....	259
5.3.4	Tribological Testing	262
5.4	Conclusions	262
5.4.1	EGDMA/LMA Polymers	262
5.4.2	DVB/DEGMA Polymers	263
5.4.3	TCDMDA/LMA Polymers	263
5.5	Future Work	264
5.6	References	265

List of Abbreviations

AFM	Atomic Force Microscopy
AIBN	Azobis(isobutyronitrile)
ATRP	Atom Transfer Radical Polymerisation
BA	Butyl acrylate
BAR	Bacterial Attachment Resistant
BMA	Butyl methacrylate
CCS	Cold Crank Simulator
CCT	Catalytic Chain Transfer
CCTP	Catalytic Chain Transfer Polymerisation
CP	Controlled Polymerisation
CRP	Controlled/living Free Radical Polymerisation
C_s	Chain Transfer Constant
CT	Chain Transfer
CTA	Chain Transfer Agent
\bar{D}	Dispersity
DCM	Dichloromethane
DDT/DDM	Dodecanethiol/Dodecyl mercaptan
DEGMA	Di(ethylene glycol) methyl ether methacrylate
DP	Degree of Polymerisation
DVB	Divinyl benzene
EA	Ethyl acetate
EGDMA	Ethylene glycol dimethacrylate
EGDPEA	Ethylene glycol dicyclopentenyl ether acrylate
EHD	Elasto-Hydrodynamic
EM	Electromagnetic
EP	Ethylene propylene
EPS	Extracellular Polymeric Matrix
FRP	Free Radical Polymerisation
GPC	Gel Permeation Chromatography

HB	Hyperbranched
HD	Hydrodynamic
HFRR	High Frequency Reciprocation Rig
hPSC	Human Pluripotent Stem Cells
IMS	Industrial Methylated Spirits
IPA	Isopropanol
KV	Kinematic Viscosity
LA	Lauryl acrylate
LMA	Lauryl methacrylate
MEHQ	Hydroquinone monomethyl ether
MMA	Methyl methacrylate
M_n	Number Average Molecular Weight
MTM	Mini Traction Machine
M_w	Weight Average Molecular Weight
MW	Molecular Weight
NMP	Nitroxide Mediated Polymerisation
NMR	Nuclear Magnetic Resonance
PAO	Polyalphaolefin
PhCoBF	Bis[(difluoroboryl)diphenylglyoximato]cobalt-(II)
RAFT	Reversible Addition Fragmentation Chain Transfer Polymerisation
RDS	Rate Determining Step
SA	Stearyl acrylate
SCs	Stem Cells
SCVP	Self-condensing Vinyl Polymerisation
SEC	Size Exclusion Chromatography
SFRP	Stable Free Radical Polymerisation
SLIM	Spacer Layer Image Mapping
SMA	Stearyl methacrylate
TCDMDA	Tricyclo[5.2.1.0 ^{2,6}]decanedimethanol
TCPS	Tissue Culture Polystyrene

THF	Tetrahydrofuran
USV	Ultra-high Shear Viscosity
2PP	Two Photon Polymerisation
3-MPA	3-Mercaptopropionic acid

1 Chapter 1: Introduction

Polymers, often known as macromolecules, are large molecules made from many, small repeating units called monomers. The process of monomers combining to form polymers is known as polymerisation. This section will first give a brief overview of polymers: how they were first discovered, their structures and properties and methods of polymerisation. It will then discuss the more specific case of free radical polymerisation and possible control methods, before introducing hyperbranched polymers, surfactants and common polymer characterisation techniques.

1.1 Background

Prior to 1930, polymers were assumed to be large clusters, or aggregates, of monomer molecules. In the 1920s, Herman Staudinger had put forward the idea that polymers were, in fact, extremely long molecules made from many smaller monomer units [1]. However, this was not proven until the 1930s, when Wallace Carothers began carefully building molecules that displayed polymeric properties through repetitive synthesis of known monomers, firmly establishing the macromolecular nature of polymers. He also classified polymerisation into two categories: step growth and chain growth. Carothers also invented Nylon: by reacting hexamethylenediamine and adipic acid in a condensation reaction, Carothers created the now widely used polyamide 6-6 [2]. Since then, thousands of polymers have been synthesised, while only a handful have been a commercial success.

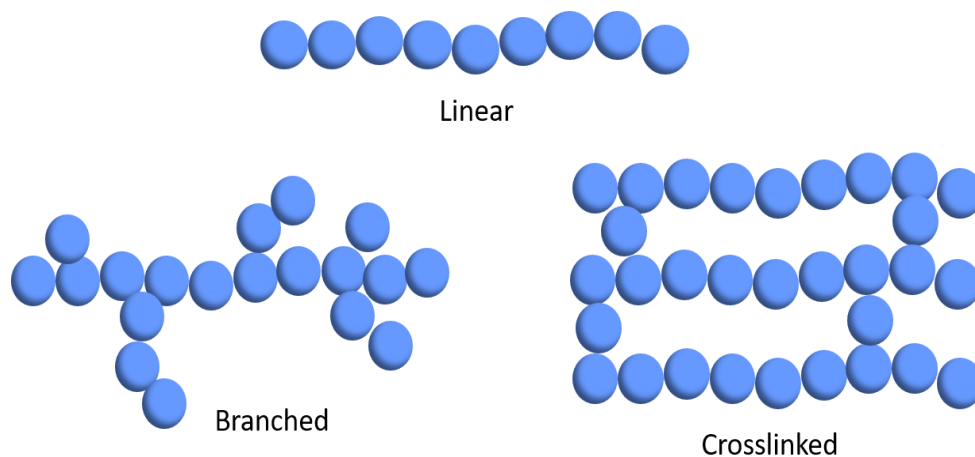


Figure 1.1. Linear, branched and crosslinked architectures for polymers.

1.2 Polymer Structures

Polymer properties are strongly dependent upon the chain structure, of which there are three main architectures: linear, branched, and networks/crosslinked polymers, shown in Figure 1.1. Linear polymers are formed from monomers that possess at least one functional group (mono-functional), while the synthesis of branched polymers requires multi-functional monomers, or a mixture of mono- and multi-functional monomers. Crosslinked polymers are three-dimensional networks, and essentially contain a very large macromolecule: such crosslinking can occur via unwanted side reactions, or through the use of specific cross-linking materials. For example, rubber is crosslinked (or vulcanised) using sulphur as the crosslinker [3].

In addition to the three main architectures, there exist a number of further structures including hyperbranched and dendrimeric structures, shown in Figure 1.2. Dendrimers are extremely highly branched, well-defined, perfectly monodisperse, three-dimensional polymers: their tree-like, porous structure, which emanates from a central core, allows small molecules to be encapsulated within them. Dendrimers were first synthesised *via* multistage, iterative reactions, independently, by Vögtle [4], Tomalia [5] and Newkome [6] as the functionality of polymers became the focus of

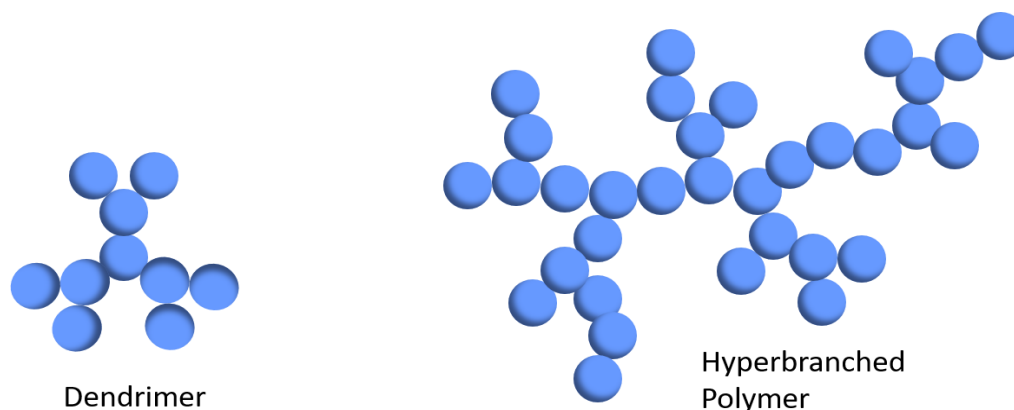


Figure 1.2 Architecture of a hyperbranched polymer.

polymer research. This led to a high level of research into using dendrimers as transport molecules for fragrances, drugs, diagnostic molecules, catalysts, light-emitting diodes, etc. [7]–[10]. However, the synthesis of dendrimers is both labour intensive and time consuming [5], [11], [12].

In contrast to dendrimers, hyperbranched polymers are polydisperse in both their molecular weight and branching factors, mainly due to the occurrence of the competitive reaction that leads to the formation of linear chains and branching [11]. Consequently, the structure of hyperbranched polymers is irregular and control over the structure produced is low: these polymers exhibit high dispersity values as a result. Additionally, they are highly susceptible to cross-linking: the propagating chains of the 3D hyperbranched polymer react with each other to form a closed, interpenetrating network. The transition, from highly branched, soluble polymer to an insoluble gel network, occurs at the gelation point: note, this is entirely separate from the gel effect (or Trommsdorff-Norish effect [13]) where the viscosity of a bulk reaction medium gets very high and chain termination is disfavoured, resulting in a loss of control of the polymerisation [21].

Polymers can be produced through the use of more than one type of monomer: by varying the monomers, monomer concentrations and polymerisation techniques

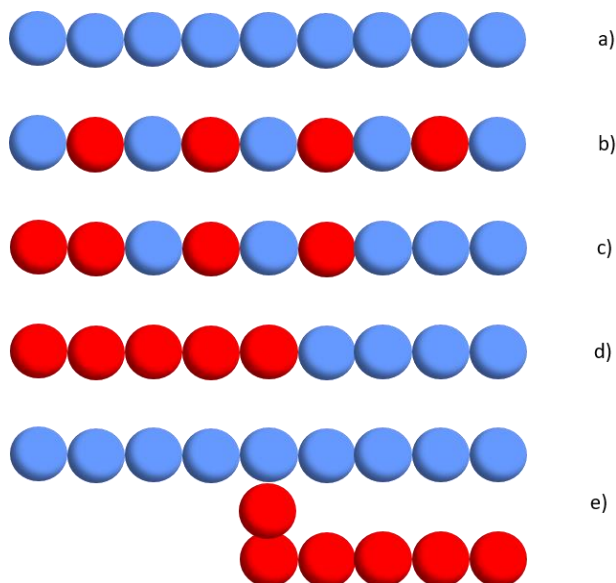


Figure 1.3. Structure of: a) homopolymer; b) alternating co-polymer; c) random co-polymer; d) block co-polymer; e) graft co-polymer.

used, a large variety of polymers with a variety of properties can be produced. Homopolymers are polymers that are composed of only one type of monomer, while polymers composed of two or more types of monomer are known as co-polymers. The main varieties of linear co-polymer are random, alternating and block/graft, and these are depicted in Figure 1.3.

Random co-polymers are also known as statistical co-polymers, where there is no repeating arrangement of monomers. In alternating co-polymers, monomers are arranged in a repeating sequence: these are difficult to produce but display some interesting properties [14]. Block co-polymers are made of 'blocks' of homopolymer which are covalently bonded together. Graft co-polymers are a form of block co-polymer, and are sometimes also classified as branched co-polymers.

1.3 Polymerisation Methods

There are two broad polymerisation mechanisms often used to categorise polymers: step growth and chain growth. More recently, controlled/living

polymerisation mechanisms, shown by the green line in Figure 1.4, have been discovered. These are discussed in more detail in Section 1.5.

1.3.1 Step Growth

Step growth polymerisation proceeds via a series of individual reactions resulting in the formation of dimers and low molecular weight oligomers, which then combine together to form longer polymer chains. The mechanism is similar to that of a conventional condensation reaction: a small molecule, such as H_2O or HCl , is often expelled as monomers combine. This condensate must be removed from the reaction mixture to prevent the reverse reaction (and hence depolymerisation) occurring.

Monomer conversion increases rapidly in the initial stage of step-growth polymerisation, though only low molecular weight oligomers are formed. Consequently, oligomers are obtained up until ~80-95% monomer conversion: after this point, the many oligomers join to form polymers, and an exponential increase in polymer molecular weight is observed, as shown in Figure 1.4 (blue line). The polymerisation rate decreases steadily as functional groups are consumed.

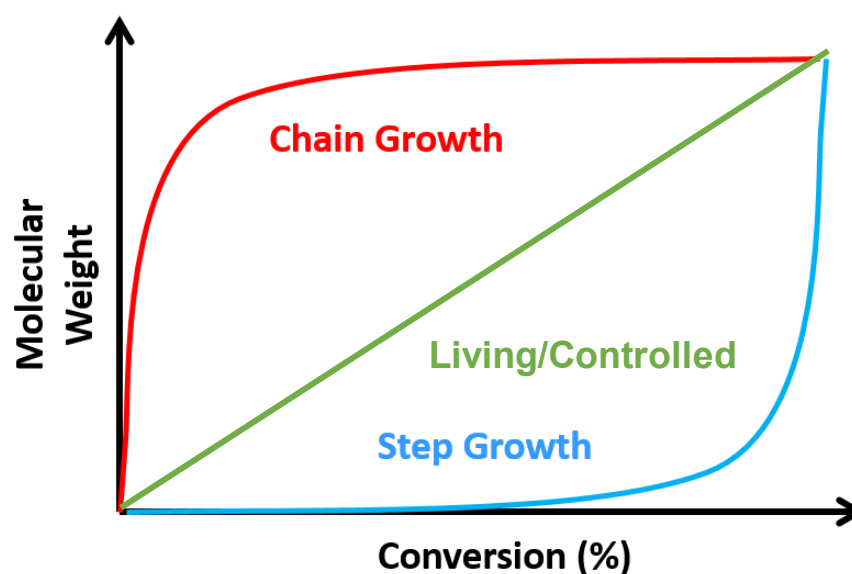


Figure 1.4. Graph of molecular weight vs conversion for step growth polymerisation (blue), chain growth polymerisation (red) and living polymerisation (green).

Nylon is an example of a polymer which can be prepared in this way: the diamine and di-acid react together, forming an amide linkage and releasing water.

1.3.2 Chain Growth

Chain growth polymerisation proceeds via the addition of a reactive species – usually a radical – to the π double bond of a monomer, producing the carbon backbone of the polymer. There are four major subcategories of chain growth polymerisation: free radical polymerisation (FRP); cationic polymerisation; anionic polymerisation and ring opening polymerisation. All such chain growth polymerisations proceed via three steps: (i) initiation, (ii) propagation, (iii) termination. [15]

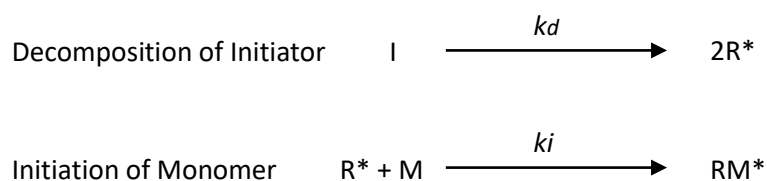
In contrast to step growth polymerisation, in chain growth polymerisation monomers sequentially join onto the end of a growing chain. Hence, high molecular weight polymers are formed early on, at low conversions, as shown in Figure 1.4 (red line) and monomer is consumed slowly. The polymerisation rate increases initially as initiating species are generated, and remains relatively constant until the monomer is depleted.

1.4 Free Radical Polymerisation

Free radical polymerisation (FRP) is the most popular polymerisation process used in industry due to its high tolerance of impurities and functional groups. FRP can also be used for a wide variety of industrially available vinyl monomers using non-stringent processing conditions. The reactive centre is a free radical, formed in the initiation step: initiation is followed by propagation and termination, which comprise the three major steps in FRP.

Initiation:

During the initiation step, the initiator (I) first decomposes (thermally or photochemically) *via* homolytic cleavage in the rate determining step (RDS) with a rate of decomposition k_d , to give a free radical, R^* , which subsequently adds to the vinyl group of a monomer, M, as outlined below in Scheme 1-1, with rate constant k_i .



Scheme 1-1. Representation of the initiation step in FRP.

The overall rate of initiation, R_i , is therefore:

$$R_i = 2k_d f [I] \quad (1-1)$$

where f is the efficiency factor, which is a measure of the fraction of initiator radicals that actually produce growing radical chains, and $[I]$ is the initiator concentration. Peroxides and azo compounds, such as azobisisobutyronitrile (AIBN), are examples of commonly used initiators.

Self-Initiation:

Certain monomers, such as the styrene monomer, are capable of self-initiation and so do not require the addition of an initiator to start the reaction. The exact mechanism of self-initiation is still under dispute, however, the two forerunning theories are the Flory and Mayo mechanisms: there is some evidence to suggest that the Mayo theory is more likely [16].

According to the Mayo mechanism, two styrene monomers undergo a Diels-Alder reaction, as shown in Figure 1.5 a, to form a dimer. Molecule-assisted homolysis

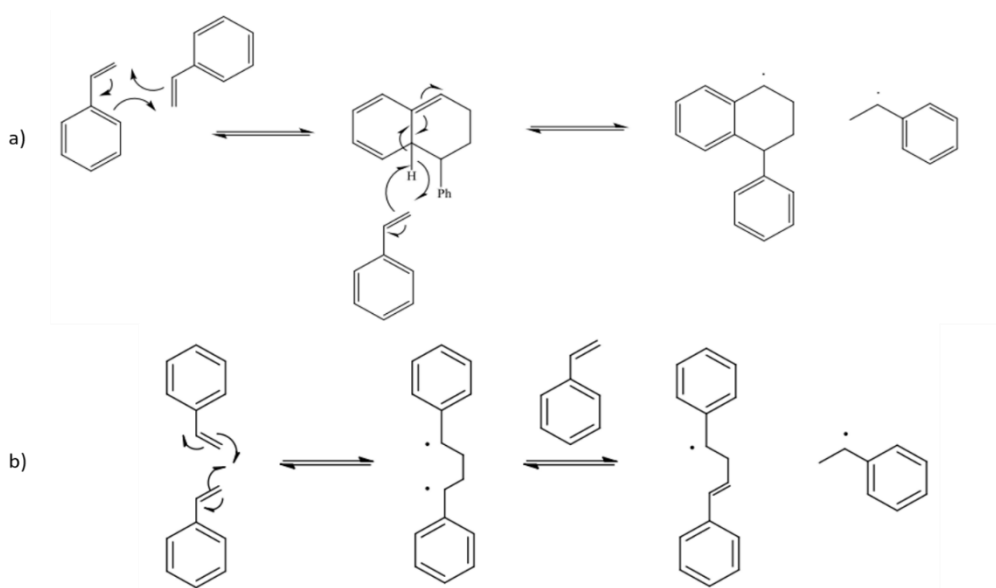


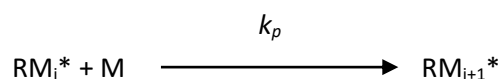
Figure 1.5. The a) Mayo and b) Flory mechanisms for self-initiation of styrene [19].

between the dimer and a third styrene monomer generates the monoradical initiators that initiate the polymerisation [16]–[18].

In contrast, Flory's mechanism first involves the dimerization of styrene monomers to form a singlet 1, 4-diradical, as outlined in Figure 1.5 b. A hydrogen is abstracted from the diradical by another styrene radical, generating the monoradical initiators used to initiate polymerisation [19].

Propagation:

Propagation is the process by which the initiated monomer, RM_i^* , combines with a radical in a head-to-tail addition to produce the growing polymer chain, shown in Scheme 1-2: it is a bimolecular reaction, and has a rate constant of propagation, k_p .



Scheme 1-2. Representation of the propagation step in FRP.

Though the monomer may contribute to the initiation process (such as in the self-initiation/autopolymerisation processes outlined above), compared to the total

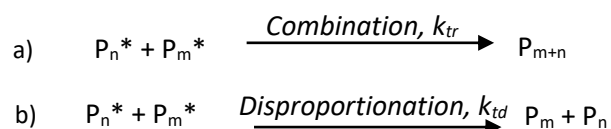
amount of monomer consumed in the production of long polymeric chains, the amount of monomer used in the initiation step is very small, and hence can be neglected. Therefore, the rate of propagation, R_p , can be related to the rate of consumption of monomer by:

$$R_p = \frac{-d[M]}{dt} = k_p[M^*][M] \quad (1-2)$$

where $[M^*]$ is the radical concentration and $[M]$ is the initial monomer concentration.

Termination:

Termination is the process by which 'dead' polymer chains are created and radicals are removed from the system. There are two forms of termination process, disproportionation and combination: the likelihood of each termination process occurring is strongly dependent upon steric and electronic effects. The combination process occurs when two growing polymer chains ($P_{m/n}$) react with each other in a head-to-head addition and form one polymer chain where growth is terminated, as shown in Scheme 1-3a.



Scheme 1-3. Representation of the a) combination and b) disproportionation termination steps in FRP.

Disproportionation involves the abstraction of a hydrogen atom from one growing polymer chain to form both saturated and vinyl-ended polymers, as shown in Scheme 1-3b. As a consequence of these two forms of termination, the final polymer chain length can vary significantly, which can affect the material properties of the final polymer.

The rate constants for combination and disproportionation are k_{tr} , and k_{td} , respectively: the rate of termination, R_t , is therefore expressed as:

$$R_t = \frac{-d[M^*]}{dt} = 2k_t[M^*]^2 \quad (1-3)$$

In addition to the initiation, propagation and termination processes described above, FRP can include another process known as chain transfer (CT) where the radical activity of the growing polymer chain is transferred to another molecule: this process will be discussed in more detail in Section 1.6 below.

1.4.1 Limitations of FRP

The lack of selectivity over the two termination processes outlined above is symptomatic of the major limitation of FRP: the lack of achievable control over the final polymer molecular weight, dispersity (\bar{D}) and architecture and copolymer composition. For example, very high molecular weight polymers are formed quickly, even at low conversion, due to the rapid propagation which is characteristic of chain growth polymerisation processes, hence producing targeted, low molecular weight polymers is difficult using FRP.

Additionally, FRP is an exothermic process which can cause potentially dangerous issues with reaction control at industrial scales. FRP reactions are conducted in sealed, degassed vessels to ensure the radicals required for polymerisation are not removed via reaction with oxygen in the atmosphere: as the reaction proceeds, large quantities of heat are released into the reaction medium, which in turn accelerates the rate of polymerisation through increasing the radical concentration, leading to high monomer conversion and high molecular weight polymer being produced and releasing yet more heat into the reaction medium. Correspondingly, this increase in polymer molecular weight greatly increases the viscosity of the reaction medium, restricting mass and heat transfer and, importantly, the termination rate. Thus, this cascade of events, leading to uncontrolled

temperature and pressure rises in the reaction vessel, results in auto-acceleration and, eventually, explosion: this effect is known as the Trommsdorff-Norrish effect (or the gel effect).

Consequently, a number of precautions are often applied to FRP reactions to reduce the chance of this effect occurring. These include restricting bulk polymerisations to low conversion or low molecular weight, and using solvents to decrease the viscosity of the reaction medium and ensure efficient heat and mass transfer. Additionally, chain transfer agents (CTAs) can be added to the polymerisation to control polymer molecular weight. This will be discussed in more detail in Section 1.6 below.

1.5 Pseudo Living/Controlled Free Radical Polymerisations

Controlled/living free radical polymerisation (CRP) was developed in the late 1980s as a means of overcoming the major limitation of FRP, taking inspiration from the fields of organic chemistry, conventional FRP and living ionic polymerisation. CRP provides high levels of control over key elements of the polymerisation process, which leads to well-defined polymers with controlled molecular weight, polydispersity, composition, chain architecture and site-specific functionality. Meanwhile, CRP retains the high tolerance of impurities and functional groups seen in FRP.

Consequently, CRP is now a versatile tool in the synthesis of more complex polymer architectures, such as block and comb copolymers. A number of CRP methods exist, but the most promising and popular are: stable free radical polymerisation (SFRP), most commonly nitroxide mediated polymerisation (NMP), in which 2,2,6,6-tetramethyl-1-piperidinyloxy (TEMPO) is used as the initiator; transition-metal-catalysed atom transfer radical polymerisation (ATRP); and

reversible addition fragmentation chain transfer polymerisation (RAFT). Other common SFRP initiator include 2,2,5-trimethyl-4-phenyl-3-azahexane-3-oxyl (TIPNO) and 2,2,5-trimethyl-4-isopropyl-3-azahexane-3-oxyl (BIPNO). Each of these methods relies on establishing a dynamic equilibrium between a low concentration of active propagating chains and a predominant number of dormant chains that are unable to propagate or terminate in order to extend the lifetime of the propagating chains.

The main characteristics of CRP are: a linear increase in molecular weight (shown in Figure 1.4 (green line)); target molecular weight polymers with narrow polydispersity can be obtained; re-initiation of polymers is possible, allowing the synthesis of complex architectures [20].

1.6 Chain Transfer

Chain transfer (CT) is the process of transferring activity from a growing polymer chain to another molecule: it has the effect of reducing the overall molecular weight of the polymer product and occurs either via unwanted side reactions or can be introduced deliberately through the addition of a chain transfer agent (CTA). The latter is often also used in order to more precisely control polymer molecular weight, by replacing the unpredictable termination mechanism with a CT mechanism. The physical and mechanical properties of polymers strongly depend on the polymer chain length, hence methods for controlling molecular weight are of great research interest.

There are four main CT processes: chain transfer to a CTA, where a weak chemical bond facilitates the process; chain transfer to a monomer, where a hydrogen atom is abstracted from a monomer by the growing polymer chain; chain transfer to a polymer, which is significant only in the latter stages of the polymerisation, when monomer concentration is low; and chain transfer to solvent, where the solvent can

act as a CTA. In conventional FRP, CT can result in branching: the growing polymer chain abstracts a hydrogen from the backbone of another polymer, resulting in a branching point. This can lead to polymers with very different properties to linear polymers. If the growing chain abstracts a hydrogen from its own backbone, this is known as 'backbiting', or intramolecular CT. In each case, the CT process results in the formation of a dead polymer chain and a CTA fragment, which contains a free radical and may go on to initiate other polymer chains. The probability of CT events occurring is defined by the chain transfer constant (C_s) of the polymer. As polymers generally have a very low C_s value, inter and intra molecular chain transfers are unlikely, and are only significant when the reaction is conducted in bulk.

1.6.1 Chain Transfer Agents

In the case of a typical chain transfer agent (T), the CTA first abstracts a hydrogen atom from the growing polymer chain (P_n^*), resulting in a dead polymer chain (P_n) and a CTA fragment containing a free radical (T^*). This CTA fragment can then go on to initiate other monomers (M), resulting in new growing polymer chains (TM^*), as summarised in Scheme 1-4.



Scheme 1-4. Representation of the chain transfer mechanism for a typical CTA.

Due to the nature of the CT mechanism, traditional CT agents introduce new functionality into the polymer backbone through the initiation step (Scheme 1-4 b). While this mechanism may be useful in producing tailored polymers with a specific second functionality introduced by careful selection of the CTA, in many cases the added functionality is undesirable; a further purification step must then be introduced

to remove the CTA fragment before the polymer can be used for its intended application.

Chain transfer agents are characterised by their chain transfer constant, C_s , which is defined as the ratio of the chain transfer and propagation rate coefficients, k_{CT} and k_p respectively. The CT constant gives a measure of the reactivity of the CTA, with a higher C_s value indicating that a lower concentration of the CTA is required to achieve a particular reduction in molecular weight for a given monomer. This is given quantitatively by the Mayo equation [21], which is expressed as:

$$\frac{1}{DP_n} = \frac{1+\alpha}{DP_{n0}} + C_s \frac{[T]}{[M]} \quad (1-4)$$

where the reciprocal of the degree of polymerisation (DP_n) is given as a function of the rate of chain growth and termination. Here, DP_{n0} , is the degree of polymerisation achieved in the absence of a CTA, α is the fraction of termination by disproportionation, $[T]$ is the concentration of CTA and $[M]$ is the concentration of monomer. Equation 1-4 is used to produce a Mayo plot of $[T]/[M]$ vs $1/DP_n$: the gradient of this line may be used to determine the C_s value of the CTA.

1.6.2 Thiol Chain Transfer Agents for FRP

Common CT agents used to reduce molecular weight in FRP are cheap and commercially available thiols, such as 1-dodecanethiol (DDT) and 3-mercaptopropionic acid (3-MPA), the structures of which are shown in Figure 1.6. Thiol-mediated FRP has been employed for a variety of mono- and multifunctional monomers, including

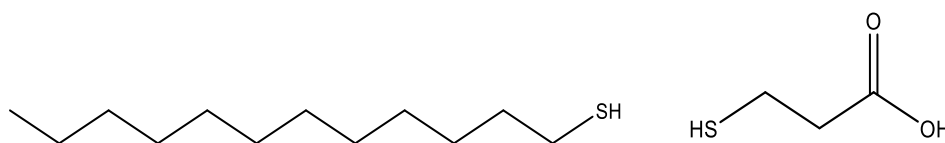


Figure 1.6. Structures of 1-dodecanethiol (left) and 3-mercaptopropionic acid (right).

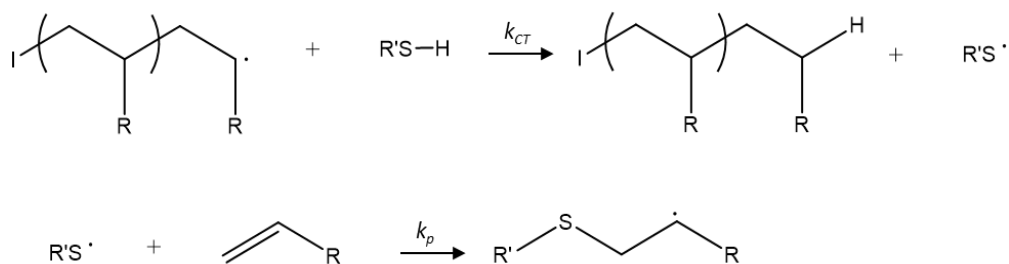


Figure 1.7. Process of chain transfer for a thiol control species.

styrene and methyl methacrylate (MMA) [22]–[25], due to their relatively efficient control of chain length. The weak S-H bond provides a labile group which may be transferred to a growing chain, generating a new, highly reactive thiyl radical (RS*) which can initiate new chains at the monomer double bond, as outlined in Figure 1.7: this is a typical FRP process, however, in the propagation step a thiyl radical is also formed, followed by addition of the radical across the vinyl group of a monomeric species, forming a thioether. This chain transfer process leads to large decreases in polymer molecular weight without significant change to the overall polymerisation rate. The resulting polymers are ‘dead’, as they are no longer propagating, and contain unreactive sulfur-containing groups called thioethers: this reaction occurs in a stoichiometric fashion.

However, thiol-based CTAs such as these have disadvantages: large quantities (5-20 mol% wrt. monomer) are required to reduce the molecular weight by a significant amount, such as when targeting oligomeric product, and they possess an undesirable odour, even when used in small quantities. Additionally, they have a high toxicity and relatively low activity: for example, DDT has a chain transfer constant, C_s ~ 1 in MMA and ~ 20 in styrene at 60°C [15], [24], [25]. Finally, their use results in the inclusion of a fragment of the thiol *via* the thioether linkage, which may impact the physical properties of the polymeric product.

1.6.3 Catalytic Chain Transfer Polymerisation (CCTP)

Thiol CTAs are undesirable for use in industrial processes for numerous reasons, as outlined in Section 0, including their toxicity and low activities, however, there is still considerable interest in producing low molecular weight polymers. One alternative and popular method is catalytic chain transfer polymerisation (CCTP).

In 1975, Boris Smirnov and Alexander Marchenko discovered a new method for controlling the molecular weight in a methacrylate polymerisation: by introducing low-spin Co^{II} catalysts, such as the substituted cobalt porphyrins or benzoporphyrins which are shown in Figure 1.8, the occurrence of chain transfer to monomer was greatly enhanced [26]. This resulted in dramatic reductions in molecular weight of the methacrylate polymers with minimal reduction in the overall polymer yield.

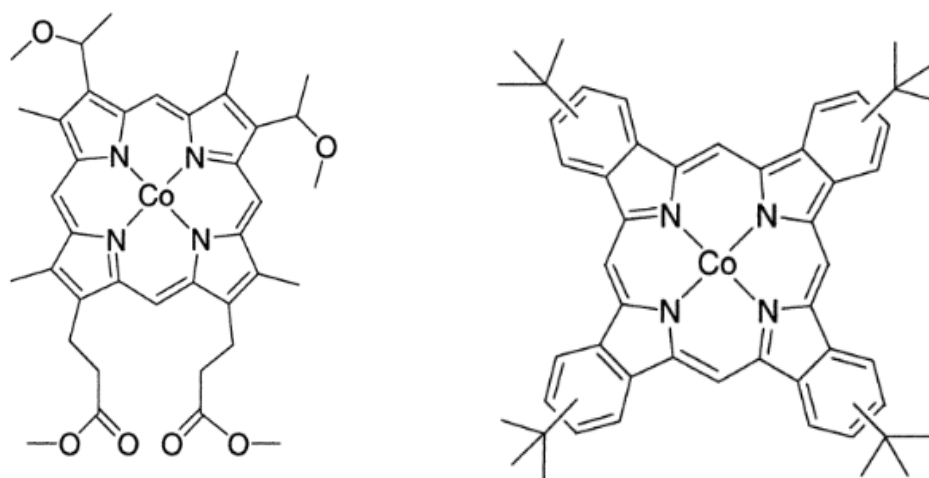


Figure 1.8. Structures of the Co complexes first used to control the polymerisation of PMMA [26].

The CCTP process is a FRP process, and the resulting linear polymer dispersities are generally in the range 1.50 – 2.50. The Co^{II} catalyst simply acts as a CTA, providing control over the polymer chain length and end group functionality similar to the thiols discussed earlier. However, the CCT process was shown to occur significantly faster

than the conventional CT process with CTAs such as thiols, while the cobalt catalysts also have high chain transfer constant (C_s) values compared to thiols [27], [28].

The cobalt porphyrins and benzoporphyrins discussed above have been found to be amongst the most efficient catalysts: reductions in molecular weight from tens of thousands to several hundred Dalton (Da) were observed using catalyst concentrations as low as 100-300 ppm, while boron based cobaloximes, such as those in Figure 1.9, have been found to exhibit the highest C_s values [26], [29]–[31]. Catalyst reactivity has also been shown to be highly dependent on the bridging groups within the cobaloximes: those with a BF_2 bridging group (Figure 1.9, right) have been shown to be more stable, and thus less sensitive to air, than those with a hydrogen bridging group (Figure 1.9, left). Consequently, these boron based cobaloximes have become the CCTP catalyst of choice.

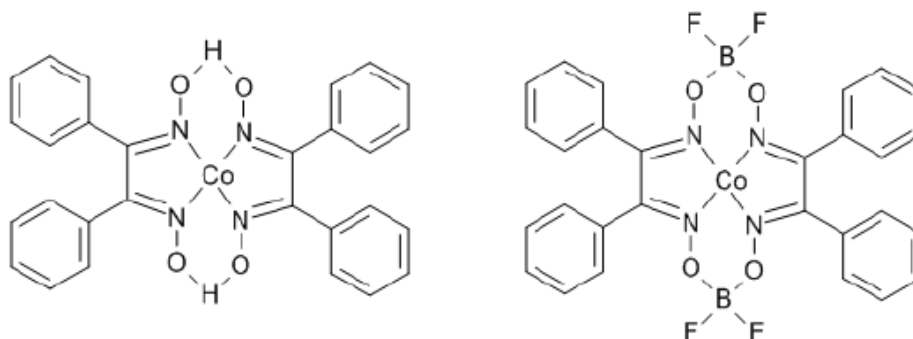


Figure 1.9. Most commonly-used cobaloximes [19].

CCTP has a number of advantages over other control mechanisms, especially with regards to the production of industrially applicable polymers/oligomers. One major limitation of controlled/living polymerisation techniques (discussed in Section 1.5), is the requirement for high levels of initiator or catalyst: each initiator molecule initiates only one macromer, making them commercially unattractive when low molecular weights are targeted. Additionally, CCTP, unlike other control techniques,

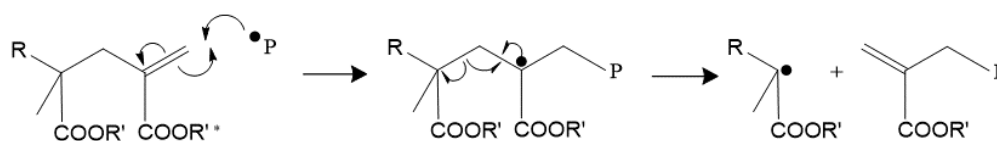
does not result in the incorporation of a fragment of the control agent into the polymer structure, but instead terminates chains with a double carbon bond, ensuring there is no added functionality or change of polymer properties. Furthermore, this terminal vinyl functionality can be exploited in secondary reactions to generate interesting, three-dimensional architectures. For example, Haddleton *et al.* have used CCTP to synthesise poly(lauryl methacrylate) and poly(methyl methacrylate) with vinyl terminal groups, which were subsequently modified: for the former, using phosphine-mediated thio-Michael addition of thioglycerol to the vinyl group [32] and for the latter through their use as in-situ CTAs for the reversible addition-fragmentation chain transfer polymerisation of various methacrylic monomers [33], [34].

More recently, a number of groups have successfully shown that CCTP can be used to inhibit gelation in hyperbranched polymers with a range on monomer types, provided that either (a) the concentration of the branching agent (a diacrylate) was kept low (5 wt %)[34], or the level of overall conversion is limited to specific levels [27], [35], [36].

1.6.3.1 CCTP-derived Macromer and β -Scission

Interestingly for the work in this thesis, low molecular weight oligomers of methacrylate monomers produced *via* CCTP have been demonstrated to exhibit chain transfer control of free radical polymerisations of other vinyl monomer types *via* a β -scission mechanism [37].

Due to the very high transfer constants associated with CCTP catalysts, it is relatively simple to prepare macromonomers of very low molecular weight, down to dimers, trimers etc. The terminal vinyl group in these macromonomers makes them susceptible to radical addition to form macromonomer-ended polymer radicals. This radical can undergo a β -scission reaction in addition to normal propagation and termination, as outlined in Scheme 1-5 for a dimeric macromer.



*Scheme 1-5. Representation of the β -scission mechanism for a dimer, where R is a thermal initiator fragment and *P is a propagating polymer chain. The propagating polymer is terminated with a fragment of the dimer and a vinyl group, while the radical segment of the dimer is released as new propagating radical.*

The result is that the ultimate unit of the macromonomer terminates the propagating radical (i.e. the polymer chain) and the remaining radical segment of the macromer is released as a new propagating radical, initiating new polymer chains: thus, the macromer acts as a CTA. Consequently, this method of chain transfer leads to a fragment of the macromeric CTA becoming an intrinsic part of the product polymer structure, as with all other stoichiometric CTAs [37].

1.6.3.2 CCTP Theory and Mechanism

In cobaloximes, the strong bonding between the metal centre and the diphenyl glyoxime ligands result in a cobalt (II) d7 species, which adopts a low spin configuration as shown in Figure 1.10. This results in the cobalt having one unpaired electron in a higher energy orbital: this unpaired electron is able to interact with a radical on a growing polymer chain, which is a key step in the CCTP mechanism [38], [39].

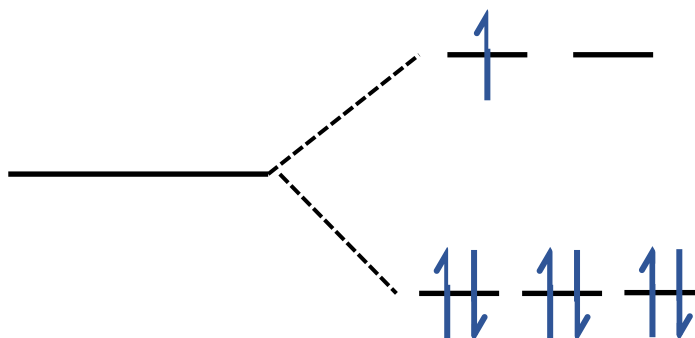


Figure 1.10. Electronic configuration of cobalt (II), a d7 low spin complex. There is one unpaired electron in a higher energy orbital.

The CCTP mechanism is outlined in Figure 1.11 for divinyl benzene polymerisation, with bis[(difluoroboryl)diphenylglyoximato]cobalt-(II) (PhCoBF) used as the catalyst. The mechanism proceeds *via* a two-step radical process: a proton is first abstracted from the growing polymer chain by the Co(II), producing a dead chain terminated with an ω -unsaturated vinyl group (the transfer product), and a Co(III) hydride complex. This is the rate determining step [39]. The Co(III)-H then reacts with a new vinyl monomer and initiates a new chain, resulting in a propagating radical and reforming the Co(II) complex.

The activity of the catalyst is greatly affected by the choice of monomer. For example, many catalysts are very active with MMA monomers due to the presence of an α -methyl group, which aids the hydrogen abstraction: the radicals formed in this process are tertiary, which are relatively stable[39]–[41]. Styrene, in contrast, does not possess an α -methyl group: only secondary radicals are formed during the CT reaction, which are less stable than tertiary radicals. Hydrogen abstraction at the α -methyl substituent is more efficient, and consequently, monomers containing an α -methyl group are very active in CCTP. In addition, tertiary radicals lead to the formation of weak cobalt-carbon bonds, thus little catalyst is lost in unwanted $\text{Co}^{\text{III}}\text{-R}_n$ complexes. In comparison, secondary radicals lead to the formation of more stable

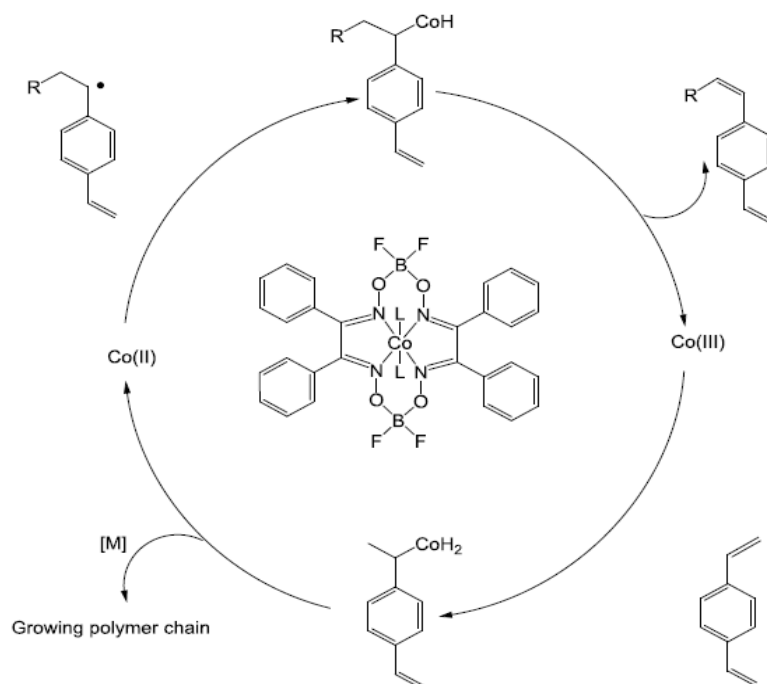


Figure 1.11. Catalytic chain transfer mechanism [19].

C-Co bonds, significantly reducing the amount of active catalyst in the system and, hence, its activity. This results in a decrease in activity from $C_s \sim 15,000-30,000$ for MMA to $C_s \sim 400$ for styrene [39]–[41].

The most notable disadvantages of CCTP relate to purification of the polymer product: in some instances, the cobalt catalyst may need to be removed post-reaction by polymer precipitation or acid/base washing, sometimes repeated to ensure minimal traces of catalyst remain. This often requires large volumes of organic solvent, which has environmental impacts.

1.7 Hyperbranched Polymers

1.7.1 History of Hyperbranched Polymers

Hyperbranched (HB) polymers are a relatively new macromolecular class in relation to reliable synthesis: the name was coined by DuPont researchers, Kim and Webster, who described dendritic macromolecules with a random topology prepared

via the single step polycondensation of AB₂-type monomers in the late 1980s, and patented the process for the preparation of hyperbranched polyarylene in 1987 [42]. However, their history (summarised in Table 1.1) can in fact be dated to the late 19th century, when Berzelius first formed a resin from tartaric acid (A₂B₂) and glycerol (B₃) [43], [44].

Table 1.1. History of hyperbranched polymers

Year	Case	Lead Author(s)	Reference
Pre- 1990	Tartaric acid + glycerol	Berzelius	[44]
1901	Glycerol + phthalic anhydride	Smith	[44]
1909	Phenolic + formaldehyde	Baekland	[45]
1929-1939	Glycerol + phthalic anhydride	Kienle	[44], [46]
1941	Molecular size distribution in theory	Flory	[47]
1952	AB _n polymerisation in theory	Flory	[48]
1982	AB ₂ + AB copolymerisation	Kricheldorf	[49]
1987	AB ₂ homopolymerisation	Kim/Webster	[42]
		Odian/Tomalia	[5]
		Frechet/Hawker	[50]

Following Watson Smith's report of the reaction of phthalic anhydride (latent A₂) or phthalic acid (A₂) and glycerol in 1901 [44], the reaction was investigated further: Kienle *et al* demonstrated that the specific viscosity of this polymer was lower than those of linear polymers such as polystyrene [46]. The ideas of a "degree of branching" and "highly branched species", however, were not introduced until the 1940s by Flory *et al*, when they calculated the molecular weight distribution of gelled 3D polymers [3], [47], [51]. Then, in 1952, Flory described the polymerisation of AB_x polymers, where $x \geq 2$, resulting in the formation of highly branched, soluble polymers, where

the risk of gelation is removed almost entirely [48]. This essentially laid the theoretical foundation for hyperbranched polymers and sparked research interest in these polymers due to their enhanced mechanical properties, increased heat resistance and improved strength-related performance, with many comparisons of their properties with their linear analogues.

However, the majority of studies initially focussed on the synthesis of dendrimers, which were discussed in more detail in Section 1.2, page 2. In contrast to dendrimers, hyperbranched polymers synthesised *via* the one-pot polymerisation of AB_x polymers, where $x \geq 2$, as outlined by Flory, are polydisperse in both their molecular weight and branching factors, mainly due to the occurrence of the competitive reaction that leads to the formation of linear chains and branching [11]. Consequently, the structure of hyperbranched polymers is less regular than dendrimers and control over the structure produced is low: these polymers exhibit high \mathcal{D} values as a result. Additionally, they are highly susceptible to cross-linking: the propagating chains of the 3D hyperbranched polymer react with each other to form a closed, interpenetrating network. The transition, from highly branched, soluble polymer to an insoluble gel network, occurs at the gelation point: note, this is entirely separate from the gel effect (or Trommsdorff-Norish effect), where the viscosity of a bulk reaction medium gets very high and chain termination is disfavoured, resulting in a loss of control of the polymerisation [52].

However, the most important difference between hyperbranched polymers and dendrimers is that these materials can be synthesised in hours using a simple one-pot method and industrially available monomers [42], [46], [52]: this is a significant improvement on the days, weeks or months required to synthesise dendrimers. Additionally, hyperbranched polymers have the potential to act as

replacements/substitutes for dendrimers, delivering the same performance and applications [52].

Consequently, since Kim and Webster first intentionally synthesised hyperbranched polyphenylene (see above), hyperbranched polymers have attracted significant and growing attention, as shown by the increasing number of publications on the topic in Figure 1.12, due to their interesting properties, wide range of potential applications, highly reactive and numerous terminal groups and greater availability than dendrimers [13], [43], [52]–[58].

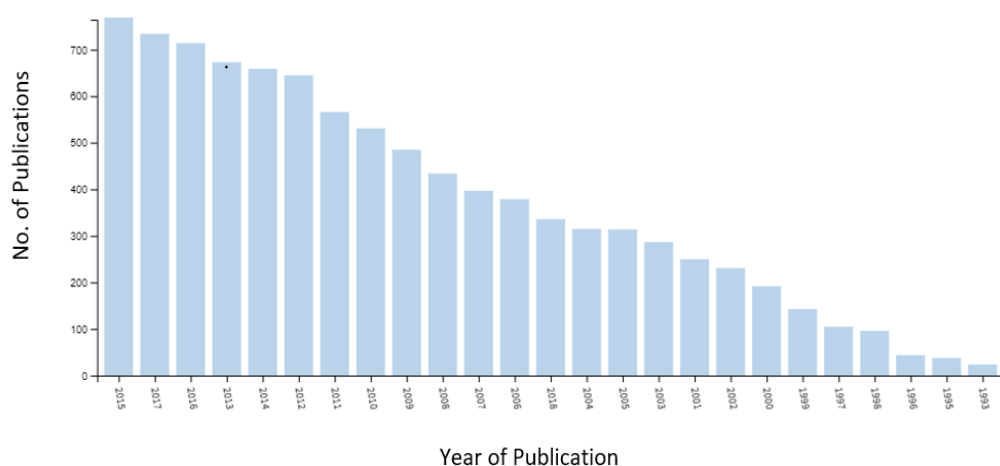


Figure 1.12. Bar chart showing rise in number of publications referencing hyperbranched polymers available on Web of Knowledge over the last 25 years [37].

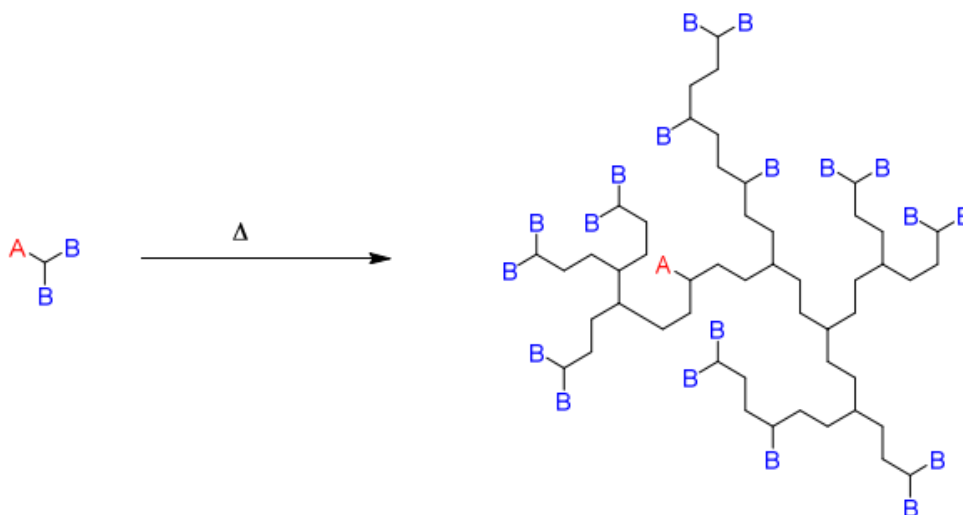
1.7.2 Synthesis of Hyperbranched Polymers

Despite the interest sparked by Flory's theory in 1952 [48], hyperbranched polymers have only been reliably synthesised since the 1990s, initially through the use of polycondensation techniques [42], [50]; self-condensing vinyl polymerisation (SCVP) [12], [57] and free radical polymerisation (FRP), controlled using chain transfer agents (CTAs) and sometimes known as CRP techniques, are also common synthesis routes [17], [59]. Many of the developments in synthesis have focussed on

attempting to develop synthesis routes that are fast, industrially viable, and that allow the formation of high yields of polymer before the onset of gelation.

1.7.2.1 Branched Polymers by Condensation Polymerisation

Condensation polymerisation, a one-pot method, uses commercially available AB_x polymers and was the first method used to produce hyperbranched polymers without reduced risk of gelation [42]. In this method, outlined in Scheme 1-6 for an AB_2 monomer, A groups only react with B groups and the relative reactivities of groups A and B are equal. Theoretically, this technique is advantageous in that if ideal selectivity between A and B groups is maintained, then cross-linking should be impossible. However, in reality cross-linking cyclisation and side reactions between B groups do occur [60]. This method allows limited control of the molecular weight of the hyperbranched product, resulting in a high dispersity.



Scheme 1-6. General reaction scheme depicting single monomer methodology self-condensation reaction of AB_2 monomers.

Many hyperbranched aliphatic polyesters are produced this way: a very popular family of dendritic materials has emerged which is based on the monomer 2,2-bis(methylol)propionic acid (bis-MPA), an AB_2 monomer [61]. This simple aliphatic molecule is readily available in bulk quantities, and has been used to

construct a range of hyperbranched polymers, including hyperbranched Boltorn™ [62], [63]. First carried out by Hult *et al.* in 1993, the carboxylic acid group of bis-MPA and a tetra-functional polyol undergo a condensation reaction to form the reactive polymer centre: subsequent reactions of the bis-MPA form the polymer arms [63]. A typical structure is shown in Figure 1.13.

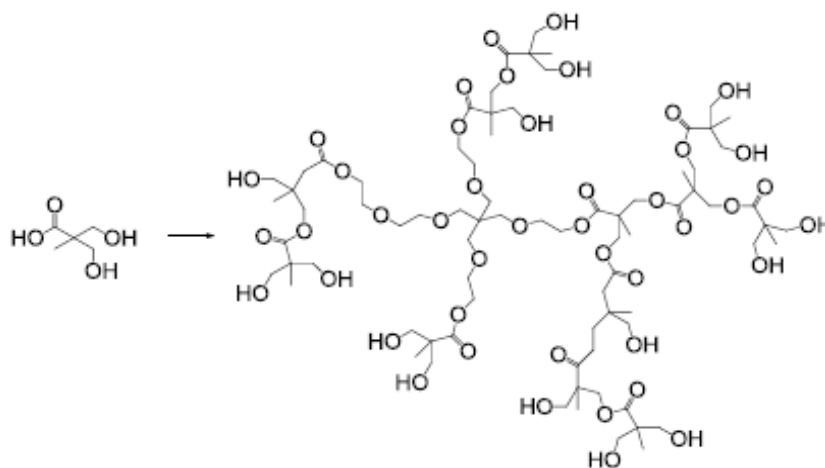


Figure 1.13. The condensation polymerisation of bis-MPA to form hyperbranched Boltorn H₂O [58]

1.7.2.2 Branched Polymers by Self-Condensing Vinyl Polymerisation

Self-condensing vinyl polymerisation (SCVP) was the first example of using vinyl polymerisation to produce hyperbranched polymers: 3-(1-chloroethyl)-ethenylbenzene, an AB type monomer where A is a vinyl group and B is a latent initiator, was first polymerised *via* a two-step process, as shown in Figure 1.14, by Frechét *et al* in 1995 [64].

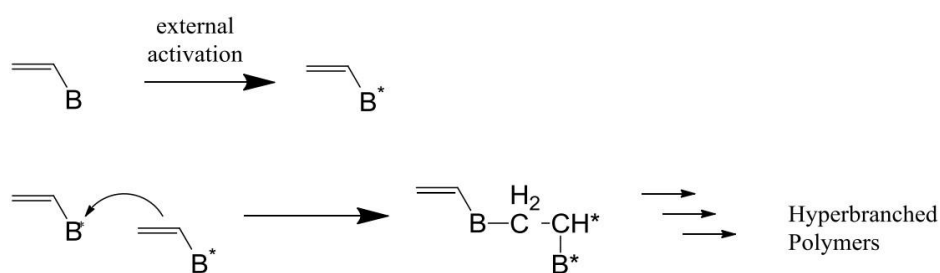


Figure 1.14. Schematic of SCVP of an AB polymer to form hyperbranched polymers [19].

The active monomer, which is in fact a mixture of species, is formed using SnCl_4 and tetrabutylammonium salt: the latter shifts the equilibrium from a free ionic structure to a dormant covalent species, as shown in Figure 1.15. As both of the monomer's resulting reactive centres have a similar reactivity, they can go on to form hyperbranched polymers.

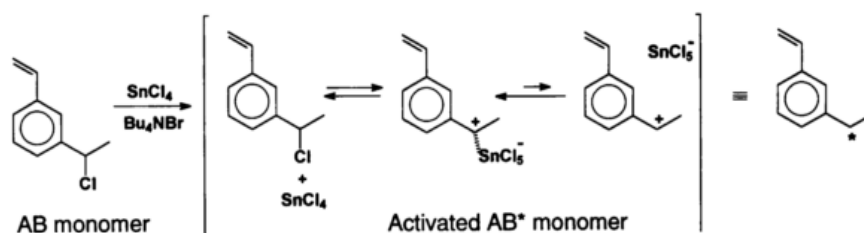
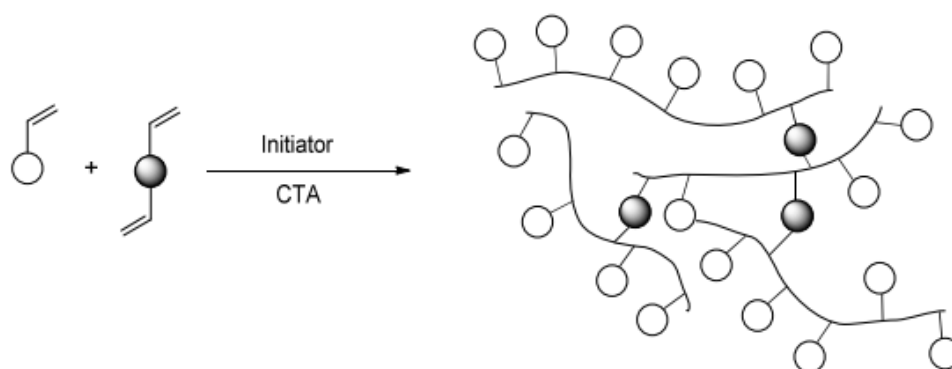


Figure 1.15. Formation of active monomer for SCVP [60].

This method was found to result in much higher yields than condensation polymerisation, with yields of $\sim 80\%$ and molecular weights in the range 30-50 kDa. However, the obvious disadvantage of SCVP is the need for the correct AB molecular structure to allow the synthesis of hyperbranched polymers *via* this method: this structure is possessed by a limited number of monomers [64].

1.7.2.3 Branched Polymers by Conventional Chain Transfer Polymerisation

Free radical polymerisation in the presence of even very low concentrations of di-functional monomer rapidly yields an insoluble, cross-linked network [65], [66]. However, the application of thiols (as discussed in Section 0) as a CTA by Sherrington *et al.* [67]–[71] was shown to enable the copolymerisation of monofunctional vinyl monomers with low concentrations of multi-functional vinyl monomers in a synthesis route now commonly known as the “Strathclyde methodology”, after the institution in which it was conceived as shown in Scheme 1-7. In the Strathclyde method, the number of molecules per kinetic chain length is reduced which delays the onset of gelation. Branched polymers may be obtained, with some polymers possessing thiol



Scheme 1-7. Synthesis of branched vinyl polymer through copolymerisation of mono- and di-vinyl monomers via the Strathclyde method.

functionality: this thiol functionality is only imparted to approximately 50 % of the chains, as each transfer event also terminates a chain with a hydrogen atom.

Polymers produced using this method generally exhibit poorly defined \bar{M} and poor control over terminal functionality. Attempts to improve this led to the application of a catalytic transfer agent.

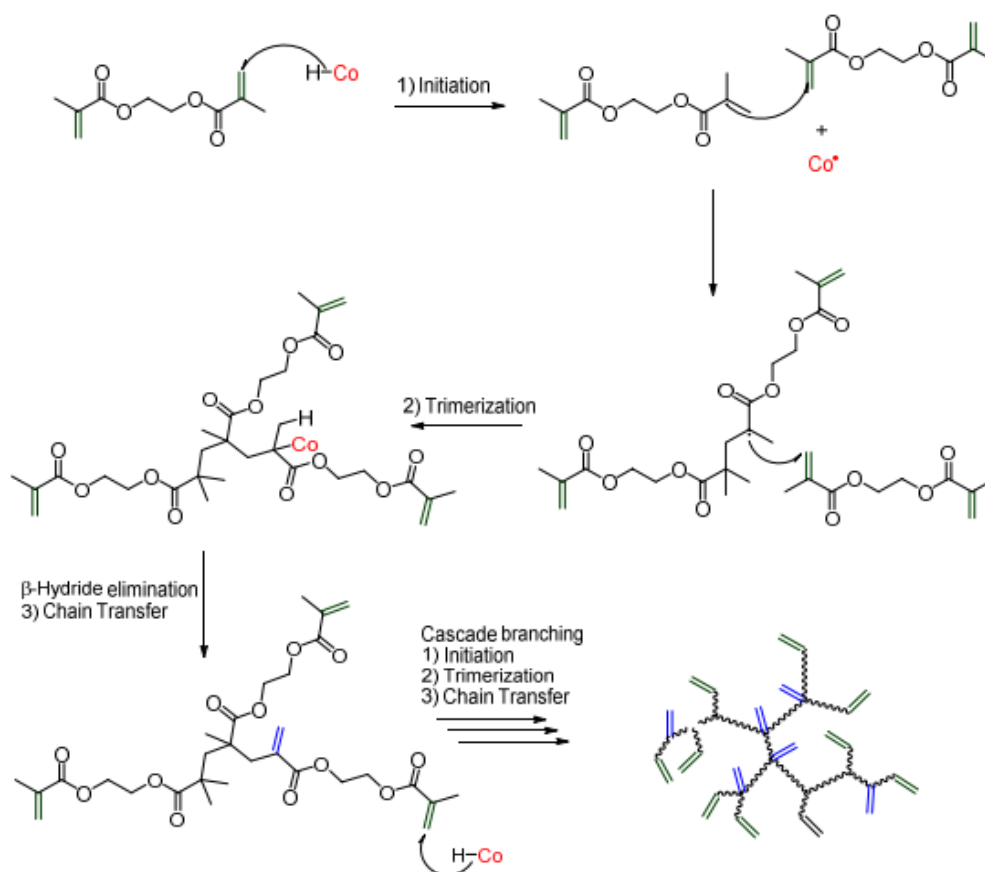
1.7.2.4 Branched Polymers by Catalytic Chain Transfer Polymerisation (CCTP)

CCTP allows the polymerisation and molecular weight control of a wide range of industrially available vinyl monomers, including multifunctional monomers, through the use of cobalt-based control agents as discussed in more detail in Section 1.6.3.

Investigations into using CCTP with multi-functional vinyl monomers first began in the 1980s with the attempted homopolymerisation of triethylene glycol dimethacrylate (TEGDMA) using a cobalt(II) (Co(II)) hematoporphyrin tetramethyl ester complex as the CTA. While soluble oligomers were produced with this method, the resulting polymers were inconsistent and not fully characterised [72]. This was followed up by the filing of a patent by Abbey in 1986 using TEGDMA and an *in situ*

Co(II) catalyst, though the large quantities of catalyst used resulted in only oligomeric products being obtained [73], [74].

More than a decade later, in 1998 Guan filled his first patent in the area, detailing the homopolymerisation of a wide variety of di- and tri- vinyl monomers, in addition to their copolymerisation with a range of mono-vinyl monomers [75]. This was later followed by its publication in academic literature, where the polymers produced were noted for their low solution viscosity, high vinyl group concentrations and the monitoring of the molecular weight through multidetector SEC, in particular viscometry [35]. The proposed mechanism was of trimerization followed by cascade branching, as shown in Scheme 1-8.



Scheme 1-8. Proposed mechanism for CCTP of EGDMA through cascade branching, leading to the formation of vinyl-terminated polymers [35].

Meanwhile Sherrington *et al.*, Viscotek and Ineos Acrylics compared the Strathclyde method to CCTP through the copolymerisation of MMA with tripropylene glycol diacrylate (TPGDA). They demonstrated that polymers produced using CCTP increased in weight average molecular weight with decreasing CTA concentration, but the number average molecular weight remained constant, suggesting backbiting was the cause, rather than branching [34].

In 2006, Kurmaz *et al.* reported the homopolymerisation of ethylene glycol dimethacrylate (EGDMA) and other di-vinyl monomers by CCTP [76], which was subsequently confirmed by Haddleton [77], McEwan and Smeets [78]. Haddleton *et al.* describe the homopolymerisation of EGDMA followed by the use of Michael addition to functionalise the polymer, confirming the significant degree of branching within these materials. Similarly, Smeets functionalised pEGDMA through reductive amination to form core-cross-linked, functionalised micelles.

More recently in 2012, work was conducted by Irvine *et al.* into the synthesis of styrenyl hyperbranched polymers through the application of CCTP to control polymerisations which use divinyl benzene (DVB) as the di-functional monomer [59]. This demonstrated that the synthesis of HB DVB “homopolymers” is possible in under one hour using high reaction temperatures (150°C) and autoinitiation, provided the high chain transfer coefficient of PhCoBF was exploited to delay gelation and the monomer conversion was limited to ~50%. It was also determined that the exact composition of the DVB mixture used affects the polymerisation rate greatly, due to the varying monomer reactivities.

1.8 Polymer Characterisation

1.8.1 Gel Permeation Chromatography (GPC)/ Size Exclusion Chromatography (SEC)

1.8.1.1 Molecular Weight Definitions

Molecular weight is one of a number of characteristics that are often used to describe polymers and to measure the efficiency of the polymerisation process. There are a number of molecular weight parameters used, the most common of those being weight average and number average molecular weight, the degree of polymerisation and the dispersity.

The weight average molecular weight, M_w , is an important parameter which is often used in industry as an indicator of the mechanical/processing properties of the polymer, particularly the polymer viscosity. M_w is expressed by Equation 1-5:

$$M_w = \frac{\sum M_i^2 N_i}{\sum M_i N_i} \quad (1-5)$$

where M_i is the molecular weight of the molecules and N_i is the number of molecules.

The number average molecular weight, M_n , is the average molecular weight of the individual macromolecules. It is expressed as shown in Equation 1-6:

$$M_n = \frac{\sum M_i N_i}{\sum N_i} \quad (1-6)$$

and indicates the average length of polymer chains.

The degree of polymerisation, DP, represents the average number of repeat units in the polymer chains, and can be calculated by dividing the M_n by the monomer's molecular mass, as shown in Equation 1-7.

$$DP = \frac{\text{Polymer } M_n}{\text{Monomer Molecular Mass}} \quad (1-7)$$

The dispersity, \mathfrak{D} , is a measure of the molecular weight distribution of a polymer: it is determined by dividing M_w by M_n , as shown in Equation 1-8:

$$\mathfrak{D} = \frac{M_w}{M_n} \quad (1-8)$$

A dispersity of 1.00 indicates that the polymer is monodisperse: all the polymer chains are equal in length, which is the best possible/ideal case.

In this work, the above metrics are all obtained using gel permeation chromatography (GPC), otherwise known as size exclusion chromatography (SEC).

1.8.1.2 GPC/SEC Overview

GPC is a widely used technique for the characterisation of polymer molecular weight (MW) distributions, which is achieved through the separation of polymers according to their hydrodynamic volumes.

This separation process occurs in the column(s) (the stationary phase), which are packed with, typically, crosslinked polystyrene/poly(divinyl benzene) porous beads: as a polymer solution (the mobile phase) flows through the column, macromers with smaller hydrodynamic volumes access many of the pores in the column. These macromers therefore take longer to pass through the column, resulting a longer retention time. Correspondingly, molecules with a larger hydrodynamic volume cannot access many of the pores and are, therefore, eluted more quickly, as is illustrated in Figure 1.16.

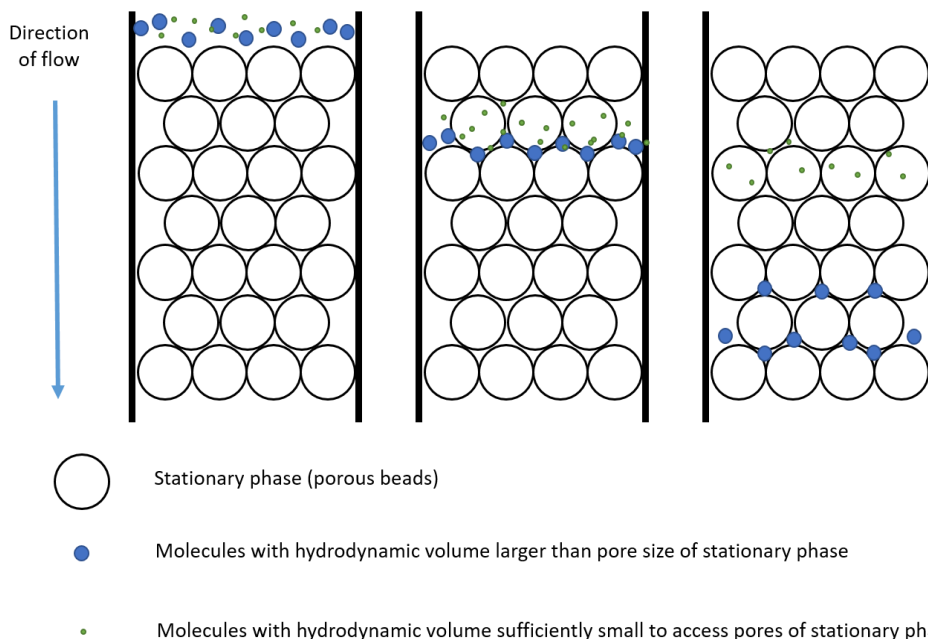


Figure 1.16. Diagram of the gel permeation chromatography mechanism.

For this work, the main detector used in the GPC was a differential refractive index (RI) detector: this method of detection relies on a comparison of the sample with polymer standards of known molecular weight, and the accuracy is dependent upon the standards and samples having the same relationship between their hydrodynamic volume and molecular weight. Here, polystyrene or poly(methyl methacrylate) standards, with \bar{D} close to 1.00 were used.

Conventional SEC is ideal for the analysis of materials with linear architectures which have minimal interaction with the stationary phase. However, substantial flaws are seen when analysing non-linear materials, where the relationship between MW and retention volume is less uniform. As the separation in SEC is not strictly dependent on MW but rather on the hydrodynamic volume of the polymer molecule, the calibration standards should be of the same architecture and composition as the sample, as both of these variables have a significant impact on the retention time. In this work, only linear standards could be obtained, hence the MW values obtained for hyperbranched polymers using SEC must be treated with caution and largely used for

comparison of similar polymers, rather than as absolute MW values. Fortunately, the \bar{D} values of HB polymers are characteristically large (>2), and so may be used as a proxy for evidence of hyperbranching.

1.8.2 Nuclear Magnetic Resonance (NMR)

NMR is a useful analytical technique for determining the content and purity of a sample, as well as the chemical structures of molecules. When a compound that contains a nucleus which possess spin, such as ^1H , ^{13}C , ^{19}F and ^{31}P , is placed in a magnetic field, the nucleus absorbs energy at a specific (radio) frequency (resonant frequency) and is promoted to a higher energy state: when the spin relaxes back to the ground state, energy of the same specific frequency is emitted. This emitted signal is detected and processed in order to yield a NMR spectrum for the compound.

The resonant frequency, energy of absorption and signal intensity are all proportional to the strength of the applied magnetic field, which would suggest that nuclei of the same type would resonate at the same frequency. However, the strength of the magnetic field that each NMR-active nucleus experiences is affected by the magnetic fields generated by the electrons around it, an effect known as shielding: generally, this shielding effect reduces the magnetic field experienced by the NMR-active nucleus. This causes a shift in the signal of each NMR-active nucleus which depends on the surrounding chemical environment, which is known as chemical shift. As a result, information about the nucleus' chemical environment can be derived from its resonant frequency.

Chemical shift is always quoted relative to reference molecule, for example tetramethylsilane (TMS) is often used as the proton reference frequency, and is given a shift of zero. If a nucleus is shielded by a higher electron density, it will be shifted

upfield (to a lower chemical shift): correspondingly, if a nucleus is less shielded by the surrounding electron density, it will be shifted downfield (to higher chemical shift). Thus, structural information about a molecule may be determined by understanding the effect of different chemical environments on the chemical shift value.

Extra structural information may be obtained from NMR signals due to an effect known as spin-spin coupling, or J coupling: if non-equivalent nuclei are separated by less than or equal to three bond lengths, the nuclei can exert an influence on each other, resulting in splitting of the NMR signal.

For polymers, NMR may also be used to determine the conversion of monomer to polymer, and in certain cases the degree of branching of the polymer.

1.8.3 Dielectric Materials, Properties and Analysis

1.8.3.1 Dielectric Materials

Dielectric materials are electrical insulators, due to their lack of free charge carriers which either possess randomly orientated dipole charges (polar dielectric materials), or dipole moments may be induced within them by the presence of an external electric field (non-polar dielectric materials) [79]–[81].

Non-polar materials are generally made of neutral diatomic molecules: in the absence of an electric field, the molecular charge distribution is equal across the molecule, however, when an external electric field is applied the charge distribution responds and moves, inducing a dipole in the material. In polar materials, the dipoles are permanent, but, in the absence of a field, are randomly orientated such that the overall material dipole is zero. Correspondingly, when an external field is applied, the dipoles rotate to align with the field, leading to a net dipole moment in the material [79]–[81].

1.8.3.2 Dielectric Properties

The dielectric properties of a material dictate how it will respond to an incident electromagnetic (EM) field. The complex permittivity, ϵ_c , is given by Equation 1-9 below:

$$\epsilon_c = (\epsilon' - j\epsilon'') \quad (1-9)$$

The complex permittivity is used when the material is considered as a dielectric (an insulator) with losses. The real part, ϵ' , is the dielectric constant, which is defined as the ratio of the permittivity of a medium (ϵ) to the permittivity of vacuum (ϵ_0), as shown in Equation 1-10 below:

$$\epsilon' = \frac{\epsilon}{\epsilon_0} \quad (1-10)$$

The permittivity, ϵ , is a measure of the electric polarizability of a dielectric material. A material with high permittivity, and thus a high dielectric constant, polarises more in response to an applied electric field than a material with low permittivity, thereby storing more energy in the material. Thus, the dielectric constant defines the extent to which a material will store energy via polarisation.

Meanwhile, the imaginary part, ϵ'' , known as the dielectric loss factor, is a measure of the loss of energy in a dielectric material through conduction, slow polarisation currents and other dissipative phenomena, and thus defines the material's ability to dissipate stored energy as heat. The peak value of the dielectric loss factor for a dielectric material with no direct-current conductivity occurs at the relaxation frequency, which is temperature related [79], [81], [82].

The loss tangent of a material relates the dielectric loss with the dielectric constant, and indicates the potential for a material to heat under the influence of an applied electric field. It is defined as shown in Equation 1-11:

$$\tan \delta = \varepsilon''/\varepsilon' \quad (1-11)$$

There is always a compromise between the values of ε' and ε'' : if a material has a high dielectric constant, it may not have a high dielectric loss. Water, for example, has a relatively high dielectric constant of 80.4 at 25 °C, but its $\tan \delta$ value is just 0.123 due to a low dielectric loss value. Conversely, ethanol's dielectric loss at 25 °C is much lower at 24.3, while the $\tan \delta$ value is 0.941, due to a higher dielectric loss [19], [83].

Frequency can have a large impact on the dielectric properties of a substance, as is illustrated in Figure 1.17, which shows the frequency dependence of water.

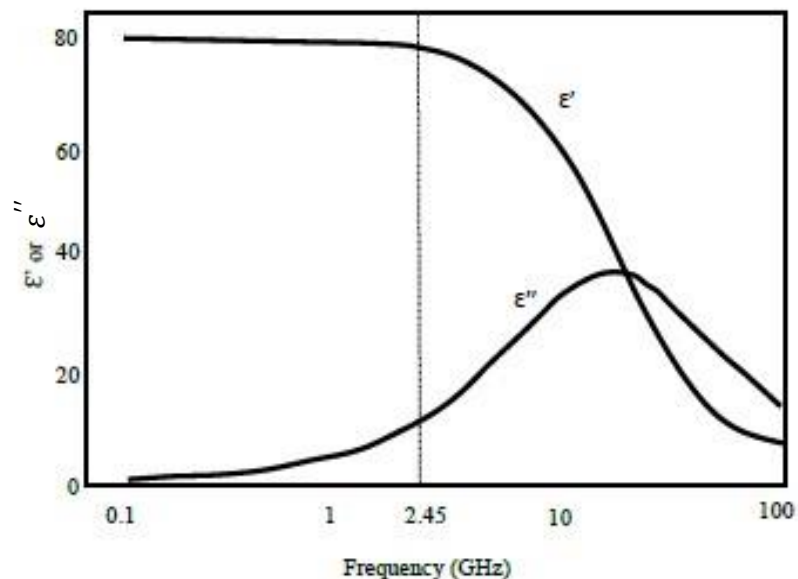


Figure 1.17. Dielectric properties of water with respect to frequency at 25 °C [83]

At low frequencies, the value of ε'' is low, indicating that no heating occurs, because the molecular dipoles are all aligned with the incident field. As the frequency increases, the value of ε'' also increases, reaching a peak at ~ 18 GHz (in the microwave region): this would be the optimum frequency to apply to the water in order to heat the sample, however, due to regulations to prevent interference, a specific frequency at 2.45 GHz must be used. Hence, the interaction is not as efficient as it could be.

The dielectric properties of a material are also temperature dependent: as the temperature increases, the molecules have more thermal energy, resulting in a greater amplitude of thermal motion. This means that the molecules are generally less closely aligned with each other, and that the orientational polarisation (and hence dielectric constant) is therefore reduced [83].

1.8.3.3 Dielectric Properties of Polymers

Polymers can be polar or non-polar depending on their chain geometries, which can significantly affect the dielectric properties. For example, PMMA, polyvinyl chloride (PVC), polyamide (PA) and polycarbonate (PC) are all polar polymers, while polytetrafluoroethylene (PTFE), polyethylene (PE), (polypropylene) PP and (polystyrene) PS are non-polar. When exposed to an alternating electric field, polar polymers require some time for the dipoles to align: at low frequencies, there is sufficient time for alignment to occur, while at high frequencies the dipoles cannot completely align before the field changes. Therefore, polar polymers generally have dielectric constants of between 3 and 9 at low frequencies and between 3 and 5 at high frequencies. For non-polar polymers, there is no dipole polarisation: instead, the applied electric field instead induces electronic polarisation, which is effectively instantaneous and results in these polymers having dielectric constants below 3 and no dependence on the frequency of the field oscillation [83].

1.8.3.4 Dielectric Property Measurements

The measurement of dielectric properties of materials has gained increasing importance, finding applications in material science, microwave circuit design, absorber development and biological research. It can provide useful electrical or magnetic characteristics of materials, and monitor changes in these characteristics in real time. For example, if an alternating, high frequency electric field is applied to a

chemical reaction mixture, the overall dielectric response measured will be a function of the dielectric properties of all the molecular species present and the interactions between them. It is, therefore, possible to follow the progress of a chemical reaction by monitoring the dielectric changes that occur, so long as they are altered by the reaction of interest [82].

1.8.3.5 Measurement Methods

There are numerous methods available for measuring the complex permittivity and permeability, with each limited to specific frequencies, materials and applications. The four most popular methods are: the transmission/reflection line method; open ended coaxial probe method; free space method and resonant (cavity) method.

The coaxial probe method is best for liquids and semi-solid materials, and is popular due to it being simple, convenient and non-destructive. In this method, the probe is pressed against/immersed in the specimen, and the reflection coefficient is measured and used to determine the permittivity. The reflection coefficient is defined as the ratio of the intensities of the reflected and incident waves. However, for small batch samples, the most accurate method of obtaining permittivity and permeability is the resonant cavity method. In this method, the dielectric properties (resonant frequency and quality factor ($1/\tan \delta$)) of an empty cavity are first measured, then compared to the properties measured in the presence of a sample, which allows the properties of the sample to be determined [84].

1.8.3.6 Dielectric Analysis of Polymers

Dielectric analysis can be used to monitor changes in viscosity and cure state of thermosetting resins, adhesives, paints, composites and other kinds of polymers or

organic substances by measuring variations in their dielectric properties. With dielectric analysis, it is possible to investigate the gel point, flow behaviour, reactivity, cure, glass transition temperature, aging, decomposition and diffusion behaviour/properties of polymers. For example, the response of a material to the application of an alternating electric field is a function of the dipole mobility. As a polymer cures, the viscosity of the sample increases and the mobility of the dipoles decreases. This causes a corresponding reduction in response signal from the sample as the level of cure increases. Thus, dielectric analysis is ideal for monitoring a curing process, or determining level of cure of a polymeric sample.

Traditionally, studies of polymerisations have used either off-line measurements of the dielectric properties [85]–[87], or specialised detectors which are often unsuitable for polymerisations due to their micrometre-sized gaps [88]–[90], which are easily blocked as the reaction viscosity increases. However, in 2014, Kamaruddin *et. al.* [79] used a coaxial probe technique to accurately follow the progress of a ring-opening polymerisation (ROP): over a broad range of temperatures and viscosities, the system clearly identified the onset of polymerisation, induction periods and end-points of the polymerisations. This allowed the reaction to be conducted for the ideal time period, thus allowing the reaction throughput, the energy efficiency and the product end quality to be maximised. Additionally, by relating the in-situ measurements to a calibration curve, it was shown that reaction rates achieved experimentally could be determined.

1.9 Overview of this Thesis

The research presented in this thesis focuses on three different topics of work, which all stem from a novel synthesis method for hyperbranched polymers: the

development and characterisation of new polymers for use as engine oil lubricant additives; investigating interesting new biologically active polymers and overcoming issues with their scale-up; and investigating the control of new monomer combinations for a wide variety of applications.

In the first section of work, chain transfer polymerisation (CTP) of a film-forming monomer with both macromeric and thiolic control agents has been implemented. The aim was to produce hyperbranched (HB) polymers which were soluble in the solvent of choice (engine oil) and which formed protective films on engine surfaces, while also proving the industrial viability of the methodology chosen. To accomplish this, the control agent had to be carefully selected and the level of incorporation of the control agent into the HB polymer optimised. Also, in collaboration with BP/Castrol, the resulting HB polymers were to undergo extensive tribological testing, to determine their suitability as engine oil additives. In addition, the polymers were synthesised at scale, and their performance compared with those produced at smaller scales. Finally, new characterisation methods were investigated, to help fast-track future copolymer formulations and monitor batch-to-batch repeatability at scale. This work has the potential to produce industrially viable additives, which result in reduced engine wear and thus improved lifetimes and efficiencies.

The next area of research focused on investigating the bio-applications of various monomers and monomer combinations which had been previously identified as bio-active *via* screening processes. The aim was to optimise and scale the synthesis of the hyperbranched polymers for use as anti-bacterial-attachment and pro-stem-cell-attachment coatings. To achieve this, various polymer control methods were employed on the di-functional monomer, tricyclodecanedimethanol diacrylate

(TCDMDA), to optimally functionalise the polymer for each application. These functionalised hyperbranched polymers were tested for biological activity and, in one case, investigated as a feedstock for additive manufacturing processes. This work will enable functionalised HB TCDMDA polymers and copolymers to be reliably and easily synthesised for various future applications.

Finally, the development of alternative functionalised copolymers for use in engine oils or metal working fluids *via* macromer controlled chain transfer polymerisation was conducted. The aim was to develop cleaner-burning and/or anti-fouling lubricant additives for future testing at BP/Castrol, and to further demonstrate the flexibility of the macromer and thiol control methods. This was achieved by using monomers which contained an increased oxygen content or the previously identified anti-fouling monomer, TCDMDA. This work was conducted in order to help reduce the economic and environmental impact of both engine oil burning and water-based filtration systems.

1.10 Reference

- [1] H. Staudinger, "Über Polymerisation," *Berichte der Dtsch. Chem. Gesellschaft (A B Ser.)*, vol. 53, no. 6, pp. 1073–1085, Jun. 1920.
- [2] American Chemical Society, "The Establishment of Modern Polymer Science By Wallace H. Carothers," *An Int. Hist. Chem. Landmark*, pp. 1–4, 2000.
- [3] P. J. Flory, "Effects of Cross-Linking and Branching on the Molecular Constitution of Diene Polymers," *Rubber Chem. Technol.*, vol. 21, no. 2, pp. 461–470, 1948.
- [4] E. Buhleier, W. Wehner, and F. Vogtle, "'Cascade'- and 'Nonskid-Chain-like'

- Syntheses of Molecular Cavity Topologies," *Synthesis (Stuttg.)*, vol. 2, pp. 155–158, 1978.
- [5] D. A. Tomalia *et al.*, "A New Class of Polymers: Starburst-Dendritic Macromolecules," *Polym. J.*, vol. 17, no. 1, pp. 117–132, 1985.
- [6] G. R. Newkome, Z. Yao, G. R. Baker, and V. K. Gupta, "Cascade Molecules: A New Approach to Micelles. A [27]-Arborol," *J. Org. Chem.*, no. 3, pp. 2003–2004, 1985.
- [7] C. C. Lee, J. A. Mackay, J. M. J. Fréchet, and F. C. Szoka, "Designing dendrimers for biological applications," *Nat. Biotechnol.*, vol. 23, no. 12, 2005.
- [8] R. M. Crooks, M. Zhao, L. Sun, V. Chechik, and L. K. Yeung, "Dendrimer-Encapsulated Metal Nanoparticles: Synthesis, Characterization, and Applications to Catalysis," *Acc. Chem. Res.*, vol. 34, no. 3, pp. 181–190, Mar. 2001.
- [9] A. W. Freeman, S. C. Koene, P. R. L. Malenfant, M. E. Thompson, and J. M. J. Fréchet, "Dendrimer-containing light-emitting diodes: Toward site-isolation of chromophores," *J. Am. Chem. Soc.*, vol. 122, no. 49, pp. 12385–12386, 2000.
- [10] H. R. Ihre, O. L. Padilla De Jesus, F. C. Szoka Jr., and J. M. Fréchet, "Polyester dendritic systems for drug delivery applications: design, synthesis, and characterization," *Bioconjug Chem.*, vol. 13, no. 3, pp. 443–452, 2002.
- [11] K. Inoue, "Functional dendrimers, hyperbranched and star polymers," *Prog. Polym. Sci.*, vol. 25, no. 4, pp. 453–571, 2000.

- [12] C. Gao, D. Yan, and H. Frey, "Promising Dendritic Materials: An Introduction to Hyperbranched Polymers," 2004.
- [13] C. Gao and D. Yan, "Hyperbranched polymers: from synthesis to applications," *Prog. Polym. Sci.*, vol. 29, no. 3, pp. 183–275, 2004.
- [14] K. Nishimori and M. Ouchi, "AB-alternating copolymers via chain-growth polymerization: synthesis, characterization, self-assembly, and functions," *Chem. Commun.*, vol. 56, pp. 3473–3483, Feb. 2020.
- [15] M. P. Stevens, *Polymer Chemistry: An Introduction*, Third. Oxford: Oxford University Press, 1999.
- [16] M. W. Lee, M. Soroush, M. C. Grady, S. Srinivasan, and A. M. Rappe, "Self-Initiation Mechanism in Spontaneous Thermal Polymerization of Ethyl and n-Butyl Acrylate: A Theoretical Study," vol. 114, no. 30, pp. 7975–7983, 2010.
- [17] J. Kolomanska *et al.*, "Design, synthesis and thermal behaviour of a series of well-defined clickable and triggerable sulfonate polymers," *Rsc Adv.*, vol. 5, no. 82, pp. 66554–66562, 2015.
- [18] F. R. Mayo, "The dimerization of styrene," *J. Am. Chem. Soc.*, vol. 90, no. 5, pp. 1289–1295, 1968.
- [19] K. Adlington, "Microwave Assisted Controlled Polymerisation and Catalysis," University of Nottingham, 2014.
- [20] C. McKee and G. R. Chaudhry, "Advances and challenges in stem cell culture," *Colloids Surfaces B Biointerfaces*, vol. 159, pp. 62–77, 2017.
- [21] F. R. Mayo, "Chain Transfer in the Polymerization of Styrene: The Reaction of Solvents with Free Radicals¹," *J. Am. Chem. Soc.*, vol. 65, no. 12, pp. 2324–

- 2329, Dec. 1943.
- [22] L. Jiang *et al.*, "Radical Polymerization in the Presence of Chain Transfer Monomer: An Approach to Branched Vinyl Polymers," *Macromolecules*, vol. 45, no. 10, pp. 4092–4100, May 2012.
- [23] J. L. O'Brien and F. Gornick, "Chain Transfer in the Polymerization of Methyl Methacrylate. I. Transfer with Monomer and Thiols. The Mechanism of the Termination Reaction at 60°1," *J. Am. Chem. Soc.*, vol. 77, no. 18, pp. 4757–4763, Sep. 1955.
- [24] O. Nuyken, "The Chemistry of Free Radical Polymerization. Von G. Moad und D. H. Solomon. Pergamon-Elsevier Science Ltd., Oxford, 1995. 408 S., geb. 75.00 £.—ISBN 0-08-42078-8," *Angew. Chemie*, vol. 109, no. 10, pp. 1173–1175, 1997.
- [25] C. Henríquez, C. Bueno, E. A. Lissi, and M. V. Encinas, "Thiols as chain transfer agents in free radical polymerization in aqueous solution," *Polymer (Guildf)*., vol. 44, no. 19, pp. 5559–5561, 2003.
- [26] A. A. Gridnev and S. D. Ittel, "Catalytic chain transfer in free-radical polymerizations.," *Chem. Rev.*, vol. 101, no. 12, pp. 3611–60, Dec. 2001.
- [27] D. M. Haddleton, D. R. Maloney, and K. G. Suddaby, "Catalytic chain transfer polymerisation (CCTP) of methyl methacrylate: Effect of catalyst structure and reaction conditions on chain transfer coefficient.," *Macromol. Symp.*, vol. 111, pp. 37–46, 1996.
- [28] K. G. Suddaby, D. R. Maloney, and D. M. Haddleton, "Homopolymerizations of methyl methacrylate and styrene: Chain transfer constants from the Mayo

- equation and number distributions for catalytic chain transfer, and the chain length dependence of the average termination rate coefficient," *Macromolecules*, vol. 30, no. 96, pp. 702–713, 1997.
- [29] A. Green, J. P. A. Heuts, B. G. E. Roberts, and J. D. Biasutti, "Catalytic Chain Transfer Polymerization: an Overview," *Aust. J. Chem.*, vol. 55, pp. 381–398, 2002.
- [30] J. P. A. Heuts and N. M. B. Smeets, "Catalytic chain transfer and its derived macromonomers," *Polym. Chem.*, vol. 2, no. 11, p. 2407, 2011.
- [31] A. Gridnev, "The 25th Anniversary of Catalytic Chain Transfer," *J. Polym. Sci. Part A Polym. Chem.*, vol. 38, pp. 1753–1766, 2000.
- [32] A. Anastasaki *et al.*, "Polymerization of long chain [meth]acrylates by Cu(0)-mediated and catalytic chain transfer polymerisation (CCTP): high fidelity end group incorporation and modification," *Polym. Chem.*, vol. 4, no. 15, pp. 4113–4119, 2013.
- [33] D. M. Haddleton *et al.*, "Radical-addition-fragmentation and copolymerization of methyl methacrylate macromonomers from catalytic chain transfer polymerization (CCTP)," *Polymer (Guildf.)*, vol. 38, no. 25, pp. 6207–6217, 1997.
- [34] P. . Costello, I. . Martin, A. . Slark, D. . Sherrington, and A. Titterton, "Branched methacrylate copolymers from multifunctional monomers: chemical composition and physical architecture distributions," *Polymer (Guildf.)*, vol. 43, no. 2, pp. 245–254, 2002.
- [35] Z. Guan, "Control of Polymer Topology through Metal Catalysis: Synthesis of

- Hyperbranched Polymers by Cobalt-Mediated Free Radical Polymerization,” *J. Am. Chem. Soc.*, vol. 124, no. 20, pp. 5616–5617, 2002.
- [36] K. Adlington, D. J. Irvine, I. Barker, and L. Stevens, “Accelerated Synthesis of Hyperbranched Divinylbenzene Polymers via Catalytic Chain Transfer Polymerisation and their Use as Gas Capture Agents - Manuscript in preparation,” Nottingham, 2017.
- [37] D. M. Haddleton, D. R. Maloney, and K. G. Suddaby, “Competition between β -Scission of Macromonomer-Ended Radicals and Chain Transfer to Cobalt(II) in Catalytic Chain Transfer Polymerization (CCTP),” *Macromolecules*, vol. 29, no. 1, pp. 481–483, Jan. 1996.
- [38] J. P. a. Heuts and N. M. B. Smeets, “Catalytic chain transfer and its derived macromonomers,” *Polym. Chem.*, vol. 2, p. 2407, 2011.
- [39] J. P. A. Heuts, G. E. Roberts, and J. D. Biasutti, “Catalytic Chain Transfer Polymerization: an Overview Review,” *Australian J. Chem.*, vol. 55, pp. 381–398, 2002.
- [40] D. M. Haddleton *et al.*, “(CCTP) in Water and Water / Alcohol Solution,” *Polym. Sci. Part A Polym. Chem.*, vol. 39, no. 14, pp. 2378–2384, 2001.
- [41] A. Gridnev, “25Th Anniversary of Catalytic Chain Transfer,” *J. Polym. Sci. Part A Polym. Chem.*, vol. 38, no. 10, pp. 1753–1766, 2000.
- [42] Y. H. Kim, “Hyperbranched polyarylene,” 4,857,630, 1989.
- [43] C. Gao and D. Yan, “Hyperbranched polymers: From synthesis to applications,” *Prog. Polym. Sci.*, 2004.
- [44] R. H. Kienle and A. G. Hovey, “The Polyhydric Alcohol-Polybasic Acid Reaction.

11. Ethylene Glycol-Phthalic Anhydride," *J. Am. Chem. Soc.*, vol. 51, no. 509, 1929.
- [45] E. M. Pearce, "Principles of polymerization (third edition), by George Odian, Wiley-Interscience, New York, 1991, 768 pp. price: \$59.95," *J. Polym. Sci. Part A Polym. Chem.*, vol. 30, no. 7, p. 1508, 1992.
- [46] R. H. Kienle, P. A. van der. Meulen, and F. E. Petke, "The Polyhydric Alcohol-Polybasic Acid Reaction. IV. Glyceryl Phthalate from Phthalic Acid," *J. Am. Chem. Soc.*, vol. 61, no. 9, pp. 2268–2271, Sep. 1939.
- [47] P. J. Flory, "Molecular Size Distribution in Three Dimensional Polymers. I. Gelation," *J. Am. Chem. Soc.*, vol. 63, no. 11, pp. 3083–3090, 1941.
- [48] P. J. Flory, *Principles of Polymer Chemistry*, 1st ed. New York: Cornell University Press, 1952.
- [49] H. R. Kricheldorf, O. Bolender, and T. Wollheim, "New Polymer Synthesis 99. Hyperbranched Poly(Ester-Imide)s Derived from 4,5-Dichlorophthalic Acid," *High Perform. Polym.*, vol. 10, no. 3, pp. 217–229, Sep. 1998.
- [50] C. J. Hawker, R. Lee, and J. M. J. Frechet, "One-step synthesis of hyperbranched dendritic polyesters," *J. Am. Chem. Soc.*, vol. 113, no. 12, pp. 4583–4588, Jun. 1991.
- [51] P. J. Flory, "Thermodynamics of High Polymer Solutions," *J. Chem. Phys.*, vol. 10, 1942.
- [52] K.-M. Kim, M. Jikei, and M. Kakimoto, "Preparation and Properties of Novel Hyperbranched Poly(dimethylsiloxane)s," *Polym. J.*, vol. 34, no. 4, pp. 275–279, 2002.

- [53] B. Voit, "New developments in hyperbranched polymers," *J. Polym. Sci. Part A Polym. Chem.*, vol. 38, no. 14, pp. 2505–2525, 2000.
- [54] W. Tian, X. Li, and J. Wang, "Supramolecular hyperbranched polymers," *Chem. Commun.*, vol. 53, no. 17, pp. 2531–2542, 2017.
- [55] A. Mashhadi Malekzadeh, A. Ramazani, S. J. Tabatabaei Rezaei, and H. Niknejad, "Design and construction of multifunctional hyperbranched polymers coated magnetite nanoparticles for both targeting magnetic resonance imaging and cancer therapy," *J. Colloid Interface Sci.*, vol. 490, pp. 64–73, 2017.
- [56] L. Zhao *et al.*, "Novel hyperbranched polymers as host materials for green thermally activated delayed fluorescence OLEDs," *Chinese J. Polym. Sci.*, vol. 35, no. 4, pp. 490–502, 2017.
- [57] W. Daniel, S. E. Stiriba, and F. Holger, "Hyperbranched polyglycerols: From the controlled synthesis of biocompatible polyether polyols to multipurpose applications," *Acc. Chem. Res.*, vol. 43, no. 1, pp. 129–141, 2010.
- [58] M. Jikei and M. Kakimoto, "Hyperbranched polymers: a promising new class of materials," *Prog. Polym. Sci.*, vol. 26, no. 8, pp. 1233–1285, 2001.
- [59] I. A. Barker *et al.*, "Catalytic Chain Transfer Mediated Autopolymerization of Divinylbenzene: Toward Facile Synthesis of High Alkene Functional Group Density Hyperbranched Materials," *Macromolecules*, vol. 45, no. 23, pp. 9258–9266, Dec. 2012.
- [60] H. Komber, A. Ziemer, and B. Voit, "Etherification as Side Reaction in the Hyperbranched Polycondensation of 2,2-Bis(hydroxymethyl)propionic Acid,"

- Macromolecules*, vol. 35, no. 9, pp. 3514–3519, 2002.
- [61] A. Carlmark, E. Malmström, and M. Malkoch, “Dendritic architectures based on bis-MPA: functional polymeric scaffolds for application-driven research.,” *Chem. Soc. Rev.*, vol. 42, no. 13, pp. 5858–5879, 2013.
- [62] A. Hult, E. Malmstrom, M. Johansson, and K. Sorensen, “DENDRITIC MACROMOLECULE AND PROCESS FOR PREPARATION THEREOF,” 5,418,301, 1995.
- [63] M. Johansson, E. Malmström, and A. Hult, “Synthesis, characterization, and curing of hyperbranched allyl ether–maleate functional ester resins,” *J. Polym. Sci. Part A Polym. Chem.*, vol. 31, no. 3, pp. 619–624, 1993.
- [64] J. M. J. Frechet, M. Henmi, I. Gitsov, S. Aoshima, M. R. Leduc, and R. B. Grubbs, “Self-Condensing Vinyl Polymerization - an Approach to Dendritic Materials,” *Science (80-.)*, vol. 269, no. 5227, pp. 1080–1083, 1995.
- [65] G. Hild and R. Okasha, “Kinetic investigation of the free radical crosslinking copolymerization in the pre-gel state, 1. Styrene/m- and p-divinylbenzene systems,” *Die Makromol. Chemie*, vol. 186, no. 1, pp. 93–110, Jan. 1985.
- [66] D. T. Landin and C. W. Macosko, “Cyclization and Reduced Reactivity of Pendant Vinyls during the Copolymerization of Methyl Methacrylate and Ethylene Glycol Dimethacrylate,” *Macromolecules*, vol. 21, no. 34, p. 1404, Dec. 1988.
- [67] N. O’Brien, A. McKee, D. C. Sherrington, A. T. Slark, and A. Titterton, “Facile, versatile and cost effective route to branched vinyl polymers,” *Polymer (Guildf)*, vol. 41, no. 15, pp. 6027–6031, 2000.

- [68] R. Baudry and D. C. Sherrington, "Synthesis of Highly Branched Poly(methyl methacrylate)s Using the 'Strathclyde Methodology' in Aqueous Emulsion," *Macromolecules*, vol. 39, no. 4, pp. 1455–1460, 2006.
- [69] F. Oise Isaure, P. A. G. Cormack, D. C. Sherrington, F. Isaure, P. A. G. Cormack, and D. C. Sherrington, "Synthesis of Branched Poly(methyl methacrylate)s: Effect of the Branching Comonomer Structure," *Macromolecules*, vol. 37, no. 6, pp. 2096–2105, Mar. 2004.
- [70] A. T. Slark, D. C. Sherrington, A. Titterton, and I. K. Martin, "Branched methacrylate copolymers from multifunctional comonomers: the effect of multifunctional monomer functionality on polymer architecture and properties," *J. Mater. Chem.*, vol. 13, no. 11, pp. 2711–2720, 2003.
- [71] F. Isaure, P. A. G. Cormack, S. Graham, D. C. Sherrington, S. P. Armes, and V. Bütün, "Synthesis of branched poly(methyl methacrylate)s via controlled/living polymerisations exploiting ethylene glycol dimethacrylate as branching agent," *Chem. Commun.*, no. 9, pp. 1138–1139, 2004.
- [72] S. R. Lowe, "Branched Polymers via CCTP with Vinyl end Groups and their Application in Wound Care Materials," University of Warwick, 2017.
- [73] J.-C. Lin and K. J. Abbey, "Lin, J. C.; Abbey, K. J. US4680354, 1987.," 4,680,354, 14-Jul-1987.
- [74] K. J. Abbey, "LINEAR ADDITION POLYESTER COPOLYMERS," 4,608,423, 26-Aug-1986.
- [75] Z. Guan, "Synthesis of multi-functional hyperbranched polymers by polymerization of di-or tri-vinyl monomers in the presence of a chain transfer

- catalyst," 5,767,211, 1998.
- [76] S. V. Kurmaz and E. O. Perepelitsina, "Cross-linking radical polymerization of di(meth)acrylates in the presence of cobalt(II) porphyrin," *Russ. Chem. Bull.*, vol. 55, no. 5, pp. 835–844, May 2006.
- [77] K. A. McEwan and D. M. Haddleton, "Combining catalytic chain transfer polymerisation (CCTP) and thio-Michael addition: enabling the synthesis of peripherally functionalised branched polymers," *Polym. Chem.*, vol. 2, no. 9, p. 1992, Sep. 2011.
- [78] D. J. Krasznai, T. F. L. McKenna, M. F. Cunningham, P. Champagne, and N. M. B. Smeets, "Polysaccharide-stabilized core cross-linked polymer micelle analogues," *Polym. Chem.*, vol. 3, no. 4, pp. 992–1001, Apr. 2012.
- [79] M. J. Kamaruddin *et al.*, "Continuous and direct 'in situ' reaction monitoring of chemical reactions via dielectric property measurement: controlled polymerisation," *RSC Adv.*, vol. 4, pp. 5709–5717, 2014.
- [80] C. Oliver Kappe, "Microwave dielectric heating in synthetic organic chemistry.," *Chem. Soc. Rev.*, vol. 37, no. 6, pp. 1127–1139, 2008.
- [81] Hyperphysics, "Dielectrics." [Online]. Available: <http://hyperphysics.phy-astr.gsu.edu/hbase/electric/dielec.html>. [Accessed: 01-Jun-2018].
- [82] M. J. Kamaruddin *et al.*, "Continuous direct on-line reaction monitoring of a controlled polymerisation via dielectric measurement," *Green Chem.*, vol. 13, pp. 1147–1151, 2011.
- [83] G. H. Haggis, J. B. Hasted, and T. J. Buchanan, "The dielectric properties of water in solutions," *J. Chem. Phys.*, vol. 20, no. 9, pp. 1452–1465, 1952.

- [84] Rhode & Shwarz, "Measurement of Dielectric Material Properties," Singapore, Jan. 2008.
- [85] C. C., R. P. A., and T. E., "Measurement method and apparatus for monitoring the kinetics of polymerization and crosslinking reactions by microwave dielectrometry," *J. Appl. Polym. Sci.*, vol. 41, no. 3-4, pp. 805–818, Jun. 1990.
- [86] C. Carlo, M. Massimo, R. P. Angelo, and T. Elpidio, "Kinetic analysis of photoinitiated polymerization by microwave dielectrometry," *J. Polym. Sci. Polym. Lett. Ed.*, vol. 23, no. 1, pp. 5–9, Jun. 2018.
- [87] C. Carlo, C. Francesco, R. Pierangelo, and T. Elpidio, "Kinetic analysis of photoinitiated polymerization of n-butyl acrylate up to high conversion by microwave dielectrometry," *J. Polym. Sci. Part B Polym. Phys.*, vol. 27, no. 1, pp. 189–197, Jun. 2018.
- [88] D. E. Kranbuehl, "Continuous dielectric measurement of polymerizing systems," *J. Non. Cryst. Solids*, vol. 131–133, pp. 930–934, Jun. 1991.
- [89] A. Cherfi *et al.*, "Application of dielectric analysis to the measurement of conversion during batch solution copolymerizations," *Chem. Eng. Process. Process Intensif.*, vol. 42, no. 2, pp. 121–128, Feb. 2003.
- [90] C. T. J. and C. K. Yong, "In-line dielectric monitoring of monomer conversion in a batch polymerization reactor," *J. Appl. Polym. Sci.*, vol. 55, no. 9, pp. 1361–1365, Jun. 2018.
- [91] A. D. Smith *et al.*, "Dielectric properties of free-radical polymerizations: Molecularly symmetrical initiators during thermal decomposition," *Ind. Eng. Chem. Res.*, vol. 49, no. 4, pp. 1703–1710, 2010.

- [92] Z. Zhou *et al.*, "High-throughput characterization of fluid properties to predict droplet ejection for three-dimensional inkjet printing formulations," *Addit. Manuf.*, vol. 29, p. 100792, Oct. 2019.
- [93] A. Miller, "The chemistry of lubricating-oil additives," *Armour Res. Found.*, 1930.
- [94] L. R. Rudnick, *Lubricant Additives: Chemistry and Applications*, 1st ed. CRC Press, 2003.
- [95] A T C, "Lubricant Additives: Use and Benefits," no. August, 2016.
- [96] "What are Friction Modifiers?" [Online]. Available: <https://www.machinerylubrication.com/Read/28815/what-are-friction-modifiers>. [Accessed: 24-Nov-2020].
- [97] R. M. Mortier and S. T. Orszulik, *Chemistry and Technology of Lubricants*. Springer US, 1994.
- [98] W. O. Winer, "Molybdenum disulfide as a lubricant: A review of the fundamental knowledge," *Wear*, vol. 10, no. 6, pp. 422–452, Nov. 1967.
- [99] L. Cizaire *et al.*, "Mechanisms of ultra-low friction by hollow inorganic fullerene-like MoS₂ nanoparticles," *Surf. Coatings Technol.*, vol. 160, no. 2–3, pp. 282–287, 2002.
- [100] Z. Tang and S. Li, "A review of recent developments of friction modifiers for liquid lubricants (2007–present)," *Curr. Opin. Solid State Mater. Sci.*, vol. 18, no. 3, pp. 119–139, 2014.
- [101] T. Cserhati, E. Forgacs, and G. Oros, "Biological activity and environmental impact of anionic surfactants," *J. Memb. Sci.*, vol. 228, no. 1, pp. 337–348,

2002.

- [102] Afton Chemical, "Viscosity Index Improvers & Thickeners | Afton Chemical." [Online]. Available: https://www.aftonchemical.com/SBU/Lubricant-Components/ThickenersViscosityIndexImprovers?__cf_chl_jschl_tk__=aa89700020d37c8f62521805968307f3ad62ebc7-1606211884-0-ARQrpKiLTanC1jEhNVskxsDHI1dqKDy5SrBtsyBFRLS10aYHn5fVqVeWo05-JtNDIpvufcVt9-dDgy3az8BFRPJ5Oclsrj63NbXU4vUeeujD5mBx8BVVtsTIGBboTntGjrqvfuE9MAUFQb6sMwF6UwvoEdHWh_Rrr-ltHqPDuQ0OR_LFcxawSolnEEYOpeHidDzqYgP2rtOL5dk5-OfopZa3VpRgajhGLrfeHONhIKrd4Z7E-9UocZAT-HHEO_IXcsd5ufV72z8y4VZSJYU0ceS0liPdv4bZ8bzKc1aBa1M1FnsfGBfRQZxXMz_JvPfZMEv_RrWGoVrocJ4jDDy19E5ryGmwemrgBgDR2wzmMAfdvU-78zSsKAuftgJM9wBbv3bd-sXXYpsgt0w5WXvzXbB5MOlmgfYPG7kTo4FghBpEOD0QtzkoMSgUI09ybKGcw. [Accessed: 24-Nov-2020].
- [103] J. W. Robinson *et al.*, "Probing the molecular design of hyper-branched aryl polyesters towards lubricant applications," *Sci. Rep.*, vol. 6, no. June 2015, pp. 1–10, 2016.
- [104] F. Wiesbrock, R. Hoogenboom, and U. S. Schubert, "Microwave-assisted polymer synthesis: State-of-the-art and future perspectives," *Macromol. Rapid Commun.*, vol. 25, no. 20, pp. 1739–1764, 2004.
- [105] C. J. Hawker, F. K. Chu, P. J. Pomery, and D. J. T. Hill, "Hyperbranched poly(ethylene glycol)s: A new class of ion-conducting materials,"

- Macromolecules*, vol. 29, no. 11, pp. 3831–3838, 1996.
- [106] T. J. Mdkern and N. C. B. Tan, “Polystyrene / Hyperbranched Polyester Blends and Reactive Polystyrene / Hyperbranched Polyester Blends,” no. January, 1999.
- [107] C. M. Nunez, B. Sen Chiou, A. L. Andraday, and S. A. Khan, “Solution rheology of hyperbranched polyesters and their blends with linear polymers,” *Macromolecules*, vol. 33, no. 5, pp. 1720–1726, 2000.
- [108] S. Uppuluri, S. E. Keinath, D. A. Tomalia, and P. R. Dvornic, “Rheology of dendrimers. I. Newtonian flow behavior of medium and highly concentrated solutions of polyamidoamine (PAMAM) dendrimers in ethylenediamine (EDA) solvent,” *Macromolecules*, vol. 31, no. 14, pp. 4498–4510, 1998.
- [109] J. Liebig, “Justus Liebig’s Annalen der Chemie.,” *Annalen der Chemie*. Meyerschen Hof-Buchh. und der Winterschen Universitäts-Buchh] ; C.F. Winter’sche ; Verlag Chemie, [Lemgo, Germany : Leipzig : Berlin, p. v., 1832.
- [110] S. chimique de France, *Bulletin*. 1866.
- [111] H. Staudinger, “Hermann Staudinger and the Foundation of Polymer Science,” *Am. Chem. Soc. Natl. Hist. Chem. Landmarks*, 1999.
- [112] A. Vazaios, D. J. Lohse, and N. Hadjichristidis, “Linear and star block copolymers of styrenic macromonomers by anionic polymerization,” *Macromolecules*, vol. 38, no. 13, pp. 5468–5474, 2005.
- [113] A. Nabifar, N. T. Mcmanus, E. Vivaldo-Lima, and A. Penlidis, “Kinetic Aspects of Styrene Polymerization with an Acyloxyamine,” *J. Macromol. Sci. Part A*, vol. 47, no. 6, pp. 496–502, Apr. 2010.

- [114] Z. Ahmad, "Polymer Dielectric Materials," in *Dielectric Material*, InTech, 2012.
- [115] C. A. Migdal, S. M. Shirodkar, T. F. DeRossa, and E. F. Miller, "FRCTION MODIFERADIOTEVE AND LUBRICATING OL COMPOSITION CONTAINING SAME," 5,066,412, 1991.
- [116] C. K. Esche, Jr., M. T. Devlin, and T.-C. Jao, "ADDITIVES AND LUBRICANT FORMULATIONS FOR PROVIDING FRCTION MODIFICATION," US 7,709,423 B2, 2010.
- [117] R. He and S. Zhang, "The friction and wear properties of divinylbenzene-grafted UHMWPE fiber-filled serpentine/PTFE composite," *Compos. Interfaces*, vol. 19, pp. 377–383, Aug. 2012.
- [118] B. Z. Poliquit, P. L. Burn, and P. E. Shaw, "Properties of PDMS-divinylbenzene based pre-concentrators for nitroaromatic vapors," *J. Mater. Chem. C*, 2020.
- [119] F. K. L. Huang, C.-J. Yoo, C. Okonkwo, D.-J. Tao, C. W. Jones, and S. Dai, "Facilely Synthesized Meso-Macroporous Polymer as Support of Poly(ethyleneimine) for Highly Efficient and Selective Capture of {CO₂}," *Chem. Eng. J.*, vol. 314, p. , 2016.
- [120] The Dow Chemical Company, "DVB - Cross-link a variety of materials for improved thermal, physical, and chemical properties," 2003.
- [121] INEOS Oligomers, "Durasyn 164 Polyalphaolefin." [Online]. Available: <https://www.ineos.com/show-document/?grade=Durasyn+164&bu=INEOS+Oligomers&documentType=Technical+Data+Sheet&docLanguage=EN&version=1d9e9f29efdefed072cf18e3c32114ec>. [Accessed: 24-Jun-2019].

- [122] L. Zou *et al.*, "Synthesis and photophysical properties of hyperbranched polyfluorenes containing 2,4,6-tris(thiophen-2-yl)-1,3,5-triazine as the core," *Phys. Chem. Chem. Phys.*, vol. 13, no. 19, pp. 8838–8846, 2011.
- [123] Y. Zheng, S. Li, Z. Weng, and C. Gao, "Hyperbranched polymers: advances from synthesis to applications," *Chem. Soc. Rev.*, vol. 44, no. 12, pp. 4091–4130, 2015.
- [124] M. Gaborieau and P. Castignolles, "Size-exclusion chromatography (SEC) of branched polymers and polysaccharides."
- [125] B. J. Hamrock and D. Dowson, "Isothermal Elastohydrodynamic Lubrication of Point Contacts: Part III—Fully Flooded Results," *J. Lubr. Technol.*, vol. 99, no. 2, pp. 264–275, 1977.
- [126] N. Marx, J. Guegan, and H. A. Spikes, "Elastohydrodynamic film thickness of soft EHL contacts using optical interferometry," *Tribol. Int.*, vol. 99, pp. 267–277, 2016.
- [127] S. Nambiar and D. J. Irvine, "Dielectric Characterization of Hyperbranched Polymers," University of Nottingham, 2016.
- [128] S. Goodwin *et al.*, "Novel, Low Viscosity Hyperbranched Lubricant Additives via Catalytic Chain Transfer Mediated Copolymerisation of Divinylbenzene and Lauryl Methacrylate," 2018.
- [129] L. Pasteur, "Scientific Papers," *The Harvard Classics*, vol. 38. P.F Collier & Son 1909-14: Bartelby.com, 2001, New York.
- [130] Encyclopedia.com: FREE online dictionary, "Plankton and Planktonic Bacteria - Dictionary definition of Plankton and Planktonic Bacteria." [Online].

Available: <http://www.encyclopedia.com/science/encyclopedias-almanacs-transcripts-and-maps/plankton-and-planktonic-bacteria>. [Accessed: 24-Apr-2017].

- [131] R. M. Donlan, "Biofilms: Microbial life on surfaces," *Emerg. Infect. Dis.*, vol. 8, no. 9, pp. 881–890, 2002.
- [132] J. W. Costerton, Z. Lewandowski, D. E. Caldwell, D. R. Korber, and H. M. Lappin-Scott, "Microbial Biofilms," *Annu. Rev. Microbiol.*, vol. 49, pp. 711–745, 1995.
- [133] T. B. Rasmussen and M. Givskov, "Quorum-sensing inhibitors as anti-pathogenic drugs," *Int. J. Med. Microbiol.*, vol. 296, pp. 149–161, 2006.
- [134] C. Cattò and F. Cappitelli, "Molecular Sciences Testing Anti-Biofilm Polymeric Surfaces: Where to Start?"
- [135] A. L. Hook *et al.*, "Combinatorial discovery of polymers resistant to bacterial attachment," *Nat. Biotechnol.*, vol. 30, no. 9, pp. 868–75, 2012.
- [136] U. Laboratory of Biophysics and Surface Analysis, University of Nottingham, Nottingham, "No Title." .
- [137] A. Gonzalez-Martin *et al.*, "Simultaneous TOC Reduction and Biofouling Prevention in BWP Processed Water," *SAE Int. J. Aerosp.*, vol. 1, no. 1, pp. 454–460, 2008.
- [138] R. F. Piola, C. Grandison, and DSTO Defence Science and Technology Organisation, "In-water Treatment of Biofouling in Internal Systems : Field Validation of Quaternary Ammonium Compound (QAC) Chemical Treatment Protocols," *US Nav. Inst.*, p. 38, 1952.

- [139] Woods Hole Oceanographic Institute (WHOI), "The Effects of Fouling," *Mar. Fouling its Prev.*, no. 580, pp. 3–19, 1952.
- [140] F. Costa, I. F. Carvalho, R. C. Montelaro, P. Gomes, and M. C. L. Martins, "Covalent immobilization of antimicrobial peptides (AMPs) onto biomaterial surfaces," *Acta Biomater.*, vol. 7, no. 4, pp. 1431–1440, 2011.
- [141] P. Li *et al.*, "A polycationic antimicrobial and biocompatible hydrogel with microbe membrane suctioning ability," *Nat. Mater.*, vol. 10, no. 2, pp. 149–156, 2011.
- [142] R. O. Darouiche, M. D. Mansouri, P. V. Gawande, and S. Madhyastha, "Efficacy of combination of chlorhexidine and protamine sulphate against device-associated pathogens," *J. Antimicrob. Chemother.*, vol. 61, no. 3, pp. 651–657, 2008.
- [143] L. Caillier, E. T. de Givenchy, R. Levy, Y. Vandenberghe, S. G ribaldi, and F. Guittard, "Synthesis and antimicrobial properties of polymerizable quaternary ammoniums," *Eur. J. Med. Chem.*, vol. 44, no. 8, pp. 3201–3208, 2009.
- [144] D. Guay, "An update on the role of nitrofurans in the management of urinary tract infections.," *Drugs*, vol. 61, no. 3, pp. 353–64, 2001.
- [145] J. I. Greenfeld, L. Sampath, S. J. Popilskis, S. R. Brunnert, S. Stylianos, and S. P. Modak, "Decreased bacterial adherence and biofilm formation on chlorhexidine and silver sulfadiazine-impregnated central venous catheters implanted in swine.," *Crit Care Med*, vol. 23, no. 5, pp. 894–900, 1995.
- [146] K. Jaeger *et al.*, "Efficacy of a benzalkonium chloride-impregnated central

- venous catheter to prevent catheter-associated infection in cancer patients,” *Chemotherapy*, vol. 47, no. 1, pp. 50–55, 2001.
- [147] K. Yorganci, C. Krepel, J. A. Weigelt, and C. E. Edmiston, “Activity of antibacterial impregnated central venous catheters against *Klebsiella pneumoniae*,” *Intensive Care Med.*, vol. 28, no. 4, pp. 438–442, 2002.
- [148] K. Adlington *et al.*, “Application of Targeted Molecular and Material Property Optimization to Bacterial Attachment-Resistant (Meth)acrylate Polymers,” *Biomacromolecules*, vol. 17, no. 9, pp. 2830–2838, 2016.
- [149] R. D. Monds and G. A. O’Toole, “The developmental model of microbial biofilms: ten years of a paradigm up for review,” *Trends Microbiol.*, vol. 17, no. 2, pp. 73–87, 2009.
- [150] M. Cloutier, D. Mantovani, and F. Rosei, “Antibacterial Coatings: Challenges, Perspectives, and Opportunities,” *Trends Biotechnol.*, vol. 33, no. 11, pp. 637–652, 2015.
- [151] P. F. Holmes, E. P. K. Currie, J. C. Thies, H. C. Van Der Mei, H. J. Busscher, and W. Norde, “Surface-modified nanoparticles as a new, versatile, and mechanically robust nonadhesive coating: Suppression of protein adsorption and bacterial adhesion,” *J. Biomed. Mater. Res. - Part A*, vol. 91, no. 3, pp. 824–833, 2009.
- [152] G. Cheng, Z. Zhang, S. Chen, J. D. Bryers, and S. Jiang, “Inhibition of bacterial adhesion and biofilm formation on zwitterionic surfaces,” *Biomaterials*, vol. 28, no. 29, pp. 4192–4199, 2007.
- [153] G. Cheng, G. Li, H. Xue, S. Chen, J. D. Bryers, and S. Jiang, “Zwitterionic

- carboxybetaine polymer surfaces and their resistance to long-term biofilm formation," *Biomaterials*, vol. 30, no. 28, pp. 5234–5240, 2009.
- [154] N. Biologicals, "Stem Cells: Novus Biologicals." [Online]. Available: <https://www.novusbio.com/research-areas/stem-cells>. [Accessed: 07-Jan-2021].
- [155] S. K. Schmitt, A. W. Xie, R. M. Ghassemi, D. J. Trebatoski, W. L. Murphy, and P. Gopalan, "Polyethylene Glycol Coatings on Plastic Substrates for Chemically Defined Stem Cell Culture," *Adv. Healthc. Mater.*, vol. 4, no. 10, pp. 1555–1564, 2015.
- [156] M. D. Kurkuri, C. Driever, G. Johnson, G. McFarland, H. Thissen, and N. H. Voelcker, "Multifunctional polymer coatings for cell microarray applications," *Biomacromolecules*, vol. 10, no. 5, pp. 1163–1172, 2009.
- [157] A. H. Broderick, S. M. Azarin, M. E. Buck, S. P. Palecek, and D. M. Lynn, "Fabrication and selective functionalization of amine-reactive polymer multilayers on topographically patterned microwell cell culture arrays," *Biomacromolecules*, vol. 12, no. 6, pp. 1998–2007, 2011.
- [158] D. S. W. Benoit, M. P. Schwartz, A. R. Durney, and K. S. Anseth, "Small functional groups for controlled differentiation of hydrogel-encapsulated human mesenchymal stem cells," *Nat. Mater.*, vol. 7, no. 10, pp. 816–823, 2008.
- [159] K. A. Kilian and M. Mrksich, "Directing Stem Cell Fate by Controlling the Affinity and Density of Ligand-Receptor Interactions at the Biomaterials Interface," *Angew. Chemie*, vol. 124, no. 20, pp. 4975–4979, 2012.

- [160] J. T. Koepsel, P. T. Brown, S. G. Loveland, W. J. Li, and W. L. Murphy, "Combinatorial screening of chemically defined human mesenchymal stem cell culture substrates," *J. Mater. Chem.*, vol. 22, no. 37, pp. 19474–19481, 2012.
- [161] Y. Liu, T. T. Yang Tan, S. Yuan, and C. Choong, "Multifunctional P(PEGMA)-REDV conjugated titanium surfaces for improved endothelial cell selectivity and hemocompatibility," *J. Mater. Chem. B*, vol. 1, no. 2, pp. 157–167, 2013.
- [162] M. Zhang, T. Desai, and M. Ferrari, "Proteins and cells on PEG immobilized silicon surfaces," *Biomaterials*, vol. 19, no. 10, pp. 953–960, 1998.
- [163] D. J. Irvine, A. M. Mayes, and L. G. Griffith, "Nanoscale clustering of RGD peptides at surfaces using comb polymers. 1. Synthesis and characterization of comb thin films," *Biomacromolecules*, vol. 2, no. 1, pp. 85–94, 2001.
- [164] S. Tugulu and H. A. Klok, "Stability and nonfouling properties of poly(poly(ethylene glycol) methacrylate) Brushes under cell culture conditions," *Biomacromolecules*, vol. 9, no. 3, pp. 906–912, 2008.
- [165] F. M. Veronese, "Peptide and protein PEGylation: A review of problems and solutions," *Biomaterials*, vol. 22, no. 5, pp. 405–417, 2001.
- [166] J. T. Koepsel and W. L. Murphy, "Patterned Self-Assembled Monolayers: Efficient, Chemically Defined Tools for Cell Biology," *ChemBioChem*, vol. 13, no. 12, pp. 1717–1724, 2012.
- [167] G. A. Hudalla and W. L. Murphy, "Immobilization of peptides with distinct biological activities onto stem cell culture substrates using orthogonal chemistries," *Langmuir*, vol. 26, no. 9, pp. 6449–6456, 2010.

- [168] O. Sanni *et al.*, “Bacterial Attachment to Polymeric Materials Correlates with Molecular Flexibility and Hydrophilicity,” *Adv. Healthc. Mater.*, vol. 4, no. 5, pp. 695–701, Apr. 2015.
- [169] A. Nasir *et al.*, “Discovery of a Novel Polymer for Xeno-Free, Long-Term Culture of Human Pluripotent Stem Cell Expansion,” *Adv. Healthc. Mater.*, vol. 2001448, pp. 1–7, 2020.
- [170] M. Javaid and A. Haleem, “Additive manufacturing applications in medical cases: A literature based review,” *Alexandria J. Med.*, vol. 54, no. 4, pp. 411–422, 2018.
- [171] N. Noor, A. Shapira, R. Edri, I. Gal, L. Wertheim, and T. Dvir, “3D Printing of Personalized Thick and Perfusable Cardiac Patches and Hearts,” *Adv. Sci.*, vol. 6, no. 11, 2019.
- [172] Y. Chen *et al.*, “Noninvasive in vivo 3D bioprinting,” *Sci. Adv.*, vol. 6, no. 23, pp. 1–11, 2020.
- [173] A. K. Miri, A. Khalilpour, B. Cecen, S. Maharjan, S. R. Shin, and A. Khademhosseini, “Multiscale bioprinting of vascularized models,” *Biomaterials*, vol. 198, no. February 2018, pp. 204–216, 2019.
- [174] M. Javaid and A. Haleem, “Current status and applications of additive manufacturing in dentistry: A literature-based review,” *J. Oral Biol. Craniofacial Res.*, vol. 9, no. 3, pp. 179–185, 2019.
- [175] “How Much Does a 3D Printed House Cost in 2021? | All3DP.” [Online]. Available: <https://all3dp.com/2/3d-printed-house-cost/>. [Accessed: 16-Feb-2021].

- [176] "NASA's Centennial Challenges: 3-D Printed Habitat Challenge | NASA." [Online]. Available: https://www.nasa.gov/directorates/spacetech/centennial_challenges/3DPHabitat/index.html. [Accessed: 16-Feb-2021].
- [177] S. A. M. Tofail, E. P. Koumoulos, A. Bandyopadhyay, S. Bose, L. O'Donoghue, and C. Charitidis, "Additive manufacturing: scientific and technological challenges, market uptake and opportunities," *Mater. Today*, vol. 21, no. 1, pp. 22–37, Jan. 2018.
- [178] S. C. Ligon, R. Liska, J. Rogen Stampfl, M. Gurr, and R. Mü, "Polymers for 3D Printing and Customized Additive Manufacturing."
- [179] S. D. Nath and S. Nilufar, "An overview of additive manufacturing of polymers and associated composites," *Polymers (Basel)*, vol. 12, no. 11, pp. 1–33, 2020.
- [180] I. Jasiuk, D. W. Abueidda, C. Kozuch, S. Pang, F. Y. Su, and J. McKittrick, "An Overview on Additive Manufacturing of Polymers," *Jom*, vol. 70, no. 3, pp. 275–283, 2018.
- [181] S. Maruo, O. Nakamura, and S. Kawata, "Three-dimensional microfabrication with two-photon-absorbed photopolymerization," vol. 22, no. 2, pp. 132–134, 1997.
- [182] "Two-photon absorption - Chemistry LibreTexts." [Online]. Available: [https://chem.libretexts.org/Bookshelves/Physical_and_Theoretical_Chemistry_Textbook_Maps/Supplemental_Modules_\(Physical_and_Theoretical_Chemistry\)/Spectroscopy/Electronic_Spectroscopy/Two-photon_absorption](https://chem.libretexts.org/Bookshelves/Physical_and_Theoretical_Chemistry_Textbook_Maps/Supplemental_Modules_(Physical_and_Theoretical_Chemistry)/Spectroscopy/Electronic_Spectroscopy/Two-photon_absorption).

- [Accessed: 23-Feb-2021].
- [183] V. F. Paz *et al.*, "Development of functional sub-100 nm structures with 3D two-photon polymerization technique and optical methods for characterization," *J. Laser Appl.*, vol. 24, no. 4, p. 042004, 2012.
- [184] A. El-Tamer, U. Hinze, and B. N. Chichkov, *Two-Photon Polymerization in Optics, Microfluidics, and Biomedicine*. 2020.
- [185] A. Koroleva, S. Gittard, S. Schlie, A. Deiwick, S. Jockenhoevel, and B. Chichkov, "Fabrication of fibrin scaffolds with controlled microscale architecture by a two-photon polymerization-micromolding technique," *Biofabrication*, vol. 4, no. 1, 2012.
- [186] N. M. B. Smeets, R. W. K. Lam, R. P. Moraes, and T. F. L. McKenna, "Catalytic chain transfer polymerization for molecular weight control in microemulsion polymerization," *Polym. Chem.*, vol. 3, pp. 514–524, 2012.
- [187] K. Adlington *et al.*, "Mechanistic Investigation into the Accelerated Synthesis of Methacrylate Oligomers via the Application of Catalytic Chain Transfer Polymerization and Selective Microwave Heating," 2013.
- [188] K. Adlington, R. Mcsweeney, G. Dimitrakis, S. W. Kingman, J. P. Robinson, and D. J. Irvine, "Enhanced 'in situ' catalysis via microwave selective heating: catalytic chain transfer polymerisation †," 2014.
- [189] K. G. Suddaby, D. M. Haddleton, J. J. Hastings, S. N. Richards, and J. P. O'Donnell, "Catalytic Chain Transfer for Molecular Weight Control in the Emulsion Polymerization of Methyl Methacrylate and Methyl Methacrylate–Styrene," *Macromolecules*, vol. 29, no. 25, pp. 8083–8091,

- 1996.
- [190] J. Fowles *et al.*, "A review of the toxicological and environmental hazards and risks of tetrahydrofuran," *Crit. Rev. Toxicol.*, vol. 43, no. 10, pp. 811–828, 2013.
- [191] C. E. Vasey *et al.*, "Amphiphilic tri- and tetra-block co-polymers combining versatile functionality with facile assembly into cytocompatible nanoparticles," *Biomater. Sci.*, vol. 7, no. 9, pp. 3832–3845, 2019.
- [192] M. Vergaelen *et al.*, "Ethyl acetate as solvent for the synthesis of poly(2-ethyl-2-oxazoline)," *Green Chem.*, vol. 22, no. 5, pp. 1747–1753, 2020.
- [193] "How to Prevent Soot Buildup in Your Car's Engine | HowStuffWorks." [Online]. Available: <https://auto.howstuffworks.com/how-to-prevent-soot-buildup-in-your-cars-engine.htm>. [Accessed: 20-Dec-2018].
- [194] D. A. Green and R. Lewis, "The effects of soot-contaminated engine oil on wear and friction: A review," *Proc. Inst. Mech. Eng. Part D J. Automob. Eng.*, vol. 222, no. 9, pp. 1669–1689, 2008.
- [195] A. D. H. Clague, J. B. Donnet, T. K. Wang, and J. C. M. Peng, "A comparison of diesel engine soot with carbon black," *Carbon N. Y.*, vol. 37, no. 10, pp. 1553–1565, 1999.
- [196] A. A. J. Dennis, C. P. Garner, D. H. C. Taylor, and A. J. Dennis, "Effect of EGR on Diesel Engine Wear," *J. Engines*, vol. 108, pp. 1185–1197, 1999.
- [197] S. Li, A. A. Csontos, B. M. Gable, C. A. Passut, and E. P. Additives, "Wear in Cummins M-1 1 / EGR Test Engin," *J. Engines*, vol. 111, no. May, pp. 2258–2271, 2002.

- [198] Z. Yang, Q. Wang, and T. Wang, "Engineering a hyperbranched polyimide membrane for shape memory and CO₂ capture," *J. Mater. Chem. A*, vol. 5, no. 26, pp. 13823–13833, 2017.
- [199] S. A. Didas, S. Choi, W. Chaikittisilp, and C. W. Jones, "Amine-Oxide Hybrid Materials for CO₂ Capture from Ambient Air," *Acc. Chem. Res.*, vol. 48, no. 10, pp. 2680–2687, 2015.
- [200] O. Wagner, M. Zieringer, W. J. Duncanson, D. A. Weitz, and R. Haag, "Perfluoroalkyl-functionalized hyperbranched polyglycerol as pore forming agents and supramolecular hosts in polymer microspheres," *Int. J. Mol. Sci.*, vol. 16, no. 9, pp. 20183–20194, 2015.
- [201] A. A. Dundas *et al.*, "Achieving Microparticles with Cell-Instructive Surface Chemistry by Using Tunable Co-Polymer Surfactants," *Adv. Funct. Mater.*, vol. 30, no. 36, 2020.
- [202] Whiteley, "Biofilms." [Online]. Available: <https://www.whiteley.com.au/biofilms>. [Accessed: 07-Jan-2021].

2 Chapter 2: Experimental Methods

2.1 General Synthetic Procedure

2.1.1 Materials

Unless otherwise stated, all reagents were used as received and without further purification, and all procedures were conducted under an inert argon atmosphere using standard Schlenk line techniques.

2.1.2 Chain Transfer Polymerisation (CTP) of Mono- or Di- functional Monomers

The required quantities of monomer(s), initiator, chain transfer agent and solvent were introduced into a Schlenk flask equipped with a magnetic stirrer bar. The mixture was degassed with an inert argon atmosphere for at least 30 minutes, then the reaction vessel was immersed in a pre-heated oil bath, which was thermostatically controlled to remain at the required reaction temperature. After the required reaction time, the vessel was removed from the heat and quenched in an ice bath to prevent further reaction.

In the case of di-functional monomers, the reaction was run once until gelation occurred, then was repeated, with the reaction being quenched at least 5 minutes prior to gelation to ensure maximum conversion was reached.

Once the mixture was cooled, polymeric product was isolated by adding the solution dropwise to a cold anti-solvent and collecting the resulting precipitate via filtration/decanting. The resulting polymeric product was then dried to constant mass. If the product was oligomeric, the product was either not isolated or isolated using vacuum distillation.

2.1.3 Note on Gelation:

Gelation was defined as the point at which the solution ceased to be a free-flowing, easily stirred liquid and became a rubbery/solidified gel. This point was a readily observable change in physical form apparent through visual inspection. However, gelation was confirmed by withdrawing a small sample and attempting to dilute it in chloroform. Where gelation had occurred, material presented as non-re-dissolvable particles in the resulting solution. The time at which this occurred was defined as the gelation time and represented a change from an oligomeric/hyperbranched system to an extended cross-linked system.

2.1.4 Gel Permeation Chromatography:

Gel permeation chromatography (GPC) was performed using a refractive index (RI) detector with HPLC THF as the eluent. Analysis was performed at 40 °C with a flow rate of 1 mL min⁻¹ through two PolarGel-M columns with a calibration range of 580–377,400 Da calibrated with 10 poly(styrene)/poly(methyl methacrylate) narrow molecular weight distribution standards. All GPC equipment and standards were supplied by Polymer Laboratories (Varian). GPC data were analysed using the Astra offline software package.

2.1.5 Nuclear Magnetic Resonance:

¹H nuclear magnetic resonance (NMR) spectra were obtained in CDCl₃ on either a Bruker AV400 and CHMNMR 400b (400 MHz) spectrometer. Chemical shifts are referenced against residual solvent signal (1 H = 7.26 ppm) and processed using the MestReNova software package.

2.2 Experimental Methods for Chapter 3

2.2.1 Materials

Divinylbenzene 80% (DVB-80, technical grade, 80% difunctional monomer (*m*- and *p*-DVB), 20% monofunctional monomer (3- and 4- ethylstyrene)), lauryl methacrylate (LMA, 96%, 500 ppm monomethyl ether hydroquinone (MEHQ) as inhibitor), lauryl acrylate (Technical Grade 90 %, 60-100 ppm MEHQ as inhibitor), stearyl methacrylate (mixture of stearyl and cetyl methacrylates, contains MEHQ as inhibitor), stearyl acrylate (97%, contains 200 ppm MEHQ as inhibitor), 1-Dodecanethiol (DDM, 98%+), cyclohexanone (99%+), toluene (99.8%), deuterated chloroform (99.8%+), tetrahydrofuran (THF, anhydrous, 99%+) and 2,2'-Azobis(isobutyronitrile) (AIBN, 98%+) were all purchased from Sigma-Aldrich. High-purity argon was purchased from BOC gases and Bis[(difluoroboryl)diphenylglyoximato]cobalt(II) (CoPhBF) was obtained from DuPont. Durasyn®164 hydrocarbon base oil (PA04) was obtained from BP Castrol.

2.2.2 Synthetic Procedures

Note that for polymerisations containing DVB, no thermal initiator species was added, as DVB is self-initiating at 150 °C (Chapter 3, Section 3.1.3). Where a catalytic chain transfer agent (CTA) is used, the process is known as catalytic chain transfer polymerisation (CCTP).

2.2.2.1 Direct Co-polymerisation of DVB and Lauryl/Stearyl Meth/Acrylate via CCTP:

Copolymers were produced through the CTP of DVB (2 ml, 1.828 g) and either LMA, LA, SMA or SA (8 mL) using a catalytic chain transfer agent (CoPhBF, 26 mg). The desired quantities of these monomers and cyclohexanone (10 mL, 9.48 g) were used. A reaction temperature of 150 °C was used. The repeat reactions were quenched 15 minutes before gelation was known to occur. The products were precipitated in cold

(0 °C) methanol and collected via filtration to provide a brown/white, viscous liquid (colouration due to PhCoBF), which was then dried to constant mass.

2.2.2.2 *Oligomerization of mono-functional LMA via CCTP*

A solution of mixed LMA oligomers was synthesised *via* CCTP of LMA monomer (100.00 mL, 80 g). Toluene solvent (5.00 mL, 4.335 g), PhCoBF CTA (78.0 mg) and AIBN initiator (866 mg, 5.274 mmol) were also used. Oligomers were targeted using relatively large quantities of CTA and initiator. A reaction temperature of 80 °C was used. After 24 hrs, the reaction was quenched, and an average oligomer concentration of 40% was obtained *via* H¹NMR.

2.2.2.3 *Preparation of Purified Lauryl Methacrylate Oligomers*

A crude oligomeric solution of LMA was synthesised by the procedure outlined above: the crude product was then vacuum distilled to increase the oligomer concentration in the solution to 81%.

2.2.2.4 *Copolymerisation of DVB and LMA Dimer via CTP*

CTP of DVB-80 (12.5 mL, 11.4 g, 0.088 mol), was conducted using LMA oligomer (50 mL, 43.4 g) as the CTA and a cyclohexanone solvent (10 mL, 9.48 g) at 150 °C for 35 minutes, followed by precipitation in cold (0 °C) methanol. The resulting precipitate was collected via filtration to provide a brown/white, viscous liquid (colouration due to PhCoBF).

2.2.2.5 *Polymerisation of DVB via CTP Using Thiol CTA*

Polymeric DVB was produced by reacting DVB monomer (1 mL, 0.914 g, 0.0070) and 60 mol % DDM (1.009 mL, 0.948 g, 0.0047 mol) in cyclohexanone solvent (1 mL, 0.948 g) at 150 °C for 360 minutes, followed by precipitation in cold (0 °C) methanol. The resulting precipitate was collected via filtration to provide a white, viscous liquid.

2.2.3 Application Testing

All tribological application testing was undertaken by BP/Castrol's Formulated Products Technology (FPT). Durasyn®164 polyalphaolefin, a hydrogenated synthetic hydrocarbon base fluid for use in fully and partially synthetic, premium, long-drain lubricating oils, industrial oils, hydraulic fluids, transmission fluids, or heat transfer fluids, was used as the control in all tests. The tribological features for the polymers produced were tested under hydrodynamic, elastohydrodynamic and boundary conditions in order to test the viscosity of the solutions, and film formation at surfaces.

2.2.3.1 Solubility Testing

The solubility of different polymers produced in the above test methods was analysed through adding a small amount (0.1 – 5.0 wt %) of the produced polymer into Durasyn®164. The tests started at room temperature, and then with stirring, the temperature of the Durasyn®164 was increased in 10 °C intervals.

2.2.3.2 Viscosity Measurements

Kinematic Viscosity (KV)

The kinematic viscosity, ν , of a material is a measure of a fluid's internal resistance to flow under gravitational forces, and can also be related to the dynamic viscosity as shown in Equation 2.1:

$$\nu = \frac{\mu}{\rho} = K_C \cdot t_f \quad (2-1)$$

where, μ is the dynamic viscosity (N s/m²), ρ is the density (kg/m³), K_C is the capillary constant and t_f is the measured flow time. The kinematic viscosity is commonly quoted in centiStoke (cSt), where 1 cSt = 1 mm²/s.

The KV of the polymeric materials produced was measured by passing concentrations of polymer of 0.0, 0.25, 0.5, 1.0 and 5.0 wt%, dissolved in base oil, through a glass capillary viscometer of known K_C (shown in Figure 2.1, top left) suspended in a thermostatically controlled water bath. The time taken for a known volume of the solution to pass through the capillary at a given temperature, t_f , was recorded and this produced the viscosity. This kinematic viscosity was recorded at 40 °C and 100 °C (KV): the results were reported in centistokes (cSt), using the methods outlined in ASTM D445. During the KV measurement, the lubrication regime is hydrodynamic.

Cold Cranking Simulator (CCS)

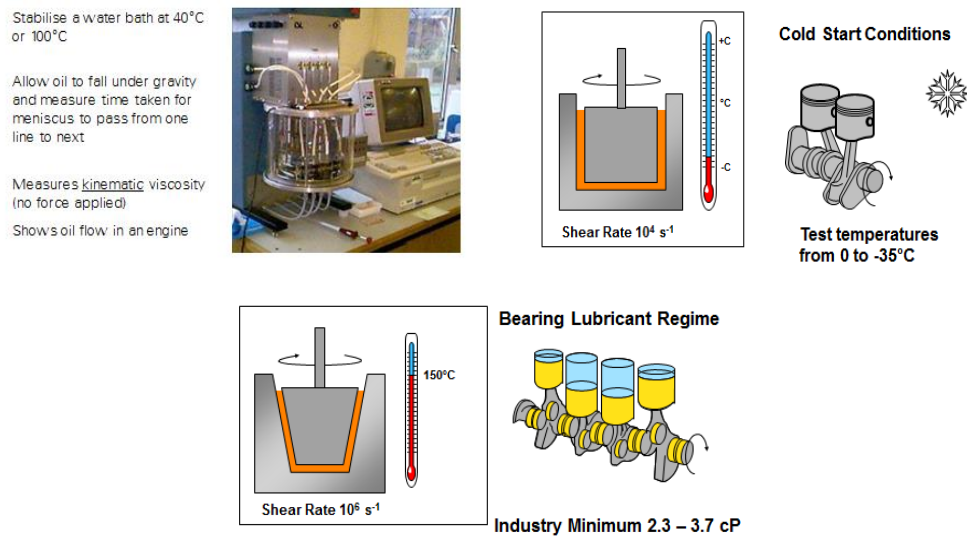


Figure 2.1. Top left: image of KV apparatus. Top right: diagram of CCS apparatus. Bottom: diagram of high temperature USV shear apparatus.

The CCS, shown in Figure 2.1 (top right) measures the apparent dynamic viscosity of oil at temperatures from -35 °C to -5 °C. The dynamic viscosity, μ , is given by Equation 2-2:

$$\mu = \frac{\tau}{\gamma} \quad (2-2)$$

where τ is the shear stress (N/m^2) and γ is the shear rate (s^{-1}) within the fluid. It is often quoted in centipoise (cP), where $1 \text{ cP} = 0.001 \text{ N s/m}^2$.

The CCS is a high shear method designed to simulate the oil viscosity under cold starting (cranking) conditions, such that the lubrication regime is hydrodynamic. The CCS contains a temperature controlled (glycol cooled) pot test chamber. The motor-controlled stator is housed within the chamber. The CCS uses a vacuum pump to inject the test sample into the test chamber, where it is cooled to the required test temperature. A motor stator with a constant current is started at a known shear rate (γ). The resistance of the stator in the sample (τ) at the test temperature is converted into viscosity using Equation 2.2.

In this work, the CCS was used to measure the apparent dynamic viscosity of polymer-oil solutions at concentrations of 1 and 2 wt% at -35°C . The test method used was ASTM D5293.

Ultra-high Shear Viscosity (USV):

Unlike kinematic viscosity, USV viscosity is measured under conditions similar to those of an operating engine. The test is conducted at up to 150°C under shear stress conditions similar to those found in very thin film lubrication areas, and as such in the hydrodynamic lubrication regime. An example is the piston ring-to-cylinder wall interface. The value obtained from this test provides an indication of the ability of the oil to maintain fluid film strength in an engine.

The dynamic shear viscosity of the polymeric materials produced was measured at 80, 100 and 150°C , over a shear range from $10^6 - 10^7 \text{ s}^{-1}$ using an Ultra Shear Viscometer shown in Figure 2.1 (bottom), which employed a coaxial cylinder system with a cylindrical rotor and stator. A brief shearing interval (typically 30 ms)

minimised shear heating in the lubricant, and allowed these high shear rates to be achieved. The test method used was ASTM D4683.

2.2.3.3 Film Formation and Wear Measurement

Mini Traction Machine (MTM):

The MTM, shown in Figure 2.2, is a multi-purpose instrument for measuring friction and traction properties of lubricated and unlubricated surface contacts under a wide range of rolling and sliding conditions, often in the mixed lubrication regime. The MTM is used to determine the friction profile of the specific ‘system’, typically recorded in the form of a Stribeck curve for metal – metal contacts.

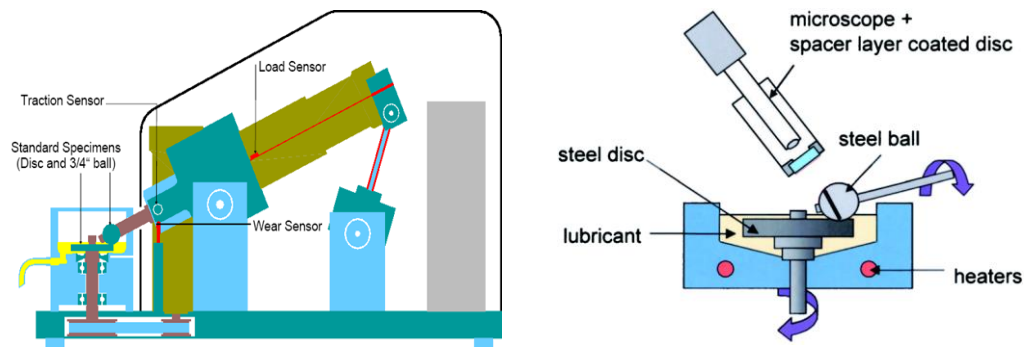


Figure 2.2. Left: schematic of MTM machine. Right: blown up diagram of equipment involved in MTM wear, film formation and friction coefficient measurement.

The MTM uses the frictional force between a rotating, highly polished spherical ball and an independently rotating highly polished glass disc. The ball is placed on the face of the disc in a reservoir of material to be measured, then the ball and disc are rotated to produce a rolling/sliding contact. The temperature of the reservoir can be increased, to allow for measurement at different temperatures. Measurements of the friction coefficient may be used to produce Stribeck curves. The coefficient of friction (COF) is a dimensionless number that is defined as the ratio between friction force and normal force. The term Stribeck curve is used to describe a plot showing the frictional characteristics of a liquid lubricant over conditions usually

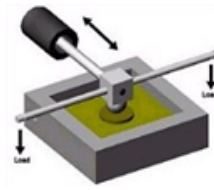
spanning the boundary, mixed and hydrodynamic regimes (see Chapter 3, Section 3.1.1.4).

The MTM was also equipped with Spacer Layer Image Mapping (SLIM). SLIM is a camera and processing system used to investigate the formation of organic films on the surface of the ball. Inorganic film formation is effectively mapped throughout the test using optical interferometry. The high-resolution digital image of the contact is captured: the colour information is then used to determine film thickness within the contact.

In this work, the ability of the HB polymer/oil solutions to form surface films was measured using the MTM. A force of 40 N was applied between the ball and the disc, which were then rotated at a speed of 100 mm s⁻¹ for 1 hour and 30 minutes with a slide/roll ratio (SRR) of 50 %, to ensure both surfaces were covered with the oil solution. The speed of the rotation was then increased to 3200 mm s⁻¹ and then reduced to 10 mm s⁻¹ at 30 °C temperature intervals between 60 – 120 °C, while measuring the frictional coefficient to produce a Stribeck curve of frictional coefficient against speed of rotation. Interferometry images were taken before and after the Stribeck curve was measured: the colour information was then used to determine film thickness within the contact after each step.

High Frequency Reciprocation Rig (HFRR):

The HFRR, shown in Figure 2.3, is a reciprocating tribometer, originally designed for analysing the lubricity of diesel fuels, but often used for screening the lubrication performance of engine oils and additives which are active in the boundary lubrication regime.



High frequency reciprocating rig (HFRR)

- Incremental increases in temperature
 - Standard test: 40 – 140 °C
 - High temperature: 60 – 270 °C
- Load: 400 g
- Frequency: 40 Hz
- Stroke length: 1 mm

Figure 2.3. Diagram of HFRR apparatus.

The HFRR was used to determine the wear rate of the polymers. A 6 mm diameter steel ball was pressed with fixed force (load 400g) onto a steel plate of defined hardness and surface roughness, and moved back and forth via a bracket in a path of the oil to be tested, with a frequency of 40 Hz and a stroke length of 1 mm. The temperature range used was 40 – 140 °C. The movement occurred at the ‘ball wear scar’: the diameter of the wear scar in microns was the HFRR value. The wear was non-linear due to the spherical nature of the test piece. Poor lubrication results in a larger wear scar, resulting in a lower surface pressure between the ball and steel plate. From this, the coefficient of friction (see pg. 77) was determined at each temperature.

Elasto-Hydrodynamic (EHD) Film Thickness Rig:

EHD rigs are used to measure the film formation/viscosity properties of a formulation in the elastohydrodynamic lubrication regime (see Chapter 3, Section 3.1.1.4).

Optical interferometry was used to measure the polymer/oil film thickness between a steel ball and glass disk at very high contact pressure conditions, as shown in Figure 2.4. Tests were run using a protocol of running from low speed to high speed (ascending speed) followed by measurements at reducing speeds (descending speed). These tests were run at 100°C under pure rolling conditions. Contact stress

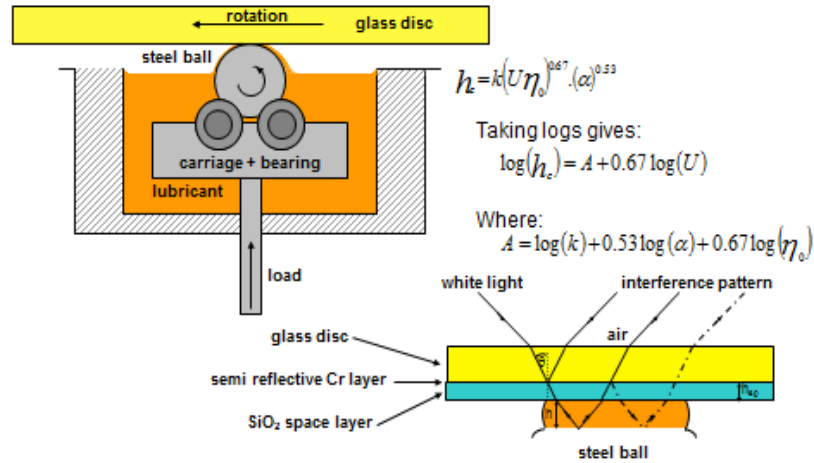


Figure 2.4. Diagram of EHD Film Thickness Rig.

in the EHD contact was approximately 0.5 GPa and shear rate in the inlet region was approximately 10^6 to 10^7 s^{-1} .

2.2.4 Film Formation Data Analysis

The thickness (nm) of the film formed by the lubricating solutions was measured by interferometry (SLIM) at each coordinate of a circular grid of fixed radius, centred on the exact middle of the wear scar. This data was plotted in 2D and 3D for each step of the MTM measurement. For the 2D scatter plots, the data was binned (i.e. grouped into a smaller number of consecutive intervals) to allow significant variations in the film thickness in each image to be observed more clearly. The mean, standard deviation, minimum and maximum thickness were calculated for each measurement. All analysis and visualisations were conducted using Python 3.7 scripts with Matplotlib visualisation libraries.

2.2.5 Dielectric Monitoring – Cavity Perturbation

0.5g of DVB-LMA copolymer (2:8 and 1:9 v/v) was dissolved in 8 mL of cyclohexanone. The samples were sent to Dr Alexis Kalamiotis (Faculty of Engineering, University of Nottingham) to carry out the dielectric measurements. The cavity perturbation technique [1] was selected for this study due to the physical form

of the samples. The experimental setup consisted of a copper resonant cylindrical cavity (dimensions: diameter 570 nm, height 50 nm) that was attached to an Agilent Technologies E5062A Vector Network Analyser, capable of producing standing waves in the cavity around 2.45 GHz. Quartz tubes were used to hold the samples during measurement. First the empty quartz tube was inserted into the rig and measurements were recorded against it with varying frequencies. Then the sample was placed into the rig via the tube placed on a step motor for measurement. The cavity has TM_{0n0} identified modes at 912 MHz, 1429 MHz, 1949 MHz and 2470 MHz. The samples were studied over a temperature range of 20 – 180 °C with a step interval of 10 °C. Each sample was measured three times.

2.2.6 Liquid Handler System

Solutions of PA04 base oil and semi-block DVB-LMA copolymer, in a ratio 2:8 (v/v) DVB:LMA, were prepared with polymer concentrations of 0.5, 1.0, 2.0 and 5.0 wt%. These samples were sent to Dr Zuoxin Zho (Centre for Additive Manufacturing (CfAM), University of Nottingham).

2mL of these samples were then loaded into a liquid handling machine. The liquid handler is a high throughput technique, which enables the testing of 96 formulations per 13 working hours. A four-channel liquid handling apparatus (Microlab STARlet, Hamilton Robotics, Inc.) was used. The liquid handler utilized air displacement pipetting as the mechanism of operation, which is similar to a handheld electronic pipette system. As the piston moves up within the channel, the air pressure is reduced, and the liquid is aspirated into the tip by the atmosphere pressure at a controlled flow rate. The liquid handler is calibrated by the manufacturer to ensure the flow rate is accurate. Each of the four parallel pipette channels was equipped with a pressure sensor to monitor pressure change during the overall process, i.e. during

both aspiration and dispensing of the samples. The pipettes automatically inject the required quantities of each component into a well plate, then the plate is heated to the chosen temperature for the required length of time. The pressure required to aspirate the resulting solution is then measured. This pressure can then be used to determine the solution viscosity. The viscosity of the polymer samples was measured at 40 °C: each test was repeated 3 times.

2.2.6.1 *Calculative Procedure to Determine Viscosity From Aspiration Data*

The pressure required to maintain a constant aspiration rate depends on the physical properties of the liquid and the geometry of the pipette. In this study, the pipette used was a two-part conical frustum. At a given time (t), the radius (R_t) and height (H_t) of the front surface of a liquid aspirated into the bottom part of the pipette were calculated. The pressures of the liquid were subjected to in the tip can be defined using $P_{gas} = P_{flow} - P_{head} - P_{interface}$, where P_{gas} was gas pressure in the channel, P_{flow} was the pressure drop caused by liquid flowing into the pipette, P_{head} was the difference in the gravitational head pressure between the liquid levels inside and outside the pipette, and $P_{interface}$ was the pressure drop across the interfacial boundary due to the surface tension. The Hagen-Poiseuille equation was used to relate P_{flow} with viscosity of the fluid if each incremented section of the pipette was simplified as a cylindrical pipe.

The above analysis was conducted using a mathematical model, generated using MATLAB 2016a (MathWorks, Inc.) and developed by Dr Zuoxin Zhou (CfAM, University of Nottingham) to fit the experimental pressure (P_{gas}) vs. time data. The sum of the square of the residual between experiment and analytical expression was taken as a minimization objective; experimental parameters, such as pressures and time, were taken as variables. MATLAB was used to apply a least-square method was

applied to minimise the objective. The computation was performed with MATLAB 2016a on a personal computer. Curve fitting was performed between 10 and 15 s as a consequence of the [actual volumetric flow rate](#) not being sufficiently accurate during the transient stage when the liquid starts to aspirate into the pipette. The influence of $P_{\text{interface}}$ is small in comparison to the other contributions beyond the transients prior to 10 s and as a consequence the terms incorporating the surface tension and contact angle were neglected during the curve fitting procedure. With a known density, the viscosity was determined using the curve fitting to best fit to the experimental data [2].

2.3 Experimental Methods for Chapter 4

2.3.1 Materials

Tricyclo[5.2.1.0^{2,6}]decanedimethanol diacrylate, (TCDMDA), butyl acrylate (BA, ≥99%, contains 10-60 ppm monomethyl ether hydroquinone as inhibitor), butyl methacrylate (BMA, 99%, contains 25 ppm monomethyl ether hydroquinone as inhibitor), cyclohexanone (≥99%), toluene (99.8%), dichloromethane (DCM, ≥99.8%), deuterated chloroform (≥99.8%), tetrahydrofuran (THF, anhydrous, ≥99%), isopropyl alcohol (IPA, >99%), methyl butyrate (99%), 3-mercaptopropionic acid (3-MPA, ≥99%), 1-dodecanethiol (DDT, 98%) and 2,2'-Azobis(isobutyronitrile) (AIBN, ≥98%) were all purchased from Sigma-Aldrich. High-purity argon was purchased from BOC gases and Bis[(difluoroboryl)diphenylglyoximato]cobalt(II) (PhCoBF) was obtained from DuPont. Industrial methylated spirit (IMS) was obtained from the School of Pharmacy. Deionised water was obtained directly from Chemistry stores.

2.3.2 Synthetic Procedures

2.3.2.1 Oligomerization of mono-functional BMA via CCTP

Oligomerization here refers to the production of macromers ($\text{BMA}_{2/3}$). Oligomers were targeted through the use of relatively large quantities of CTA and initiator. BMA monomer (20 mL), toluene solvent (1 mL), PhCoBF CTA (800 ppm, 8 mg) and AIBN (1.0 wt%, 89 mg) were reacted at 80 °C for 24 hrs before quenching, according to the procedure outlined in Section 2.1.2. Monomer conversion was achieved in the range 22 – 25 %.

2.3.2.2 Polymerization of TCDMDA via CTP

CTA used included thiols (3-MPA or DDM), or PhCoBF. The di-functional TCDMDA monomer, toluene solvent, required CTA and AIBN initiator were reacted at 65 °C and quenched 5-15 minutes prior to the gelation time to prevent crosslinking. The product was isolated using a cold (0 °C) hexane antisolvent, and was collected via filtration and dried to constant mass, according to the procedure outlined in Section 2.1.2.

2.3.2.3 Copolymerization of TCDMDA and BMA Macromer via CTP

Degassed TCDMDA (2 mL), toluene (9 mL) and AIBN (0.5 wt %) was transferred to a Schlenk flask containing BMA macromer ($\text{BMA}_{2/3}$, 1 mL), a magnetic stirrer bar and an inert argon atmosphere. The resulting solution was heated to 65 °C by immersion in a pre-heated oil bath until gelation occurred at 155 minutes. The reaction was then repeated and quenched after 140 minutes to prevent gelation. The polymeric product was collected as described above (Section 2.1.2) using a cold hexane antisolvent.

2.3.2.4 *Two Photon Printing of Scaffolds of HB pTCDMDA Synthesised via CTP*

All work on formulation and printing was conducted by Andrea Konta (CfAM, University of Nottingham).

Formulations were prepared in 5ml amber glass vials in UV-free environment. Formulations containing only linear PEGDA or TCDMDA were prepared by adding the monomer to the vial, followed by the previously weighted amount of photoinitiator. The vial was left stirring on a hotplate at 60°C for 1 hour. Formulations containing only hyperbranched materials were prepared by adding the polymers to the vial, followed by the photoinitiator amount and leaving the vial stirring for 2 hours at room temperature. Formulations containing both hyperbranched polymer and linear monomer were prepared by adding the materials to the amber vial and mixing them at low stirring on a hotplate for 1 hour. Once well mixed, photoinitiator was added to the vial and the formulation was left stirring for another 2 hours at room temperature.

Structures were printed using a commercial two-photon system (Nanoscribe Photonic Professional GT) equipped with a 780 nm wavelength fibre laser, a pulse frequency of 80 MHz, and a pulse duration of 120 fs. The laser beam was focused with an oil immersion objective (63X, Numerical Aperture (NA) =1.4). The structures were manufactured by moving the laser beam in X-Y direction with mirrors and by moving the piezo stage in the Z direction (printing in galvo-mode).

A glass coverslip was used as the substrate for printing. Thus, a drop of the test formulation was loaded onto the coverslip which was then mounted into the 2PP system's sample holder. This was then loaded into the Nanoscribe system to allow printing to commence. The structures were designed on AutoCAD software. To eliminate unpolymerized material being retained in the final structures, the specimens were washed after printing by immersing the samples in propylene glycol monomethyl ether acetate (PGMEA) for between 2 and 24 hours. The structures were

then thoroughly washed in isopropanol for 10 minutes, to remove any residual solvent and air-dried.

2.3.2.5 *Biocompatibility Studies of HB pTCDMDA Scaffolds*

LIVE/DEAD Biocompatibility tests and all associated work up were performed on HBpTCDMDA printed scaffolds by Dr Adja Toure (CfAM).

3T3 cell cultures:

3T3 fibroblasts were harvested and cultured from mice. After thawing, the 3T3 cells were grown in Alpha MEM Medium (BioWhittaker Reagents, Lonza Walkerville Inc, United States). Cell culture media was complemented with 10% foetal bovine serum (Sigma Aldrich; UK), 1% antibiotic and antimycotic (100 mg/ml penicillin, 100 mg/ml streptomycin, and 0.25 mg/ml amphotericin B; Sigma Aldrich; UK) and 1% of L-Glutamine (Sigma Aldrich; UK). Cell cultures were maintained in T75cm² flasks (Costar, Corning Inc., Corning, NY, USA) in standard culture conditions of 37°C and 5% CO₂, cells were passaged every 3 days after harvesting them by trypsinization using 0.05% Trypsin-EDTA solution (Gibco R, Fisher Scientific UK) at 70% culture confluence and further sub-cultivated into culture flasks.

Preparation of the samples for direct viability assessment:

The scaffolds were sterilised using UV radiation for 20 minutes then rinsed 3 times using phosphate-buffered saline (PBS). Following this step, the scaffolds were covered with 2.5 mL of media and placed in an incubator under standard culture conditions of 37°C and 5% CO₂.

Cell seeding:

3T3 cells were counted using the Trypan blue (Sigma-Aldrich, UK) and a hemocytometer. 10000 cells were seeded on top of the scaffolds placed in a 6 well-

plate. Well plates were incubated under standard conditions of 37°C and 5% CO₂ for 24 hours.

LIVE/DEAD Staining protocol:

A solution of 2 µM calcein AM and 4 µM Ethidium homodimer-1 (EthD-1) in PBS was prepared. Media was removed from the scaffold and the scaffolds were delicately washed once with PBS. Staining solution was then added, and the well plate was incubated for 1 hour. Fluorescence microscope images were taken using a Leica fluorescence microscope and a Lumen dynamic Mercury Source at an exposition of 500ms.

2.3.2.6 UV Polymerisation of TCDMDA and BA and Well Plate Preparation

All work conducted on UV-initiated polymerisations was completed by Dr Jordan Thorpe and Dr Aishah Nasir (School of Pharmacy, University of Nottingham).

First, the tissue culture plastics (well plates) were etched using oxygen plasma for 10 minutes, at 100 W and 2x10⁹ mbar. Next, the monomer and photoinitiator solutions were prepared. The correct volume of monomer (10 µL/96-well, ~125 µL 6-well, in 2:1 v/v TCDMDA:BA) were pipetted into the wells. Photoinitiator solution, which was heated to fully dissolve the photo initiator, was then added to the well at a concentration of 1%. The monomer/initiator solution were degassed for 15 minutes at 30 °C using a sonicator. Argon gas was run over the de-gassed monomer solution for several seconds before closing the scintillation vial. The monomer solutions were then applied to the tissue culture plastic inside a glove box. First, the plates and solutions were taken into the main chamber, where the oxygen levels were controlled to be ≤200 ppm. The monomer was applied to the well plates, then irradiated with UV for 60 minutes, with the bulb raised approximately 20 cm. The plates were then removed from the incubation chamber. Finally, the plates were washed to remove

any residual toxic reagents and unreacted monomer. The plates were washed with IPA three times, then with DI water three times. The plates were then incubated with 2-3 mL DI water at 37 °C in an oven for at least 48 hours. The DI water was changed every 24 hours after performing five washes with DI H₂O per 24 hours.

2.3.2.7 Summary of Stem Cell Culture Well Plate Preparation for HB Polymer

To prepare polymer/solvent solutions at 35 g/L, 42.08 mg of the polymer was first weighed into vial. A micropipette was used to add 1.2 mL of solvent to the vial. The vial was placed on vortex machine to help dissolve polymer at room temperature. If elevated temperature was required to enable polymer dissolution, the vial was heated with stirring in an oil bath. A visual inspection was used to ensure that the polymer was completely dissolved.

To prepare well plates and check for solvent compatibility, the well plate was first placed on a shaker. A micropipette was used to add 150 µL of polymer/solvent solution into each well. Complete coverage of well was ensured *via* by shaking the plate manually if necessary. The plates were allowed to dry in fume hood overnight, then washed with IMS and DI H₂O three times. The plates were then soaked in 2-3 mL DI H₂O over 48 hours at room temperature. Following each washing/soaking step, the plates were visually inspected for any residual odours, whitening, crazing, cracking or general opacity.

Subsequently, for plates not displaying crazing/cracking/whitening/smell at this point, the plates were washed with IMS and DI H₂O three more times, then incubated in 2-3 mL DI H₂O at 37 °C for 48 hours, to ensure all remaining residual monomer/solvent was leached out. The plates were once again visually inspected for surface effects.

The following work was conducted by Dr Thorpe/Nasir (School of Pharmacy). To prepare the plates for cell culture, they were sprayed inside and out with 70% IMS. The plate lid and wells were then soaked in 70% IMS for 20 minutes at room temperature in a class II tissue culture cabinet. The IMS was then removed with a glass aspirator and rinsed three times with DI water. The plates were re-suspended with DI water, UV sterilised (with lids on) using a tissue culture safety cabinet UV lamp for 30 minutes, then placed in an incubator overnight. The plates were then rinsed with DI water 3 times before further use. The plates were then pre-incubated in E8 supplemented with 0 μ M Y-27632 (ROCKi, Tocris Bioscience #1254/10) for 15-60 minutes at 37°C.

2.3.2.8 Stem Cell Growth Studies

All cell culture preparations were performed by Dr Thorpe/Dr Nasir (School of Pharmacy) in a type II Biological Safety Cabinet and humidified incubator, at 37°C and 5% CO₂ (Heracell). Human pluripotent stem cells (hPSCs) were routinely maintained in E8 medium (LifeTechnologies #A1517001) on 1:100 MT (Corning #356235)-coated plasticware (Nunc) and were removed for seeding onto prepared polymer plate using TryPLE. Cells were then resuspended in E8 supplemented with 10 μ M Y-27632 (ROCKi, Tocris Bioscience #1254/10) and seeded onto polymer plates (~70K/well). Cells were cultured to confluency (usually 72 h) with media exchanged daily (without addition of ROCKi). Serial passages are achieved using TryPLE.

2.4 Experimental Methods for Chapter 5

2.4.1 Materials

Divinylbenzene 80% (DVB-80, technical grade, 80% difunctional monomer (*m*- and *p*-DVB), 20% monofunctional monomer (3- and 4- ethylstyrene)), lauryl

methacrylate (LMA, 96%, 500 ppm MEHQ as inhibitor), ethylene glycol dimethacrylate (EGDMA, 98 %, 90-110 ppm MEHQ as inhibitor), di(ethylene glycol) methyl ether methacrylate (DEGMA, 95 %, 100 ppm MEHQ as inhibitor), diethylene glycol dimethyl ether (diglyme, anhydrous, 99.5 %), toluene (99.8%), deuterated chloroform (99.8%+), tetrahydrofuran (THF, anhydrous, 99%+), acetone (>95.5 %), methanol (>98.5 %) and 2,2'-Azobis(isobutyronitrile) (AIBN, 98%+) were all purchased from Sigma-Aldrich. High-purity argon was purchased from BOC gases and Bis[(difluoroboryl)diphenylglyoximato]cobalt(II) (PhCoBF) was obtained from DuPont. Durasyn®164 hydrocarbon base oil (PA04) was obtained from BP Castrol.

2.4.2 Synthetic Procedures

2.4.2.1 Oligomerization of mono-functional LMA and DEGMA via CCTP

Solutions of both mixed LMA oligomers and DEGMA oligomers were synthesised *via* CCTP of LMA and DEGMA monomers, respectively (see Section 2.1.2). For the LMA (100.00 mL, 80 g), toluene solvent (5.00 mL, 4.335 g), PhCoBF CTA (78.0 mg) and AIBN initiator (866 mg, 5.27 mmol) were also used, while for the DEGMA (5.00 mL, 5.10 g), diglyme solvent (0.25 mL, 0.24), toluene solvent (0.25 mL, 0.25 g), PhCoBF CTA (6.0 mg, 1000 ppm) and AIBN initiator (51 mg, 1.0 wt %) were used. Oligomers were targeted using relatively large quantities of CTA and initiator. A reaction temperature of 80 °C was used. After 24 hrs, the reaction was quenched, and an oligomer concentration of 40% was obtained.

2.4.2.2 Synthesis of DVB/DEGMA, TCDMDA/LMA and EGDMA/LMA copolymers via CTP

All CTP reactions were conducted following the standard synthesis method outline in Section 2.1.2.

CTP of DVB was conducted using DEGMA oligomer as the CTA, with volume ratios of DVB:DEGMA of 1:9, 2:8, 3:7, 4:6 and 5:5 (v/v). Cyclohexanone solvent (1:1 v/v with DVB) was also used. Each mixture was reacted at 150 °C between 10 minutes (5:5 v/v) and 90 minutes (1:9 v/v), before being quenched and precipitated in cold (0 °C) methanol. The resulting precipitate was collected via filtration to provide a brown/white, viscous liquid (colouration due to PhCoBF).

CTP of TCDMDA was conducted using LMA oligomer as the CTA, with a volume ratio of TCDMDA:LMA of 2:8 (v/v). Toluene solvent and 1.0 wt % AIBN initiator was also used. The mixture was reacted at 65 °C for 24 hours, before being quenched and precipitated in cold (0 °C) hexane. The resulting precipitate was collected via filtration to provide a brown/white, viscous liquid (colouration due to PhCoBF).

CTP of EGDMA was conducted using LMA oligomer as the CTA, with volume ratios of EGDMA:LMA of 1:9, 2:8, 3:7, 4:6 and 5:5 (v/v). Toluene and diglyme solvent (1:1 v/v with EGDMA), and 0.5 – 1.0 wt % AIBN initiator was also used. Each mixture was reacted at 80 °C between 5.5 hours (5:5 v/v) and 24 hours (1:9 v/v), before being quenched and precipitated in cold (0 °C) methanol. The resulting precipitate was collected via filtration to provide a brown/white, viscous liquid (colouration due to PhCoBF).

2.5 References

- [1] A. D. Smith *et al.*, “Dielectric properties of free-radical polymerizations: Molecularly symmetrical initiators during thermal decomposition,” *Ind. Eng. Chem. Res.*, vol. 49, no. 4, pp. 1703–1710, 2010.
- [2] Z. Zhou *et al.*, “High-throughput characterization of fluid properties to predict droplet ejection for three-dimensional inkjet printing formulations,” *Addit. Manuf.*, vol. 29, p. 100792, Oct. 2019.

3 Chapter 3: Synthesis and Testing of Novel, Low Viscosity Hyperbranched Lubricant Additives synthesised *via* Chain Transfer Polymerisation with Catalytic, Thiolic and Macromeric Control Agents

This chapter outlines the synthesis of hyperbranched (HB) copolymers of divinyl benzene (DVB) and lauryl methacrylate (LMA) using chain transfer polymerization (CTP), and the subsequent testing, optimisation and scale up of these copolymers. A new polymerization method was investigated for the synthesis of more structured HB copolymers, to optimise copolymer solubility in the target solvent. These copolymers were then subject to extensive tribological testing to investigate their potential for use as low-viscosity friction modifiers/lubricants in engine oils, in collaboration with industrial partner, BP/Castrol. Promising candidates were scaled up and retested to prove reproducibility and industrial viability. New synthesis routes to higher-yielding oil-soluble HB polymers are investigated using thiol control agents. New methods for quality control and future copolymer screening were developed in order to prove the feasibility of the copolymerisation strategy on an industrial scale.

3.1 Introduction & Background

3.1.1 Overview of Lubricants

Since the early 20th century, lubricants have evolved to enable their application performance to match the increasingly stringent demands made of them. For example, the requirements of lubricant materials have extended from providing simple wear reduction and heat transfer in cast-iron machinery, to acting as antioxidants and protective film coatings in modern combustion engines [1], [2].

The primary function of a lubricant is the reduction of friction and wear between moving mechanical parts, which is achieved by providing a fluid film within

the lubricated contact to prevent metal-to-metal contact. The viscosity of the oil is critical in maintaining optimum oil film thickness within acceptable limits. Too low a viscosity means insufficient metal surface separation and increased friction and wear due to metal-to-metal contact. Too high a viscosity means high frictional losses in “churning” the viscous fluid and also poor lubricant flow. As such, two common components of current industrial lubricants are viscosity and friction modifiers. These are added to engine oil to improve the performance of the engine by reducing wear and increasing operational efficiency [3].

3.1.1.1 Friction Modifiers

While the base oil itself is the primary friction modifier, additives are used to further improve fuel economy. Friction modifiers, or boundary lubrication additives, are oil soluble chemicals which are instrumental in reducing friction in key metal-metal contact points. Friction modifiers also help to increase fuel economy, reducing energy losses in the form of heat generated by internal friction, while they also reduce engine wear, pitting, scoring and noise by creating and maintaining boundary films on internal surfaces. Traditionally, friction modifiers are amphiphilic molecules, which contain both a straight-chain hydrocarbon “tail” group and a polar “head” group (See CH1 Sect 1.8) such as esters and natural and synthetic fatty acids [4]. Common head groups include amines, amides, carboxylic acids and phosphoric or phosphonic acids [5]. Alternatively, molybdenum compounds are also extensively used: these form a molybdenum disulphide (MoS_2) deposit on the metal surface, which exhibit a crystal structure that allows sliding and shearing to occur [3], [6]. More recently, the use of MoS_2 nanoparticles has been found to give an ultra-low friction coefficient of 0.04 compared to hexagonal MoS_2 [7], [8]. The final choice of head group is guided by the expected level of pressure in the working environment.

When used as a lubricant additive, the polar head group attaches itself to metal surfaces within the engine, as shown in Figure 3.1, and forms a coating that serves to minimise friction caused by metal-to-metal contact.

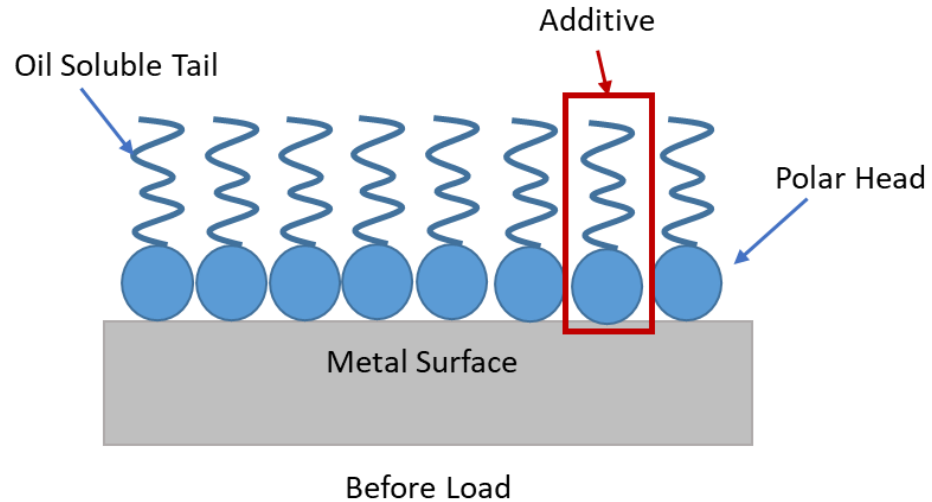


Figure 3.1. A representation of how friction modifiers for protective films on metal surfaces.

The hydrocarbon tail group is key to the oil solubility of the modifier and ensures the film-forming properties of the additive. As long as the frictional contact is light, these molecules provide a cushioning effect when one surface connects with another coated surface. If the contact is heavy, then the molecules are brushed off, eliminating the potential benefit of the additive. If heavier contact is expected, a stronger friction modifier is selected, examples of which are often characterised as anti-wear additives. For example, zinc dialkyldithiophosphate (ZDDP) is a common anti-wear agent, which reacts with the metal surface when the temperature is sufficient, providing sacrificial surface protection. For extreme pressure applications with high loading and metallic contact, the strength of the additive and reaction process must increase further, leading to the use of sulphur-phosphorus based extreme pressure (EP) chemicals. The EP additives form organo-metallic salts on the loaded surfaces, and protect against aggressive surface damage. Phosphorus and sulphur are part of a set of temperature dependent EP additives, which also includes boron and chlorine: the chemical reaction between the additive and the metal surface

is driven by the heat generated by the friction and pressure. Following the reaction, these additives form new compounds such as iron chlorides, iron phosphides and iron sulphides, which produce a chemical film that acts as a barrier to reduce friction, wear and metal scoring [4], [8].

3.1.1.2 Kinematic vs Dynamic Viscosity

The viscosity of a fluid is a measure of its resistance to gradual deformation by shear stress or tensile stress. The shear resistance in a fluid is caused by inter-molecular friction exerted when layers of fluid attempt to slide by one another. There are two related measures of fluid viscosity, dynamic (or absolute) viscosity and kinematic viscosity.

Absolute (dynamic) viscosity (μ) is a measure of internal resistance and is defined as the tangential force per unit area required to move one horizontal plane with respect to another plane at a unit velocity, whilst maintaining a unit distance between the two planes within the fluid. It can be expressed as shown in Equation 3-1:

$$\mu = \frac{\tau}{\gamma} \quad (3-1)$$

where τ is the shearing stress (N/m^2) and γ is the shear rate (s^{-1}). Dynamic viscosity is often expressed using the metric CGS system in units of centipoise (cP) where 1 cP is equivalent to 0.001 N sm^{-2} .

Kinematic viscosity (ν) is the ratio of absolute/dynamic viscosity to density (ρ), and can be obtained by dividing the absolute viscosity of a fluid by the fluid mass density, as outlined in Equation 3-2:

$$v = \frac{\mu}{\rho} \quad (3-2)$$

Commonly, the unit Stoke (St) is used for kinematic viscosity, where 1 St is 1 cm²s⁻¹, or the centiStoke (cSt), where 1 St is 100 cSt.

The viscosity index (VI) of a material is often quoted, which is an arbitrary, unit-less measure of a fluid's change in viscosity relative to temperature change. It is mostly used to characterize the viscosity-temperature behaviour of lubricating oils. The lower the VI, the more the viscosity is affected by changes in temperature. The higher the VI, the more stable the viscosity remains over temperature fluctuations. For oils with VI values of 0-100, the VI is calculated using Equation 3-3:

$$VI = \begin{cases} 100 \frac{L-U}{L-H} & \text{If } VI \leq 100 \\ 100 + \left(\exp\left(\frac{\log H - \log U}{\log Y}\right) - 1 \right) / 0.00715 & \text{If } VI > 100 \end{cases} \quad (3-3)$$

where U is the oil's kinematic viscosity at 40 °C (104 °F), Y is the oil's kinematic viscosity at 100 °C (212 °F), and L and H are the viscosities at 40°C for two hypothetical oils of VI 0 and 100, respectively, having the same viscosity at 100°C as the oil whose VI we are trying to determine. That is, the two oils with viscosity Y at 100°C and a VI of 0 and 100 would have a viscosity of L and H , respectively, at 40°C. These L and H values can be found in tables in ASTM D2270 [9].

3.1.1.3 Viscosity Index Modifiers

Viscosity index modifiers are often high molecular weight linear polymers, which are added to improve the viscosity index of the oil such that the viscosity is less sensitive to temperature changes, as outlined in Figure 3.2.

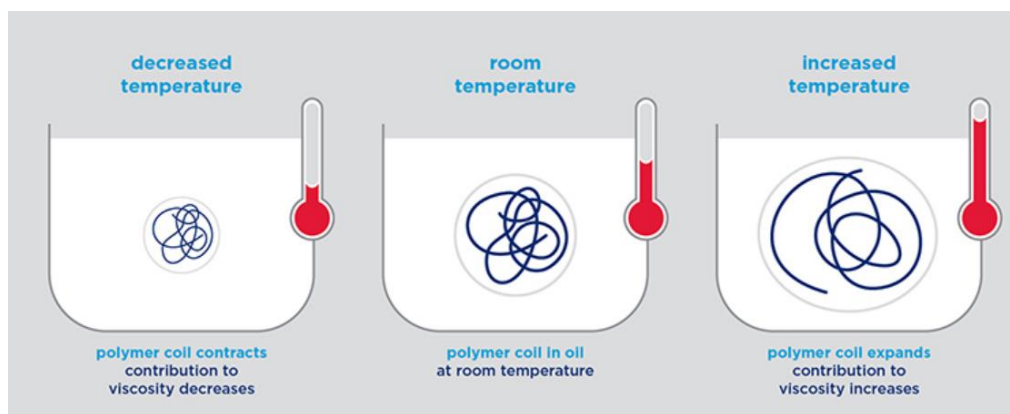


Figure 3.2. An overview of the effect of temperature on the viscosity contribution of polymeric lubricant additives [10].

Mineral oil lubricants become less effective at high temperatures as the high temperature reduces their viscosity and film-forming ability: viscosity modifiers enable this problem to be overcome and thus remove the need for the traditional seasonal oil changes that were required in the past. When viscosity index modifiers are added to low-viscosity oils, they effectively thicken the oil as temperature increases. This is due to the expansion of the polymer which impedes the free movement of the oil more than the smaller coiled oleochemical molecular structures discussed above. At low temperatures, the polymer coil energy is reduced and it contracts, ensuring its contribution to the oils viscosity at low temperatures is small. The thickening impact of the polymer is therefore greater at higher temperatures than low temperatures, leading to the “viscosity index improver” effect [10]. This allows the oil to operate efficiently over a wider range of temperatures. These multi-grade oils enable easier cold cranking and starting, leading to improved fuel efficiency. Commonly used viscosity modifiers are olefin copolymers such as ethylene-propylene copolymers, hydrogenated styrene-diene copolymers and polyalkylmethacrylates [3].

When creating a viscosity index improver, a balance between the thickening efficiency and shear stability of the polymer is important. During routine engine operation and continued use, engine oils are exposed to more extreme shearing mechanism that break down the polymer, reducing the overall oil molecular weight. This can lead to viscosity loss and a subsequent decrease in oil film thickness. In severe cases, this can cause undesired friction and engine wear. The effect of increasing shear is outlined in Figure 3.3.

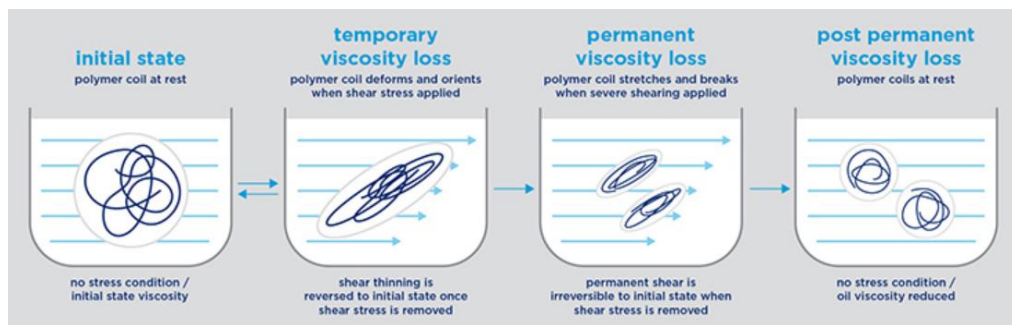


Figure 3.3. Overview of response of polymer to increasing shear regimes and resulting effect on viscosity [10].

Under conditions with no shear or flow, the polymer coil is roughly spherical in shape. As the oil begins to flow, the flexible polymer coil responds to the velocity gradient within the oil and deforms, becoming elongated and aligned in the direction of flow. The distorted coil impedes the oil's flow less than the spherical coil did, thus the oil's observed viscosity falls in what is known as "shear-thinning" behaviour. From this point, if the shear is removed the distorted coil returns to its original shape and the oil viscosity returns to its original value. If the level of shear increases further and becomes too severe, the polymer coil may stretch and break irreversibly, reducing the molecular weight of the oil and leading to permanent viscosity loss [10]. Thus, higher molecular weight polymers typically make better thickeners but tend to be less resistant to mechanical shear. Correspondingly, lower molecular weight polymers are more shear resistant, but do not improve the viscosity index as effectively at higher temperatures and must be used in larger quantities [11].

3.1.1.4 Lubrication Regimes

Lubrication regimes describe the type of lubrication film that is created under specific operating conditions, and these are dependent on the degree of contact between surfaces. There are three primary lubrication regimes: boundary, mixed and hydrodynamic, which may be summarised using a Stribeck curve (see 3.3.4.3), which depicts how the coefficient of friction changes with rolling speed [12].

During boundary lubrication, opposing surfaces meet with little or no oil film separation as shown in Figure 3.4a. Thus, metal-to-metal contact between two sliding surfaces occurs, typically at low speeds. This regime is common during initial start-up or shutdown of some equipment or under heavily loaded conditions. Friction is often highest in this regime, with up to 70 % of wear occurring during start-up/shutdown phases. Protective, anti-wear additives that promote sliding rather than welding of surface asperities (i.e. topographical features on the surface of the metal) prevent damage. These additives may react with the asperities by reacting to the increased

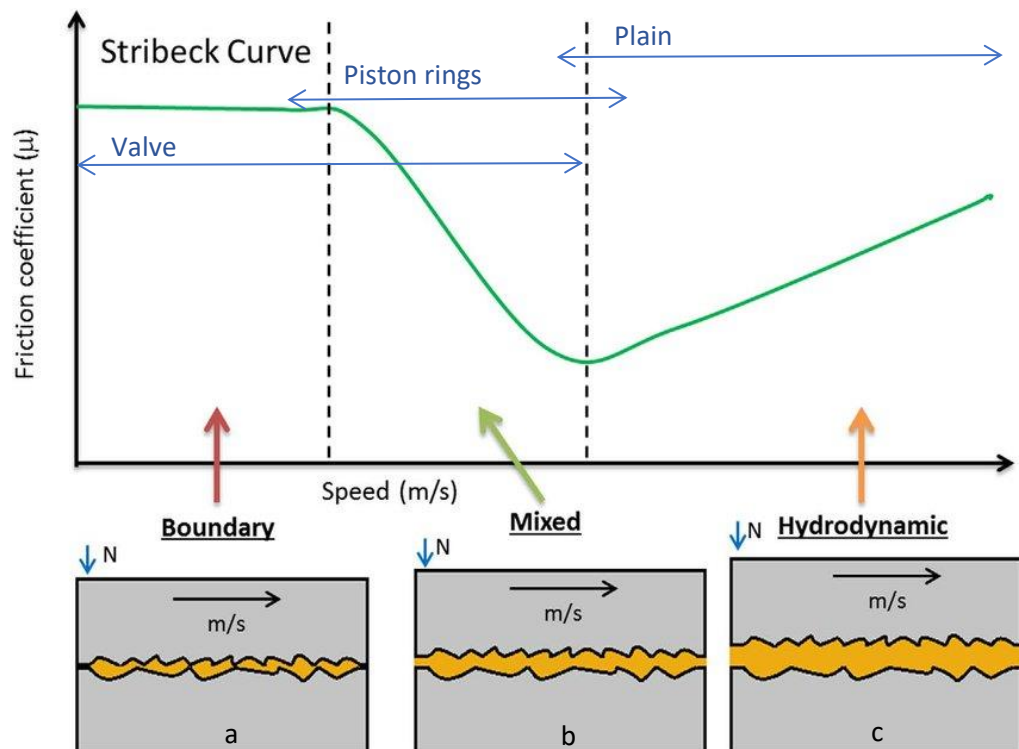


Figure 3.4. Representations of a) boundary, b) mixed and c) hydrodynamic lubrication regimes, which may occur simultaneously in engines. [12]

pressure and temperature of contact and forming an altered ductile film on the metal surface. The film then acts sacrificially, being worn away instead of the metal surface. However, obtaining the correct viscosity in this regime is vital. Too low a viscosity will not keep the metal surfaces separated, while too high a viscosity will increase the oil's molecular friction, causing internal oil shearing and, in turn, increasing operational temperatures and energy loss.

During hydrodynamic (HD) lubrication, moving parts are completely separated by a viscous fluid film, as shown in Figure 3.4c. This regime typically occurs at high speeds between sliding surfaces, after the speeds and loads are such that a wedge of oil has formed between the two surfaces. There is little risk of asperity contact, thus this is a desirable condition to avoid wear. Any remaining friction is located within the lubricant itself, as the molecular structures of the oil slide past each other during operation. For HD lubrication to be effective, the oil's viscosity must be such that the HD condition is maintained under every operating condition, i.e. over the full range of expected operational temperatures and speeds. If the oil's viscosity is too high, the internal drag will reduce the operating efficiency and increase temperatures.

Meanwhile, mixed lubrication occurs during the transition from low to high-speed operation when boundary and hydrodynamic conditions coincide. As sliding speeds increase, boundary lubrication is reduced, creating a wedge of lubricant film between the two surfaces, as shown in Figure 3.4b. The potential for asperity contact is reduced and film thickness is increased, while the friction coefficient drops dramatically to the condition known as mixed lubrication. In this regime, the asperities of boundary surfaces will extend through the film and occasionally come into contact.

Another type of lubrication regime is elastohydrodynamic (EHD): this is similar to HD, however EHD lubrication conditions occur when a rolling motion exists between the moving elements and the contact zone has a low degree of conformity, such as between a ball and raceway (i.e. the metal plate in contact with the rolling element). This leads to very small contact areas which, as a result of their size, experience high pressures. As the oil enters the contact zone between the ball and raceway, the oil's pressure rises sharply, which in turn increases the oil's viscosity and load-holding ability. This concentrated load will slightly deform the metal of the rolling elements in the contact zone: the deformation only occurs at the contact zone and the metal elastically returns to its normal form as the rotation continues. Incorrect or abnormal operating temperatures will affect the viscosity of the oil and hence interfere with the formation of the EHD lubricating film. Such films are often of the order of 1 micron, though EHD lubrication (EHL) is considered to operate on a full fluid film (as with HD) and so asperities do not come into contact.

3.1.2 Hyperbranched (HB) Polymers as Lubricants

Straight-chain/linear polymers, such as these those mentioned above for use as both friction and viscosity modification, inherently demonstrate strong, attractive intermolecular interactions. While this is a desirable property for viscosity modifiers at high temperature, this is not usually beneficial for friction modifiers. This is because it can limit the minimum oil viscosity that can be achieved at low temperatures due to the ability of the chains to pack together efficiently.

These inter-chain reactions may be reduced through the use of non-linear polymer structures. Such structures, sometimes known as architectural polymers, include comb-graft, star, hyperbranched and dendrimeric polymers [13]–[15]. Of these, hyperbranched and dendrimeric polymers have been shown to exhibit the

greatest difference from linear materials in terms of viscosity build that is observed when they are added to liquid media [16]. It has been hypothesised that the high level of branching within these structures reduces inter-chain reactions significantly, resulting in what is referred to as a “globular” molecular structure.

Hyperbranched (HB) polymers can be synthesised much more rapidly, i.e. in hours rather than weeks, and hence much more cheaply than dendrimers (see Chapter 1, Section 1.7 for more discussion of dendrimers). This synthesis can be achieved using relatively inexpensive, simple one-pot methods and a wide variety of industrially available monomers are applicable [17]–[19]. Meanwhile, these methods produce structures similar to those of dendrimers, though they are far less well defined. This gives them the potential to act as replacements or substitutes for dendrimers, delivering the same performance and applications [17] at much reduced cost.

During the synthesis of hyperbranched polymers, care must be taken to avoid cross-linking: this leads to the formation of an insoluble gel [17], rather than the desired solvent-soluble HB material. This coupling can occur in conventional free radical polymerisation even at very dilute monomer concentrations ($\ll 10\%$ monomer) and at low monomer conversion ($< 20\%$) [20].

Recently, researchers including Guan, Sherrington, Haddleton and Irvine have reported the use of catalytic chain transfer polymerisation (CCTP, see Chapter 1, Section 1.6.3) to synthesise HB polymers [20]–[23]. CCTP is an industrially viable polymerisation control strategy, first reported in the 1980’s, for the control of the free radical polymerisation of mono-functional vinylic monomers. Typically, a cobalt organometallic complex is used as the chain transfer agent, (CTA). These species are catalytic in nature, which means that very low molecular weight polymer (e.g.

dimers/trimers) can be produced using only very low (i.e. parts per million (ppm)) quantities of CTA with some monomer types [24] (see Chapter 1, Section 1.7.2 for more details). Additionally, any CCT-terminated methacrylate polymer has vinyl group as the terminal group, resulting in an increase in concentration of vinyl chain ends compared to other common CTAs, such as thiols, leaving room for post-modification/polymerisation [20].

Additionally, low molecular weight CCTP oligomers of methacrylate monomer have been demonstrated to exhibit chain transfer control of free radical polymerisations of other vinyl monomer types *via* a β -scission mechanism. Due to the very high transfer constants associated with CCTP catalysts, it is relatively simple to prepare macromonomers of very low molecular weight, i.e. down to dimers, trimers etc. The terminal vinyl group in these macromonomers makes them susceptible to radical addition to form macromonomer-ended polymer radicals. This radical can undergo a β -scission reaction in addition to normal propagation and termination (see Chapter 1, Section 1.6.3.1 and 1.4). The result is that the ultimate unit of the macromonomer terminates the propagating radical (i.e. the polymer chain) and the remaining radical segment of the macromer is released as a new radical free to initiate new polymer chains. Hence, the macromer acts as a CTA. Consequently, this method of chain transfer leads to a fragment of the macromeric CTA becoming an intrinsic part of the product polymer structure, as with all other stoichiometric CTAs [25], see Chapter 1, Section 1.6.1. As when thiol molecules are employed as control agents, this allows tailoring of the HB polymer structure and properties, as the majority of these fragments will proliferate around the outside of the globular HB structure when chain ends are terminated. This results in the formation of a structure with a “core” composed of the chosen di-functional monomer and a “corona” composed of the chosen mono-functional monomer.

Importantly for lubricant applications, HB polymers, whether synthesised using catalytic, thiolic or macromeric control agents, cannot efficiently pack and so exhibit intrinsically low viscosities, while also possessing the high molecular weights common to currently used viscosity modifiers [26]. Their globular structures should also enable improved shear resistance compared to linear polymers, while their many functionalisable chain ends may allow improved interaction at the surfaces within the engine. Thus, they are an exciting new architecture to investigate as lubricant additives.

3.1.3 Styrene and Divinyl Benzene

Styrene, otherwise known as ethylbenzene or vinylbenzene, is a naturally occurring monomer: its polymerised form, polystyrene, was first discovered in 1839 by Eduard Simon, who found that the oily styrene monomer had thickened over time [27]. However, this process was not recognised as polymerisation until 1866 [28], and it was 80 years after that when Herman Staudinger discovered that heating styrene initiates the polymerisation process [29]. Since then, polystyrene has grown in popularity worldwide, and it often copolymerised to make it less brittle, widening its potential applications further [30].

Divinylbenzene (DVB) is a commercially produced monomer which is related to styrene by the addition of another vinyl group. It is typically available as a molecular mixture defined as DVB 80%, indicating it is actually made up of 80% di-functional para- and meta-DVB and 20% mono-functional para- and meta-ethylstyrene, as illustrated in Figure 3.5.

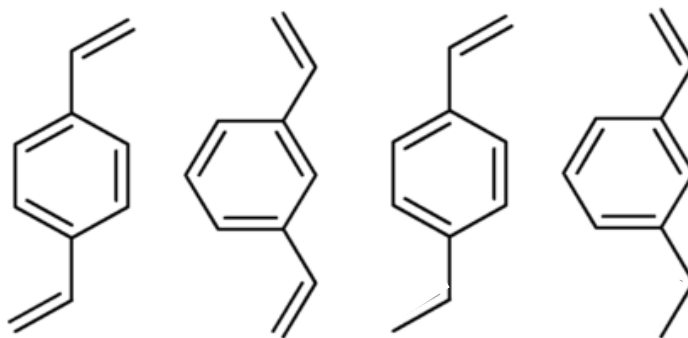


Figure 3.5. Structure of (left to right) *para*-DVB, *meta*-DVB, *para*-styrene and *meta*-styrene [33].

However, the addition of a second vinyl group means that when this monomer is polymerised, its di-functional vinyl groups act as branching points, allowing it to form branched, and hyperbranched, polymers, in contrast to linear polystyrene.

DVB, like styrene, undergoes thermal self-initiation (see Chapter 1, Section 1.4), the advantage of which is that no conventional initiators, which may be toxic, explosive and expensive, are required. However, the reaction temperature must be higher than for conventional initiators to ensure that the reactions defined by the Mayo mechanism proceed at a rate which is sufficient to allow the polymerisation to be both stable and repeatable (batch-to-batch). This also has the fortunate side-effect of increasing the rate of propagation, thus reducing the overall reaction time.

In 2012, work was conducted by Irvine *et al.* into the synthesis of styrenyl hyperbranched polymers through the application of CCTP to control polymerisations which use DVB as the di-functional monomer. This demonstrated that the synthesis of HB DVB “homopolymers” is possible in under one hour using high reaction temperatures (150°C) and auto-initiation, provided the high chain transfer coefficient of bis[(difluoroboryl)diphenylglyoximato]cobalt-(II) (or PhCoBF) was exploited to delay gelation and the monomer conversion was limited to ~50%. It was also determined that the exact composition of the DVB mixture used affects the polymerisation rate greatly, due to the varying monomer reactivities [31].

Hyperbranched DVB (HB DVB) contains a high density of functional, reactive vinyl end groups. Copolymerisation of DVB using CCTP with other monomers that are capable of interacting with vinyl groups and behaving as CTAs means that HB-DVB can be used as a 'backbone' or 'skeleton', where each chain is terminated by the alternate monomer. Thus, HB DVB can be functionalised to enhance its potential range of applications, which is determined by the properties of the monomer used for copolymerisation.

3.1.4 Dielectric Monitoring for Batch Repeatability

Traditional free radical polymer synthesis (FRP) is a well understood chemistry, and from an engineering perspective is a well proven 'technology'. Many processes have been successfully deployed on industrial scales and been commercial successes. However, more recently a number of controlled polymerisation (CP) techniques which allow finer control over many aspects of the polymerisation and resulting polymer. These characteristics include the molecular architecture, molecular weight and polydispersity. CCTP is typically regarded as one of these techniques, for the free radical polymerisation of the specific monomer types discussed earlier. For these reagents, adopting CCTP enables the synthesis of three-dimensional polymer structures such as graft, star and hyperbranched polymers.

However, despite their popularity in academia, very few CP methods have been successfully scaled up to a commercial level. This is due to the requirement for stringent process conditions, lack of availability of control agents and the need for accurate process monitoring to follow the reaction's progress. These difficulties may be solved using dielectric property measurements to monitor the degree of cure and molecular weight of polymers, either continuously during synthesis or batch to batch as has been previously reported for linear polymers [32]–[37].

However, first, it must be determined whether dielectric property measurement can be effectively used in characterising these novel HB polymers empirically. In particular, it needs to be demonstrated whether dielectric analysis is more accurate, cheaper and industrially applicable than current monitoring techniques such as gel permeation chromatography/size exclusion chromatography (see Chapter 1 Section 1.9.1).

3.1.5 Liquid Handler Screening

When new copolymer formulations are developed for engine additives, they must undergo performance testing. At present, the lubricant polymers produced in this work are tested on a variety of large-scale, very specialised pieces of apparatus. As a result, they tend to be sited at the lubricant company's testing facility (such as the sponsor of this project). For example, the properties typically evaluated include film formation, shear and kinematic viscosity. These tests require large quantities of these new copolymers to be synthesised, often putting a strain on the ability of the academic laboratory to produce enough material to allow the evaluation to be conducted. Furthermore, typically the testing is slow, requiring specialist rigs and a large amount of manpower.

Therefore, it would be highly beneficial to develop a lab-scale screening process for new copolymer formulations. One crucial property for the lubricant materials discussed in this work is their viscosity. The hypothesis of this section of study is that the target HB polymers should not drastically increase the viscosity of the oil when added in low concentrations, unlike linear polymers, due to their decreased hydrodynamic volumes and decreased entanglement. However, the extent of the observed change in viscosity will be dependent on the degree of branching achieved in each new HB polymer, which may be dependent on the

monomer or reaction conditions used. If the viscosity profile of each new copolymer can be quickly determined using only a few milligrams of polymer, this would help accelerate the development of new, suitable copolymers in future work.

3.2 Aims and Objectives

3.2.1 Aims

- To synthesise and test the tribological properties of novel hyperbranched polymers in collaboration with BP/Castrol, to evaluate whether they can be used to deliver high levels of wear protection, friction reduction and/or improved low temperature oil fluidity.
- To investigate methods of enabling the large-scale, efficient production and monitoring of these HB polymers, to improve their economic viability.

3.2.2 Objectives

- CCTP will be used to synthesise macromers of LMA, confirmed using GPC/NMR analysis.
- The LMA macromers will be used as control agents, in both their crude and purified forms, for the polymerisation of DVB, to synthesise HB polymers of two architectures (known as semi-block and block, respectively) with room-temperature solubility in a hydrocarbon base oil on a 5 mL scale.
- Kinematic viscosity testing at 40 and 100 °C, dynamic viscosity testing on a Cold Crank Simulator at -35 °C, and Ultra High Shear Viscometry will be used to evaluate the viscosity-modifying properties of the HB polymers.
- Film formation/friction reduction properties of the HB polymers across a range of lubrication regimes will be tested using a Mini Traction Machine and an Elastohydrodynamic Rig.
- The mechanical performance of the two HB polymer architectures will be evaluated by comparing to the performance of a linear ethylene-propylene copolymer currently used as an industrial standard, as well as to each other.

- The HB polymer architecture which performs best in the above testing will be synthesised on a larger (50 mL) scale.
- The 50 mL batch will undergo the same tribological testing as the 5mL batch for comparison, to determine the scalability and batch-to-batch reproducibility of the synthesis methodology.
- Thiol (DDM) mediated-chain transfer polymerisation, with DDM concentrations in the range 0-65 mol%, will be used to synthesise oil soluble HB DVB, with higher yields than the macromer-control method.
- The DDM-controlled HB DVB polymers will also undergo tribological testing to enable their performance to be compared to the lower-yielding HB DVB/LMA polymer.
- The dielectric constant and loss of semi-block HB DVB/LMA polymer samples of different molecular weights and copolymer ratios (including 1:9 and 2:8 v/v) will be measured *via* a cavity perturbation method and compared to traditional SEC analysis, to investigate the potential for the use of dielectric analysis as an in-line monitoring method or method of ensuring quality control.
- A liquid handling machine will be used to measure the viscosity of a small (2 mL) volume of 2:8 DVB/LMA semi-block copolymer in a high-throughput manner:
- The viscosity data obtained from the liquid handler will be compared to that obtained from previous Kinematic Viscosity testing to evaluate whether the liquid handler may be used as a high-throughput screening method for future HB polymer formulations.

3.3 Results and Discussion

3.3.1 Synthesis of Oil Soluble Hyperbranched Polymers

In this work, a hyperbranched (HB) polymer capable of being delivered as part of a liquid lubricant formulation and forming protective films on hot engine surfaces was desired.

Hyperbranched divinylbenzene (HB-DVB) homopolymers and copolymers have previously exhibited high solvent solubility and the potential to cross-link *in-situ* upon hot surfaces to produce protective films [38]–[43]. Thus, in work conducted within the group (Dr Amy Stimpson), DVB was chosen as the di-functional monomer for use in the development of HB polymer lubricant additives. However, an initial inspection of the HB-DVB solubility identified that HB-DVB was essentially insoluble in the solvent of interest, Durasyn®164 hydrocarbon base oil (also known as PA04) [44], which was attributed to the Poly(DVB)s highly aromatic nature. Hence, DVB monomer (Figure 3.6a) was initially directly copolymerised *via* CCTP with a range of mono-olefin acrylate/methacrylate monomers (structures shown in Figure 3.6b-e) with long pendant alkyl chains in an attempt to improve the solubility in the base oil of the subsequent HB copolymers.

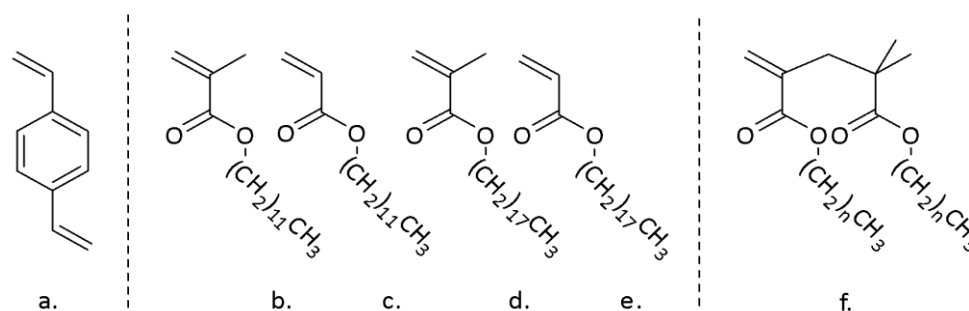


Figure 3.6. Structures of materials used in synthesising functional HB polymers. a. DVB b. lauryl methacrylate c. lauryl acrylate d. stearyl methacrylate e. stearyl acrylate f. dimer made from lauryl/stearyl methacrylate.

It was observed that using a ratio of either 1:9 or 2:8 (v/v) of DVB:mono-olefin monomer produced oil soluble hyperbranched copolymers with identifiable gel points. As these copolymers were the result of direct copolymerisation of DVB and the chosen alkyl containing reagent, they were proposed to be statistical/random copolymers, with the structure having a purely random mix of DVB and mono-functional monomer: a representation of this structure is shown in Figure 3.7a.

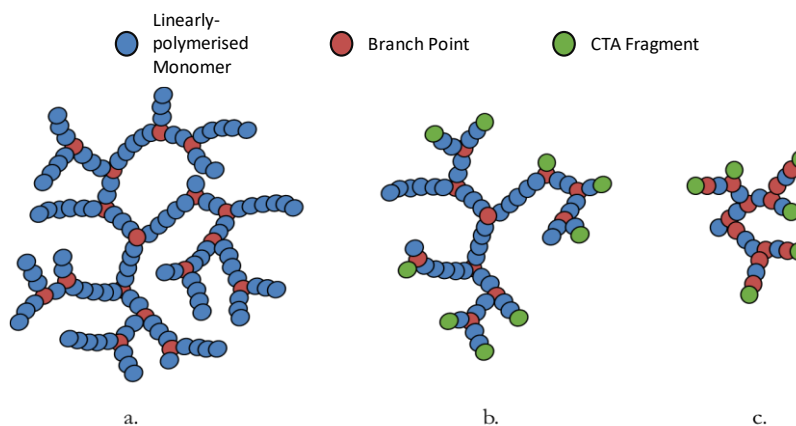


Figure 3.7. Structures of the a. random, b. semi-block and c. block, HB copolymers.

The copolymer synthesised from DVB and lauryl methacrylate (LMA, Figure 3.6b) was chosen as the best candidate for further study. This was because this copolymer demonstrated both the greatest level of solubility in the base oil, fully dissolving in the Durasyn®164 at 50 °C (Table 3.1), and also the physical form that the reagents and polymers exhibited resulted in the greatest relative ease in processing when compared to copolymers of DVB and the species c – e in Figure 3.6. Indeed, the low melting point of LMA, -7 °C, was the key reason that this copolymer was subsequently chosen for further study, as it would require minimal additional processing to transport and deliver in an industrial setting. Correspondingly, the high melting points of 18-20 °C for stearyl methacrylate (SMA, Figure 3.6d) and 32-34 °C for stearyl acrylate (SA, Figure 3.6e) meant that lengthy mixing times and heating would be required to deliver these reactants as homogenous liquid mixtures, which is undesirable from an industrial view-point.

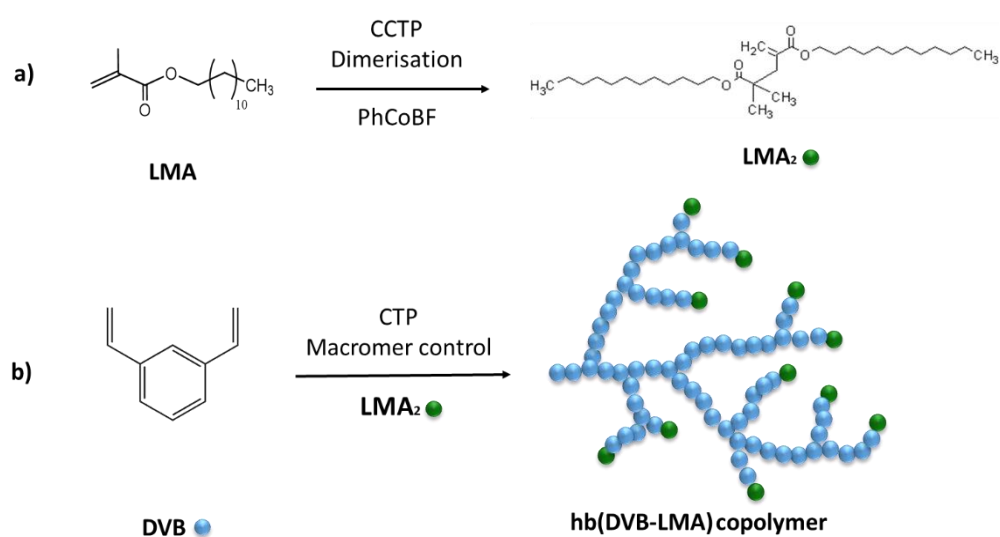
Table 3.1. Solvation properties of random structure co-polymers in base oil.

Co-monomer	Solvation Temperature (°C)	Appearance in Solution
SA	70	Colloidal Suspension
SMA	70	Clear Soln.
LA ^a	-	-
LMA	50	Clear Soln.

^a. Species was unable to be isolated from the reaction mixture.

However, whilst the monomer combination of DVB and LMA was found to give the best solubility of those evaluated, it was observed that the direct CCT copolymerisation of DVB and LMA was inefficient. Thus, insufficient levels of LMA were being incorporated into the random structure, which limited the achievable solubility of the final copolymer, as demonstrated by the heating required to fully solvate the polymer.

In order to improve both the efficiency of copolymerisation and the achievable level of control over the copolymer structure, subsequent work within our research group (Dr Richard Moon) focussed on a new copolymerisation strategy. The new method centred on first producing low molecular weight oligomers of LMA from the pure monomer, by employing a high concentration of the CCTP catalytic chain transfer agent (catalytic CTA), PhCoBF as shown in Scheme 3-1a. This strategy involved adding sufficient concentration of CTA to reduce the molecular weight of the resultant polymers to just 2-3 units in length. At this length, the polymers were capable of acting as stoichiometric CTA in its own right.



Scheme 3-1. Idealised representation of a) LMA monomer undergoing CCTP to produce LMA dimer; b) LMA dimer being used to control the polymerisation of DVB monomer to produce a hyperbranched structure with a largely DVB "core" and LMA "corona" for enhanced base oil solubility.

In this way, a solution of LMA monomer/dimer/trimer species, with an average oligomer yield of ~40 %, was achieved, with the results confirmed through NMR analysis, an example of which is shown in Figure 3.8.

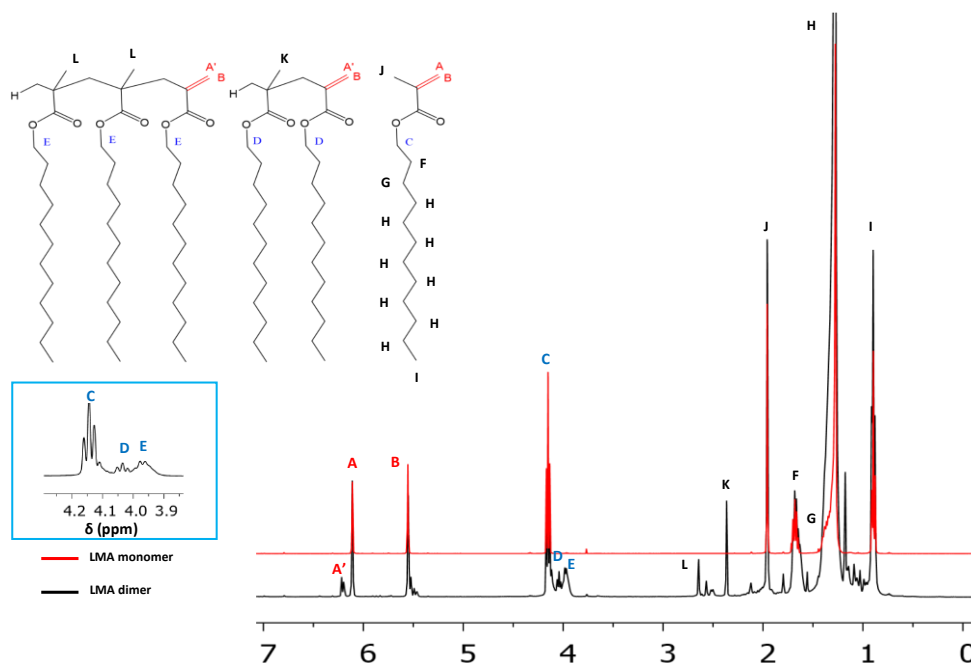
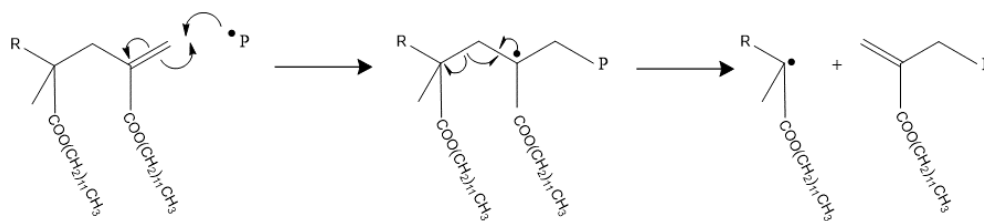


Figure 3.8. A typical ^1H NMR of LMA monomer (red trace) and LMA oligomeric mixture (black trace) synthesised via CCTP. Characteristic vinyl peaks (A, A', B) can be observed between $\delta = 5.6$ and 6.4 ppm. The peak at $\delta = 4.15$ ppm due to the ester linkage of the monomer (C) can be seen in the LMA monomer spectrum. In the oligomer spectrum, this peak can also be observed, in addition to new peaks at $\delta = 4.03$ and 3.97 ppm, which originate from the dimer (D) and trimer (E) species respectively, due to the change in environment experienced by the ester protons within these macromers, indicating conversion has been achieved. This region of the spectrum has been expanded in the blue box to enable these peaks to be observed more clearly.

Comparison of the ^1H NMR of the LMA monomer (red trace) and oligomeric solution (blue trace) reveals the growth of new oligomeric ester peaks at $\delta = 4.03$ and 3.97 ppm, which are highlighted in the expansion in Figure 3.8. The oligomer peaks appear at lower shifts due to the increased shielding the “backbone” of the oligomer provides compared to the monomer. Comparing the intensity of the oligomer peaks to the monomer peak at $\delta = 4.15$ ppm, an estimate of the conversion was determined.

As stated, the dimer/trimer species are capable of acting as stoichiometric chain transfer agents in their own right, and so have the potential to simultaneously control the polymerisation of DVB to produce HB-DVB and to introduce the hydrocarbyl character required for this work, as outlined in Scheme 3-1b. This is

because the oligomer species splits *via* a β -scission reaction as outlined in Scheme 1-5 (see Section 3.1.2) which leaves the growing polymer chain terminated with a segment of the LMA oligomer plus an olefin end group, thus incorporating the lauryl functionality into the polymer.



Scheme 3-2. Representation of the β -scission mechanism for a dimer, where R is a thermal initiator fragment and *P is a propagating polymer chain. The propagating polymer is terminated with a fragment of the dimer and a vinyl group, while the radical segment of the dimer is released as new propagating radical.

Meanwhile, the other segment of the oligomer initiates the growth of another polymer chain, again incorporating the lauryl functionality into the HB polymer. This approach leads to a high density of lauryl functionality proliferated around the outside of each HB polymer due to the high density of chain ends in HB polymers.

Once the LMA oligomer solutions had been synthesised, they were used in two different ways to make hyperbranched copolymers. Firstly, to produce what were referred to as “semi-block” structures (Figure 3.7b), the products of the CCTP reaction were used to control the DVB polymerisation in a ratio of 2:8 DVB:LMA oligomers (v/v) without any further purification. The term “semi-block” refers to the fact that, through the use of the monomer/dimer/trimer solution, some of the polymer end groups will be terminated with lauryl-functionalised olefin groups, but that there will also be some LMA monomer present which will be involved in random structure polymerisation. This means that the morphology of the HB polymer will also contain some random polymer character.

Secondly, “block” structures (Figure 3.7c) were synthesised by reacting DVB with a solution of the LMA CCTP oligomer products that had been purified *via* distillation, in order to reduce the LMA monomer concentration in the solution from 60 % to 19 %. This resulted in a significantly increased concentration of the dimer/trimer chain transfer agent. Consequently, there was a higher probability of the HB polymer end groups being terminated with the LMA CTA fragment, resulting in a greater number of the terminal groups on the block HB copolymer being these olefin functionalised groups and in much reduced/no random character being present.

Subsequent testing demonstrated that both the semi-block and block copolymers were fully soluble in the PA04 base oil at room temperature, indicating the successful incorporation of LMA. Furthermore, since the copolymers synthesised *via* direct CCTP required heating to 56 °C to achieve full solubility in the base oil, this indicated that increased solubility was achieved when using the LMA oligomer as the CTA compared, which indicated improved LMA incorporation had been achieved. As a general procedure, all HB polymers were synthesised until the gel point of the reaction was reached, then a repeat reaction was performed which was quenched at least 5 minutes prior to the identified gel point, and the polymer was then precipitated. The results of these reactions are summarised in Table 3.2.

Table 3.2. Yield and molecular weight data of HB DVB-LMA (2:8 v/v) copolymers of random, semi-block and block structures.

Entry	Structure	Crude Yield % ^a	M _n ^b (kDa)	Đ ^b
1	Random	53	3644	4.9
2	Semi-Block	66	37062	102.7
3	Block	65	9815	118.1

^a Determined gravimetrically. ^b Determined *via* gel permeation chromatography.

Furthermore, an example GPC trace for a semi-block HB polymer product is shown in Figure 3.9.

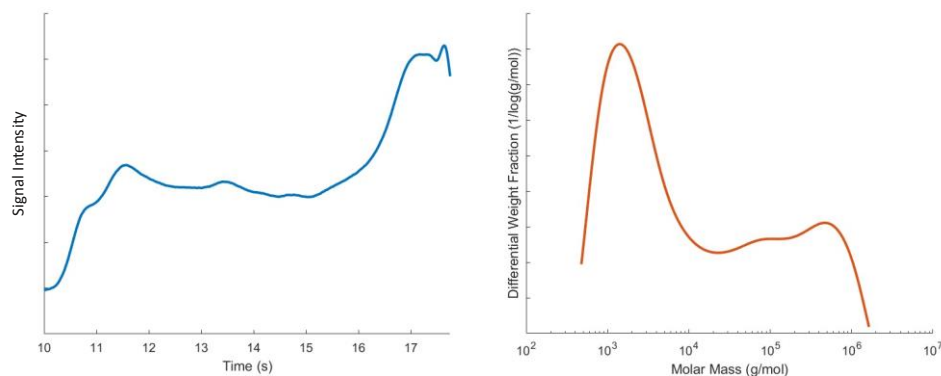


Figure 3.9. SEC traces of DVB-LMA homopolymer, plotted against retention time and molar mass to illustrate the broad peaks obtained, which are characteristic of HB polymers.

The crude yield, i.e. where no further purification methods have been applied post reaction, of the polymer is reported rather than that of the pure polymer due to difficulties drying the copolymers and to give an overall indication of the efficiency of the reaction. This is because all the polymers synthesised here exhibited a glass transition point (T_g) below room temperature. The T_g for a polymer indicates the temperature around which the polymer changes from a rigid, “glassy” material to a viscous or rubbery state as the temperature is increased. As such, the precipitation product was in its viscous form and could not be completely separated from the anti-solvent without risk of cross-linking the polymer collected, which would lead to erroneously high yield values.

From the data in Table 3.2, it was apparent that these reactions all demonstrated a high crude yield compared to other HB reactions in the literature [21], [45]–[48], and that sufficient material could be generated to go on to application testing. The lower molecular weight (MW) of the block structure compared to the semi-block was attributed to the higher concentration of the CTA moieties in the

distilled reagent mixture used for the block structure, which resulted in more chain transfer, thus decreasing the MW of the polymers.

The polydispersity value of the random polymer was observed to be the lowest at $\bar{D} = 4.9$, while the semi-block and block copolymers have dispersity values of \bar{D} greater than 100. The dispersity value for the random copolymer was higher than would be expected for a standard free radical polymerisation, which would not be expected to exceed $\bar{D} = 1.2$. It is likely that the random reaction was in the early stages of hyper branching when the reaction was quenched due to the highly efficient nature of the control agent used, which resulted in very short inter-branch distances. In addition to this early-stage termination, the expected polymer retardation associated with the use of PhCoBF was also thought to contribute to both the lower dispersity and the lower yield of the random copolymer compared to the semi-block and block copolymers. The high values for the dispersity displayed by the semi-block and block copolymers were characteristic of HB polymers, which do not necessarily exhibit a proportional relationship between their hydrodynamic volume and MW due to their non-linear nature [49]. Equally, HB polymers do not interact with the GPC columns in the same manner as a linear polymer due to both their branched structures and the high functional group densities, factors which also contribute to elongated peak areas, as seen in Figure 3.9, and high dispersity values. As a result, the MW values obtained for hyperbranched polymers using SEC must be treated with caution. They should largely be used for comparison of similar polymers and verification of hyperbranching, rather than as absolute MW values. More accurate values may be achieved by combining GPC/SEC with viscometry, however, this data was unfortunately unavailable here.

3.3.2 Application Testing of Controlled Morphology Hyperbranched Polymers

The semi-block and block polymers described above were subjected to various application tests by BP/Castrol to determine their suitability and performance as lubricant additives. Testing was conducted by technicians at BP/Castrol, all analysis and interpretation of the results were conducted by the author. First, their kinematic viscosities were determined, with a view to understanding whether these polymeric additives may be used as viscosity modifiers. Further tribological tests were then conducted to analyse the performance of these polymers with regard to film formation and wear prevention across a range of lubrication regimes.

3.3.2.1 Viscosity Testing

Hyperbranched semi-block and block copolymer and a standard linear ethylene-propylene (EP) copolymer were dissolved in base oil at concentrations of 0.0, 0.25, 0.50, 1.0, and 5.0 wt%, and 0.0, 0.13, 0.25, 0.38 and 0.63 wt%, respectively.

The kinematic viscosities, in centistokes (cSt), of these solutions were recorded at both 40 °C and 100 °C, and this data is shown in Figure 3.10. Centistokes are used as this is the ASTM standard unit for kinematic viscosity measurements within the industry, where $1 \text{ cSt} = 1 \text{ mm}^2 \text{ s}^{-1}$.

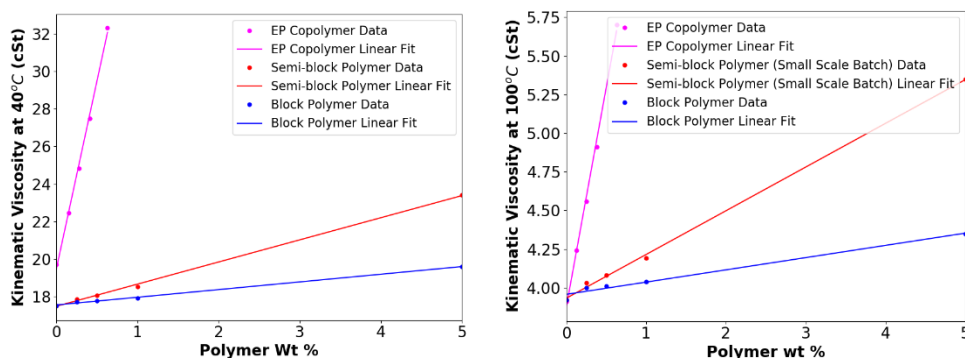


Figure 3.10. Plot of the change in viscosity of both linear and HB polymer/base-oil solution, measured at 40 °C (left) and 100 °C (right), where the EP copolymer (pink) is the current commercial linear polymer used in industrial formulations. The solid lines represent linear best fits to the data.

It was apparent that the viscosity for each solution increased as the concentration of polymer increased, with the viscosity for the standard linear EP copolymer increasing at a significantly greater rate than that of either HB polymer. This was attributed to the branched/globular structure of the HB polymer, which due to the polymer extending from a central core was much more tightly compacted and, as such, less easily penetrated by solvent than the linear EP copolymer. This resulted in a lower hydrodynamic volume for the HB polymer, compared to the linear polymer, and produced a lower increase in viscosity as the concentration of the polymer was increased. Additionally, the overall magnitude of the viscosity was observed to be lower at 100 °C than at 40 °C as expected, due to the temperature-induced thinning of the solution.

It was also clear from Figure 3.10 that the increasing viscosity trend within the HB variations followed the molecular weight of the polymers produced, as the highest molecular weight semi-block structure exhibited a higher viscosity than the lower molecular weight block structure at the same concentration. However, even the highest molecular weight HB polymer, when included into the formulation at a 5 wt % concentration, produced a significantly lower viscosity increase than was observed for the linear copolymer at one fifth the concentration. This suggested that significantly higher concentrations of the HB polymer may be added to an oil formulation, compared to the linear formulation, before the viscosity is significantly affected at working engine temperatures. It also suggested that polymers of this architecture cannot be used as viscosity modifiers at the usual loadings, which was an application considered initially for these polymers, due to their reduced impact on the solution viscosity.

The HB polymers were also tested on the Cold Cranking Simulator (CCS), which simulates engine start-up conditions: the results are shown in Figure 3.11. Here centipoise (cP) are used, as these are the ASTM standard units of dynamic viscosity, where 1 cP = 1 mPa s. Centipoise are related to centistokes unit used earlier for kinematic viscosity measurements by the density of the medium (see Section 3.1.1.2, Equation 3.2).

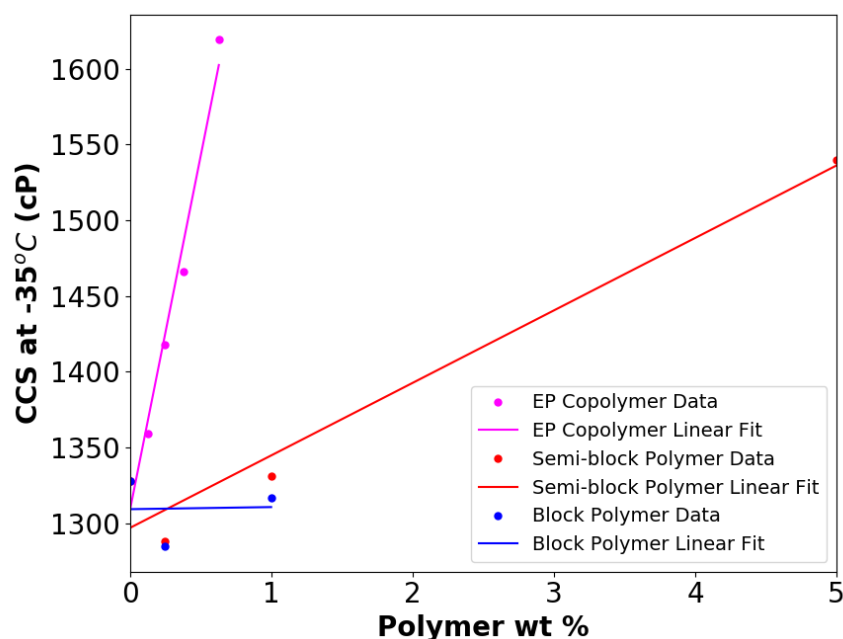


Figure 3.11. Plot of the change in viscosities of both linear and HB polymer/base oil solution measured in the Cold Cranking Simulator at $-35\text{ }^{\circ}\text{C}$, where the EP copolymer (pink) is the current commercial linear polymer used in industrial formulations. The solid lines represent linear best fits to the data.

Similar behaviour to that seen at 40 and 100 $^{\circ}\text{C}$ was observed for the semi-block polymer, with the viscosity of the polymer-oil solution increasing as the concentration of polymer increased. Too few data points could be collected for the block copolymer to draw meaningful conclusions regarding the trend with increasing concentration. However, both HB polymers were seen to cause insignificant (<500 cP) increase in base oil viscosity below 1 wt% loading. This was a much smaller increase than caused by the linear EP copolymer at the same loading, and even caused the oil viscosity to decrease below the unloaded value at 0.25 wt% loading. This

indicated that the HB polymers did not adversely affect the performance of the engine at low temperatures. This was attributed to a large reduction in the hydrodynamic volume of the HB polymers at these temperatures.

However, due to their reduced impact on the viscosity index of the base oil at 40 and 100 °C, these polymers would not be suitable for use solely as viscosity modifiers. Hence, an alternative application for these low viscosity polymers was considered, namely friction modifiers *via* the formation of surface films.

3.3.2.2 Film Formation Testing

Copolymer solutions in base oil were investigated in order to determine their ability to form surface films. This was conducted using a mini-traction machine (MTM), a schematic of which is shown in Figure 3.12.

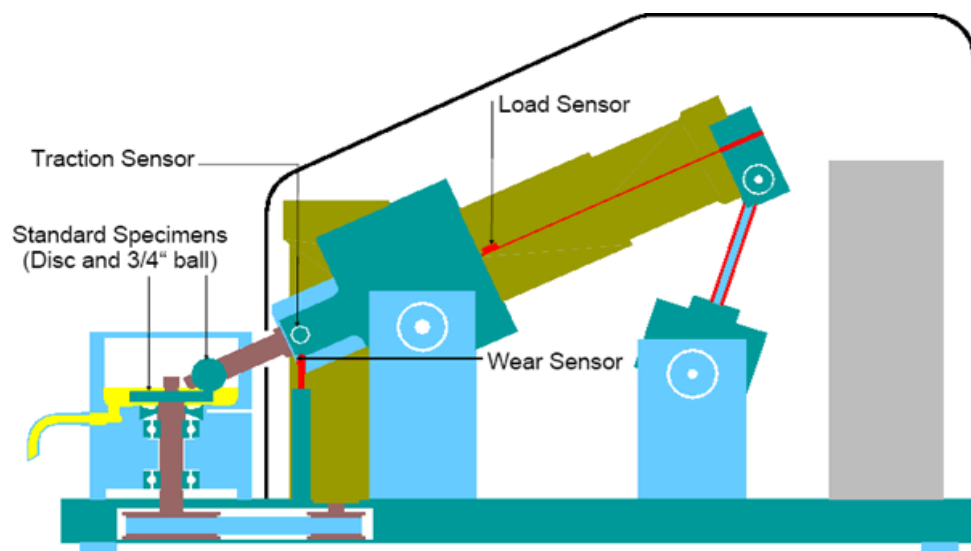


Figure 3.12. Schematic of MTM machine, courtesy of BP/Castrol.

Interferometry images of the wear scar that developed between a rotating steel ball and disk were taken both before and after Stribeck curves were measured at 60, 90 and 120 °C. These images provided a measurement of the thickness of the film between the surfaces, as well as an indication of the level of wear between the two surfaces. The lubricant film thickness at any point in the image can be accurately

calculated by measuring the wavelength of light at that point. Figure 3.13 shows the interferometry images of the contact between the ball and disc in pure oil, with no polymer additives.

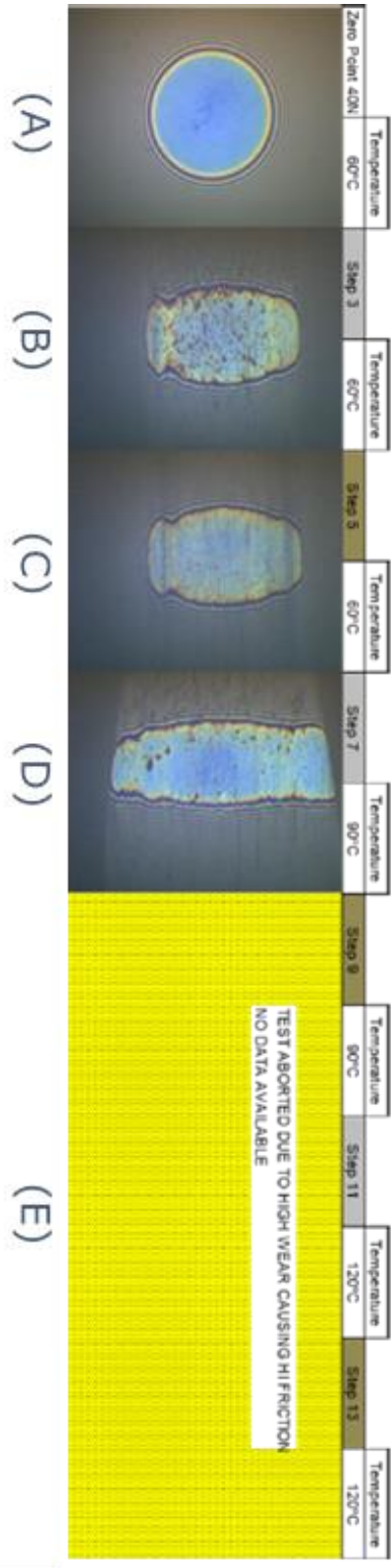


Figure 3.13. Interferometry images for MTM experiment using pure oil only as the lubricant.

The zero-point interferometry image (Figure 3.13A) shows the contact at 60 °C before any rolling was commenced, where the contact is perfectly round with no deformation. The next image (Figure 3.13B) shows the contact after the ball has been rolled at a constant 100 mm s⁻¹ for 1 hour 15 minutes, while Figure 3.13C is an image of the contact immediately following a Stribeck curve measurement, which involves varying the rolling speed between 10 and 3200 mm s⁻¹. Elongation of the contact can be seen in both of the images (B and C), indicative of wear having occurred between the surfaces during these steps. The final image (Figure 3.13D) shows the contact immediately after the test temperature was increased to 90 °C, in which further elongation and wear can be seen. After this image was recorded, the test had to be abandoned (Figure 3.13E) due to significant wear having occurred to the test surfaces.

An important observation here was that the interferometry image increased in brightness from the start of the testing (Figure 3.13B) to the end (Figure 3.13D), indicating qualitatively that no surface film was produced and that, in fact, the film provided initially by the oil became thinner with time, temperature and extended rolling. However, this image did not provide a great deal of information on its own about how the film thickness changes at each pixel of the image, hence further analysis of the data was required.

To extend this analysis, the interferometry images were used to provide a more quantitative view of the thickness and nature of the film that is formed. To achieve this, over a circle of set radius, centred on the exact centre of each interferometry image/wear scar, the thickness of the film formed by the polymer/oil solution was measured and recorded for each pixel. This film thickness data was then plotted graphically for each step of the MTM measurement (Chapter 2.2.4).

This film thickness data for the pure oil formulation is presented in Figure 3.14, where a 2D scatter plot (top) and 3D surface plot (bottom) of the film thickness for each step are shown. In the case of the scatter plot, the data was binned (i.e. grouped into a smaller number of consecutive intervals), which allowed significant variations in the film thickness in each image to be observed more clearly than in the interferometry images in Figure 3.13. By comparison, the surface plot was a 3D representation of the raw film thickness across the imaged area. These visualisations highlight how, in Figure 3.14B, a film of significant thickness did initially form, while in some regions the film thickness exceeded 150 nm. However, this film was not homogeneous, with large regions thinner than 10 nm, which was especially visible in the 3D surface plot.

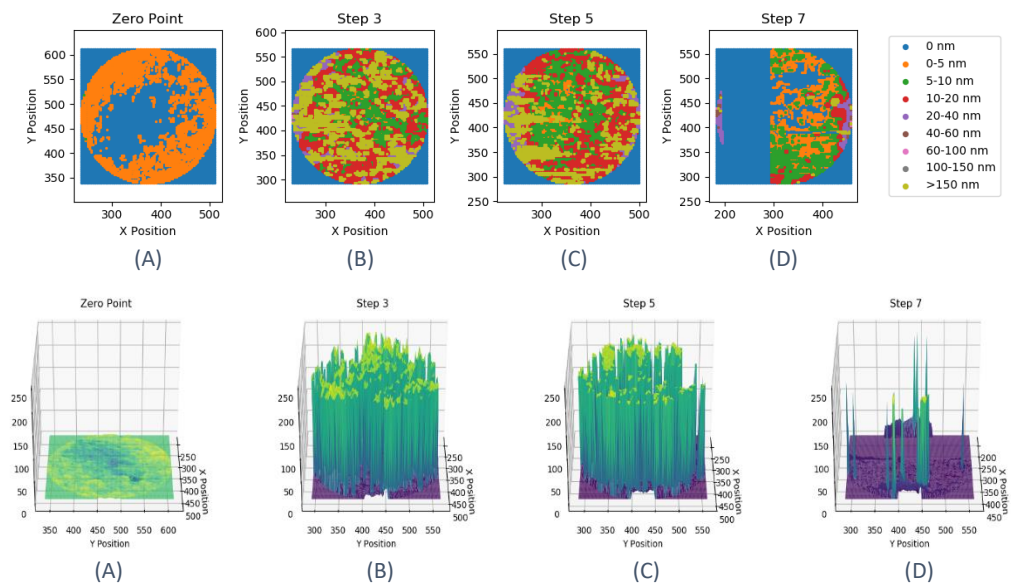


Figure 3.14. Plots of the film thickness (nm) for a pure oil formulation. Top: 2D scatter plots for each step, where the data has been binned, as indicated in the legend. Bottom: 3D surface plots for each step. The labels (A, B, C and D) correlate across the two plots and with the labels in Figure 3.13: A – zero point, $T = 60\text{ }^{\circ}\text{C}$; B – step 3, $T = 60\text{ }^{\circ}\text{C}$, rolling speed = 100 mm s^{-1} ; C – step 5, $T = 60\text{ }^{\circ}\text{C}$, after Stribeck, D – step 7, $T = 90\text{ }^{\circ}\text{C}$, rolling speed = 100 mm s^{-1} .

Following the $60\text{ }^{\circ}\text{C}$ Stribeck curve measurement, Figure 3.14C indicated that the overall maximum thickness of the film was not significantly changed from the previous image. However, an increased proportion of the film was now at less than 10 nm thick, which suggested that varying the rolling speed had the effect of wearing

away sections of the film. Meanwhile, when the test temperature was increased to 90 °C in Figure 3.14D, the film thickness decreased significantly across the image, with the majority of the film being less than 10 nm thick. This suggested that the effect of increasing temperature was a significant reduction in film thickness, likely due to a decrease in the oil viscosity. This also suggested that the effect of increasing temperature on the film thickness was more pronounced than that of varying rolling speed for the pure oil solution.

The film thickness data from the interferometry images was then processed to determine the average (mean), minimum and maximum thickness across the image area, and the standard deviation of the average thickness was also calculated, as summarised in Table 3.3.

Table 3.3. Summary of the film thickness data obtained from interferometry for a pure oil solution. The blue shading indicates that the measurement was made after film build up (i.e. following a period with no change of temperature or rolling speed). The orange shading indicates that the measurement was made after a Stribeck Curve measurement was made.

Step No	Max (nm)	Min (nm)	Mean (nm)	Std (nm)	Temp (°C)
Zero Point (A)	5.00	-10.0	0.265	1.45	60
Step 3 (B)	241	-10.0	71.1	89.4	60
Step 5 (C)	233	-6.00	54.0	83.0	60
Step 7 (D)	240	-10.0	4.51	19.8	90

A graphical visualisation of the data was also generated, shown in Figure 3.15. As a general observation, the average surface film thickness decreased from a maximum at Step 3 (A) over the duration of the test. The Stribeck measurement was performed between Steps 3 and 5 (B and C, in Figures 3.13 and 3.14) and after Step 7 (D in Figures 3.13 and 3.14). As there was no change in temperature between B and C, it was concluded that the changing rolling speed during the Stribeck measurement

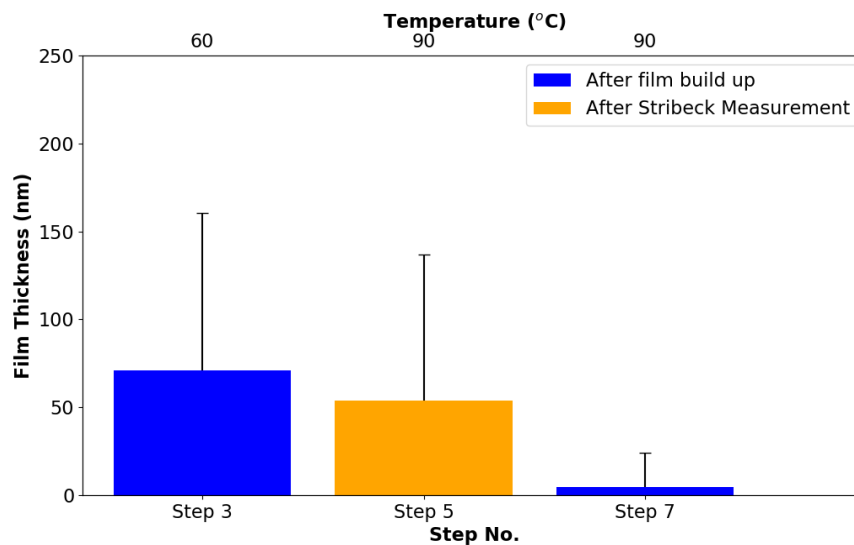


Figure 3.15. A visual representation of the data in Table 3, Entries B-D. It contains the plot of the film thickness in nm for these entries. The overall data in this Figure and Table 3 represent the summary of the film thickness data obtained from interferometry for a pure oil solution. The blue shading indicates that the measurement was made after film build up (i.e. following a period with no change of temperature or rolling speed). The orange shading indicates that the measurement was made after a Stribeck Curve measurement was made.

caused a decrease in the average surface film thickness of ~ 17 nm, from ~71 nm to ~54 nm. However, the decrease in average thickness between C and D of ~50 nm, which corresponded to an increase in test temperature from 60 to 90 °C, was considerably greater than that caused by the Stribeck measurement. This supported the earlier conclusions drawn from the raw data in Figure 3.14, that temperature appeared to have a greater impact on the thickness of the film formed for a pure oil solution than rolling speed.

The interferometry results for a comparative experiment which utilised a 1 wt% solution of the semi-block HB polymer in the base oil are shown in Figure 3.16. It was first apparent that the measurements were able to be conducted at 120 °C (Figure 3.16F and G) without having to abandon the test due to excessive wear. Comparing the semi-block polymer solution to that of the pure base oil, it was also apparent that very little wear occurred between the surfaces throughout the duration of the test: this was evidenced by the lack of elongation of the contact point. The interferometry images also became steadily darker throughout the testing as the

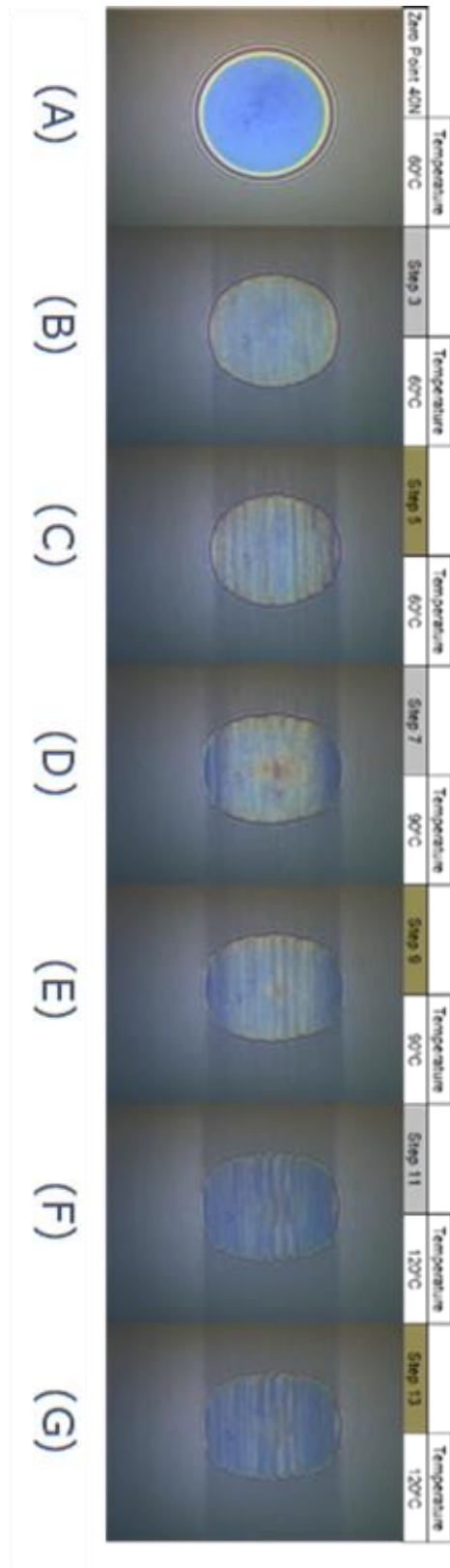


Figure 3.16. Interferometry images for MTM experiment using semi-block HB polymer in oil, 1 wt%.

different rolling and temperature regimes were performed, indicative of the formation of a tribological film at the contact point between the surfaces.

The formation of this film has been visualised in Figure 3.17, where the thickness of the film measured at each pixel of a circular area centred on the middle of the wear scar has been plotted.

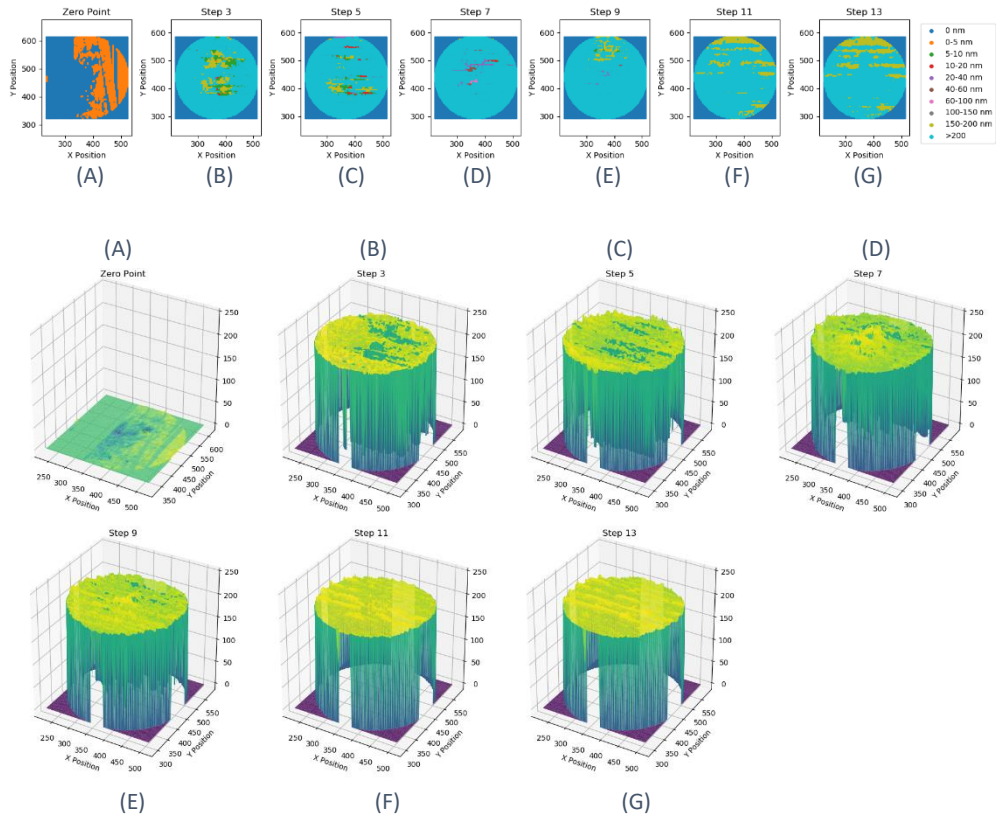


Figure 3.17. Plots of the film thickness (nm) for a 1 wt % semi-block HB polymer and base oil formulation. Top: 2D scatter plots for each step, where the data has been binned, as indicated in the legend. Bottom: 3D surface plots for each step. The labels (A - G) correlate across the two plots and with the labels in Figure 17.

From both the 2D scatter plot (top) and the 3D surface plot (bottom), it was clear that a significant film formed rapidly, with the majority of the measured film having a thickness >200 nm in plot B. From this Step, the film thickness continued to grow and become more uniform as the test progressed, with very little variation in film thickness seen after plot F. This indicated that varying rolling speed and increasing temperature caused an increase in the thickness of the film formed when the semi-block HB polymer was incorporated into the formulation, and the formation of a protective, robust film was observed.

The film thickness summary statistics for this test, shown in Table 3.4, corroborate the previous observation.

Table 3.4. Summary of the film thickness data obtained from interferometry for a 1 wt % semi-block HB polymer/base oil formulation. The blue shading indicates that the measurement was made after film build up (i.e. following a period of constant temperature and rolling speed).

Step No	Max (nm)	Min (nm)	Mean (nm)	Std (nm)	Temp (°C)
Zero Point (A)	4.00	-10.0	0.174	1.29	60
Step 3 (B)	217	0.00	180	67.9	60
Step 5 (C)	231	0.00	184	63.0	60
Step 7 (D)	241	7.00	196	53.6	90
Step 9 (E)	230	0.00	200	35.4	90
Step 11 (F)	216	127	202	3.39	120
Step 13 (G)	219	74.0	202	4.17	120

Initially, at step 3 (B), the average film thickness was 180 nm. The film then grew to a peak average thickness of 202 nm at step 13 (G) at 120 °C. Similarly, at this point the calculated errors (standard deviations) reduced significantly from ~35 to ~3 nm, indicating little variation in the film thickness across the wear scar. These statistics were visualised in Figure 3.18.

Comparing the semi-block polymer solution data in Table 3.4 that of the pure base oil in Table 3.3, it was noted that the trend of decreasing film thickness with time/temperature observed for pure oil was reversed here. Rather than the surface contact increasing, due to loss of film at the contact point, thus the root cause of the wear for the pure oil case, in this case the thin film was found to grow with increasing temperature and rotation regimes (i.e. after Stribeck measurements). This demonstrated that the addition of HB polymer resulted in the formation of a thin film,

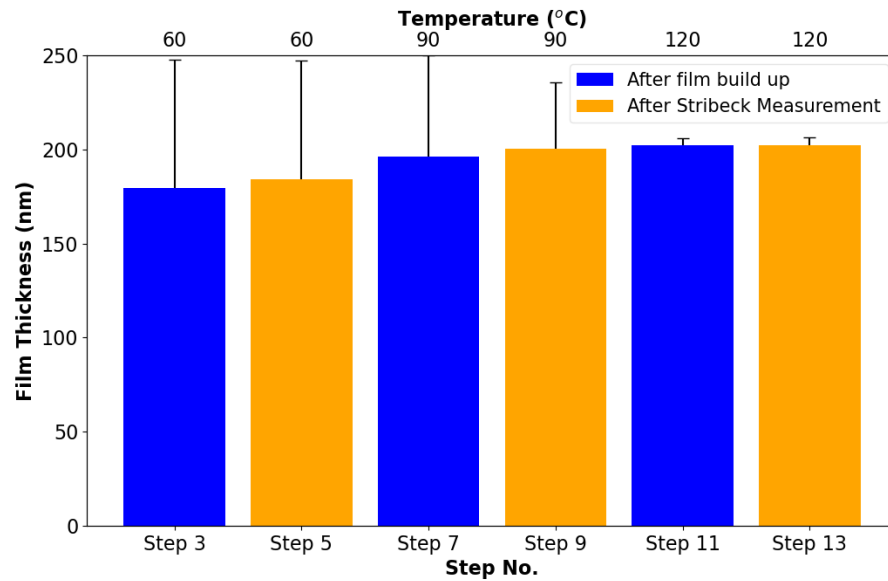


Figure 3.18. A visual representation of the data in Table 4, Entries B-G. It contains the plot of the film thickness in nm for these entries. The overall data in this Figure and Table 3 represent the summary of the film thickness data obtained from interferometry for a 1 wt % semi-block HB polymer/base oil formulation. The blue shading indicates that the measurement was made after film build up (i.e. following a period of constant temperature and rolling speed). The orange shading indicates that the measurement was made after a Stribeck Curve measurement was made.

which was not worn down with increasing temperature and applied force between two surfaces. However, it is worth noting that the errors on the average values overlapped significantly, suggesting that the growth was not statistically significant.

Similarly, the interferometry data for a 1 wt % solution of block HB polymer in oil are shown in Figure 3.19. The interferometry images in Figure 3.19 again showed a lack of elongation, which indicated very little wear occurred between the surfaces, as well as the formation of a significant surface film over the course of the test, as shown by the darkening of the contact point.

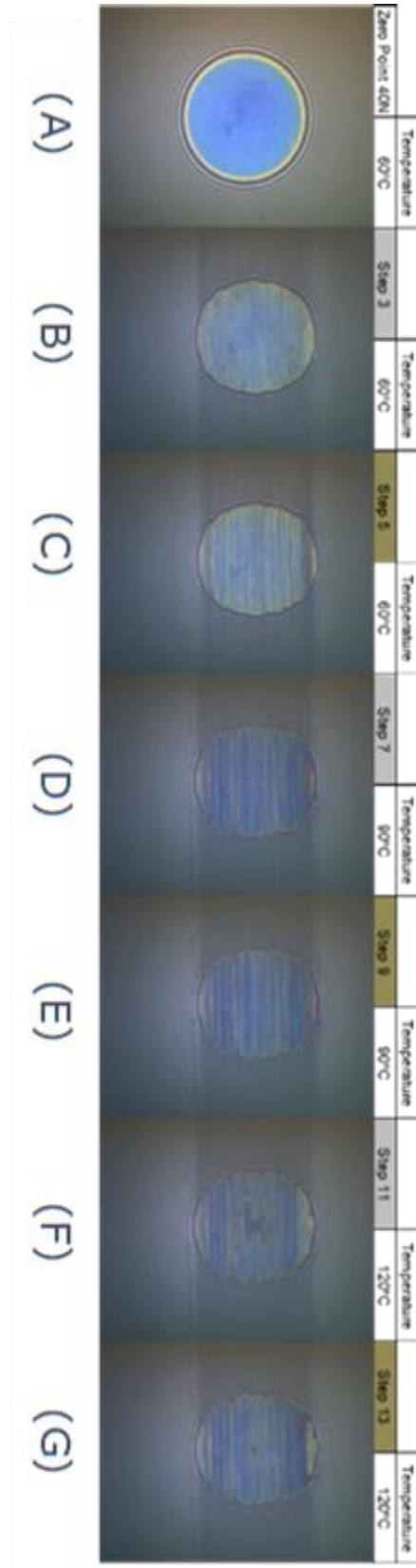


Figure 3.19. Interferometry images for a MTM experiment utilising a 1 wt % block HB polymer in oil solution.

The formation of this film has again been visualised in Figure 3.20, where the thickness of the film measured at each pixel of a circular area centred on the middle of the wear scar has been plotted.

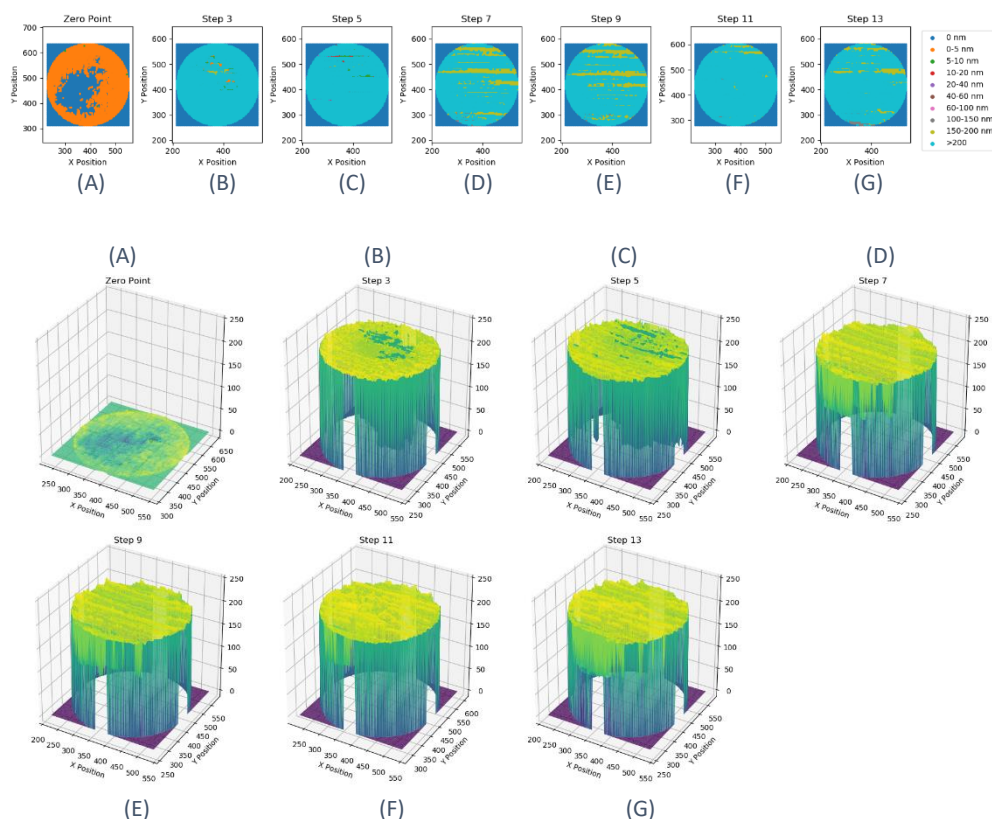


Figure 3.20. Plots of the film thickness (nm) for a 1 wt % block HB polymer and base oil formulation. Top: 2D scatter plots for each step, where the data has been binned, as indicated in the legend. Bottom: 3D surface plots for each step. The labels (A - G) correlate across the two plots and with the labels in Figure 20.

In a similar manner to the semi-block polymer, a significant film formed rapidly, with the majority of the measured film having a thickness >200 nm in plot B. From this Step, the film thickness continued to grow minimally and became more uniform as the test progressed, with very little variation in film thickness seen after plot D.

This suggested that the block HB polymer formed a more robust film more rapidly than the semi-block copolymer, as it stabilised earlier in the test and was not affected as greatly by changes in temperature and rotation regime, though the difference was minimal. This may have been due to the structure of the block polymer. The greater concentration of chain transfer agent (CTA) in the distilled oligomer mixture used to synthesise the block copolymer compared to the semi-block polymer meant the block copolymer possessed a greater density of vinyl end groups.

The crosslinking of these end groups was likely the origin of the observed film formation: if the block polymer possessed a greater density of end groups, the cross-link density within the film formed would also be greater, potentially leading to a more robust film being formed more quickly.

When the summary data for the block copolymer shown in Table 3.5, and summarised in Figure 3.21, was compared with that for the semi-block polymer (Table 3.4, Figure 3.18).

Table 3.5. Summary of the film thickness data obtained from interferometry for a 1 wt % block HB polymer/base oil formulation. The blue shading indicates that the measurement was made after film build up (i.e. following a period of constant temperature and rolling speed). The orange shading indicates that the measurement was made after a Stribeck Curve measurement was made.

Step No	Max (nm)	Min (nm)	Mean (nm)	Std (nm)	Temp (°C)
Zero Point (A)	6.00	-10.0	0.749	1.73	60
Step 3 (B)	218	-3.00	195	44.6	60
Step 5 (C)	227	1.00	194	46.6	60
Step 7 (D)	223	80.0	200	12.1	90
Step 9 (E)	227	118	201	9.91	90
Step 11 (F)	223	75.0	204	8.84	120
Step 13 (G)	220	118	201	13.3	120

It was observed that the average initial thickness of the film formed by the block HB polymer solution was greater, with an initial average film thickness at Step 3 (B) of 195 nm compared to 180 nm for the semi-block polymer. This film, like that in the semi-block case, was not degraded with increasing temperature, time, or rolling speed and grew to a maximum average thickness of 204 nm at Step 11 (F). This was very similar to the 202 nm maximum average thickness observed for the semi-block polymer, though the overall difference in thickness of 9 nm was not significant compared to the associated errors and their overlap. However, for the block polymer

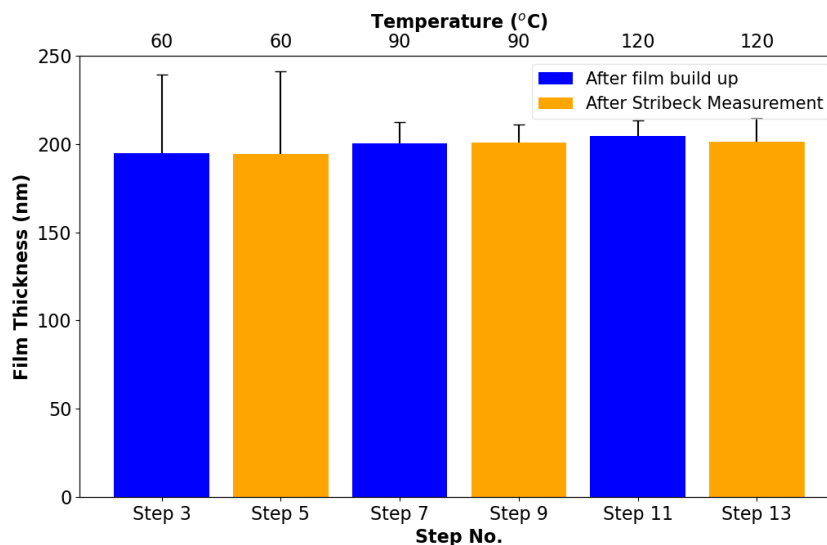


Figure 3.21. A visual representation of this data of Table 5, Entries B-G. It contains the plot of the film thickness in nm for these entries. The overall data in this Figure and Table 5 represent the Summary of the film thickness data obtained from interferometry for a 1 wt % block HB polymer/base oil formulation. The blue shading indicates that the measurement was made after film build up (i.e. following a period of constant temperature and rolling speed). The orange shading indicates that the measurement was made after a Stribeck Curve measurement was made.

the errors became very small by Step 7, which indicated that a uniform film developed rapidly, much more so than for the semi-block polymer which did not become uniform until Step 11 (F). Once 90 °C was attained, the average film thickness was very similar for the two HB polymer solutions. It was thought that the film formation evidenced by both HB polymer solutions could be due to crosslinking between the HB polymer molecules at elevated temperature.

Thus, it was thought that this reduced film build-up and higher viscosity of the block polymer compared to the semi-block polymer was due to the lower molecular weight of the block polymer. This lower weight was less able to crosslink during the experiment, due to the decreased volume occupied by the smaller polymer, making polymer interaction less likely. Interestingly, the average film thickness after the Stribeck measurement at 120 °C (Step 13, G) was decreased compared to before the measurement (Step 11, F), suggesting that the film formed by the block polymer was actually less robust than that of the semi block polymer, and was capable of being

destroyed, which again suggested less crosslinking had occurred between the polymer molecules.

3.3.2.3 Friction Coefficient Testing – Stribeck Measurements

Stribeck measurements were performed between Steps 3 and 5 (B and C) at 60 °C, between Steps 7 and 9 (D and E) at 90 °C, and between Steps 11 and 13 (F and G) at 120 °C for each HB polymer solution. Unfortunately, no data was available for the errors of these measurements, and the data was not made available for manipulation. Instead, plots produced by BP/Castrol technicians were made available and are presented here.

The results for the pure base oil are shown in Figure 3.22, where the 120 °C measurement was not performed to prevent damage to the analytical equipment.

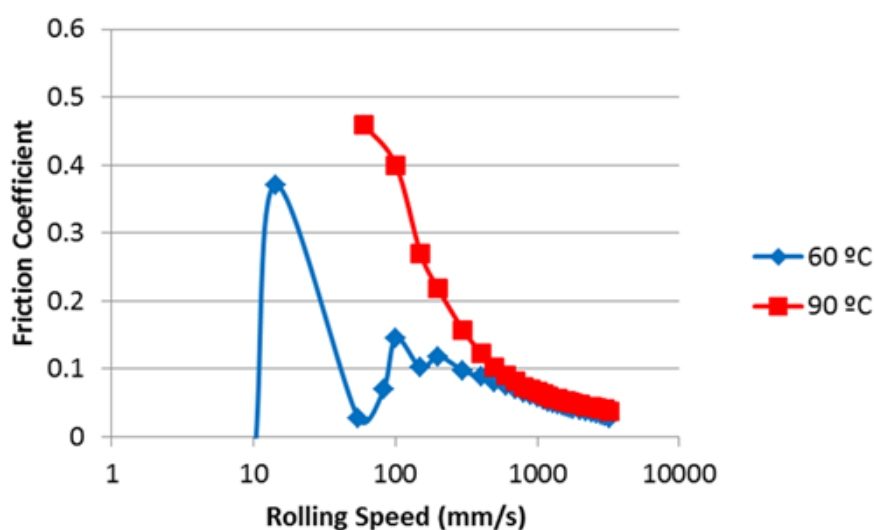


Figure 3.22. Stribeck curve from an experiment using pure oil as the lubricant.

The overall observed trend was an increase in the dimensionless friction coefficient as the speed of rotation was decreased. This was because at slower speeds the surfaces were less able to entrain the material being measured, which was forced out of the inter-surface space due to the force applied between the surfaces. This led to a change in the lubrication regime, and thus a change in the friction coefficient.

At 60 °C the trace for the friction coefficient fluctuated considerably, though it tended to increase with decreased rolling speed, with a maximum coefficient of 0.38 being achieved. Meanwhile, at 90 °C the friction coefficient rose to a maximum of 0.46, at which point the test was stopped to prevent apparatus damage. The friction at higher temperature was greater due to a decrease in the viscosity of the oil at higher temperature, meaning that the entrainment of the oil is decreased, allowing for greater wear.

By comparing this to the data from the HB polymer solutions shown in Figure 3.23, it was immediately apparent that the friction coefficient is markedly decreased on addition of both the semi-block (left) and block (right) HB polymer.

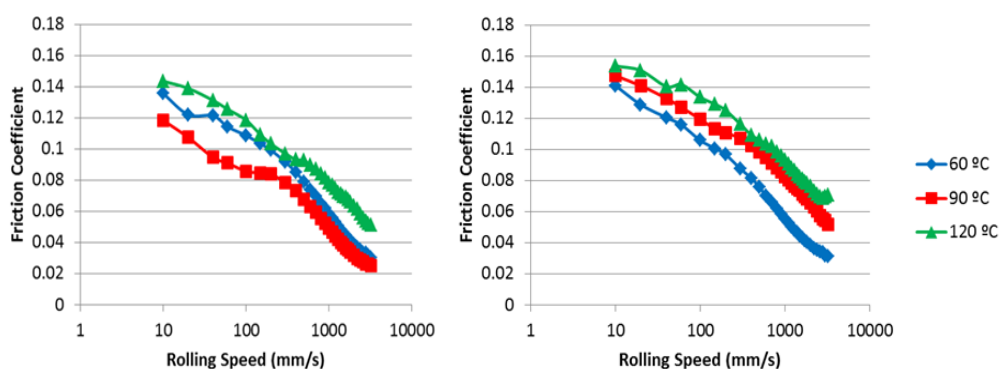


Figure 3.23. Stribeck curve from an experiment using a 1 wt % semi-block HB polymer in oil solution (left) and a 1 wt % block HB polymer in oil solution (right) as the lubricant.

Even at low entrainment speeds the hyperbranched polymer solutions outperformed the pure base oil. For example, in the 60 °C test, the HB results peaked at ~ 0.14 , compared to 0.38 for the oil without polymer. For the semi-block polymer (Figure 3.23, left), the expected trend of increasing friction coefficient with increasing temperature was reversed in the 90 °C measurement, where the friction coefficient was consistently lower than in the 60 °C case. Cross-referencing this observation to the average film thickness data in Table 3.4, this decrease in friction was accompanied by a substantial increase in the average film thickness of 16 nm, suggesting that the observed decrease in the friction coefficient was due to the formation of greater film

depth. The results from the 120 °C curve show increased friction compared to the 60 and 90 °C curves, as would be expected due to the decreased solution viscosity at elevated temperature. This was likely because the average film thickness only increased by 2 nm between the 60 and 90 °C tests, so there was very little additional film to further decrease friction.

For the block polymer (Figure 3.23, right), the expected trend of increased friction with increased temperature was seen for all three temperatures. While the block solution produced a lower friction coefficient than the pure base oil case, it is interesting to note that the friction was higher at each of the temperatures measured for the block polymer solution when compared to the semi-block polymer. This was despite a thicker film having been formed for the block solution, at lower temperatures (comparing the film thickness for the block and semi block polymers at 60 °C of 195 nm and 180 nm respectively). However, the block polymer solution was observed to undergo a lower increase in average film thickness (6 nm) than the semi-block polymer solution (22 nm) as the test proceeded, and therefore the increase in average film thickness did not produce the same decrease in friction as observed with the semi-block material.

3.3.2.4 *Elasto-Hydrodynamic Film Thickness Measurement*

Previous testing had focussed on boundary/very thin film conditions, which are the dominant regimes in an engine. However, rolling bearings are the second most used machine components. The small contact area and large pressures between rolling elements and raceways due to the non-conformity of their surfaces lead to very thin lubricant films, a regime of lubrication known as elastohydrodynamic (EHD).

Thus, the performance of the HB semi-block and block materials were tested in the EHD regime using 0.5 wt% polymer solutions. The film thickness was measured for each HB polymer using an EH rig with both ascending and descending entraining speed tests. The results are shown in Figure 3.24. The pure base oil was also measured for comparison.

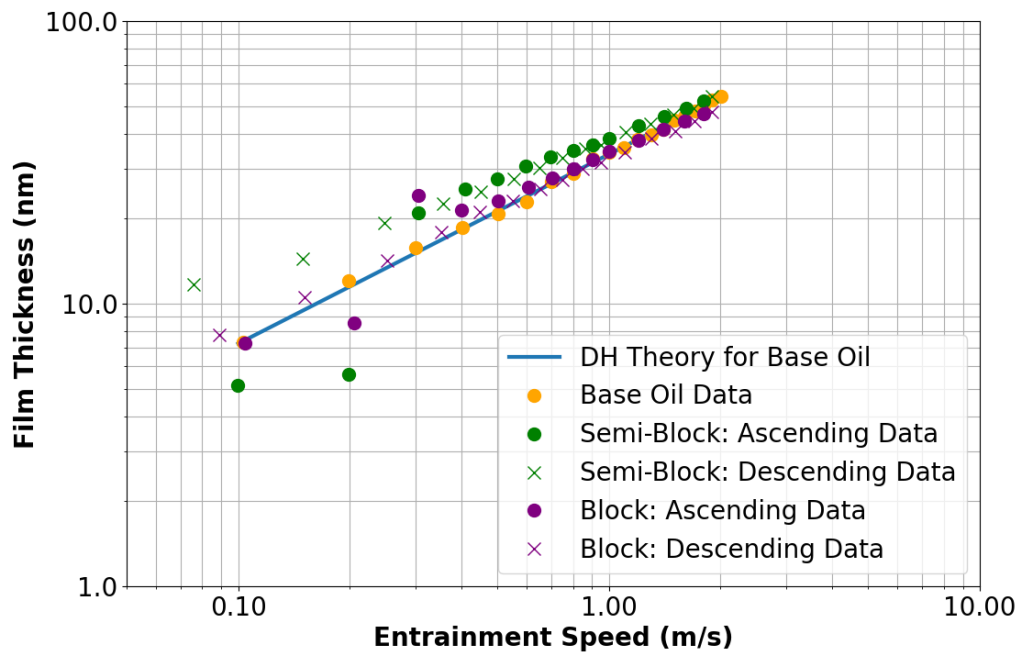


Figure 3.24. EHD data for PA04 Base oil (orange plots), 0.5 wt% semi-block copolymer in solution (green plots) and 0.5 wt% block copolymer in solution (purple plots). The circular data points represent data measured when the entraining speed was increasing, while the data point represented by 'x' show the data obtained when the entraining speed was decreasing. The straight-line fit represents the theoretical values for an ideal (pure oil) solution

For the Durasyn 164, the data, shown by the orange circles in Figure 3.24, demonstrated the expected variation in film thickness as a function of entraining speed. According to Dowson-Hamrock (DH) theory [50] a plot of film thickness versus entraining speed should give a straight line of slope 0.67 when plotted with logarithmic axes, which is known as ideal behaviour. This plot can be used to predict the film thickness at a given entraining speed, and is plotted as a straight line in Figure 3.24, as calculated by BP/Castrol. The experimental data (orange circles) for the base oil closely matched the theoretical data as expected.

For the semi-block copolymer, the data for which is shown in the green plot in Figure 3.24, two occurrences of non-ideal behaviour were observed. When running from low to high speed, at the two lowest speeds, the film thickness measured was smaller than expected for an ideal solution. This was probably due to the phenomenon of inlet rejection, where the polymer molecules were not fully solvated and were unable to enter the EHD contact. As the speed increased further, the polymer was able to enter the contact and the solution behaved more ideally. When running from high to low speeds, there was a notable increase in measured film thickness compared to that expected for an ideal solution. This indicated that the polymer from the solution had adsorbed onto the ball and/or disc and formed a protective film. It was also noted that the film thickness at an entrainment speed of 1 m/s was higher than that of the base oil alone, which indicated the polymer had a thickening effect.

For the block copolymer, the data for which is shown in the purple data in Figure 3.24, the data followed essentially the same trend as for the pure base oil. While a small amount of inlet rejection was seen when entrainment speed was ascending, when descending there was no evidence of either non-ideal behaviour or increased oil film thickness at 1 m/s. This indicated this polymer had only a limited thickening effect under these high stress high shear conditions. This contrasted with the trend seen for the semi-block polymer, which was attributed to the higher molecular weight of the semi-block polymer and its greater ability to act as a viscosity modifier.

At higher entrainment speeds both polymer-base oil solutions behaved as constant viscosity fluids, which was evidenced by the fact that the gradients of their

measurements were parallel to that of the base oil. This suggested shear-thinning of the polymers occurred at these increased entrainment speeds [51].

3.3.2.5 Conclusions from Small Scale Batch Testing

Overall, both the semi-block and block HB polymers demonstrated excellent film formation and wear prevention properties across a range of lubrication regimes when synthesised on a 1-2 mL scale, indicating good potential for their use as friction modifiers. However, their viscosity improvement was too low for them make suitable viscosity modifiers at normal operation temperatures. While the block polymer was found to produce a thicker film, on average, than the semi-block polymer, their overall performance was very similar. Certainly, any performance difference between the two polymers was not significant enough to warrant the extra distillation step required for the synthesis of the block copolymer. Hence, the semi-block polymer was chosen as the best candidate polymer for further scale up and testing and is the focus of the remainder of this Chapter.

3.3.3 Synthesis Scale Up of HB Semi-Block Polymer

If the HB semi-block polymer was to be of any use on an industrial scale, proof of scale up potential and batch-to-batch reproducibility was needed. Hence, work was conducted to scale-up the synthesis of the semi-block HB polymer. Using the same reactant ratios and methods outlined above, the synthesis was scaled up by approximately an order of magnitude to produce 30-60 mg of semi-block HB polymer per batch, an increase in yield of ~20-30 fold. From this point, the polymers discussed

previously which were produced on a 1-2 mL scale will be known as Batch 1, while those produced at larger scale will be known as Batch 2.

The Batch 2 semi-block polymer was analysed by GPC, the results of which are summarised in Table 3.6.

Table 3.6. Yield and molecular weight data of HB DVB-LMA copolymer of semi-block structure, produced on a 20-30 mL scale.

Entry	Structure	Crude Yield ^a (%)	M _n ^b (kD)	M _w ^b (D)	Đ ^b
1	Semi-Block	64.0	653.10	4360.00	6.68

^a Determined gravimetrically. ^b Determined via gel permeation chromatography.

By comparing this with the data for the Batch 1 semi-block polymer (Table 3.2), it was clear that while the Batch 2 polymer was higher molecular weight than the Batch 1 polymer, it was more lightly branched. For example, the number average molecular weight (M_n) for the Batch 2 semi-block polymer was 653.1 kDa, while the Batch 1 semi-block polymer was only 37.1 kDa, however the polydispersity of the Batch 1 polymer was 102.7, compared to 6.68 for the larger-scale Batch 2 polymer.

There are a number of possible explanations for these observations. For example, the concentration of dimeric transfer agent in the oligomeric mixture may have been lower in the Batch 2 polymer: this would result in an increased molecular weight for the Batch 2 polymer, compared to the Batch 1 polymer. However, given that the average oligomer conversion rarely deviated from $40 \pm 3\%$, this effect would be minor. Alternatively, the increased scale of the polymerisation may have impacted the architecture of the polymer product, though this requires further investigation. A reduction in heat and mass transfer in the larger scale Batch 2 polymerisation may have led to a reduction in the production of initiating radicals in the initiation step. This would have resulted in fewer, higher molecular weight polymers being produced with lower overall polydispersity. Thus, in future, to obtain polymer of a similar molecular weight and branching density to that produced on a small scale, it may be

necessary to increase the initiator concentration, which should increase the number of chains initiated and thus reduce the molecular weight of each chain and increase dispersity. Alternatively, as the chain transfer process would be influenced by diffusion, it may be that a reduction in mass transfer within the larger batch reactions reduced the ability of the CTA to find radicals, which would have reduced the level of chain transfer achieved and so resulted in an increased molecular weight.

However, the Batch 2 polymer was still hyperbranched, as evidenced by the dispersity value of 6.68 and the broad peaks in the SEC spectrum, shown in Figure 3.25, which indicated that the polymer was suitable for the current application and could be sent for tribological testing.

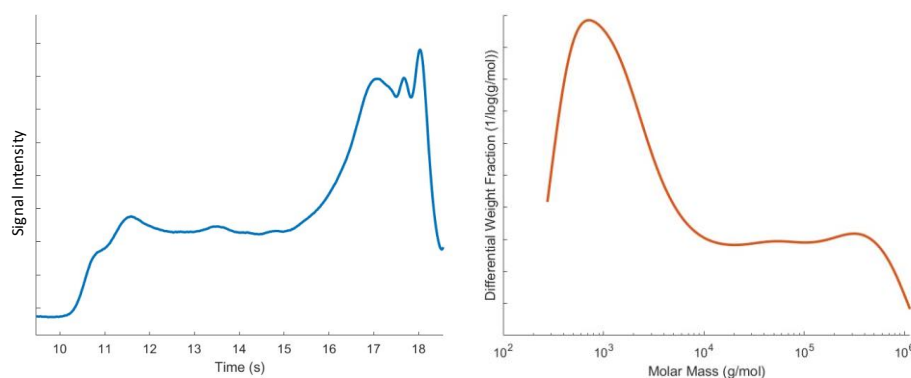


Figure 3.25. SEC traces of DVB-LMA homopolymer made at 50 mL scale, plotted against retention time and molar mass to illustrate the broad peaks obtained, which are characteristic of HB polymers.

3.3.4 Further Application Testing of HB Semi-Block Polymer at Increased Scale

The scaled-up Batch 2 HB polymer product was then subjected to the same testing as the polymer produced on a smaller scale (Batch 1), starting with kinematic viscosity testing and moving on to wear and film formation property testing, to ensure the scale up process had not affected the overall behaviour of the polymer. Due to the larger quantity of polymer available, further testing, including shear testing and high frequency reciprocation were also conducted on the Batch 2 polymers. From this

point, all synthesis, analysis and interpretation was completed by the author, while tribological testing was conducted by BP/Castrol technicians.

3.3.4.1 Viscosity Testing

The kinematic viscosity (KV) of the Batch 2 HB polymer was tested under the same conditions outlined above and the results are shown in orange in Figure 3.26: the data obtained for the Batch 1 HB polymer is also presented (red) for easier comparison (see Figure 3.10 for more detail).

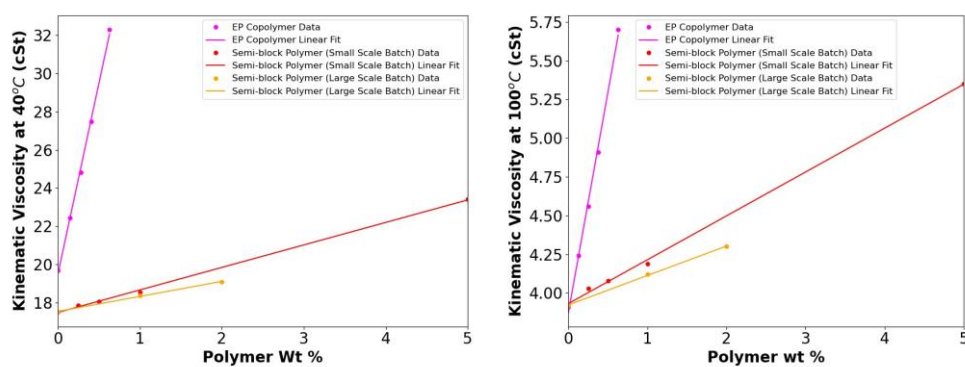


Figure 3.26. Plot of the change in viscosity of both Batch 1 (red) and Batch 2 (orange) HB semi-block polymer/base-oil solution, measured at 40 °C (left) and 100 °C (right), where the linear EP copolymer (pink) is the current commercial linear polymer used in industrial formulations. The solid lines represent linear best fits to the data.

As observed previously, the KV increased with increasing polymer concentration at both 40 °C (Figure 3.26, left) and 100 (Figure 3.26, right), though not so significantly as the linear EP copolymer standard. Due to the slightly altered testing range and limited scope of the KV testing conducted on the Batch 2 semi-block polymer, it was difficult to draw quantitative conclusions from comparing this data to that from the Batch 1 semi-block polymer (Figure 3.26, red). However, it could be observed that the general trend for Batch 2 polymer at 40 °C was delivering a slightly increased KV at each polymer loading when compared to the Batch 1 polymer. This was possibly due to the reduction in branch density observed in the GPC results for the Batch 2 polymer, where reduced levels of branching may have resulted in the polymer experiencing greater entanglement, and thus increased the viscosity of the

polymer. Meanwhile, at 100 °C the KV values were very similar when compared to the Batch 1 polymer, indicating that any extra entanglement of the more lightly branched Batch 2 polymer was less significant at increased temperature, likely due to the thermal expansion of the polymer.

The Batch 2 semi-block polymer was also tested on the Cold Cranking Simulator (CCS), and the results are shown in Figure 3.27: the data for the Batch 1 polymer is also shown for easier comparison (see Figure 3.11 for more detail).

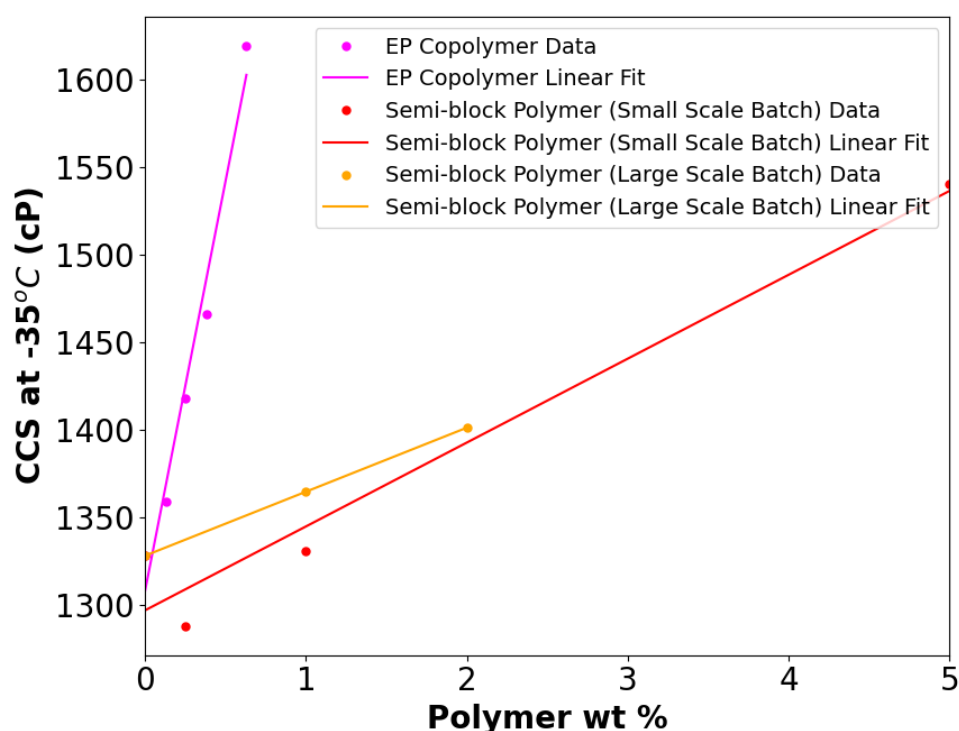


Figure 3.27. Plot of the change in viscosities of both the Batch 1 (red) and Batch 2 (orange) HB semi-block polymer/base oil solution measured in the Cold Cranking Simulator at $-35\text{ }^{\circ}\text{C}$, where the EP copolymer (pink) is the current commercial linear polymer used in industrial formulations. The solid lines represent linear best fits to the data.

Again, similar behaviour to that seen at 40 and 100 °C, and to that observed for the Batch 1 polymer was observed for the semi-block Batch 2 polymer, where the viscosity of the polymer-oil solution increased as the concentration of polymer increased. Additionally, the Batch 2 semi-block polymer was seen to cause insignificant (<500 cP) increase in base oil viscosity below 2 wt% loading, a much smaller increase than caused by the linear EP copolymer at the same loading. The

decrease in viscosity from the unloaded value seen previously at 0.25 wt% loading for the Batch 1 polymer was not repeated here. However, the testing range was not the same and 0.25 wt% loading was not tested for the Batch 2 polymer, only 1 and 2 wt%, hence this behaviour may just have been masked.

Clearly, the small change in architecture between the two batches of HB polymer had not greatly affected the performance of the polymer, as the KV and CCS values measured were still significantly lower for the HB polymer than those for the EP copolymer, and the overall behaviour trends were not changed.

3.3.4.2 *Film Formation Testing*

The film formation properties of the Batch 2 semi-block polymer were then evaluated using the MTM, as described previously.

The interferometry images obtained for a 5 wt % solution of the Batch 2 semi-block polymer in oil are shown in Figure 3.28. It was clear that, as previously (Figure 3.16), the measurements were able to be conducted to a temperature of 120 °C (Figure 3.28F) without having to abandon the test, and very little wear occurred between the surfaces, as shown by a lack of significant elongation of the contact wear scar across the rolling and temperature regimes. Similarly, a tribological film was formed at the contact point between the two surfaces, as evidenced by the darkening of the image as the test progressed. However, some scarring of the image could be seen, with dark furrows apparent in Figure 3.28D-G for the Batch 2 polymer, which was not observed for the Batch 1 polymer.

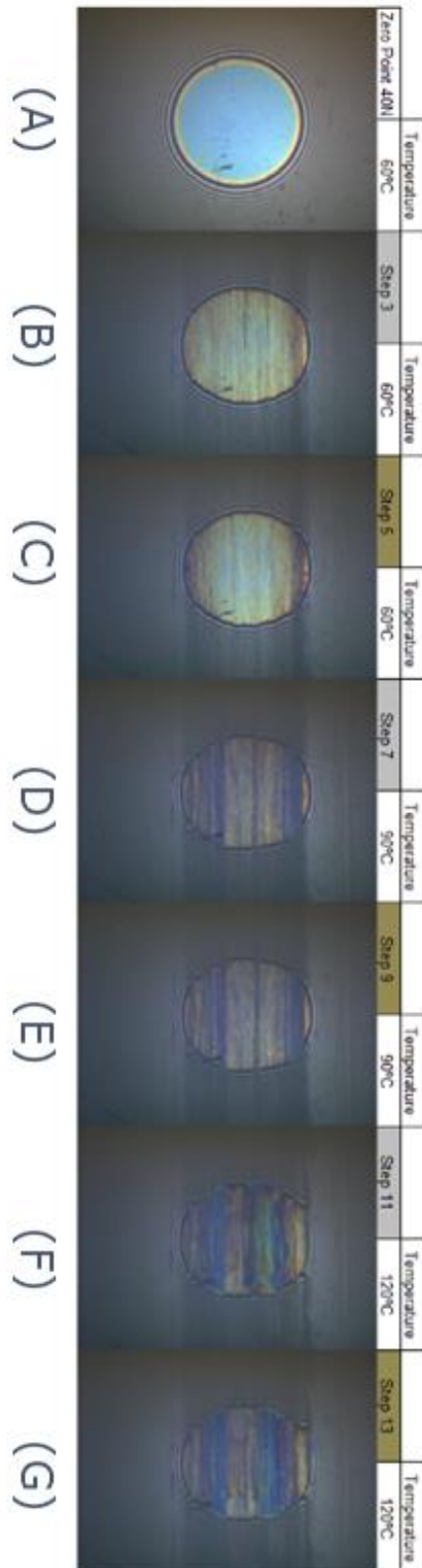


Figure 3.28. Interferometry images of scaled-up/Batch 2 semi-block HB polymer in oil solution, 5 wt%.

The film thickness data collected from the interferometry measurement was visualised for the Batch 2 semi-block polymer in the same way as described previously

for the Batch 1 polymer (Figure 3.17), and the data is presented in Figure 3.29, as both a 2D scatter plot (top) and 3D surface plot (bottom).

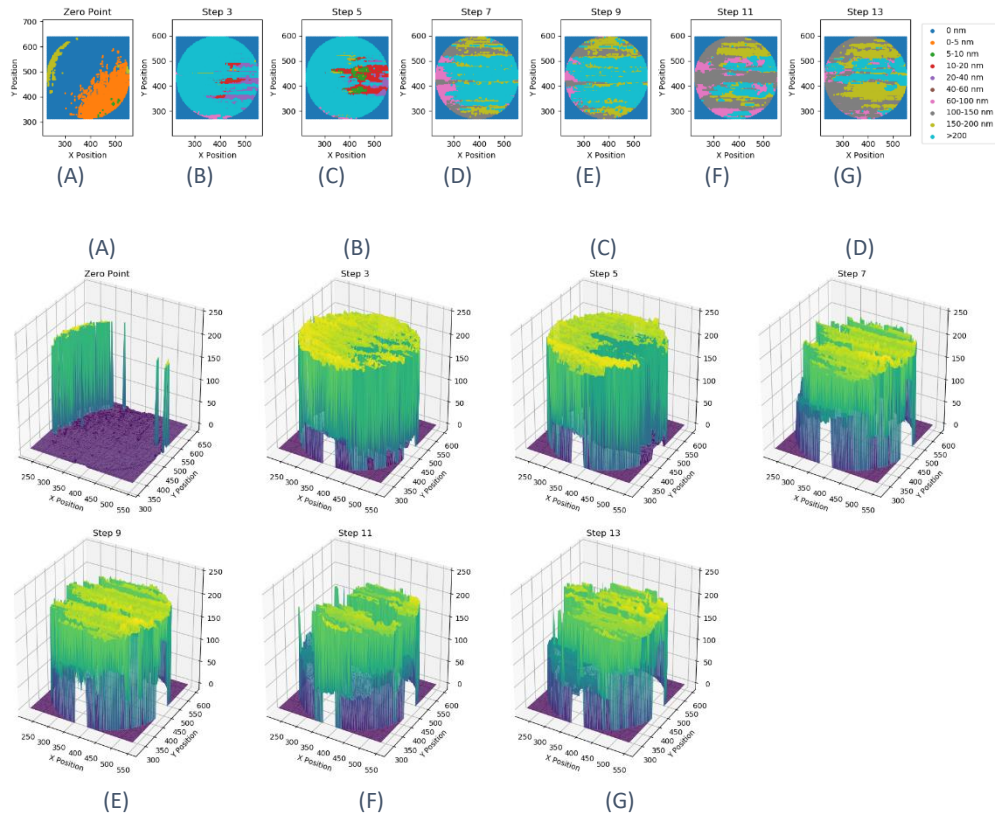


Figure 3.29. Plots of the film thickness (nm) for a 5 wt % Batch 2 semi-block HB polymer and base oil formulation. Top: 2D scatter plots for each step, where the data has been binned, as indicated in the legend. Bottom: 3D surface plots for each step. The labels (A - G) correlate across the two plots and with the labels in Figure 3.15.

These plots indicated that, as for the Batch 1 polymer, a significant film formed rapidly, with the majority of the measured film having a thickness >200 nm in plot B. However, it was interesting to note that, despite the Batch 2 polymer being included at an increased concentration compared to the Batch 1 polymer (5 wt % for the Batch 2/oil solution, 1 wt % for the Batch 1/oil solution), the initial film thickness achieved was similar for the two batches. This may have been due to increased levels of polymer crosslinking occurring in solution, rather than at the surface, due to the increased availability of vinyl groups in solution. Beyond this Step, wear scars were observed to form which increased in depth and width as the test progressed from image B to F. For example, large portions of the film moved from the >200 nm

thickness designation to 150-200 nm thickness, and some striations were seen with thicknesses in the range 100-150 nm, while other small areas had a thickness as low as 60-100 nm, as indicated by the legend on the 2D scatter plot. The striations were also observed in the surface plot, which very clearly indicated visually the non-uniformity of the surface by image F. However, some recovery of the film thickness was seen in image G, where areas of the film which were only 100-150 nm thick (or less) in image F increased to 150 – 200 nm following the 120 °C Stribeck curve measurement.

The striations could also be analysed by taking a slice through the 3D surface image, as shown in Figure 3.30, to show the profile of the surface. Here, the film thickness was plotted as a function of the Y-coordinate of each image, with a set value of the X-coordinate of 401, for both the Batch 1 (top) and Batch 2 (bottom) semi-block polymers for comparison. From these, it could be observed that films of similar structure and thickness were initially formed in Step B for both batches. In the case of the Batch 1 semi-block polymer, the film was seen to grow steadily, with areas of low thickness being gradually “filled in” as the test progressed until a uniform thickness was achieved at Step F. In comparison, the Batch 2 polymer showed good overall film growth, as by Step D there were no further regions of zero thickness. However, beyond Step D, regions of the film became slightly worn, with areas of the film reduced in thickness by up to ~100 nm, up to Step F as was observed in Figure 3.29. At Step G, some of the striations became narrower in extent, while others recovered completely, which suggested that the polymer was continually forming the film throughout the test and was capable of regenerating the film in areas where damage occurred.

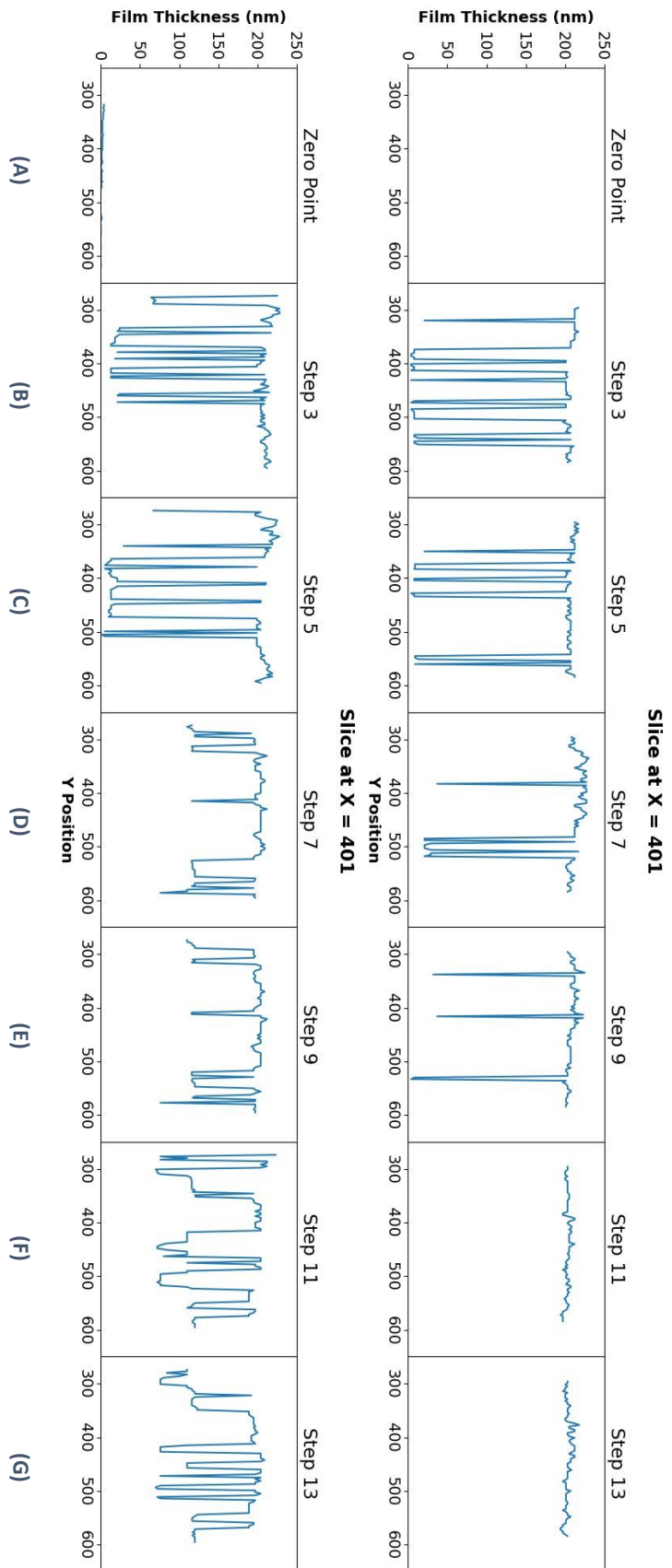


Figure 3.30. Plots showing how the film thickness varies across the y-coordinate of the interferometry images for the Batch 1 (top) and Batch 2 (bottom) semi-block polymer in base oil solution at 1 wt % (Batch 1) and 5 wt % (Batch 2) at x = 401. The labels (A - G) correlate across the two plots and with the labels in Figures 10 and 17.

It was further hypothesised, when reviewing this data and the pattern of damage relating to the applied conditions, that the gouging of the thin film surface

evidenced in both Figure 3.29 and Figure 3.30 may have been the result of residual metal catalyst in the Batch 2 polymer. This may have been present in larger concentrations than in the Batch 1 polymer due to issues with precipitating larger quantities of viscous liquid polymer. This may be resolved in future work through the application of multiple precipitation steps, which will help to ensure that as much CTA is removed as possible. However, this was not applied here due to the large quantities of anti-solvent required when working on a tens-of-gram scale.

The film thickness data for the Batch 2 semi-block polymer was then processed to obtain the summary statistics for each Step/image, the data for which is shown in Table 3.7 and visualised in Figure 3.31.

Table 3.7. Summary of the film thickness data obtained from interferometry for a 5 wt % Batch 2 semi-block HB polymer/base oil formulation. The blue shading indicates that the measurement was made after film build up (i.e. following a period of constant temperature and wear rate). The orange shading indicates that the measurement was made after a Stribeck Curve measurement was made.

Step No	Max (nm)	Min (nm)	Mean (nm)	Std (nm)	Temp (°C)
Zero Point (A)	198	-10.0	5.99	35.4	60
Step 3 (B)	233	4.00	167	79.9	60
Step 5 (C)	233	-1.00	154	88.5	60
Step 7 (D)	227	58.0	164	52.0	90
Step 9 (E)	227	56.0	173	46.1	90
Step 11 (F)	233	62.0	129	48.2	120
Step 13 (G)	227	58.0	148	48.1	120

Comparing the data in Table 3.7 to that for the Batch 1 semi-block polymer (Table 3.4), little trend was observed across the test, although in 2 of the 3 cases the average film thickness appeared to increase following a Stribeck curve measurement (Steps E and G). Additionally, the average film thickness for the Batch 2 polymer was reduced at all stages of the testing, with a peak average thickness of 173 nm at image (E), a reduction of 29 nm compared to the smaller scale Batch 1 polymer. This could be attributed to the reduced branching of the copolymer because the film growth was

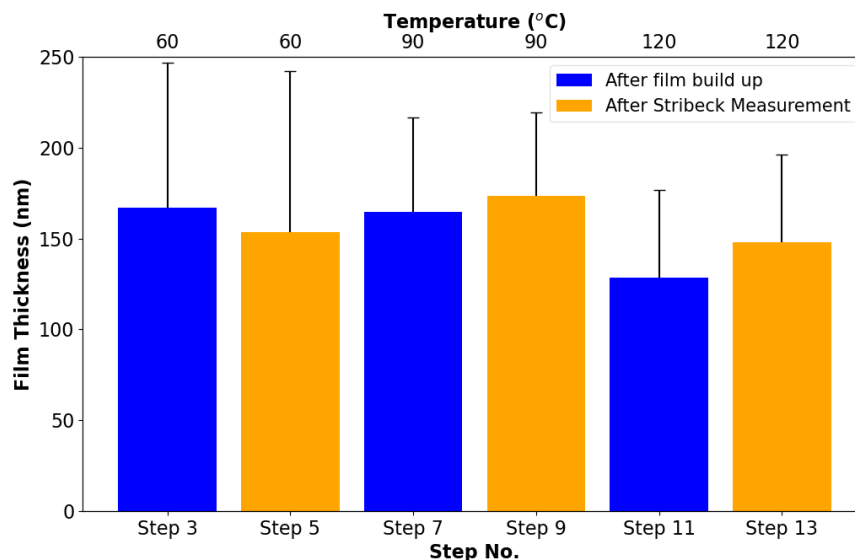


Figure 3.31. A visual representation of the data in Table 7, Entries B-G. It contains the plot of the film thickness in nm for these entries. The overall data in this Figure and Table 3 represent the summary of the film thickness data obtained from interferometry for a 1 wt % Batch 2 semi-block HB polymer/base oil formulation. The blue shading indicates that the measurement was made after film build up (i.e. following a period of constant temperature and rolling speed). The orange shading indicates that the measurement was made after a Stribeck Curve measurement was made.

believed to be enabled by the large number of cross-linkable vinyl end groups available in the HB polymer, resulting from both from the chain transfer product and unreacted DVB bonds. Therefore, if the branching was reduced, there would be fewer vinyl groups available for cross-linking, resulting in reduced film formation. The reduced film thickness at 120 °C (Step F) may have been due to the degradation of these shorter chains due to the film being less cross-linked and thus weaker. However, these mean values may have been heavily influenced by the gouging of the film under entrainment, caused by the CTA contaminant, that was evident in Figure 3.29 and Figure 3.30, and which was reflected in the large errors seen for each Step. In fact, these errors were so large that the difference in the average film thickness between each Step appeared not to be significant.

Despite the observed differences, it was clear that the addition of the Batch 2 HB polymer resulted in the formation of a thin film of comparable thickness (peak thickness within ~30 nm) to that measured for the Batch 1 polymer, which was not

significantly worn down with increasing temperature, applied force between two surfaces, and changing rolling speeds.

3.3.4.3 Friction Coefficient Testing – Stribeck Measurements

The Stribeck curve for the Batch 2 polymer/base oil solution measured by the MTM machine between Steps 3 and 5 (B and C) at 60 °C, between Steps 7 and 9 (D and E) at 90 °C, and between Steps 11 and 13 (F and G) at 120 °C is shown in Figure 3.32.

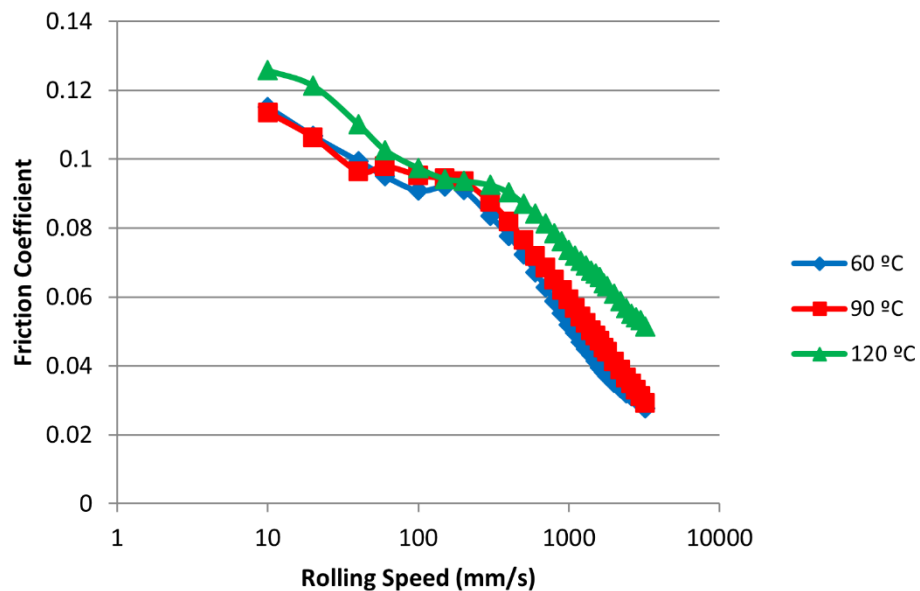


Figure 3.32. Stribeck curve from an experiment using a 5 wt% Batch 2 semi-block HB polymer in oil as the lubricant.

The observed trend was an increase in the dimensionless friction coefficient with decreasing rotation speed. Comparing this to the data from the pure base oil solution (Figure 3.22), it was apparent that the friction coefficient was markedly decreased on addition of the semi-block HB polymer even at low entrainment speeds, as seen for the Batch 1 polymer previously, with the 60 °C test peaking at 0.115, compared to 0.38 for oil without the polymer. Comparing to the data obtained previously for the Batch 1 semi-block polymer, which peaked at 0.14 at 60 °C, it was clear that the overall trend of the friction coefficient was very similar for both batches,

as were the absolute values. The expected trend of increasing friction coefficient with increasing temperature was observed for all temperatures, unlike the data obtained for the Batch 1 polymer, possibly be due to marked decrease in average film thickness observed at Step F. For the Batch 2 polymer, the friction coefficients measured at 60 and 90 °C were observed to be extremely similar, while the coefficients measured at 120 °C were significantly higher. This could be attributed to the dramatic decrease in average film thickness observed at 120 °C (Table 3.7F). Additionally, at low rolling speeds, the expected trend of increasing friction coefficient with increasing temperature was reversed in the 60 and 90 °C measurement. From the average film thickness data in Table 3.7D, this decrease in friction may have been due to the increased average film thickness, which suggested that the decrease in friction was due to the formation of greater average film depth. However, at higher rolling speeds where entrainment was increased, the trend returned to the expected increase in friction coefficient with increasing temperature.

3.3.4.4 Conclusions from Comparison of Small- and Large-Scale Batch Testing

In summary, the film thickness achieved was more variable for the larger-scale polymer batch (Batch 2) when compared to the Batch 1 polymer. This was likely due to a combination of reduced branching and an increase in the amount of abrasive contaminant leading to increased damage to the film. In future, removal of excess PhCoBF may help to improve the performance of the larger-scale batch of polymer. However, the film thickness obtained was still significant, especially compared to that for oil without a polymer additive (Table 3.3), which indicated that the scale-up process had not affected the film formation properties of the HB polymer in any significantly adverse way. Additionally, the trends and values observed in the friction coefficient for the Batch 2 polymer were comparable to those seen for the Batch 1

polymer, indicating both that the scale-up process had not affected the friction-reduction properties of the HB polymer, and that the branching of the HB polymer also had little effect on the measured friction coefficient.

3.3.4.5 Further Tribological Testing

In the case of the Batch 2 polymer, sufficient polymeric material was synthesised to extend the tribological testing further. This included testing on the High Frequency Reciprocating Rig (HFRR) and the Ultra-high Shear Viscometer (USV).

HFRR Analysis

The average friction coefficient measured for a pure base oil solution at 60, 90 and 120 °C is shown in Figure 3.33. Lower rotation speeds were used during this testing than during the Stribeck measurement, resulting in the boundary regime being examined in this case.

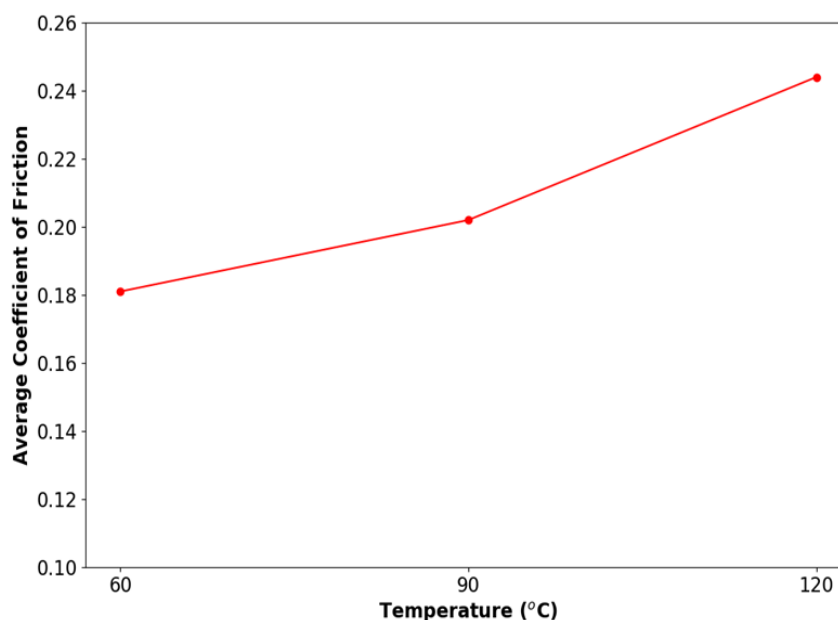


Figure 3.33. Average friction coefficient of PA04 base oil over temperature range 60 - 120 °C.

The observed trend was of increasing friction coefficient with increasing temperature, which was consistent with the Stribeck curve measured in Figure 3.22.

The friction coefficient was lowest at 60 °C, with a value of at 0.182 and rose to a peak of 0.244 at 120 °C. This increase in friction with increasing temperature was attributed to the thinning of the oil and reduced entrainment with increased temperature, as discussed previously.

The Batch 2 semi-block HB polymer was dissolved in base oil at concentrations of 1.0, 2.0 and 5.0 wt%. The average friction coefficient for each concentration was recorded at temperatures in the range 40 – 140 °C, and this data is shown in Figure 3.34.

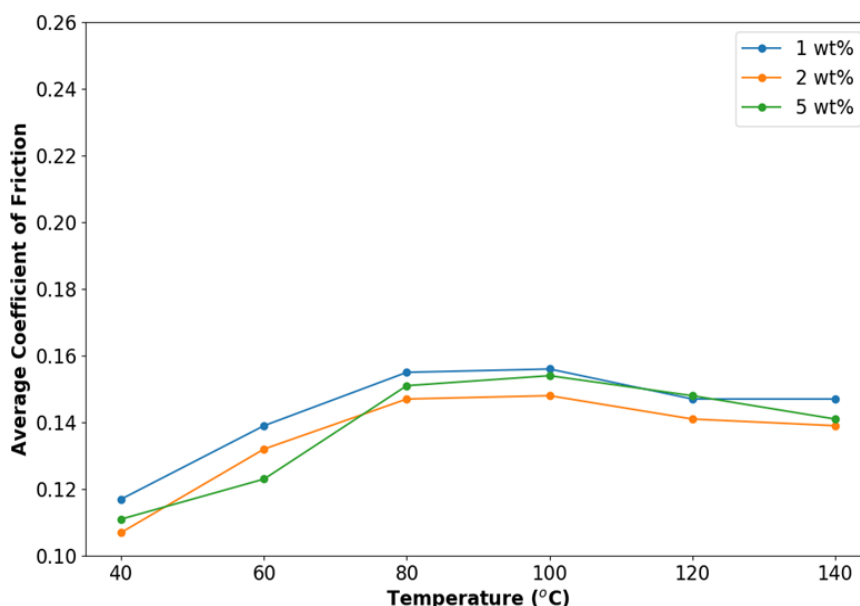


Figure 3.34. Average friction coefficient of semi-block HB polymer over temperature range 40 - 140 °C at loadings 1 wt% (blue), 2 wt% (orange) and 5 wt% (green).

The average friction coefficient was observed to increase with increasing temperature up to approximately 80 °C, which again was consistent with earlier results (Figure 3.32). However, above this temperature, the friction stopped increasing and even begin decreasing with further increases in temperature. Given that these polymers had been previously found to form protective films under stress and temperature (Figure 3.29), it seemed likely that this decrease in friction was caused by the formation of a protective film on the surfaces due to thermally-induced cross-linking of residual vinyl groups within the polymer. This indicated that these

polymers performed well as friction modifiers under more extreme temperature conditions in the boundary regime, and that the film forms most significantly above temperatures of 80 °C. Once again, little difference in the measured friction coefficient was seen between 1 and 5 wt% polymer loading, which indicated that the level of loading did not greatly affect the friction reduction properties of these polymers.

USV Analysis

In order to test the performance of the semi-block polymer under much more extreme and realistic conditions than previously used, the polymer was analysed using an Ultra-high Shear Viscometer, the data for which is summarised in Figure 3.35. Data on the errors associated with these measurements was not available.

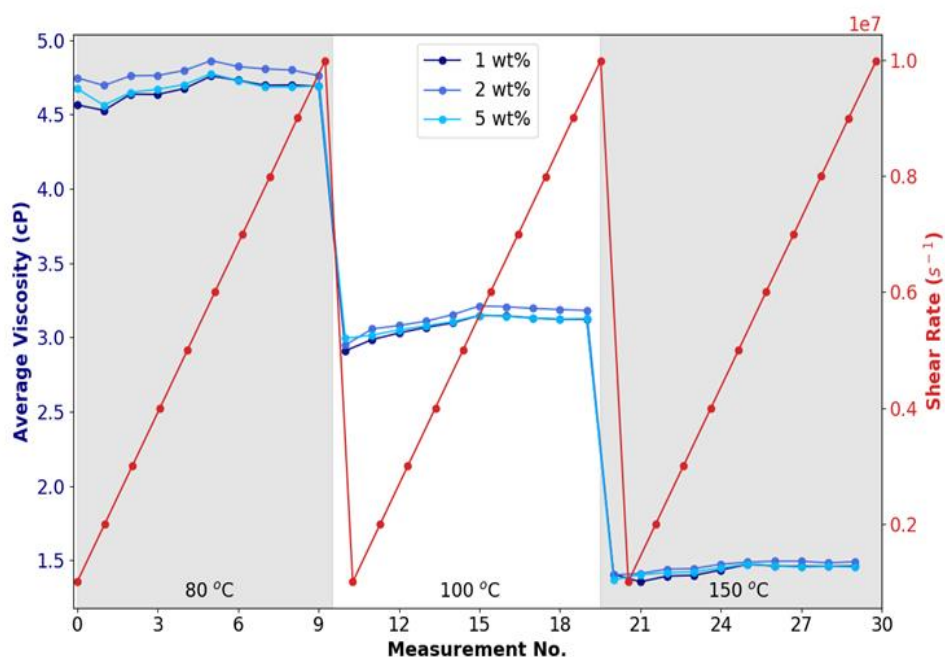


Figure 3.35. The measured average viscosity at 80, 100 and 150 °C, over a range of shear rates (indicated by the red plot) for 1 wt% (dark blue), 2 wt% (mid blue) 5 wt % (light blue) semi-block polymer in PA04.

The Batch 2 semi-block HB polymer was dissolved in base oil at concentrations of 1.0, 2.0 and 5.0 wt%. Each polymer solution was then subject to high shear rates, which increased steadily from $1 \times 10^6 - 1 \times 10^7 \text{ s}^{-1}$, (illustrated by the red plot in Figure 3.35) at

a fixed temperature, and the average dynamic viscosity of each polymer/oil solution, shown by the blue plots in Figure 3.35, was recorded across the shear range. This was repeated at three different temperatures, 80 (left section), 100 (centre section) and 150 °C (right section).

Firstly, it was clear from Figure 3.35 that the viscosity of all three polymer/oil solutions decreased with increasing temperature, from a maximum of ~4.7 cP at 80 °C to a minimum of ~1.4 cP at 150 °C, as was expected given the reduced viscosity modification abilities of the HB polymer and the decreased oil viscosity associated with increased temperature. Interestingly, however, the magnitude of the shear rate appeared to have no effect on the viscosity of the solutions at any fixed temperature, indicating that the polymer/oil solutions behaved as shear-resistant Newtonian fluids in the hydrodynamic lubrication regime. This was in direct contrast to the usual behaviour of linear polymers under high shear rates, where shear thinning behaviour is observed when the polymer is distorted along the direction of flow. This was likely related to the ‘globular’ structure that HB polymers form: the reduced hydrodynamic volume and more robust 3D network, which may result in a reduction in the amount of deformation under shear, with the HB polymers behaving more like solid/deformable spheres than linear polymers.

Comparing the results for each polymer loading, the greatest difference in average viscosity was noted to be in the 80 °C testing regime, where the 2 wt% loading (mid-blue plot) was measured as ~0.2 cP greater than the cases with 1wt% (dark-blue plot) and 5 wt% (light-blue plot) loading. However, it was not possible to get a quantitative evaluation of the errors for these tests, and as the differences observed were very small, this suggests it may not be statistically significant. Certainly, in the

100 °C and 150 °C region, there was no significant difference between the average viscosities of each polymer loading.

3.3.5 Using Thiol CTA to Develop Oil Soluble Polymers

So far, the process for developing base-oil-soluble polymers had focussed on the incorporation of hydrocarbon character into DVB polymer *via* macromer control of the DVB polymerisation. While this process successfully generated oil soluble HB copolymers, it involves a two-step process, where the first step takes a full 24 hours. Additionally, as a crude mixture of LMA oligomers is used, the structure of the HB polymer obtained could vary between batches, depending on the level of dimer/trimer available to act as the CTA. This introduced an added level of uncertainty and variability. Moreover, the yields obtained using CTP were relatively low, limiting the attraction for industry due to the poor economics. While it may be possible to reduce wastage by recovering the unreacted monomer and cobalt CTA (through distillation or filtration etc.), this introduces yet another costly step into the process, further reducing the economy of this route.

Consequently, thiol-controlled chain transfer polymerisation was investigated to define if this strategy could provide a more controlled, rapid and economic method of producing oil-soluble HB polymers. Due to the nature of the chain transfer process, when a thiol is used as the CTA, a fragment of that thiol will be incorporated into these HB polymers. Thus, by choosing a thiol with a high hydrocarbon content, the chain ends of a HB DVB polymer may be functionalised with a long hydrocarbon chain to encourage base oil solubility in a single step. Additionally, previous work within the research group has shown that vastly improved yields may be achieved using thiol CTAs for hyperbranched polymerisations.

Thus, the chosen thiol was dodecanethiol, also known as dodecyl mercaptan (DDM), which contained a chain of 12 carbon atoms, similar to LMA. A range of concentrations of DDM (5-60 mol %) was used with a 1:1 mixture of DVB monomer and cyclohexanone solvent at 150 °C to produce a range of HB polymers with differing levels of incorporated DDM, on a 1 mL scale. The gelation times associated with these polymer reactions can be seen in Figure 3.36, where a roughly linear relationship can be seen between DDM concentration and gelation time.

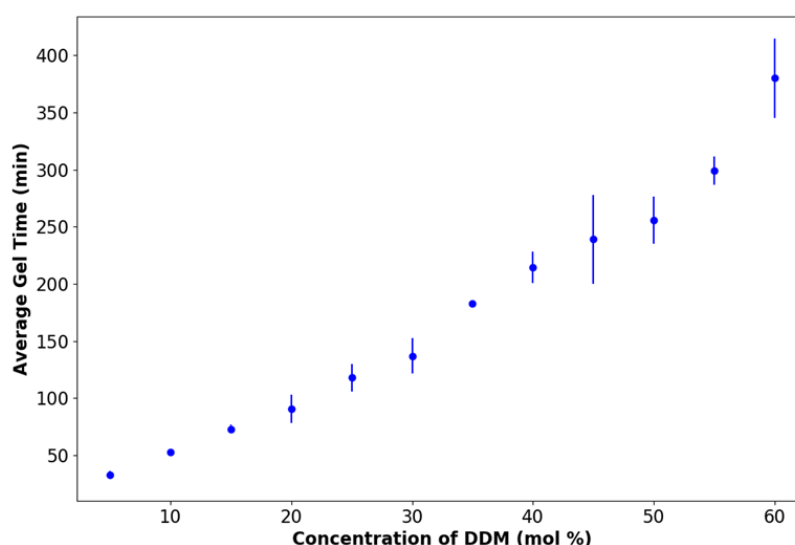


Figure 3.36. The average gelation time over three repeats, obtained for DVB polymerisations using CTA (DDM) concentrations from 0-60 mol %. The circles represent the mean values, while the error bars indicate the standard deviation across these repeat measurements.

This was expected, because a) the thiol was consumed in a stoichiometric manner, and b) as the CTA concentration increased, the average branch length within the polymeric solution was reduced and the probability of chains undergoing transfer with each other was reduced, thus reducing the rate of gelation.

A selection of these DVB polymers were then analysed *via* GPC and tested for solubility in PA04 base oil, as summarised in Table 3.8, using a polymer concentration of 1 wt% and heating up to 56 °C. The actual composition of the polymers was not determined due to time constraints, as it was the solubility of these polymer in the base oil that was of interest, rather than the exact structures achieved.

Table 3.8. Measured yield, molecular weight and dispersity for representative samples of pDVB made using 5-60 mol% DDM chain transfer agent. The solubility of 1 wt% of each polymer in PA04 base oil is also indicated., with Y = fully soluble, P = partially soluble, N = insoluble.

Entry	DDM (mol %)	Yield ^a (%)	Mn ^b (kDa)	Mw ^b (kDa)	Đ ^b	Soluble in PA04?
1	5.0	131	3.8	13.6	3.5	N
2	30.0	76	2.7	25.1	9.3	N
3	40.0	68	2.8	86.2	30.8	N
4	45.0	79	3.1	159.2	52.1	P
5	55.0	81	3.3	188.0	57.0	P
6	60.0	75	2.1	6.2	2.9	Y

^a Determined gravimetrically. ^b Determined *via* gel permeation chromatography.

First, the high yield obtained for 5.0 mol % DDM (Entry 1) was likely due to the presence of residual solvent, which could not be fully removed due to the nature of the polymer sample.

Meanwhile, the molecular weight data indicated that all the polymers were hyperbranched ($\text{Đ} > 2.5$), and the number average molecular weights recorded were very similar across all polymerisations (2.1 – 3.8 kDa). However, it also highlighted three distinct regimes. In the first regime, where the relative concentration of CTA was low, the polymers were observed to be lightly branched, with relatively low dispersity values observed from 5.0 mol% to 30.0 mol % (Entry 1 and 2). This was likely due to the low CTA concentration, which would have resulted in the HB polymers developing fewer, relatively long branches. In the next regime, as the concentration of CTA increased from 40.0 (Entry 3) to 55.0 mol % (Entry 5), the dispersity increased significantly up to a maximum of 57.0, indicating highly branched polymers were produced. This suggested that this range of CTA concentration may have been the optimal range for HB polymer production, likely due to the balance between increased reaction times, which allowed the facile isolation of HB polymer,

and the reduction in branch length, due to the presence of appreciable quantities of CTA. For the polymerisation conducted with 60.0 mol % CTA (Entry 6), the dispersity was the smallest seen, indicating that these conditions resulted in polymers with the lightest branching, likely due to the large quantity of CTA present which would have terminated all branches very quickly. Furthermore, this reaction had to be quenched further from the true gelation time due to time constraints, which would have resulted in a reduced level of branching.

To determine solubility in the PA04 base oil, polymer/oil mixtures (1 wt %) were heated for up to 24 hours with stirring, and dissolution was measured by visual inspection. For the polymers with 5-40 mol % DDM, the pDVB was found to be insoluble in the PA04 base oil. For those with 45-55 mol% DDM, the pDVB was found to initially be soluble in the PA04 base oil after a minimum of 1 hour heating and stirring. However, once these solutions were removed from the heat, the pDVB dropped out of solution to form a cloudy dispersion. For the pDVB with 60 mol% DDM, the pDVB dissolved completely and remained dissolved once removed from the heat. This trend was caused by the increased incorporation of hydrophobic DDM fragments into the pDVB with increased CTA concentration, which enhanced the solubility of the polymer in the hydrocarbon oil. The yield of the 60 mol % polymerisation was the lowest seen, which was likely due to a combination of physical losses during work up and the polymerisation being quenched a little further from the gel point, as the reaction had to be stopped due to time constraints. However, the yield was still higher than most of the dimer/trimer-controlled HB polymerisations conducted previously in this work, and the polymer produced was confirmed to be branched (see above).

Thus, the pDVB synthesised using 60 mol % DDM was chosen as the best candidate for further testing in this work. The synthesis was scaled by a factor of 50 to ensure sufficient polymer was available for testing. The resulting polymer is summarised in Table 3.9.

Table 3.9. Yield and molecular weight data of HB DVB homopolymer produced using 60 mol % DDM as the transfer agent on a 50 mL scale.

Entry	Structure	DDM % (mol%)	Crude Yield ^a (%)	Mn ^b (kD)	Mw ^b (D)	Đ ^b
1	pDVB	60	91	2.14	7.09	3.31

^a Determined gravimetrically. ^b Determined via gel permeation chromatography.

Comparing this to the smaller 1 mL scale reaction outlined in Entry 5 of Table 3.8, it was first apparent that the yield obtained was considerably higher for the larger scale polymerisation. This was attributed to physical losses associated with precipitating and recovering viscous polymers. The 1 mL scale polymerisations resulted in relatively large physical losses during work up as a percentage of the materials synthesised when compared to the 50 mL scale polymerisations, hence the associated yields were lower for the 1 mL scale polymerisations. The molecular weight and dispersity data obtained for the 50 mL scale polymer were very similar to those obtained for the smaller scale polymerisation (Table 3.8), which demonstrated that the polymer was hyperbranched and indicated that the scale-up did not adversely affect the resulting polymer architecture.

Following solubility testing which confirmed that the polymer was still fully soluble in the PA04 base oil, the 50 mL scale sample of pDVB was subjected to tribological testing at the BP/Castrol laboratories. Unfortunately, due to government restrictions, this testing was unable to be conducted in the required time frame, thus we do not have confirmation of the effectiveness of the pDVB polymer as a lubricant additive.

3.3.6 Dielectric Monitoring for HB Polymer Quality Control

For the DVB/LMA HB polymers described above, a robust method of polymer characterisation will be required to provide a quality control mechanism if they are ever to become industrially viable. This is because their structures and molecular weights (MWTs) must be within a specific tolerance, if every batch of polymer is to function as expected. However, the method of characterisation most widely used to measure polymer molecular weight and polydispersity (\mathcal{D}), Gel Permeation Chromatography (GPC), possess inherent limitations with respect to highly branched polymers such as hyperbranched polymers (see Chapter 1, Section 1.9.1).

Due to the proven applicability of dielectric analysis to HB polymeric samples [52], dielectric analysis (Chapter 2.2.5) was chosen as the analysis method to investigate, in an attempt to develop a more accurate method of characterisation. It was decided to conduct this testing on the HB LMA/DVB polymers which have been of most interest so far, to provide a new viable industrial strategy for polymer characterisation.

A range of HB polymers based around the semi-block HB copolymer described above were produced to investigate whether dielectric analysis could be used to monitor the reproducibility of HB reactions. Three samples of 8:2 v/v HB LMA-DVB semi-block copolymer were synthesised under identical reaction conditions (see Table 3.10, 1-3).

Table 3.10. The number average (M_n) and weight average (M_w) molecular weights, and dispersity (\mathcal{D}) of all polymer samples subject to dielectric property testing.

Entry	LMA:DVB (v/v)	Reaction Time (min)	M_n^a (kD)	M_w^a (kD)	\mathcal{D}^a
1	8:2	35	653.1	4360.0	6.7
2	8:2	35	624.5	4139.4	6.6
3	8:2	35	4.4	254.2	58.4
4	8:2	30	4.2	311.1	74.7
5	8:2	20	8.3	55.2	6.7
6	8:2	10	2.5	13.7	5.5
7	9:1	75	614.5	2992.5	4.8

^a Determined *via* gel permeation chromatography.

Additionally, to further investigate whether dielectric analysis would be suitable for monitoring HB polymer cure using in-line analysis, 8:2 v/v HB LMA-DVB semi-block polymerisations were reacted for 10 minutes, 20 minutes and 30 minutes (Table 3.10, 4-6) before being quenched. Finally, in order to determine whether dielectric analysis could distinguish between copolymers of similar molecular weight but different copolymer ratios, a HB LMA-DVB polymer with monomer ratio 9:1 v/v (Table 3.10, 7) was synthesised and compared to the 8:2 semi-block structure (Table 3.10, 1).

These polymers were subjected to dielectric analysis, which was conducted by Dr Alexis Kalamiotis (Faculty of Engineering). The dielectric properties of these HB LMA-DVB copolymers were studied over a temperature range of 20 – 180 °C with a step interval of 10 °C. Cavity perturbation technique was selected for this study due to the physical form of the samples. The experimental setup consisted of a copper resonant cylindrical cavity with TM_{0n0} identified modes at 912 MHz, 1429 MHz, 1949 MHz and 2470 MHz (see Chapter 2.2.5). A small sample (1-2 mL) of each polymer was used. The GPC results for these polymers were also measured for comparison (see Table 3.10).

3.3.6.1 Determining Batch-to-Batch Repeatability

Firstly, three isolated 8:2 HB polymer samples produced under identical conditions were analysed. The GPC data for these polymerisations are shown in Figure 3.37, 1-3, while Figure 3.37a and b show the dielectric constant and loss values versus frequency, respectively.

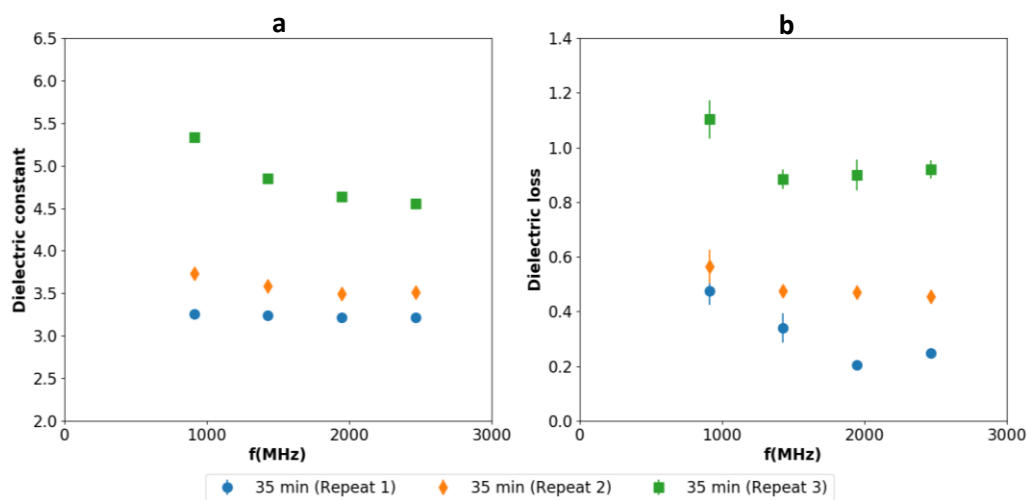


Figure 3.37. a) Dielectric constant and b) dielectric loss versus frequency (MHz) for 8:2 LMA2-DVB copolymer repeats. Error bars are included for both plots, though they are small enough to be indistinguishable for the dielectric constant data.

Here, Repeat 1 corresponds to Table 3.10.1, Repeat 2 corresponds to Table 3.10.2 and Repeat 3 corresponds to Table 3.10.3. Looking first at the dielectric data, two of the samples displayed similar dielectric properties (Repeat 1 and 2), indicating structural similarity. However, the third batch (Repeat 3) displayed an increased dielectric constant, suggesting the structure was changed or molecular weight was significantly lower: smaller polymer chains demonstrate increased dielectric properties, since they have greater freedom of movement due to decreased entanglement and thus respond more readily than longer chains to the incident electric field. Similarly, the GPC analysis in Table 3.10 indicated that the molecular weight of Repeat 3 was significantly lower than Repeats 1 and 2, while dispersity was increased, confirming the validity of the dielectric analysis to differentiate different HB structures.

The results above supported the hypothesis that dielectric properties could be used to differentiate between different types of HB structure. Additionally, Repeat 3 was observed visually to be less viscous than Repeats 1 and 2. This difference in polymer structure was attributed to the fact that in the process that produced Repeat 3, the LMA oligomer mixture produced in the first step of the polymerisation was used directly at the 5°C overnight storage temperature. As the process for Repeat 1 and 2 used LMA at room temperature, this effectively increased the gelation time of the polymerisation. As a result of the increased time required for Repeat 3 to reach reaction temperature, this meant that, at 35 minutes, this reaction was quenched further away from the gel point of the reaction than Repeats 1 and 2. This strategy was adopted to show that dielectric analysis could indicate the presence of such procedural, and thus molecular differences in the HB polymerisation process.

Compared to the results from previous work, [52] the difference in the dielectric properties and molecular weights/PDI between batches was significant. This was due to the change in manufacturing process adopted, and the dielectric property measurement was capable of capturing these differences between batches. This suggests that dielectric analysis may provide a simple and potentially in-line method of both ensuring batch-to-batch repeatability and possibly monitoring the level of cross-linking to maximise yield and branching of HB polymerisations.

3.3.6.2 Monitoring Polymerisation Progress and Level of Cure

Next, the three 8:2 LMA-DVB copolymers quenched at 10, 20 and 30 minutes (Table 3.10, 4-6) to form, polymers of low (entry 6), mid (entry 5) and high (entry 4) molecular weight, respectively, were analysed. The dielectric properties of these polymers are shown in Figure 3.38.

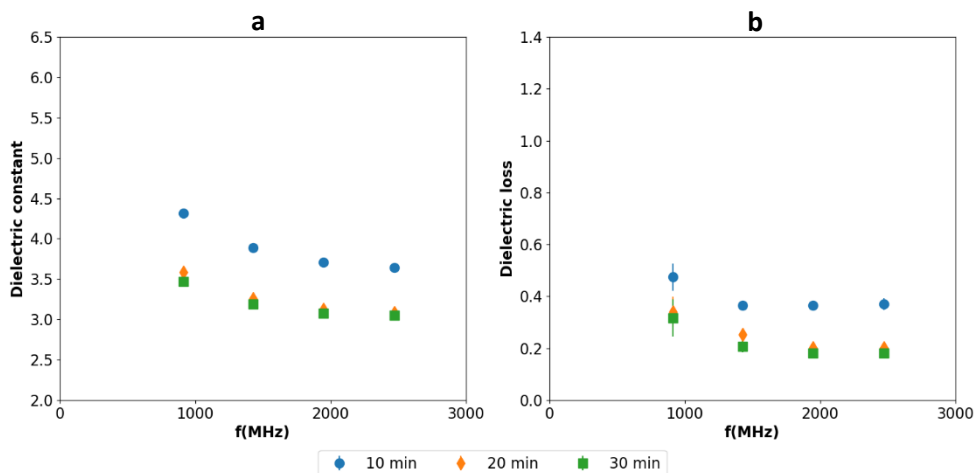


Figure 3.38. a) Dielectric constant and b) dielectric loss versus frequency (MHz) for a low molecular weight polymer (10 min reaction time), a mid-molecular weight polymer (20 min reaction time) and a high molecular weight polymer (30 min reaction time) of 8:2 LMA2-DVB. Error bars are included for both plots, though they are small enough to be indistinguishable for the dielectric constant data.

It was observed that both dielectric constant and loss decreased as the reaction time increased. This was the expected trend: in previous work, and in the section above, it had been shown that the response from the polymer was weaker than that of the monomer/lower MWT polymer, hence a higher molecular weight polymer should result in lower dielectric property values.

Looking at the GPC data in Table 3.10, 4-6 demonstrates the difficulty of relying on GPC data for HB polymers: the M_n values did not follow the expected trend, as the 20-minute reaction had the highest M_n value. This was likely due to problems with the calibration standard, and the M_w values should be considered more reliable for highly branched polymers, as these are related more to the mechanical behaviour of the polymer than the chemistry. As such, the M_w values follow the expected trend, where the 10-minute reaction demonstrated the lowest M_w and the 30-minute reaction demonstrated the highest M_w polymer as was expected. Thus, the M_w data corroborated the data obtained from dielectric analysis, which proved to be able to distinguish HB polymers of various molecular weights. This suggested it may be a useful technique for monitoring cure in-line in future applications.

3.3.6.3 Distinguishing HB Copolymers with Different Molecular Weights

Finally, the copolymer synthesised using a 9:1 v/v ratio of LMA:DVB (Table 3.10, 7) was analysed. This polymer contained an increased level of the monofunctional LMA than the 8:2 copolymer. Figure 3.39a and b show the dielectric constant and loss values for the 9:1 and an 8:2 LMA-DVB copolymer (Table 3.10.7 and 1, respectively).

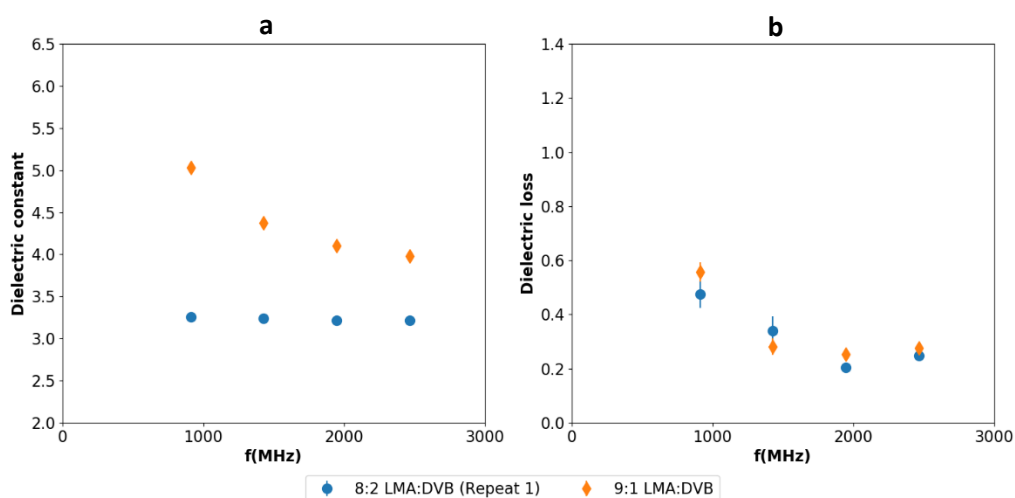


Figure 3.39. Dielectric responses of two ratios of LMA-DVB copolymers. Part a) shows the dielectric constant, part b) shows the dielectric loss vs frequency (MHz). Error bars are included for both plots, though they are small enough to be indistinguishable for the dielectric constant data.

Looking first at the GPC data for these two polymers, it can be seen that the M_n value of the 9:1 polymer was similar to those of the 8:2 polymer in Entries 1 (Repeat 1) and 2 (Repeat 2). However, the M_w value for the 9:1 polymer was considerably reduced, as was the dispersity, indicating lighter branching in this copolymer. This was likely due to the reduction in cross-link density, as the relative amount of di-functional monomer was reduced by 10% in the case of the 9:1 polymer. This reduction in cross-link density and increased incorporation of a flexible, hydrocarbyl species should have resulted in greater chain flexibility and mobility, and hence in a greater interaction with the incident field, and thus an increased dielectric response would be expected. The sample of 8:2 polymer (Entry 1) was chosen for comparison because its molecular weight was closest to that of the 9:1 copolymer.

Focussing now on the dielectric constant data in Figure 3.39a, the measured dielectric constant was seen to be greater in the polymer with greater LMA content across all frequencies, as expected. This was likely due to that fact that the cross-link density of the co-polymer decreased. The addition of a greater proportion of the monofunctional, flexible LMA monomer to the structure increased the mobility of the polymer chain, which resulted in an increased interaction of the polymer with the incident electromagnetic field and an increase in the ability of the polymer to store energy. This was in agreement with work previously reported by He et al., that the relative permittivity of DVB-based copolymers was related to the extent of the cross-link density in the copolymer, which was related to the concentration of di-functional monomer, DVB. It was also in agreement with the results seen in the previous work within the group for HB-DVB [52]. Meanwhile, the dielectric loss data was comparable for the 8:2 and 9:1 copolymers, which may reflect their similar M_n values.

Thus, this indicated that the dielectric analysis data could also provide information about the relative PDI of the HB polymer, where the data above suggested that the dielectric loss gave the clearest indication of the relative M_n of the HB polymer. This was because this property indicated the ability of the material to transfer stored energy into heat *via* intermolecular friction. Thus, globular polymers of the same M_n could transfer similar amounts of energy into intermolecular friction. However, the dielectric constant, which gives an indication of how much energy a molecule can store, would be influenced by the level of end group density and degree of flexibility in the structure (i.e. the level of branching achieved in the polymer). The greater the “accessible” flexibility, the greater the energy a molecule can store. This data showed that the polymer which possessed the lesser branching and/or greater flexible hydrocarbyl end group recorded the greater dielectric constant.

The loss tangent ($\tan \delta$, Chapter 1, Equation 12) was then calculated for the two copolymers, as visualised in Figure 3.40.

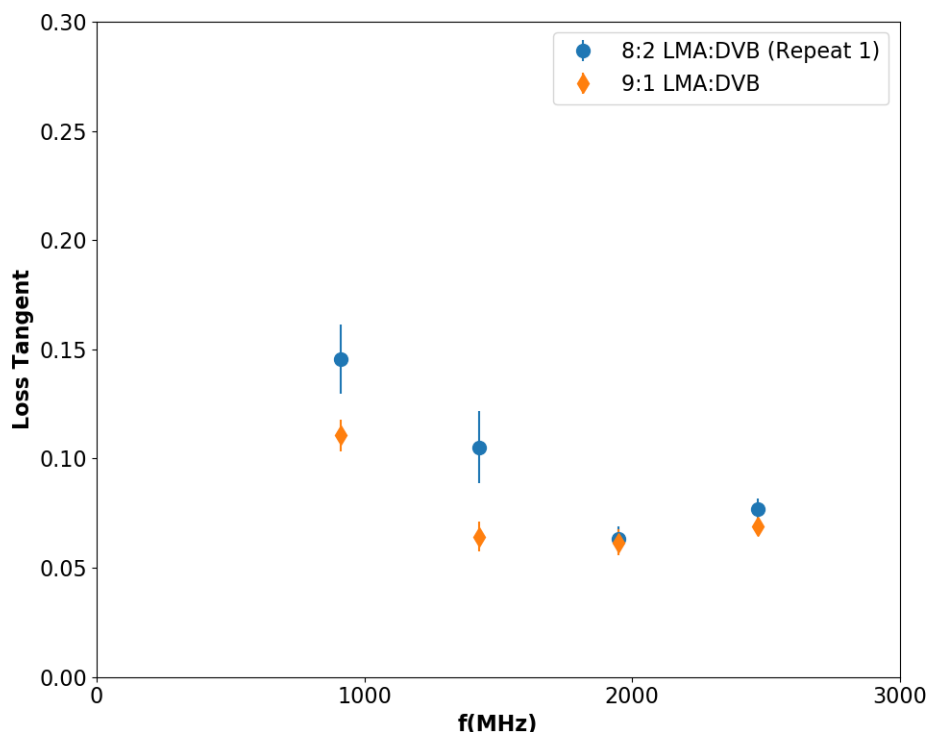


Figure 3.40. Loss tangent for 8:2 (blue circle) and 9:1 (orange diamond) v/v LMA:DVB copolymers.

Generally, it was observed that the 8:2 copolymer demonstrated a higher $\tan \delta$ than the 9:1 copolymer, especially at lower frequencies. The observed differences in $\tan \delta$ values between the two copolymers were attributed to difference in architecture between the two polymers, with the more flexible 9:1 copolymer storing more of the incident radiation than the 8:2 copolymer.

Overall, this data demonstrated that it should be possible to differentiate HB polymers with varied monomer ratios using dielectric spectroscopy, due to the change in the value of the dielectric constant observed with a change in concentration of DVB, where the dielectric properties measured increased as the concentration of DVB decreased. This was due to the change in the degree of branching, where the addition of more LMA resulted in a more flexible, linear structure, which increased the

ability of the dipoles to align themselves with the external field. However, care must be taken, as any difference in molecular weight between the two polymers could also contribute to the difference in dielectric properties observed, though the contribution from a reduction in molecular weight appeared to be a smaller effect than that of varying copolymer ratio. A more thorough investigation, using copolymers with a variety of ratios of more similar molecular weights should be conducted to verify this result. Also, it has been demonstrated that reviewing both dielectric constant and loss data can give different information about the relative polymer structure.

3.3.7 High Throughput Copolymer Viscosity Screening

Previously, all the kinematic viscosity testing of HB polymers in this study was conducted using large scale apparatus on-site at BP/Castrol. This testing was essential for any new polymeric additive, however, this experimental work was problematic for a number of reasons: each test required tens-of-grams of sample, the testing site was not local to the synthetic laboratory, the testing process was time consuming, and each sample (polymer concentration) had to be prepared and loaded manually.

Hence, a faster, more convenient alternative method of screening new polymeric additives was investigated. A liquid handling system (Microlab STARlet, Hamilton Robotics, Inc. [53]) was employed in the attempt to develop a high-throughput alternative for viscosity testing: a diagram of the liquid handling system is shown in Figure 3.41 (see Chapter 2.2.6)).

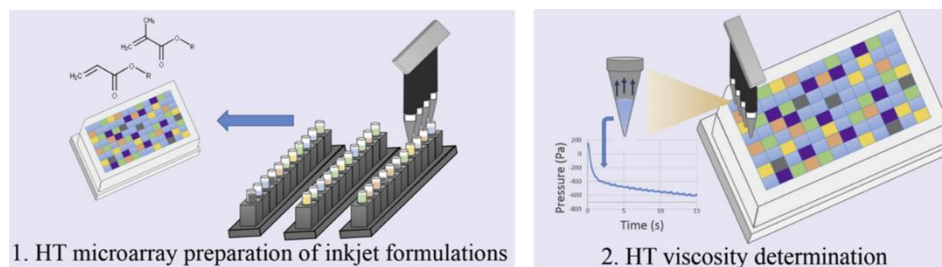


Figure 3.41. Diagram of the process used to determine viscosity in the liquid handler system [53].

This high throughput technique enables the testing of 96 formulations per 13 working hours. It involves a series of pipettes which automatically inject the required quantities of each component into a well plate, heats the well plate to the chosen temperature, and then measures the pressure required to aspirate the resulting solution. This pressure can then be used to determine the solution viscosity. Additionally, only a few mL of sample is required per test in this system, making this much more suitable for screening new copolymers, which are often only produced on a milligram scale, than the larger scale apparatus currently in use in the industrial laboratories. As this was a proof of concept, the evaluation was conducted on one copolymer formulation.

Previously, kinematic viscosity data at 40 °C for semi-block (crude LMA oligomers used) DVB:LMA copolymers were obtained from large scale testing at the industrial sponsor's site using a capillary rheometer (see Figure 3.26). Thus, in this work, solutions of PA04 base oil [44] and the semi-block DVB-LMA copolymer, in a ratio 2:8 (v/v) DVB:LMA, were prepared with polymer concentrations of 0.5, 1.0, 2.0 and 5.0 wt%. These formulations were then tested on a liquid handing apparatus in order to determine their viscosity *via* this method. This section will discuss the results of these viscosity measurements and how they may be useful in providing a fast and simple screening process for future copolymers and compare the results to those obtained from larger scale testing. Testing was conducted in collaboration with Dr Zuoxin Zhou of the CfAM group at the University of Nottingham.

3.3.7.1 Comparing Liquid Handler and KV Results

The 40 °C kinematic viscosity data discussed previously (see Section 3.3.4.1) for the semi-block DVB-LMA (see Figure 3.26) is shown in the purple and blue plots in Figure 3.42 (EP copolymer and semi-block copolymer, respectively). As discussed previously, Centistokes are the unit used, as this is the ASTM standard unit for kinematic viscosity measurements within the industry, where $1 \text{ cSt} = 1 \text{ mm}^2 \text{ s}^{-1}$.

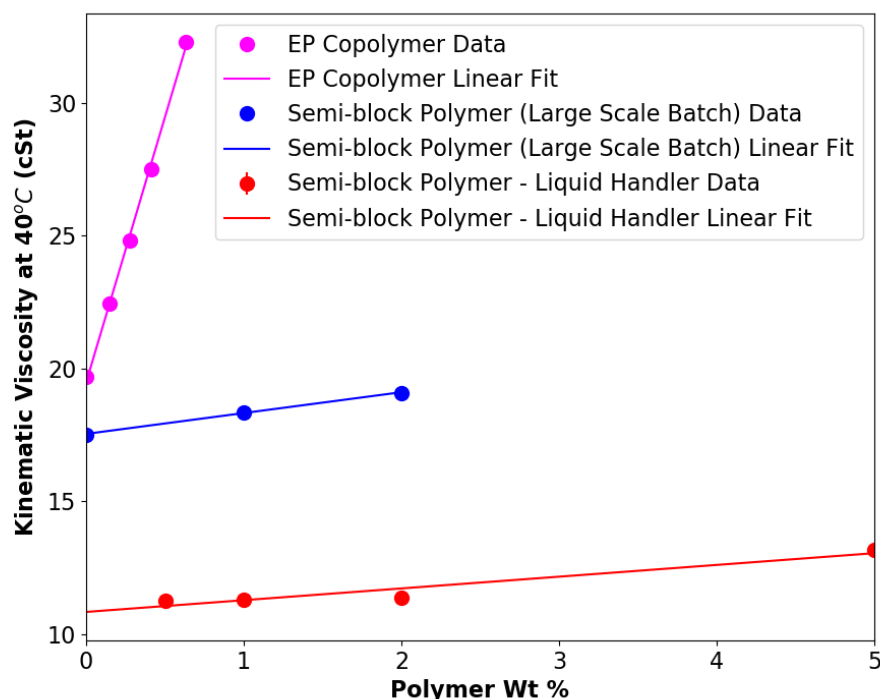


Figure 3.42. Viscosity data for 2:8 DVB:LMA copolymer. The purple and blue data was obtained from large scale kinematic viscosity testing apparatus on-site at the BP/Castrol. Purple: linear ethylene-propylene (EP) copolymer, used as standard lubricant additive. Blue: semi-block DVB:LMA copolymer. The data shown in red was obtained on the liquid handling system for a semi-block DVB:LMA copolymer. Straight lines represent a linear fits to the data. Data on the errors was not available.

When compared to data obtained for a standard linear ethylene propylene (EP) copolymer (shown in the purple plot in Figure 3.42), which is commonly used as a lubricant additive, it was observed that the viscosity of the oil was only marginally increased with addition of the HB polymer, even up to 5.0 wt% loading, due to the globular structure of the HB polymer.

The viscosity data obtained for the semi-block HB polymer from the liquid handler apparatus is shown in the red plot in Figure 3.42. Comparing to the data from the KV capillary rheometer (blue plot), it was observed that the trend observed for increased viscosity with increased polymer loading was very similar. The straight-line fit possessed a similar gradient, which indicated that the polymer tested on the liquid handler behaved in a similar manner to the sample tested in the capillary rheometer.

However, it was also clear that there was an offset of ~ 7 cSt between these two data sets. This discrepancy could be due the level of shear associated with the measurements made *via* the liquid handler. KV measurements in a capillary rheometer are not measured under high shear conditions, as the only force acting on the sample is gravity. Meanwhile, the liquid handler uses high pressure to force the polymer out of the pipette tips, which creates shear in the polymer. Thus, the offset could have been due to the fact that the shear forces in the liquid handing system caused a small and consistent amount of shear thinning of the polymer during the measurement, and therefore reduced its apparent viscosity. Alternatively, the offset may be due to an error in the conversion from pressure to viscosity, however it is difficult to be sure with just one dataset: similarly, due to error-bar overlap, the fit gradient may not be accurate. Another possible source of error would be differences in the molecular weight/dispersity and architecture of the two polymer samples. The GPC data for the two polymer samples tested are shown in Table 3.11: these are the same two polymers outlined in Table 3.10.1 and 2 respectively.

Table 3.11. The number average (M_n) and weight average (M_w) molecular weights, and dispersity (\mathcal{D}) of sample sent to BP for large scale testing on KV capillary rheometer apparatus (1) and sample tested on liquid handler system. These correspond to entries 1 and 2 in Table 10.

Entry	LMA:DVB (v/v)	Reaction Time (min)	M_n^a (kD)	M_w^a (kD)	\mathcal{D}^a
1	8:2	35	653.1	4360.0	6.7
2	8:2	35	624.5	4139.4	6.6

^a Determined *via* gel permeation chromatography.

It was observed that the two polymer samples displayed very similar molecular weights and dispersities, hence differences in architecture are unlikely to be responsible for the observed offset.

Despite the offset, this initial dataset did indicate that the liquid handler could be used to give a more rapid estimation of a mixture's viscosity that is in the range of interest to fuel lubricants. However, to improve the reliability of this data in future, further oil-soluble HB copolymers should be tested, with a wider range of loadings, which would also make use of the automation available with the liquid handler. Furthermore, polymer samples which have undergone more thorough testing at BP/Castrol on their large-scale apparatus, and are well characterized and understood, should also be tested on the liquid handler: this will allow a direct comparison to be made on a much larger array of samples.

3.4 Conclusions

3.4.1 Synthesis and Tribological Testing of HB DVB/LMA

- Successfully synthesised two architectures of low viscosity, oil soluble hyperbranched copolymer of DVB and LMA, using oligomeric control agents to enhance control and oil solubility at < 5 mL scale – semi block (using crude monomer/oligomer mixture) and block (using pure dimer/trimer).

- Kinematic Viscosity testing indicated that HB polymers displayed significantly reduced viscosity compared to linear EP copolymer, up to 5 wt% loading.
 - HBPs not suitable as viscosity index improvers, as would need much greater loading to achieve same effect, which would be more expensive
- CCS indicated that inclusion of HBPs in a formulation would not adversely impact low temperature performance.
- HBPs underwent tribological testing to determine that they act to reduce friction and wear across a range of lubrication regimes.
 - MTM data indicated both semi-block and block copolymers form thin, robust protective films with increasing temperature and rolling speed, which reduced friction between the moving parts.
 - HBPs crosslink on surface at elevated temperature, thus films increased in thickness as the experiment was run.
 - The block polymer solution underwent a lower overall increase in film thickness than the semi-block polymer as the test proceeded, and the increase in film thickness did not produce the same decrease in friction for the block copolymer as the semi-block.
 - This was due to the lower molecular weight of the block polymer compared to the semi-block: the lower weight polymer was less able to crosslink during the experiment due to the decreased volume occupied by the smaller polymer, which made polymer interactions less likely than for a higher molecular weight polymer.
 - The film produced by the Block polymer was also less strong and more capable of being destroyed compared to the semi-

block film, which supported the idea that there was less crosslinking between the polymer molecules.

- From EHD measurements, the addition of semi-block polymer caused a thickening effect and formed a protective film under elastohydrodynamic lubrication regimes. Meanwhile the block polymer did not display thickening behaviour or film formation. Both polymers were seen to act a constant viscosity fluids, which suggested shear thinning occurred at these high entrainment speeds.
- Both HBPs demonstrated excellent film formation and wear prevention properties, with good potential for use as friction modifiers, but not viscosity modifiers.
- Identified semi-block polymer as best option for further study as compromise between performance and synthesis cost.
- Scaled up synthesis of semi-block copolymer by order of magnitude, sent to BP/Castrol for tribological testing.
 - KV, CCS and MTM testing show comparable results for the large-scale polymer batch.
 - Slight reduction in film thickness due to slightly reduced molecular weight and metal contaminant.
 - Extra purification step may be required in future to remove PhCoBF contaminant
 - Overall, performance differences were insignificant, and scale up was a success.
- Further tribological testing:

- HFRR confirmed semi-block polymer reduced friction at low rolling speeds (in boundary regime) over a wide temperature range, and that films formed most significantly above 80 °C due to crosslinking.
- USV confirmed polymers behave as shear-resistant Newtonian fluids in the hydrodynamic lubrication regime – contrary to EHD results.

3.4.2 Using Thiol CTAs to Synthesise Higher-Yielding Oil Soluble HB Polymers

- Aimed to improve yields and make the HB polymer synthesis a faster, more economic, one-step process.
- Successfully synthesised pDVB using thiol (DDM) control at variety of DDM concentrations on 1 mL scale.
- 60 mol% DDM was identified as concentration which gave best oil solubility.
 - While 40.0 – 55.0 mol % DDM were the best conditions for producing HBPs, the resulting polymers in this range were insoluble in PA04 base oil.
- Synthesis of pDVB controlled with 60.0 mol % DDM was scaled to 50 mL scale.
 - pDVB was found to still be oil soluble.
 - Yield further improved to 91 %.
- Tribological testing of pDVB could not be conducted due to COVID 19 restrictions.

3.4.3 Dielectric Monitoring of HBPs for Batch-to-Batch Reproducibility

- Wanted to find new, more accurate characterisation method for HBPs, which may potentially be able to monitor HB polymerisations in-situ and monitor batch-to-batch repeatability.

- Measured the dielectric properties of range of hyperbranched co-polymers synthesised from mono-functional lauryl methacrylate (LMA) and di-functional DVB *via* CCTP.
- Measurements of the dielectric constant and loss were used to determine the effect of molecular weight and polymerisation time on the dielectric properties of LMA-DVB samples with the same LMA:DVB ratio, and to determine batch-to-batch repeatability.
- Demonstrated that dielectric spectroscopy can be used to differentiate HBPs with varied monomer ratios, observing that, as the concentration of LMA increased, the dielectric constant measured increases due to a decreasing degree of branching: the addition of LMA resulted in a more linear, flexible structure, which increased the ability of the dipoles to align themselves with the external field.
- Both dielectric loss and constant were found to be good indicators of variance in the molecular weight/structure of different batches of the same HBP: this work supported the observations made by Nambiar previously [52].
- Findings largely corroborated by GPC data, while also indicating the need for this new measurement technique for HBPs.

3.4.4 Liquid Handler For Screening New Copolymers

- Aimed to develop a faster screening method which requires less material per test, and the possibility of automation.
- Viscosity profiles of new copolymers can be obtained through the use of a liquid handling system: may be possible to screen the viscosity profiles of future lubricant formulations quickly and efficiently, while requiring only a few milligrams of sample to do so.

- This will significantly increase the speed at which new copolymers may be developed and optimized in future.
- More testing is required to confirm whether offset is due to science or equipment.

3.5 Future Work

3.5.1 Synthesis and Tribological Testing of HB DVB/LMA

The DVB:LMA 2:8 v/v semi-block copolymer has been proven to perform well as a low viscosity lubricant, while the methodology used to synthesise it has also proven robust up to the 50g scale. However, further scale up of the synthesis of the is needed in order to prove the industrial viability of this methodology, and to provide sufficient material for extended tribological testing and formulation optimisation. Thus, it would be valuable to investigate and optimise the synthesis of the semi-block copolymer using a 5kg rig, such as that available in the Faculty of Engineering, to further develop the batch processing methodology for this polymerisation.

However, large-scale batch processing of a free radical polymerisation carries inherent risk, due to large volumes being non-uniformly heated and the potential for runaway propagation due to reduced mass and heat transfer efficiencies. Therefore, future work should also investigate the synthesis of HB semi-block polymer in a flow rig with microwave heating. This would enable the development of a continuous flow methodology, which would both reduce the risk associated with large scale polymer heating and allow polymer to be produced on a further increased scale in a more economic and efficient manner.

Once these large-scale methodologies are developed, extended testing of the polymer should be conducted. This will ensure the scale up process does not impact the performance of the polymer, and enable testing over a wider range of conditions.

For example, the polymer should be tested in full-scale engine rigs under realistic conditions, to ensure that the results obtained from small-scale tribological tests are representative of real-world results. Additionally, the polymer should be tested in combination with all of the additional additives required in the full engine oil formulation, to investigate whether the interactions between the additives results in any adverse (or synergistic) effects.

Additionally, similar scale up and testing should be conducted on polymers synthesised using different monomer combination, developed to further optimise performance or reduce emissions (see Chapter 5 for more details).

3.5.2 Using Thiol CTAs to Synthesise Higher-Yielding Oil Soluble HB Polymers

The polymerisation of DVB using DDM as the control agent proved that this methodology could produce oil-soluble polymers and help increase the yields of HB polymers. Now, these polymers need to undergo tribological testing at BP/Castrol laboratories in order to determine whether they may be of use as lubricant additives. Following these tests, the polymerisation may have to be further optimised, as outlined for the semi-block polymers above, or a new application identified.

3.5.3 Dielectric Monitoring of HBPs for Batch-to-Batch Reproducibility

Dielectric monitoring demonstrated promise as a method of accurately monitoring the batch-to-batch reproducibility of HB polymers. However, a wider range of monomers and monomer ratios should be tested to ensure that these results are applicable to all HB polymers.

Additionally, to extract the most value from this characterisation technique, the use of a coaxial probe to monitor HB polymerisation in-situ should be investigated. This would enable continuous flow synthesis, such as that described above, to be

monitored in real time, ensuring the polymerisation remains optimised and any deviations from the ideal conditions can be quickly rectified.

3.5.4 Liquid Handler For Screening New Copolymers

The results obtained so far indicate that using the liquid handler to screen the rheological properties of various HB copolymers should, in theory, be possible. However, repeat testing is needed to determine whether the offset in viscosity values compared to the KV viscometer seen here is significant, or simply due to a calculation error. Additionally, it would be beneficial to test some polymers which have previously been used by BP/Castrol, and which are already well characterised, in order to calibrate liquid handler with KV viscometer. Furthermore, it would be useful to use this wide range of pre-measured additives to make use of the of the automation inherent in the liquid handling system, which would enable the testing of a wider range of additives at wider range of concentrations.

3.6 References

- [1] A. Miller, "The chemistry of lubricating-oil additives," *Armour Res. Found.*, 1930.
- [2] L. R. Rudnick, *Lubricant Additives: Chemistry and Applications*, 1st ed. CRC Press, 2003.
- [3] A T C, "Lubricant Additives: Use and Benefits," no. August, 2016.
- [4] "What are Friction Modifiers?" [Online]. Available: <https://www.machinerylubrication.com/Read/28815/what-are-friction-modifiers>. [Accessed: 24-Nov-2020].
- [5] R. M. Mortier and S. T. Orszulik, *Chemistry and Technology of Lubricants*.

- Springer US, 1994.
- [6] W. O. Winer, "Molybdenum disulfide as a lubricant: A review of the fundamental knowledge," *Wear*, vol. 10, no. 6, pp. 422–452, Nov. 1967.
- [7] L. Cizaire *et al.*, "Mechanisms of ultra-low friction by hollow inorganic fullerene-like MoS₂ nanoparticles," *Surf. Coatings Technol.*, vol. 160, no. 2–3, pp. 282–287, 2002.
- [8] Z. Tang and S. Li, "A review of recent developments of friction modifiers for liquid lubricants (2007–present)," *Curr. Opin. Solid State Mater. Sci.*, vol. 18, no. 3, pp. 119–139, 2014.
- [9] ASTM, "ASTM Compass." [Online]. Available: [https://compass.astm.org/EDIT/html_annot.cgi?D2270+10\(2016\)](https://compass.astm.org/EDIT/html_annot.cgi?D2270+10(2016)). [Accessed: 02-Aug-2021].
- [10] T. Cserhati, E. Forgacs, and G. Oros, "Biological activity and environmental impact of anionic surfactants," *J. Memb. Sci.*, vol. 228, no. 1, pp. 337–348, 2002.
- [11] Afton Chemical, "Viscosity Index Improvers & Thickeners | Afton Chemical." [Online]. Available: https://www.aftonchemical.com/SBU/Lubricant-Components/ThickenersViscosityIndexImprovers?__cf_chl_jschl_tk__=aa89700020d37c8f62521805968307f3ad62ebc7-1606211884-0-ARQrpKiLTanC1jEhNVskxsDHI1dqKdy5SrBtsyBFRLS10aYHn5fVqVeWo05-JtNDIpvufcVt9-dDgy3az8BFRPJ5Oclsrj63NbXU4vUeeujD5mBx8BVVtsTIGBboTntGjrqvfuE9MAUFQb6sMwF6UwvoEdHWh_Rrr-ltHqPDuQ0OR_LFcxaWsolnEEYOpeHidDzqYgP2rtOL5dk5-

OfoPZa3VpRgajhGLrfeHONhIKrd4Z7E-9UocZAT-
HHEO_IXcsd5ufV72z8y4VZSJYU0ceS0liPdv4bZ8bzKc1aBa1M1FnsfGBfRQZxX
Mz_JvPfZMEv_RrWGoVrocJ4jDDy19E5ryGmwemrgBgdR2wzmMAfdvU-
78zSsKAuftgJM9wBbv3bd-
sXXYpsgt0w5WXvzXbB5MOImgfYPG7kTo4FghBpEOD0QtkzoMSgUI09ybKGcw.
[Accessed: 24-Nov-2020].

- [12] J. W. Robinson *et al.*, “Probing the molecular design of hyper-branched aryl polyesters towards lubricant applications,” *Sci. Rep.*, vol. 6, no. June 2015, pp. 1–10, 2016.
- [13] F. Wiesbrock, R. Hoogenboom, and U. S. Schubert, “Microwave-assisted polymer synthesis: State-of-the-art and future perspectives,” *Macromol. Rapid Commun.*, vol. 25, no. 20, pp. 1739–1764, 2004.
- [14] C. J. Hawker, F. K. Chu, P. J. Pomery, and D. J. T. Hill, “Hyperbranched poly(ethylene glycol)s: A new class of ion-conducting materials,” *Macromolecules*, vol. 29, no. 11, pp. 3831–3838, 1996.
- [15] D. A. Tomalia *et al.*, “A New Class of Polymers: Starburst-Dendritic Macromolecules,” *Polym. J.*, vol. 17, no. 1, pp. 117–132, 1985.
- [16] T. J. Mdkern and N. C. B. Tan, “Polystyrene / Hyperbranched Polyester Blends and Reactive Polystyrene / Hyperbranched Polyester Blends,” no. January, 1999.
- [17] K.-M. Kim, M. Jikei, and M. Kakimoto, “Preparation and Properties of Novel Hyperbranched Poly(dimethylsiloxane)s,” *Polym. J.*, vol. 34, no. 4, pp. 275–279, 2002.
- [18] R. H. Kienle, P. A. van der. Meulen, and F. E. Petke, “The Polyhydric Alcohol-

- Polybasic Acid Reaction. IV. Glyceryl Phthalate from Phthalic Acid," *J. Am. Chem. Soc.*, vol. 61, no. 9, pp. 2268–2271, Sep. 1939.
- [19] Y. H. Kim, "Hyperbranched polyarylene," 4,857,630, 1989.
- [20] P. . Costello, I. . Martin, A. . Slark, D. . Sherrington, and A. Titterton, "Branched methacrylate copolymers from multifunctional monomers: chemical composition and physical architecture distributions," *Polymer (Guildf)*., vol. 43, no. 2, pp. 245–254, 2002.
- [21] Z. Guan, "Control of Polymer Topology through Metal Catalysis: Synthesis of Hyperbranched Polymers by Cobalt-Mediated Free Radical Polymerization," *J. Am. Chem. Soc.*, vol. 124, no. 20, pp. 5616–5617, 2002.
- [22] D. M. Haddleton, D. R. Maloney, and K. G. Suddaby, "Catalytic chain transfer polymerisation (CCTP) of methyl methacrylate: Effect of catalyst structure and reaction conditions on chain transfer coefficient.," *Macromol. Symp.*, vol. 111, pp. 37–46, 1996.
- [23] K. Adlington, D. J. Irvine, I. Barker, and L. Stevens, "Accelerated Synthesis of Hyperbranched Divinylbenzene Polymers via Catalytic Chain Transfer Polymerisation and their Use as Gas Capture Agents - Manuscript in preparation," Nottingham, 2017.
- [24] N. O'Brien, A. McKee, D. C. Sherrington, A. T. Slark, and A. Titterton, "Facile, versatile and cost effective route to branched vinyl polymers," *Polymer (Guildf)*., vol. 41, no. 15, pp. 6027–6031, 2000.
- [25] D. M. Haddleton, D. R. Maloney, and K. G. Suddaby, "Competition between β -Scission of Macromonomer-Ended Radicals and Chain Transfer to Cobalt(II) in Catalytic Chain Transfer Polymerization (CCTP)," *Macromolecules*, vol. 29, no.

- 1, pp. 481–483, Jan. 1996.
- [26] K. Inoue, “Functional dendrimers, hyperbranched and star polymers,” *Prog. Polym. Sci.*, vol. 25, no. 4, pp. 453–571, 2000.
- [27] J. Liebig, “Justus Liebig’s *Annalen der Chemie.*,” *Annalen der Chemie. Meyerschen Hof-Buchh. und der Winterschen Universitäts-Buchh* ; C.F. Winter’sche ; Verlag Chemie, [Lemgo, Germany : Leipzig : Berlin, p. v., 1832.
- [28] M. Berthelot, “Sur Les caractères de la benzine et du styrolène, comparés avec ceux des Autres carburetors d’hydrogène,” *Bull. Soc. Chim. Fr.*, vol. 6, no. 2, p. 294, 1866.
- [29] H. Staudinger, “Hermann Staudinger and the Foundation of Polymer Science,” *Am. Chem. Soc. Natl. Hist. Chem. Landmarks*, 1999.
- [30] A. Vazaios, D. J. Lohse, and N. Hadjichristidis, “Linear and star block copolymers of styrenic macromonomers by anionic polymerization,” *Macromolecules*, vol. 38, no. 13, pp. 5468–5474, 2005.
- [31] I. A. Barker *et al.*, “Catalytic Chain Transfer Mediated Autopolymerization of Divinylbenzene: Toward Facile Synthesis of High Alkene Functional Group Density Hyperbranched Materials,” *Macromolecules*, vol. 45, no. 23, pp. 9258–9266, Dec. 2012.
- [32] C. T. J. and C. K. Yong, “In-line dielectric monitoring of monomer conversion in a batch polymerization reactor,” *J. Appl. Polym. Sci.*, vol. 55, no. 9, pp. 1361–1365, Jun. 2018.
- [33] M. J. Kamaruddin *et al.*, “Continuous and direct ‘in situ’ reaction monitoring of chemical reactions via dielectric property measurement: controlled polymerisation,” *RSC Adv.*, vol. 4, pp. 5709–5717, 2014.

- [34] D. E. Kranbuehl, "Continuous dielectric measurement of polymerizing systems," *J. Non. Cryst. Solids*, vol. 131–133, pp. 930–934, Jun. 1991.
- [35] Z. Ahmad, "Polymer Dielectric Materials," in *Dielectric Material*, InTech, 2012.
- [36] A. Cherfi *et al.*, "Application of dielectric analysis to the measurement of conversion during batch solution copolymerizations," *Chem. Eng. Process. Process Intensif.*, vol. 42, no. 2, pp. 121–128, Feb. 2003.
- [37] M. J. Kamaruddin *et al.*, "Continuous direct on-line reaction monitoring of a controlled polymerisation via dielectric measurement," *Green Chem.*, vol. 13, pp. 1147–1151, 2011.
- [38] C. A. Migdal, S. M. Shirodkar, T. F. DeRossa, and E. F. Miller, "FRCTION MODIFERADIOTEVE AND LUBRICATING OL COMPOSITION CONTAINING SAME," 5,066,412, 1991.
- [39] C. K. Esche, Jr., M. T. Devlin, and T.-C. Jao, "ADDITIVES AND LUBRICANT FORMULATIONS FOR PROVIDING FRCTION MODIFICATION," US 7,709,423 B2, 2010.
- [40] R. He and S. Zhang, "The friction and wear properties of divinylbenzene-grafted UHMWPE fiber-filled serpentine/PTFE composite," *Compos. Interfaces*, vol. 19, pp. 377–383, Aug. 2012.
- [41] B. Z. Poliquit, P. L. Burn, and P. E. Shaw, "Properties of PDMS-divinylbenzene based pre-concentrators for nitroaromatic vapors," *J. Mater. Chem. C*, vol. 8, no. 47, pp. 16967--16973, 2020.
- [42] F. K. L. Huang, C.-J. Yoo, C. Okonkwo, D.-J. Tao, C. W. Jones, and S. Dai, "Facilely Synthesized Meso-Macroporous Polymer as Support of Poly(ethyleneimine) for Highly Efficient and Selective Capture of {CO₂},"

- Chem. Eng. J.*, vol. 314, p. , 2016.
- [43] The Dow Chemical Company, “DVB - Cross-link a variety of materials for improved thermal, physical, and chemical properties,” 2003.
- [44] INEOS Oligomers, “Durasyn 164 Polyalphaolefin.” [Online]. Available: <https://www.ineos.com/show-document/?grade=Durasyn+164&bu=INEOS+Oligomers&documentType=Technical+Data+Sheet&docLanguage=EN&version=1d9e9f29efdefed072cf18e3c32114ec>. [Accessed: 24-Jun-2019].
- [45] A. Mashhadi Malekzadeh, A. Ramazani, S. J. Tabatabaei Rezaei, and H. Niknejad, “Design and construction of multifunctional hyperbranched polymers coated magnetite nanoparticles for both targeting magnetic resonance imaging and cancer therapy,” *J. Colloid Interface Sci.*, vol. 490, pp. 64–73, 2017.
- [46] L. Zou *et al.*, “Synthesis and photophysical properties of hyperbranched polyfluorenes containing 2,4,6-tris(thiophen-2-yl)-1,3,5-triazine as the core,” *Phys. Chem. Chem. Phys.*, vol. 13, no. 19, pp. 8838–8846, 2011.
- [47] W. Tian, X. Li, and J. Wang, “Supramolecular hyperbranched polymers,” *Chem. Commun.*, vol. 53, no. 17, pp. 2531–2542, 2017.
- [48] Y. Zheng, S. Li, Z. Weng, and C. Gao, “Hyperbranched polymers: advances from synthesis to applications,” *Chem. Soc. Rev.*, vol. 44, no. 12, pp. 4091–4130, 2015.
- [49] M. Gaborieau and P. Castignolles, “Size-exclusion chromatography (SEC) of branched polymers and polysaccharides,” *Anal. Bioanal. Chem.*, vol. 399, pp. 1413–1423, 2011.

- [50] B. J. Hamrock and D. Dowson, "Isothermal Elastohydrodynamic Lubrication of Point Contacts: Part III—Fully Flooded Results," *J. Lubr. Technol.*, vol. 99, no. 2, pp. 264–275, 1977.
- [51] N. Marx, J. Guegan, and H. A. Spikes, "Elastohydrodynamic film thickness of soft EHL contacts using optical interferometry," *Tribol. Int.*, vol. 99, pp. 267–277, 2016.
- [52] S. Nambiar and D. J. Irvine, "Dielectric Characterization of Hyperbranched Polymers," University of Nottingham, 2016.
- [53] Z. Zhou *et al.*, "High-throughput characterization of fluid properties to predict droplet ejection for three-dimensional inkjet printing formulations," *Addit. Manuf.*, vol. 29, p. 100792, Oct. 2019.

4 Chapter 4: Synthesis and Optimisation of Bio-Active Hyperbranched Polymers

This chapter outlines the synthesis and optimisation of hyperbranched (HB) polymers and copolymers of tricyclo[5.2.1.0^{2,6}]decanedimethanol diacrylate (TCDMDA) using chain transfer polymerization (CTP) with catalytic, thiolic and macromeric control agents. It also details the subsequent optimisation and scale up of these (co)polymers for use as bacterial attachment resistant and pro-stem cell attachment surfaces, which is described in the application testing reported later in the chapter. A new polymerization method was investigated for the synthesis of more controllable and structured HB TCDMDA copolymers, to optimise monomer mixing in the final copolymer and improve the polymer yield and gel time repeatability. These copolymer coatings were then subject to application testing. Furthermore, the thiol-controlled TCDMDA was investigated as an improved feedstock material for two photon polymerisation (2PP). Macromer-controlled HB pTCDMDA underwent biological testing to investigate its potential for use as improved stem cell culture surfaces. Successful candidates were scaled up for further biological testing.

4.1 Introduction

4.1.1 Biofilms and Anti-Fouling Surfaces

Following their discovery by Pasteur [1] microorganisms were classified as planktonic, indicating they were single celled creatures living as floating organisms, much as plankton does [2]. Biofilms, on the other hand, are microorganisms that live in a self-organised, cooperative communities. They attach to a substrate and cover themselves in a self-produced matrix of extracellular polymeric substances (EPS) [3], [4] essentially forming a slimy, slippery coating. This process is illustrated in Figure 4.1.

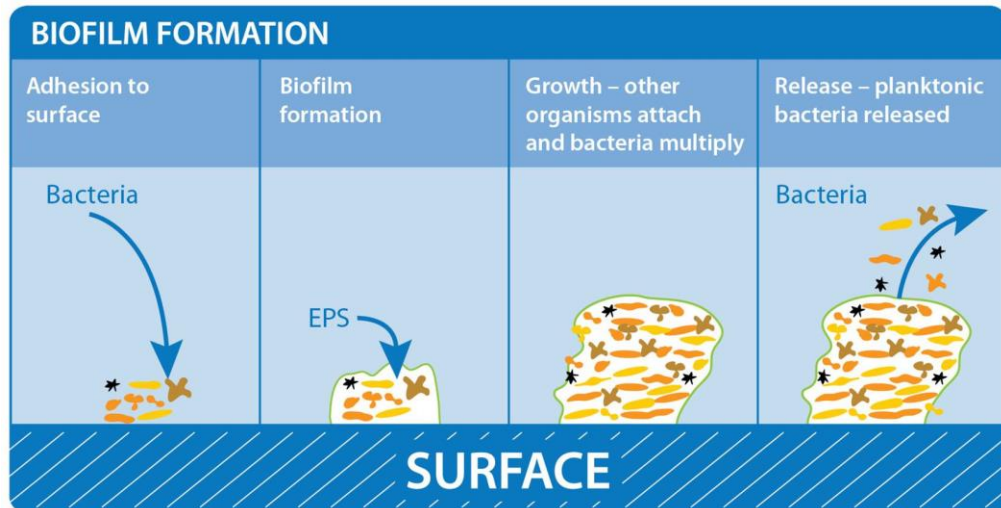


Figure 4.1. Diagram outlining the process for biofilm formation on a surface [89].

The EPS are natural, high molecular weight (MW) polymers secreted by microorganisms into their environment to establish the functional and structural integrity of the biofilm. They are also the fundamental component in determining the physicochemical properties of a biofilm. Importantly, biofilms exhibit vastly different characteristics to their planktonic counterparts. For example, they have been found to exhibit up to 1000 times higher resistance to antibacterial agents or, in medicine, to the host's immune defences [5].

On the global scale, the impact of biofilm formation is almost incalculable, with billions of dollars spent throughout different sectors of the economy to prevent their occurrence or remove them once they have formed[6]. In the medical sector, it has become widely known in recent years that healthcare-associated infection is a frequent problem in hospitals. Up to 80% of such infections involve biofilms [7], which can give rise to life-threatening systemic infections. These contribute to post-operation morbidity, mortality, protracted hospitalisation, higher re-operation rates, and increases in the need for diagnostic tests and treatments, which creates a large medical and financial burden.

Biofouling is also an issue in other market sectors, such as aerospace [8], marine structures [9] and in oil recovery [9], and may affect a variety of systems and devices such as: plumbing, medical implants, food processing facilities, and heating and air conditioning systems. The result is a reduced industrial yield, efficiency and physical degradation of industrial systems, due to problems during device use or application. An example that is relevant to this study is an increased fuel demand in transportation due to increased drag and blockage, or erosion/obstruction of pipes [10].

Therefore, developing materials or coatings that are more resistant to biofouling than the current commercial benchmarks will bring many social and economic benefits. Traditionally, strategies to alleviate the effects of biofilm formation have focussed on cleaning and disinfection treatments aimed at killing the microbes following surface attachment. This strategy is shown in the first window of Figure 4.1. However, these strategies were not proven to be totally effective, as biofilm microorganisms have features that provide successful conditions for microbial life, including enhanced tolerance to antibiotic and biocide treatments. Multiple factors appear to contribute to the overall resistance of biofilm bacteria. These include reduced metabolic and growth rates, protection by extracellular polymeric substances and specific resistance mechanisms conferred by the altered physiology of biofilm bacteria compared with planktonic bacteria. The failure of antibacterial agents to rapidly penetrate all areas of a biofilm has been considered as a contributing factor to biofilm resistance. Reports indicate that species-composition of biofilms and the choice of antibiotic have a marked impact on antibiotic penetration. Biofilm cells have been shown by several investigators to have reduced growth rates, and this is believed to impact the effectiveness of antibiotics that target rapidly multiplying cells. Therefore, antibiotics such as the fluoroquinolones or macrolides may be better

therapeutic choices than β -lactams when treating biofilm infections. Altered physiological states of biofilm cells compared with planktonic cells have been demonstrated for several bacteria. The activation of specific resistance genes in biofilms has been demonstrated in a few instances. Specific resistance mechanisms should, therefore, be considered when treating biofilm infections. Furthermore, resistance towards many antibiotics has increased in several microbes, reducing the chances to effectively treat infections and increasing the risk of complications and fatal outcomes [11].

Consequently, in the past 20 years, research has addressed the development of preventative strategies. For example, in relation to medical devices, methods for reducing infections associated with biofilms generally focus on modifying the materials that are used to manufacture implantable devices by incorporating antibiotics or antimicrobial agents that kill bacteria on contact. These materials include silver salts, nitrofurazone, chlorhexidine, polymerised quaternary ammonium surfactants, antibacterial peptides and anionic nanoporous hydrogels [7], [12]–[19].

The above materials can be classified as drug-releasing or non-releasing biomaterials. Drug-releasing materials are applied to biomaterials by physical absorption, impregnation in a polymer matrix, complexation or conjugation. They are designed to work as carriers of biocides which are transferred to attached microbial cells and released in high local concentrations during the critical post-implantation period, in order to inhibit the initial surface colonization and prevent biofilm formation. These include antibiotic-, silver-, furanone- and nitric oxide-releasing materials.

However, these materials have a number of drawbacks. They can be: expensive, toxic, have a lifetime that is limited by depletion of the active agents over

time and potentially contribute to the development of antibiotic resistant bacteria. The latter effect arises because the biocidal material cannot maintain the correct, therapeutic dose throughout the lifetime of the device, thus it tends to be used in larger concentrations than should be required [7], [20]. This overdosing eventually leads to the development of biocide resistant strains with time. Thus, new non-drug releasing materials have been developed, which are based on coatings that are, in principle, able to counteract bacterial adhesion and biofilm formation when microorganisms come in contact with a coated surface. Most of these coatings are based on either polymers possessing antimicrobial activity by themselves or photoactive metal-oxide NPs. However, some polymer biocides have also been investigated. These are commonly cationic polymers which are capable of binding to the membrane proteins of microbial cells. Additionally, photoactive coatings based on metal-oxide nanoparticles, which are capable of producing reactive oxide species (ROS) in the presence of UV or visible radiation have been developed. These species can damage organic biomolecules including carbohydrates, lipids, proteins and DNA, and therefore are responsible for bacterial cell death. Several metal-oxide NPs, such as TiO_2 , CuO and ZnO , have been reported to possess potent antimicrobial activity in relation to the oxidative stress induced by photogenerated ROS. NPs are more efficient in ROS generation than their bulk counterparts likely due to the high NP surface area providing better interaction with UV irradiation [21].

More recently, the focus has shifted to attempting to develop new polymeric materials that possess an inherent resistance to bacterial attachment, known as antifouling coatings, such that the resistance is achieved from the structure and ordering of the polymer rather than any additive [22]. These polymers interrupt the interaction of the bacteria with the surface, and thus prevent attachment. Additionally, it has been found that the polymers do not kill the bacteria and so do

not promote antimicrobial resistance. These bacterial attachment-resistant (BAR) materials can be used on their own or in combination with traditional additives to improve the effectiveness of coatings [23]. So far, only a small number of these materials have successfully been used as coatings. Such microbial repellent coatings are based on (i) hydrophilic polymers, mainly PEG; (ii) zwitterionic materials or (iii) superhydrophobic low surface energy materials possessing nanoscale surface topology. For example, reductions in bacterial attachment of between 1.4- and 2.5-fold have been seen from poly(ethylene glycol) brushes, [24] and zwitterionic polymers [25], [26], respectively, compared to a native glass surface. Coatings able to affect biofilm architecture, mainly based on the immobilization of enzymes either interfering with bacterial quorum sensing or degrading the biofilm matrix, can be also considered antifouling because, even if they do not properly prevent microbial adhesion, they facilitate the process of biofilm removal [21].

PEG is the most frequently used polymer to impart the biomaterial surfaces with resistance to protein adsorption. PEG antifouling properties have been widely investigated and are believed to be related to both hydration and steric hindrance effects. In the early 1990s, Jeon et al. [27] proposed a theory to justify the interaction between proteins and PEG-functionalized surfaces. According to this study, the approach to the surface by proteins is hindered by the repulsive electric forces resulting from the compression of the highly mobile PEG chains. In addition, the compression of polymer chains would need the thermodynamically unfavourable removal of water molecules from the hydrated polymer. The formation of this tightly bound water layer interacting with the polymer seems to act as a physical barrier for the adsorption of protein and bacteria [21].

Zwitterionic coatings have been recently investigated in terms of resistance ability to proteins and prevention of bacterial adhesion [28]. As for PEG, also in this case, the antifouling properties are tightly related to the hydration layer formed on the polymer and act as a physical barrier for the adhesion of proteins and bacteria [29]. However, in poly-zwitterionic materials, water molecules bind more strongly by ionic interactions. The strength of surface hydration is also related to surface packing, self-assembled monolayers (SAMs) being the most efficient [21].

Since the discovery of the 'lotus leaf effect', superhydrophobic surfaces have revealed a plethora of unique functional properties and potential applications [30]. Also, in the medical field, material superhydrophobicity has been shown to play a key role in reducing bacterial adhesion and enabling easy cleaning of the surface [31]. A measure of surface hydrophobic/hydrophilic features is the contact angle (θ) that, for ideal smooth surfaces, is defined by the Young's equation [21]. When the contact angle is 0° , the wetting is complete, whereas when it is 180° , the liquid does not wet the material and the droplet stands on the surface. The surface is hydrophilic when θ is less than 90° and hydrophobic when higher than 90° . Superhydrophobic surfaces are those having θ higher than 150° . It is now well accepted that two crucial factors govern surface wetting features – surface chemical composition and surface roughness [32]. Indeed, low surface energy materials, mainly fluorinated compounds, can reach a maximum contact angle of 119° [33]. To obtain θ higher than 119° , a rough surface is required as found in the lotus leaf where hierarchical micro/nanostructures are present together with a waxy hydrophobic film [32]. For these kinds of surfaces, heterogeneous wetting occurs with water droplets sitting on the top of the surface protrusions due to the air entrapped inside the roughness grooves, thus hindering liquid penetration [34], [35]. This significantly reduces the adhesion force between the water droplet and the surface with a consequent droplet rolling off when the

surface is tilted. Therefore, dirt particles as well as bacterial cells deposited on these surfaces can be taken away by the water droplet rolling off (easy-to-clean property). With this in mind, investigation into the influence of superhydrophobicity on microbial adhesiveness has been initiated [21].

4.1.2 Stem Cells and Pro-Stem Cell Attachment Surfaces

Stem cells (SCs) are cells with the capacity to self-renew and the ability to differentiate into specialised cell types, such as muscle cells and active cells in an immune system, depending on their environment. Pluripotent SCs are capable of unlimited self-renewal and can differentiate into almost any of the over 200 types of cell in the body, a representative summary of which is shown in Figure 4.2.

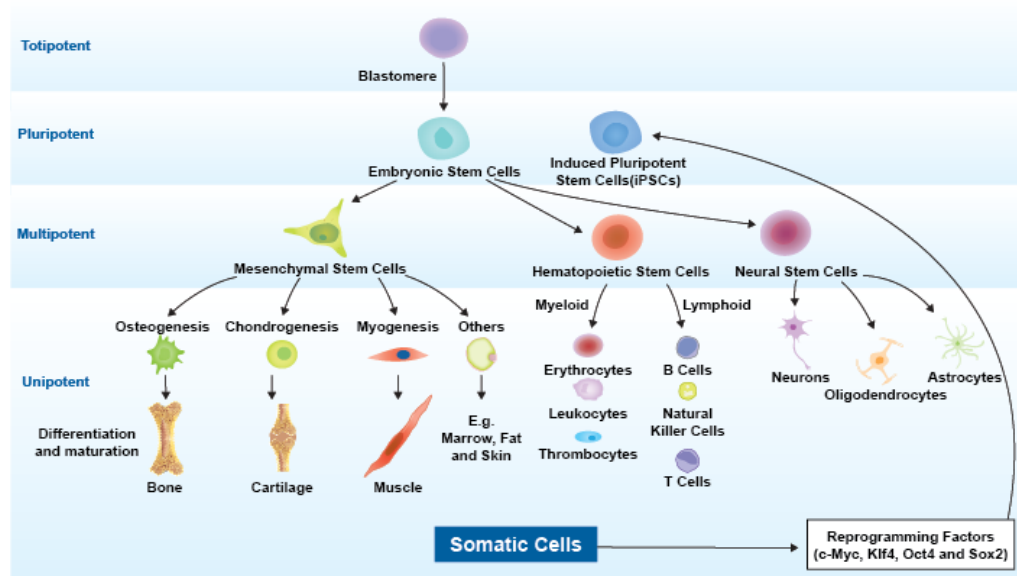


Figure 4.2. Diagram summarising the differentiation pathways of stem cells [37].

There are two sources of pluripotent SCs. The first, embryonic stem cells (ESCs) are derived from the inner cell mass of a pre-implantation blastocyst. The blastocyst is a structure formed in the early development (gestation period) of mammals. It possesses an inner cell mass (ICM) which subsequently forms the embryo. The outer layer of the blastocyst consists of cells collectively called the trophoblast. Second, induced pluripotent stem cells (iPSCs) are laboratory-engineered stem cells created

from reprogrammed cells. Other types of SCs include mesenchymal stem/stromal cells (MSCs), which are isolated from adult sources (e.g. bone marrow and adipose tissue), or perinatal tissues, (e.g. umbilical cord, cord blood, placenta and amniotic fluid). Unlike pluripotent SCs, MSCs are multipotent and differentiate into only limited cell types [36], [37].

As such, SCs show great promise for a variety of applications, including: cell therapy, tissue engineering, regenerative medicine and in pharmaceutical and biotechnological applications. However, all of these applications require both (a) a high quantity and quality of SCs, which requires both a large-scale growth in the number of SCs (expansion) and (b) homogeneous differentiation into the required derivative. Traditionally, SCs are propagated as a monolayer in two-dimensional (2D) plastic culture plates, and often require undefined or xenogenic materials, e.g. attachment substrates, cytokines and growth factors, as well as serum. These monolayer cultures require routine passaging (transfer to new media) to maintain the self-renewal and potency of the cells, which is highly inefficient for large-scale expansion of cells and may result in cells losing their clonal and differentiation capacity after long-term passaging [36]–[38].

Regulation of fundamental stem cell behaviour using 2D synthetic templates in vitro is of immense importance in regenerative medicine. Control over cell adhesion, proliferation, and differentiation behaviour may facilitate increased therapeutic applications of stem cells. Chemically defined growth of stem cells allows for quantifiable cell–material interactions and hence, control over these cell behaviours. However, cells are traditionally grown on tissue culture polystyrene (TCPS), which is low cost, sterile, and semi-reusable, leading to its widespread use over other materials such as glass. TCPS undergoes rapid adsorption of proteins when put in contact with

biological fluids, creating a poorly defined surface for cell studies, where identity, density, and orientation of the proteins is unknown.

To better understand the substrate factors that influence cell behaviour, a substantial amount of research has focused on creating synthetic 2D substrates for chemically defined cell culture. These include self-assembled monolayers (SAMs), hydrogels, polymer brushes, thin films, and layer-by-layer films [39]–[44]. Many of these systems use poly(ethylene glycol) (PEG) to provide a “blank slate” background to cells and prevent nonspecific protein adsorption [45]–[47]. This is because, it is easy to functionalise with biomolecules using a variety of chemistries [48]. For example, SAMs terminated with oligoethylene glycol chains and functionalized with specific peptides can present a powerful platform for regulating stem cell behaviour. They are formed easily and facile functionalization with peptides can be achieved using a wide variety of distinct chemistries [49], [50]. The use of multiple substrate types is often desirable, in order to explore additional factors, such as the effect of substrate stiffness on cell behaviour or the utilization of the optical clarity of the substrate for imaging. Thus, it is highly desirable to have a chemically defined coating that is compatible with multiple substrate types and is stable over long term in cell culture conditions. For example, Schmitt *et al.* used a polyethylene glycol copolymer to coat plastic substrates for hMSC culture. The coating was functionalised with peptides *via* thioester or amide linkages. The amides exhibited more stable linkages and so presented the attached peptides for longer period when under serum-containing conditions. Furthermore, the coating was found to promote hMSC adhesion and spreading, and support multiple human cell types. The coating also enabled successful passaging on the plastic surfaces, and the possibility of reusability from the coatings [38].

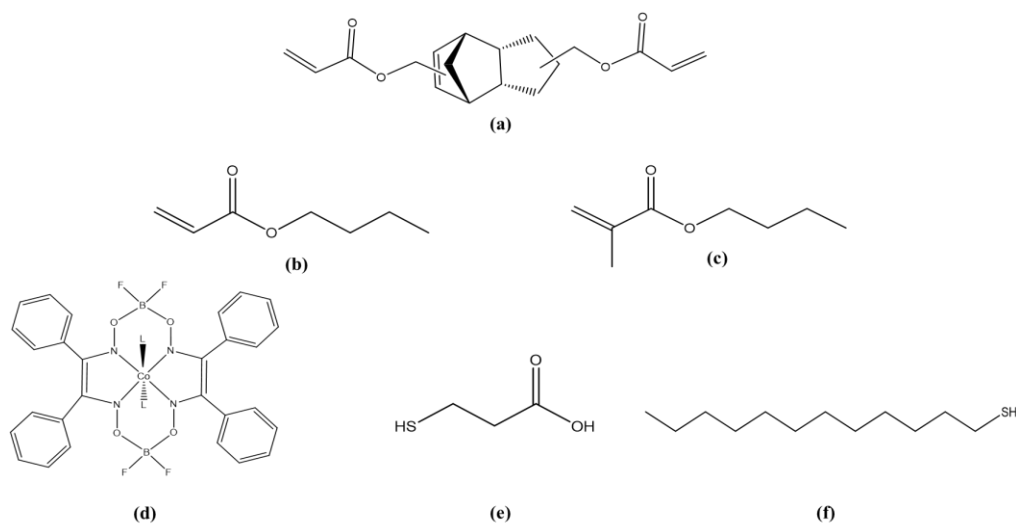
4.1.3 Hit Polymers

In recent years, high-throughput 2-dimensional, micro-array screening methods have led to the discovery of new classes of synthetic polymers which display both high BAR and show promise for use as improved culture plate surfaces. However, up to this point these have only been tested at small scales (in a 96-well plate).

For example, Hook *et al.* reported the screening of more than 1300 unique copolymers in almost 2000 different bacterial attachment assays. This led to the discovery of a new class of polymers which exhibited up to a 30-fold reduction in inherent bacterial attachment compared to conventional silver hydrogel catheters, due to a combination of the weak amphiphilic nature and the molecular rigidity of the polymers' pendant groups [7], [51]. The anti-fouling materials identified all contained both ester and cyclic hydrocarbon moieties that substantially reduced the attachment of pathogenic bacteria (*Pseudomonas aeruginosa*, *Staphylococcus aureus* and *Escherichia coli*) in a similar fashion to that observed for zwitterionic polymers.

Following on from this study, in 2016, Adlington *et al.* reported the optimisation and scale up of these high BAR polymers: they found that copolymerisation of these "hit" monomers with diethylene glycol ethyl ether methacrylate (DEGMA) decreased the glass transition temperature, T_g , and so increased the flexibility of these materials such that they are suitable for use in catheters. For example, the ideal ratio of an ethylene glycol dicyclopentenyl ether acrylate EGDPEA:DEGMA copolymer was found to be 75:25 mol %. This copolymer performed well as a functional coating with regards to flexibility and BAR performance (compared to existing benchmarks)[20].

A variety of other monomers have emerged from these screening processes. One such monomer that has subsequently received significant attention is tricyclo[5.2.1.0^{2,6}]decanedimethanol diacrylate, (TCDMDA), structure shown in Scheme 4-1a.



Scheme 4-1. Structures of (a) TCDMDA, (b) butyl acrylate, (c) butyl methacrylate, (d) CoPhBF, (e) 3-mercaptopropionic acid, (f) dodecane mercaptan.

Homopolymers of TCDMDA have shown anti-biofilm formation properties, while statistical copolymers of TCDMDA with the mono-functional monomers butyl acrylate (BA) (Scheme 4-1b) and butyl methacrylate (BMA) (Scheme 4-1c), have been reported to display relatively high levels of stem cell attachment [7], [52].

Due to its di-acrylate functionality, TCDMDA can undergo controlled free radical polymerization to form hyperbranched structures. As described in detail earlier in this study, (Chapter 3), hyperbranched (HB) polymers are extremely highly branched, polydisperse, three-dimensional macromolecules, with a high density of end groups. They can be regarded as being closely related to the more ordered and widely studied dendrimer polymer architectures [53]–[55]. However, as has been detailed in Chapter 3, HB polymers can be more rapidly, cheaply and flexibly synthesized than dendrimers [56]–[58], to produce structures similar to those of dendrimers, but less well defined. This gives them the potential to act as

replacements or substitutes for dendrimers, delivering the same performance and applications at much reduced cost [56]. Importantly, HB polymers possess a high density of end groups, which can help improve attachment properties and allows better incorporation of end group functionality, such as stem cell attachment.

4.1.4 Additive Manufacturing for Bio-Applications

Additive manufacturing (AM), also commonly known as 3D printing, is a process where parts are created layer-by-layer from 3D computer model data. 3D printing technologies involve a 3D object being “sliced” into computer-modelled layers. The structure is then created by the deposition of each layer at a time. The term AM refers to the deposition of layer upon layer so that no material is wasted. This contrasts with subtractive methods such as the use of tooling boards, where the final shape is “drilled” out of a block of material that is larger than the final target article. AM was first introduced commercially in 1987 with stereolithography (SLA) by 3D Systems. Since then, AM has evolved rapidly, particularly in the last decade, due to its many advantages, including its ability to deliver low-cost complexity, customisation, small part number batches, short lead times and minimal waste materials.

As a result, AM has found applications in a wide variety of industries. Lightweight materials and structures manufactured by AM have potential use in marine and aerospace industries. The medical sector is utilizing the advantages of AM by printing organs, tissues, blood vessel stents, etc. AM is able to 3D print small quantities of customised products with relatively low costs. This is specifically useful in the biomedical field, whereby unique patient-customised products are typically required. For example, using AM, it is possible to produce a wide variety of medical implants from CT-imaged tissue replicas [59]–[62]. In dentistry, AM is used to print

custom-sized teeth, implants, and dental moulds at reduced cost and with reduced fabrication times [63]. In architecture, AM processes are utilised to visualize and materialize ideas and even buildings more cheaply than using conventional construction methods [64]. In addition, recent NASA initiatives for MARS colonization have generated a great deal of enthusiasm for 3D printed habitats [65]. Nevertheless, there are some serious limitations to AM, many of which centre on the limited number of materials that are currently available for use in AM techniques. These technical challenges still need to be addressed for meeting engineering demands such as customized geometry, building scalability, material heterogeneity, and structural reliability [63], [66]–[69].

4.1.4.1 Two Photon Polymerisation

Among the additive manufacturing processes, two-photon polymerization (2PP) is one of the most flexible and high-resolution of processes. It enables the production of arbitrary three-dimensional structures on the basis of computer-aided design (CAD) models and is capable of delivering resolutions of less than 100 nm. These properties open up new possibilities for the development of novel and miniaturized components for different applications, so that today 2PP is successfully being used in various areas of research.

2PP is an additive manufacturing process that can be classified in the group of 3D lithography processes and can be traced back to a study carried out by Maruo et al. [70]. It differs from the well-known 3D lithography methods, which are mainly based on the application of UV radiation, by the application of short-pulsed laser radiation in the visible to near-infrared range. It also exploits nonlinear effects, namely, two-photon absorption [71]. In 2PP, 3D structures are produced by direct laser writing in the volume of a transparent photoresist, as shown in Figure 4.3.

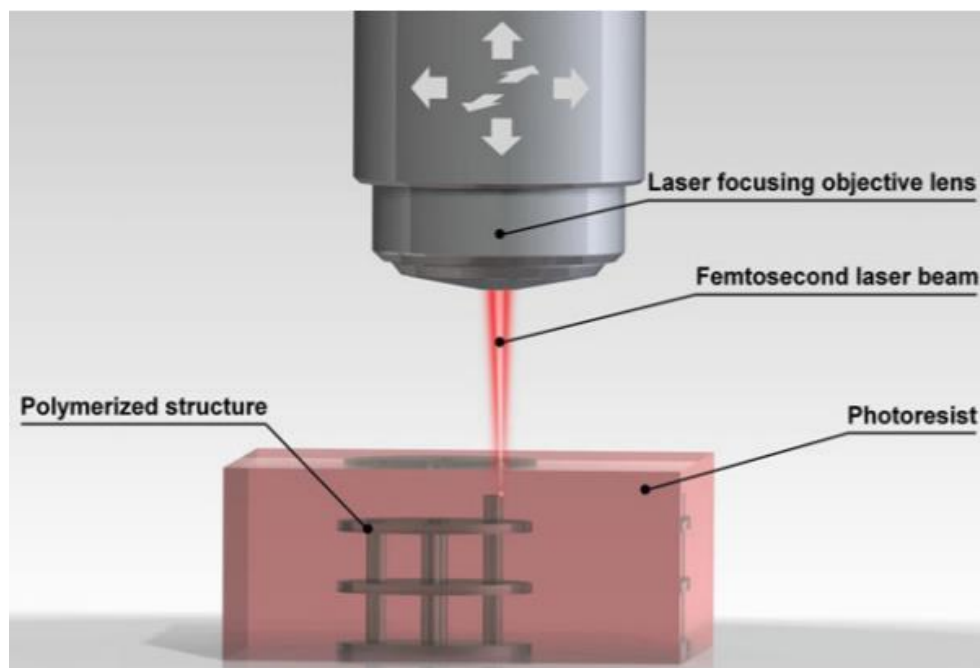


Figure 4.3. Principle of the three-dimensional structuring process using two-photon polymerization [73].

Thereby, a limited photochemical reaction is induced by two-photon absorption in the small volume of the photoresist that is impinged by a strongly focused femtosecond laser beam. The resist within this volume solidifies by polymerization initiated by exposure to the laser energy. Computer-controlled three-dimensional movement of the focus through the material allows almost any three-dimensional structure to be produced. As stated above, structure resolutions down to the sub-100 nm level have been demonstrated by some groups, such as Ferreras Paz et al. [72]. In comparison to other lithography methods, 2PP does not depend on a strict layered construction method, which offers greater design freedom. The high resolution and the possibility to produce any three-dimensional (3D) objects are unique features of this technology.

Due to its closeness to conventional photolithographic processes, 2PP today benefits from there being a number of available materials, enabling this promising production technology to open up a wide range of applications in a relatively short time. Typical applications of 2PP are characterized by the necessity of a high structure

resolution and a high structuring flexibility, whereby the maximum size of the required structures lies in the micrometre to single-digit centimetre range. Applications today include micro-optics, micromechanics, microfluidics, microelectronics, as well as medicine and biology [73].

4.1.4.2 Bio-Applications

Since the beginning of the millennium, biomedicine has become one of the most important applications of 2PP. The advantages of 2PP, such as high precision and flexibility, make it interesting for various biomedical applications. It therefore opens up new possibilities for the production of novel biological structures and, as a result, shows great potential to be of great importance for the delivery of developments in this field. One of its most important applications today is the development of scaffolds in the field of tissue engineering. However, it is also increasingly used for the rapid prototyping of medically relevant structures and the construction of micro-structured implants [73].

4.1.4.3 Challenges of 2PP

However, to date, 2PP is not commonly used for biological applications due to the toxicity of many of the feedstock materials, and the need for the monomers that are 2PP processable to typically have to contain multiple functional groups to achieve the necessary spread of cure. Thus, these two elements result in difficulties in producing mesoscale structures that are relevant for biological applications. Thus, most 2PP polymers have been adopted from established SLA technologies, but this means that they have not been specifically formulated for either 2PP or biological applications. In addition, the nanoscale precision offered by 2PP is also a source of weakness for this processing method, because structures with small-scale features

require relatively slow fabrication speeds. To increase the manufacturing rates, strategies such as soft lithography replication of a 2PP-fabricated master structure have been demonstrated [20], [74]. However, these strategies must be regarded as stop gap measures and do not overcome the key existing weaknesses. Novel photopolymers exhibiting increased 2PP sensitivity and optics and that are able to process larger volumes must be developed to enable large-scale commercial translation [73].

4.2 Aims and Objectives

4.2.1 Aims

- To increase the scale and optimise the synthesis of TCDMDA homopolymer and TCDMDA/BMA copolymer for large scale biological testing as anti-attachment and pro-attachment surfaces, respectively.
- To investigate whether HB TCDMDA can help improve conversion (and thus reduce toxicity) and allow faster, lower power (and thus higher resolution) printing compared to a commercial TCDMDA monomer feedstock in two-photon polymerisation (2PP).
- To determine optimum conditions for coating polystyrene tissue culture plastic with HB TCDMDA/BMA for stem cell work.

4.2.2 Objectives

- Synthesise HB TCDMDA homopolymer using catalytic (PhCoBF) and thiolic (3-mercaptopropionic acid (Scheme 4-1e), and dodecanethiol/dodecyl mercaptan (DDT/DDM, Scheme 4-1f)) control agents to determine most controlled, efficient and industrially viable synthesis route for the production of anti-bacterial attachment polymers at increased scale.

- Use 2PP to print cuboidal scaffolds with a HB TCDMDA-based feedstock over a range of laser powers (10-100%) and speeds (2-25 mm/s), to determine processing range, and compare to commercial TCDMDA monomer feedstock.
 - Use a LIVE/DEAD biocompatibility test to determine whether HB TCDMDA retains its bio-activity following 2PP printing.
- Synthesise HB TCDMDA using butyl methacrylate oligomers as the control agent on a 50 g scale.
- Test solubility of TCDMDA/BMA polymer in range of non-toxic, tissue culture plastic-compatible solvents.
- Determine coating, washing and drying protocols for HB TCDMDA/BMA in 6-well and 96-well plates.
- Use pluripotency, integrin and mechanistic testing of the coated plates to determine viability as stem cell culture plastic.

4.3 Results and Discussion

4.3.1 TCDMDA Homopolymers *Via* CCTP

In previous work by the School of Pharmacy (Dr Andrew Hooke), a limited scale-up of the production of HB pTCDMDA had been attempted using CCTP, to produce sufficient polymer for testing (microgram scale). A 1:1 (v/v) mixture of TCDMDA monomer and toluene solvent, 0.5 wt % of AIBN initiator and approximately 2000 ppm of PhCoBF (Scheme 4-1d) were used with standard catalytic chain transfer polymerisation (CCTP) techniques (see Chapter 2, Section 2.1.2). The mixture was degassed for 30 minutes and reacted at 70 °C for approximately 6 hours. However, further scale up would be required for future bacterial assay work, which could not be conducted easily within Pharmacy due to equipment and procedural limitations.

Hence, the scale-up and optimisation work was out-sourced to become part of this project. Initially, the targets were to: a) synthesise a larger batch of pTCDMDA for further biological testing; b) decrease the reaction time to 3 hours to enable more rapid synthesis.

The CCTP method outlined above was used as a starting point. CCTP was the preferred method, as it results in the polymer chain ends being terminated with vinyl groups and does not add any other functionality to the polymer. This enabled polymers with similar structures to those generated previously, using UV-initiated polymerisation at a small scale, to be produced.

4.3.1.1 Optimising CCTP Using Previously Reported Conditions

Throughout this section of the study, all the reactions were conducted following the same strategy. An initial reaction was first run until gelation occurred, in order to determine the gelation time associated with the specific set of conditions adopted. Then, the reaction was repeated but quenched 10 minutes prior to the identified gelation time to obtain solvent soluble HB polymer for analysis. Table 4.1

Table 4.1. Summary of the reaction conditions used for TCDMDA polymerizations. Average values of the yield, number average molecular weight (M_n), weight average molecular weight (M_w) and dispersity (\bar{D}) are also reported. CH = cyclohexanone.

Reaction	Mon:sol	Solvent	Temperature (°C)	AIBN (% wt)	PhCoBF (ppm)	Reaction/Gel Time	Yield ^a	Mn ^b (kD)	Dispersity, ^b \bar{D}
1	1:1	Toluene	80	0.5	~2000	13 min	7 %	153.9	3.737
2	1:4	CH	80	0.5	~1000	>19 hrs	34 %	328.8	3.940
3	1:2	CH	80	0.5	~2000	4 min – 5hr 30	-	-	-
4	1:1	CH	80	0.5	~2000	10 min – 4hr 7	-	-	-
5	1:1	Toluene	70	0.5	~2000	1hr – 1hr 30	-	-	-
6	1:1	Toluene	65	0.5	~2000	1hr 33 – 3hr 35	-	-	-
7	1:1	Toluene	70	0.5	~2000	60 min	5.6 %	1.6	6.015

^a Determined gravimetrically. ^b Determined *via* gel permeation chromatography.

summarises the initial reaction conditions and average results obtained for this investigation. A variety of reactions conditions were altered simultaneously because the main aim with this work was simply to achieve a viable polymerisation strategy which reliably produced polymer over an ~3hr time frame; the exact conditions required and resulting polymer characteristics were secondary considerations. The AIBN concentration was not altered, as 0.5 wt% was considered a sensible lower limit, while increasing the concentration of initiator in CCTP reactions has minimal impact due to the dominant catalytic transfer and initiation processes.

First, in order to decrease the reaction time, the reaction temperature was increased from 70 °C (used at small scale as outlined above) to 80 °C in order to increase the rate of polymerisation, as outlined in Table 4.1, Entry 1. Hyperbranched polymer was successfully obtained, with a number average molecular weight of 153.9 kDa. However, the reaction time achieved (13 minutes) was considerably shorter than the desired 3 hours, making the isolation of highly converted HB polymer challenging, and the yield (7 %) was low.

To combat these issues, the reaction conditions were slightly altered, as shown in Table 4.1, Entry 2. First, the solvent was switched to cyclohexanone (CH) as both PhCoBF (the CTA) and TCDMDA monomer were considerably more soluble in cyclohexanone than toluene, hence this should remove any miscibility issues and so lead to improved yield. Secondly, the monomer-to-solvent ratio was decreased, reducing the concentration of monomer and thus reducing the propagation rate but potentially increasing the diffusion through the medium as polymerisation occurred. Finally, the level of the CTA was dropped to see if this increased the yield by reducing the potential for a chain transfer event to occur. These changes proved to have mixed results. A significant increase in the reaction time in excess of 19 hours was observed.

This was much too slow for the purposes of this study, indicating that a higher monomer-to-solvent (M-S) ratio was required. However, the yield increased to 34 %, indicating that the solvent change had the desired result and appeared to solve the issue of low yield. In addition, the molecular weight of the polymer obtained (328.8 kDa) more than doubled compared to Entry 1, likely due to the relative decrease in the concentration (ppm) of PhCoBF compared to Entry 1.

In an attempt to achieve a ~3-hour reaction time, the M-S ratio was next increased from 1:4 to 1:2 and then 1:1 (Table 4.1, Entry 3 and 4 respectively) in order to increase the rate of propagation. However, despite numerous repeats, these reaction conditions resulted in random and non-reproducible gelation times, making isolation of a representative, solvent soluble HB polymer unfeasible. While acrylates are known for their relatively high reactivity and reduced amenability to CCTP compared to methacrylates due to their lack of an easily abstractable hydrogen on an α methyl group, this level of unpredictability had not been expected. Three main hypotheses were initially suggested for this irreproducibility: a) poor degassing; b) degradation of initiator and c) variable fume hood temperature. Hence, further reactions were conducted to investigate the validity of these hypotheses.

In the case of hypothesis a), it was thought that the mixture may not be fully degassed each time, resulting in varying levels of oxidant in the reaction which would retard the polymerisation at different rates: degassing with inert gas is not always the most effective method, though it is the most industrially viable. Therefore, the reaction mixtures were degassed for one hour, rather than the 30 minutes used previously, however, this had no impact of the variability of the results.

In the case of hypothesis b), it was thought that initiator efficiency may have been lower than expected due to thermal degradation prior to the reaction. The AIBN

initiation mechanism is thermally activated. At elevated temperatures, thermally labile C-N bonds are broken, creating nitrogen gas and two radical fragments which then initiate the free radical polymerisation. Consequently, in order to prevent premature thermal degradation, AIBN is stored between -5.0 and -1.0 °C and exposure to room temperature is limited, as far as possible, prior to use. However, the AIBN used in this work was a communal reagent, thus there was the possibility that it may have been exposed for extended periods to room temperatures and, subsequently, have undergone thermal degradation. Consequently, a new sample of AIBN was obtained and used. However, there was no positive impact on the variation of the measured gelation points.

In the case of hypothesis c), it was observed that the ambient temperature of the fume hood varied noticeably day-to-day and between reactions, which may have lead to varying levels of initiator degradation during the 30-60 minute degassing period. Hence, the reaction mixtures were placed in an ice bath during the degassing stage to ensure a stable temperature was maintained and to prevent radical formation until the reactant mixture was immersed in the heated oil bath. Once again however, this measure had no noticeable impact on the variability of the gelation times measured for the conditions used in either Entry 3 or Entry 4, and nor did any combination of these factors.

Therefore, the remaining possibility was that cyclohexanone, and by extension PhCoBF, were not a suitable solvent or control agent for this polymerisation. Enhanced solubility of the PhCoBF control agent seemed to increase the variability of the gelation times, suggesting that PhCoBF was not an ideal control agent for TCDMDA. However, due to the desire to produce HB polymers with vinyl end groups, work with the PhCoBF CTA was continued. Consequently, toluene was

once again used as the solvent for this polymerization, as the variability of the gel time was significantly reduced compared to when cyclohexanone was used.

Therefore, it was decided to return to the original polymerization method and attempt to replicate the results obtained previously on the small scale. The data for this reaction is shown in Table 4.1, Entry 5. A gelation time of approximately 6 hours was expected, however this was not observed. Instead, the gelation time was again variable, though less widely than with the cyclohexanone solvent, with all repeats falling between 60 and 90 minutes. In an attempt to better control the reaction by reducing the reaction rate, the polymerization was then repeated at 65 °C, shown in Table 4.1, Entry 6. However, this appeared to increase the range of the gelation times observed further, though the range did shift towards slightly longer times as expected.

The reaction conditions detailed in Entry 5 were noted to have resulted in the narrowest gelation time window. Thus, these conditions were chosen for the next stage of the investigation. The polymerization was conducted for 60 minutes (the minimum gelation time recorded for these conditions) before quenching, outlined in Table 4.1, Entry 7. The product obtained was of very low molecular weight (1,600 g/mol), indicating that the material was oligomeric. Given that TCDMDA monomer has a molecular weight of 304.38 g/mol, the material obtained likely largely contained pentameric structures. A broad dispersity (~6.0) was obtained, which suggested a broad range of molecular weights was obtained. This was attributed to the fact that the polymerisation had to be quenched a significant length of time prior to its actual gelation time. It was proposed that the relatively high concentration of CTA used may have been a significant factor in the low molecular weight obtained. The ~2000 ppm quoted in the protocol was higher than is often seen with CCTP when polymeric

product is desired, thus the CTA concentration may have been so high that all chains were terminated prior to the formation of polymeric product.

4.3.1.2 Optimising CCTP Using New Conditions

Clearly, the reaction conditions devised in the prior internal reports were not ideal for this polymerisation at scale, and, as a consequence, the reaction could not be reliably reproduced. These problems with optimization prevented either of the original aims from being met, hence new reaction strategies were investigated for this monomer. The data for the resulting reactions is summarised in Table 4.2.

Table 4.2. Summary of the reaction conditions used for two TCDMDA polymerizations, using (1&2) toluene solvent and (3) DCM solvent. Average values of the yield, number average molecular weight (M_n), weight average molecular weight (M_w) and dispersity (\bar{D}) are also reported.

Entry	Mon: sol	Solvent	Temperature (°C)	Initiator (% wt)	CoPhBF (ppm)	Reaction Time (min)	Yield ^a (%)	M _n ^b (kDa)	M _w ^b (kDa)	\bar{D} ^b
(1)	1:1	Toluene	70	0.5 (AIBN)	~800	36	6.6	1154.5	3158.1	2.7
(2)	1:3	Toluene	65	0.5 (AIBN)	~1000	113	17	36.2	253.7	7.0
(3)	1:3	DCM	35	0.5 (V70)	~500	65	4.8	1619.1	3419.4	2.3

^a Determined gravimetrically. ^b Determined *via* gel permeation chromatography.

As previously, a variety of reactions conditions were altered simultaneously because the main aim with this work was simply to achieve a viable polymerisation strategy which reliably produced polymer over a reproducible time frame; the exact conditions required and resulting polymer characteristics were secondary considerations. The initiator concentration was not altered, as 0.5 wt% was considered a sensible lower limit, while increasing the concentration of initiator in CCTP reactions has minimal impact due to the dominant catalytic transfer and initiation processes.

Firstly, the reaction was repeated using a significantly lower concentration (~800 ppm) of PhCoBF, shown in Table 4.2, Entry 1 and this resulted in the reaction

forming a gel after ~41 minutes. In this case, the reaction time became significantly more reproducible, with all repeats falling between 40 and 43 minutes. This concentration of CTA was chosen as a balance between gelation time and molecular weight achieved. As the reaction must be quenched at least 5 minutes prior to gelation to prevent unwanted gelation during cooling, gelation times shorter than ~30 minutes can lead to difficulty in isolating any significantly hyperbranched polymer before significant cross-linking occurs. In free radical polymerisations, the addition of a CTA slows the gelation process by shortening branch lengths, but also leads to lower molecular weight polymer being produced for the same initial monomer concentration. Thus, CTA concentration should be kept as low as possible when high molecular weight polymers are desired.

Upon quenching this reaction at 36 minutes, a polymer of relatively high molecular weight (1154.5 kDa) was produced, which indicated that the reduction in CTA concentration did have the desired effect of increasing the polymer product's molecular weight. However, the yield (6.6 %) and dispersity (2.7) were low, which indicated that it was very likely that predominantly linear polymer was being formed *via* this method. This conclusion was supported by the fact that a) polymer theory would predict that branching in these types of systems does not occur below 20 % conversion and b) dispersity is correlated to the degree of branching for HB polymers, with 2.7 being only slightly higher than the dispersity obtained from the CCTP polymerisation of a linear polymer [20], [75], [84], [76]–[83]. This lack of hyperbranching was attributed to the short reaction time observed for these conditions: the architectural transition from lightly branched, to hyperbranched, to cross-linked polymer occurs very rapidly for this diacrylate polymer, thus the HB polymer could not be isolated over the timescale of this reaction.

Thus, the optimisation of the reaction was furthered by lengthening the gelation time and the branched-polymer-to-gel transition period to attempt to increase the chance of isolating HB polymer. The result of this experiment is shown in Table 4.2, Entry 2. In this polymerisation the solvent-to-monomer ratio was increased to 3:1, the temperature was decreased to 65 °C and the CTA concentration was increased slightly to ~1000 ppm. These conditions resulted in the greatest achieved yield (17 %) and branching, though molecular weight was sacrificed. The reaction time increased to 113 minutes and the dispersity value to 7.0. The reduction in molecular weight was expected, given the increased CTA concentration relative to Entry 1. However, in comparison to typical CCTP hyperbranching reactions, the yield remained low. It was concluded that the toluene solvent was likely the limiting factor, as this had been observed earlier to be a non-ideal solvent for this system. Thus, the best way to increase the yield further would be to find a new solvent in which the reactants showed good solubility, but which did not adversely affect the reproducibility of the gelation time.

Previous work by the research group at Nottingham [20] had shown that DCM-based reaction conditions provided good control over the polymerization of a related mono-functional monomer, ethylene glycol dicyclopentenyl ether acrylate (EGDPEA) due to good reactant solubility. Hence, these conditions were adapted for the di-functional TCDMDA monomer in an attempt to determine whether improved monomer and CTA solubility at significantly reduced reaction temperature resulted in greater control over the reaction and/or improved the yields obtained compared to the toluene-based system.

The reaction conditions used for the DCM-based reactions are shown in Table 4.2, Entry 3. Due to the difference in the boiling temperatures of the solvent used,

the reaction temperature with DCM (35 °C) was significantly reduced compared to with cyclohexanone and toluene; a suitable thermal initiator (2,2'-Azobis(4-methoxy-2,4-dimethylvaleronitrile), or V70) with a lower half-life temperature was therefore used in place of AIBN. The CTA concentration was reduced to ~500 ppm due to its enhanced solubility in DCM. Unfortunately, the only improvement observed when using DCM rather than toluene solvent was to the molecular weight (1619 kDa), which was attributed to the reduced CTA concentration used. The yield achieved (4.8 %) was still very low, which suggested that the solvent choice was not, in fact, the limiting factor for the yield. There were also some issues with using DCM as a solvent. Due to its high volatility, appreciable quantities of solvent evaporated during the degassing phase, making the results unreliable. In future work, repeating these polymerisations using a two-part degassing technique may prevent this issue: degassing the DCM solvent separately, then transferring the required volume into the degassed reaction vessel would ensure the expected quantity of DCM was used. However, this was not pursued in this work due to the continued poor performance/yield of these polymerisations.

Overall, it was concluded that it could not simply be poor solvation that was causing the issues with yield and variable gelation times. Furthermore, given that all of these parameters were linked to the growth/termination of HB polymer chains, which were controlled by the CTA, it seemed likely that the CTA PhCoBF was simply a very poor control agent for TCDMDA. This was not entirely unexpected, as acrylates are known to be poorly controlled by CCTP compared to methacrylates due to the lack of an α -methyl group for facile hydrogen abstraction. However, the extent of the issue was surprising, and a new control method was needed to provide a viable method for the synthesis of HB pTCDMDA at larger scales.

4.3.2 TCDMDA Homopolymers *Via* Chain Transfer Polymerisation (CTP) with Thiol CTA

Due to the extremely poor yields and control observed when attempting to synthesise HB pTCDMDA *via* CTP, use of a new control agent was investigated and the thiol, 3-mercaptopropionic acid (3-MPA), was chosen to replace PhCoBF. In order to optimise the new reaction conditions for 3-MPA, which had not previously been used during this work, the effect of CTA and initiator concentration on the TCDMDA homopolymerisation was investigated, with the aim of determining appropriate quantities of each to enable a suitable reaction timescale. These thiols were chosen due to a) their potential to add interesting new functionality to the polymer and b) to tie in with another project being run simultaneously by a peer.

4.3.2.1 *Determining Appropriate Starting Conditions*

Firstly, an investigation into the effect of the thiol CTA concentration on the gelation time of the reaction was conducted. The monomer-to-solvent ratio (1:2), weight percentage (0.1 wt%) of AIBN initiator and reaction temperature (65 °C) were kept constant, while the concentration of 3-MPA was varied from 5 – 65 mol %. The data which looked firstly at the average gelation times obtained with increasing CTA concentration are displayed in Figure 4.4.

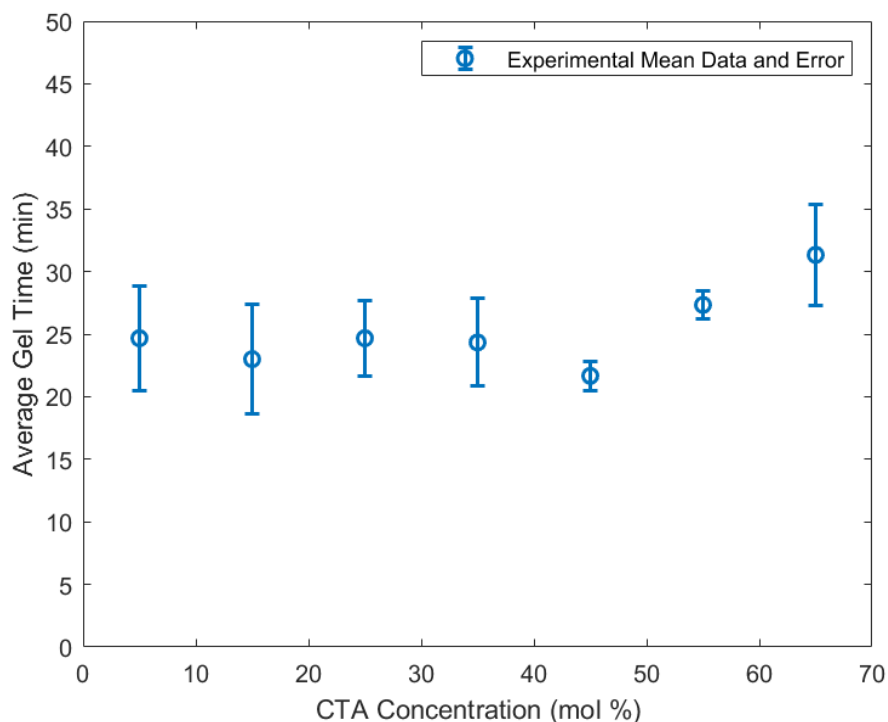


Figure 4.4. The average gel time over three repeats, obtained for TCDMDA polymerizations using CTA concentrations from 0 – 65 mol%. The circles represent the mean values, while the error bars indicate the standard deviation error across these repeat measurements.

It was clear that the CTA had a negligible impact on the gelation time until the concentration reached 55 mol % or above: beyond this point, the gelation time rose marginally with increasing CTA concentration to a peak of 31 minutes. This effect was due to the reduction in branch length that occurred when the CTA acted to transfer the radical from the growing chain to a new chain. The levelling-off of the effectiveness of the CTA below 55 mol% could be attributed to the CTA concentration becoming so low relative to monomer and solvent concentration that the effect of the CTA was negligible. However, once the extent of the error bars for this data were taken into account, no significant trend could really be identified due to the large overlap. The use of more than 65 mol % of thiol CTA was not investigated, as this would prove uneconomical at larger scales. Consequently, 65 mol % was identified as the most suitable CTA concentration for use in future experiments.

Further optimization involved investigating the effect of initiator concentration on the gelation time. The monomer-to-solvent ratio (1:2), concentration of thiol CTA (65 mol%) and temperature (65 °C) were kept constant while the initiator concentration was varied from 0.1 – 3.0 wt%; the average gelation times obtained for initiator concentrations of 0.1, 0.3, 0.5, 0.7, 1.9, 2.0 and 3.0 wt% are summarised in Figure 4.5.

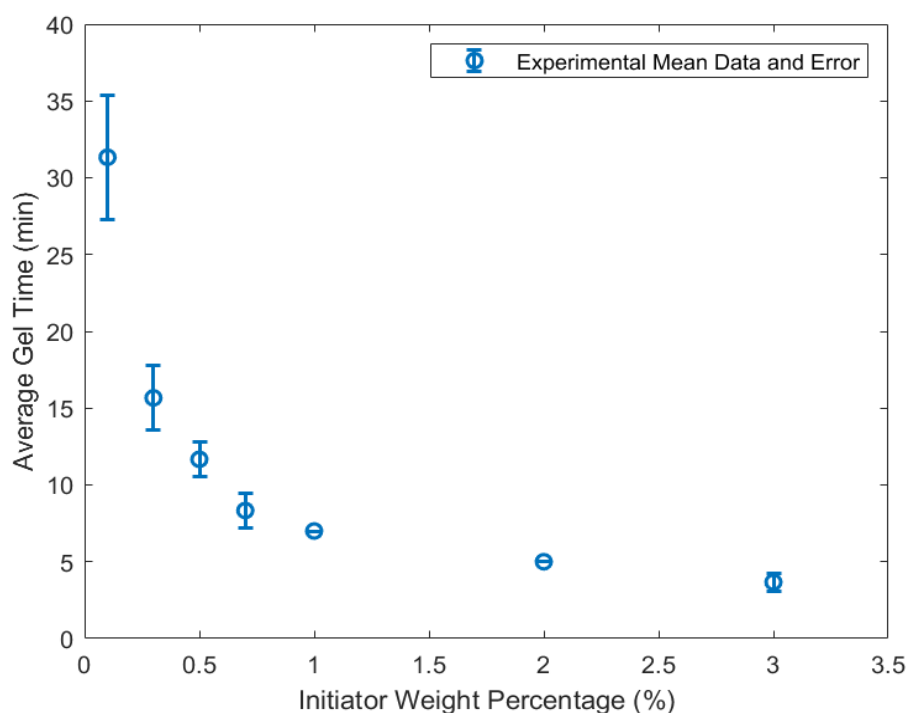


Figure 4.5. The average gel time over three repeats, obtained for TCDMDA polymerizations using initiator concentrations from 0.1 – 3.0 wt %. The circles represent the mean values, while the error bars indicate the standard deviation error across these repeat measurements.

At low initiator concentration, the gelation time was seen to decrease rapidly with increasing initiator weight percentage, from an average of 31 minutes at 0.1 wt% to 7 minutes at 1.0 wt%. Above the latter concentration, the effect of increasing initiator concentration on the gelation time became less pronounced, though a small decrease in gelation time to 4 minutes was noted as the initiator concentration was tripled to 3.0 wt%. This trend was due to the increased availability of radicals for chain initiation with increasing initiator concentration, which lead to a greater number of

propagating chains for the same quantity of monomer. As the reaction with 0.1 wt% of AIBN had the longest gelation time, these conditions were chosen for the subsequent synthesis of HB-pTCDMDA. This was to ensure that a practical amount of time was available to maintain a repeatable termination point for these reactions.

4.3.2.2 Investigating Chosen Conditions

Thus, 65 mol% CTA and 0.1 wt% initiator was used to synthesise HB pTCDMDA. The reaction was quenched at 25 minutes to prevent gelation: the data for three repeats are shown in Table 4.3.

Table 4.3. Summary of the yields, molecular weights and dispersities of three identical TCDMDA polymerizations using 65 mol % 3-MPA CTA and 0.1 wt % AIBN initiator.

Entry	Reaction Time (min)	Yield ^a	Mn ^b (kDa)	Mw ^b (kDa)	Đ ^b
1	25	95%	8.02	61.04	7.61
2	25	75%	8.94	24.75	2.77
3	25	82%	15.19	100.70	6.63

^a Determined gravimetrically. ^b Determined via gel permeation chromatography.

The resulting polymers demonstrated relatively low molecular weights compared to the CCTP-derived polymers discussed earlier, as might be expected from such a high CTA concentration. However, the dispersity values were high indicating branching had occurred. Importantly, the yields for these polymerisations were very high, ranging from 75 – 95 %. This was considerably higher than a standard hyperbranching reaction (35-45 %), possibly due to a higher efficiency of interaction between the monomer and thiol compared to between the monomer and PhCoBF. It was, therefore, tentatively concluded that CTP with a thiol CTA was a more feasible route to synthesizing hyperbranched pTCDMDA than CCTP.

This was confirmed by repeating the CTP reactions above using dodecanethiol/dodecyl mercaptan (DDM) as the CTA in place of 3-MPA. The same conditions (65 mol % CTA, 0.1 wt% AIBN, 1:3 monomer:solvent ratio) were used, resulting in an average gelation time of 52 minutes. This reaction was then repeated and quenched 7 minutes prior to the average gelation time to ensure maximum conversion, as summarised in Table 4.4.

Table 4.4. Summary of the yields, molecular weights and dispersities of three identical TCDMDA polymerizations using 65 mol % DDM CTA and 0.1 wt % AIBN initiator.

Entry	Reaction Time (min)	Yield ^a	M _n ^b (kDa)	M _w ^b (kDa)	Đ ^b
1	45	78%	8.27	241.82	29.2
2	45	71%	6.99	68.02	9.7
3	45	75%	7.21	89.56	12.4

^a Determined gravimetrically. ^b Determined *via* gel permeation chromatography.

0

The resulting polymer demonstrated similarly high yields (average 74.7 %) to that produced using 3-MPA (min 75 %). The number average molecular weights obtained for the DDM controlled polymer (average M_n = 7.5 kDa) were also similar to those for the 3-MPA-controlled polymers (average M_n = 10.7 kDa), which indicated that the increased control observed for 3-MPA was not an isolated incident. The weight average molecular weights and dispersities, however, were slightly increased for the DDM-controlled polymers, indicating that a more branched structure was achieved when using DDM. This may have been due to the extended reaction time obtained when using DDM (45 minutes) compared to 3-MPA (25 minutes), as this would have allowed the reaction to be quenched closer to the true gelation time for the DDM control. Consequently, the higher levels of branching would have been achieved for the DDM-controlled polymer.

Comparing the results of these DDM-controlled reactions to a similar reaction using DVB as the di-functional monomer (Chapter 3, Section 3.3.5), it was clear that similar yields were obtained, with a DVB (60 mol % DDM) average yield of 83 %, compared to 74.7 % for TCDMDA. However, the molecular weights achieved for TCDMDA were significantly higher than for DVB, despite the increased concentration of DDM used (60 mol % for DVB, 65 mol % for TCDMDA). This was attributed to the DDM providing less control over the TCDMDA compared to the DVB. This was expected, given the difficulties observed in this work of controlling the polymerisation of the TCDMDA monomer. Additionally, the reaction times were quite different: for pDVB, the gelation time at 65 mol % DDM was > 420 minutes, which was considerably longer than the 52 minutes seen for TCDMDA. It is likely that this was due to the relative reactivity ratios of styrenyl vinyl groups and acrylate groups. Styrenyl vinyl groups are generally more stable than acrylates due to resonance of the vinyl group π -electrons with the delocalized π system of the benzene ring. Consequently, it is less likely to undergo radical addition than the acrylate group, resulting in slower radical reactions for styrenyl monomers.

An additional advantage to polymers made in this way is that they may possess some interesting amphiphilic properties due to the CTA mechanism. When a growing polymer chain is terminated by chain transfer with thiol, a hydride radical fragment is added to the end of the chain. The functional sulphur-containing species then possesses a radical, which may initiate another chain or attach to a pendant acrylate group. Thus, having a large CTA concentration should lead to high levels of sulphur-containing functionality in the final products. Thus, due to the acidic and hydrophilic nature of this thiol in the case of 3-MPA, and the carbon-rich nature of the TCDMDA monomer, an amphiphilic structure was created. This may be proven by determining the acid value of the polymer, which should be done in future work.

Additionally, contact angle measurements and the determination of critical micelle concentration (CMC) could also be used to determine the level of amphiphilicity. This may help to increase the anti-attachment properties of the polymer, by introducing increased levels of amphiphilicity similar to that seen for anti-biofilm zwitterionic polymers (see Section 4.1.1).

Similarly, DDM possesses a long hydrocarbon chain, which introduces new hydrocarbon character to the polymer, increasing its hydrophobicity. This, in turn, increased the solubility of the polymer in hydrocarbon-based solvents (see Chapter 3 Section 3.3.5). Furthermore, by substituting in other thiol CTAs with different properties, the polymer could be tailored for a specific application by deliberately introducing a second functionality. Thus, this new thiol-based hyperbranching method may constitute a way to synthesise functionalized, high-yielding HB polymers from a variety of di-functional monomers which otherwise prove difficult to control using a PhCoBF CTA.

4.3.2.3 Scaling up 3-MPA-Controlled Polymer Synthesis

The HB pTCDMDA polymerisation was then scaled up to a 10 g scale, in order to prove the industrial viability of this methodology and to provide sufficient polymer for future application testing. The data from this polymerisation is summarised in Table 4.5.

Table 4.5. Summary of the conversion, yield, molecular weight and dispersity of 10g scale TCDMDA polymerizations using 65 mol % 3-MPA CTA and 0.1 wt % AIBN initiator.

Entry	Reaction Time (min)	Conversion (%) ^a	Yield ^b	Mn ^c (kDa)	Mw ^c (kDa)	Đ ^c
1	25	60.0	121.9%	3.31	12.92	3.90

^a Determined by ¹H-NMR. ^b Determined gravimetrically. ^c Determined *via* gel permeation chromatography.

The polymer was precipitated as a very viscous liquid, which was likely the origin of the > 100 % yield, as the polymer could not be vacuum-dried. The molecular weights achieved were similar to those observed at a smaller scale (Table 4.3). However, they were slightly reduced at the larger scale, possibly due to the reduction in heat and mass transfer efficiency at scale, which would have limited CTA and radical diffusion.

The proposed material testing to define if these HB pTCDMDA polymers were suitable for use as anti-bacterial attachment coatings when an acid functionality was included could not be completed. This was because while testing of the HB-pTCDMDA/3-MPA for use as a high BAR coating for water-based emulsion polymerisation mesh filters was planned in collaboration with BP/Castrol, Covid-19 restrictions closed both BP and University of Nottingham labs.

However, the suitability of HB pTCDMDA for use in 2PP was investigated, using a sample of the polymer synthesised in Table 4.5.

4.3.2.4 Two Photon Printing of 3-MPA Controlled HB pTCDMDA for Bio-Applications

In work conducted by Andrea Konta (Centre for Additive Manufacturing), commercial TCDMDA monomer and HB pTCDMDA synthesised using 3-MPA as the CTA were compared in a 2PP formulation. Both were used as a feedstock to print an array of 3D, rectangular scaffolds across a range of printing speeds (2 – 25 mm/s) and laser powers (10 – 100%). These scaffolds are presented in Figure 4.6.

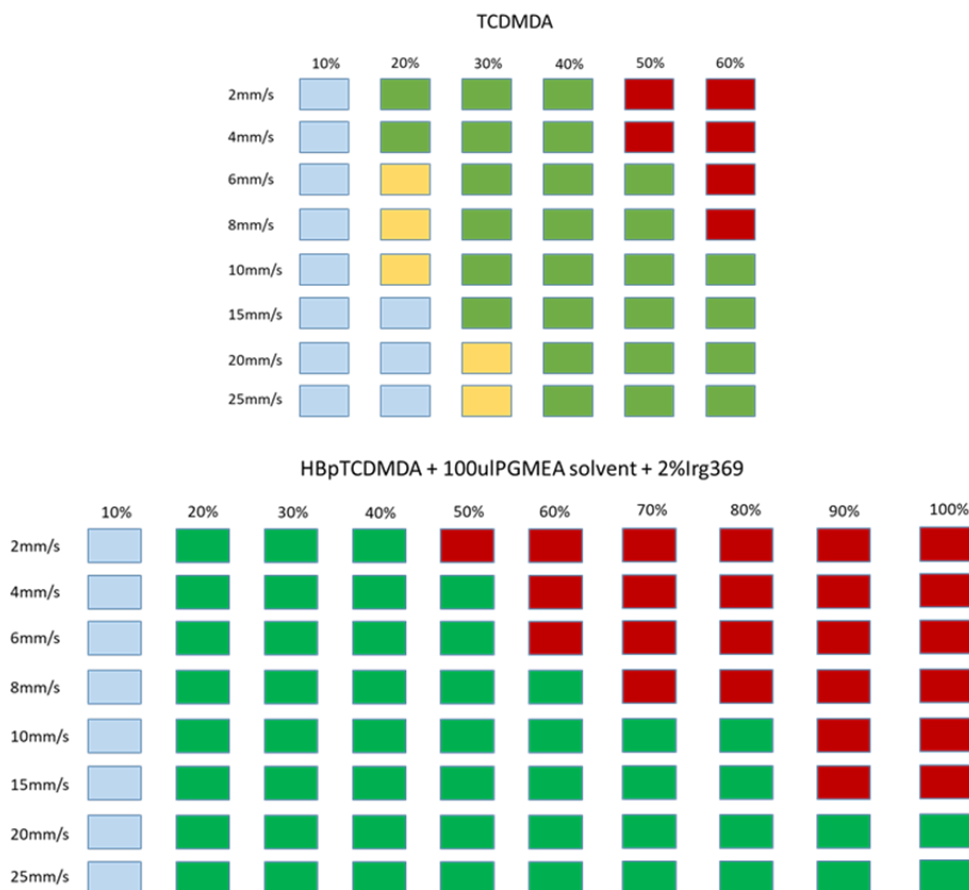


Figure 4.6. Array of scaffolds produced using 2PP to print commercial TCDMDA (top) and HB pTCDMDA (bottom) across printing speeds in the range 2 – 25 mm/s and laser powers from 10 – 100 %. Red indicates conditions where the final cuboid was burned. Yellow indicates conditions where insufficient polymerisation occurred, such that the final shape was not representative of the CAD shape. Green indicates conditions where polymerisation occurred, and well-structured shapes were produced. Blue indicates conditions where no polymerisation was observed.

Here, the colour assigned to the scaffold indicates the quality of the final product produced for each combination of conditions. Red indicated conditions where the final cuboid was burned. Yellow indicated conditions where insufficient polymerisation occurred, such that the final shape was not representative of the CAD shape. Green indicated conditions where polymerisation occurred and well-structured shapes were produced. Blue indicated conditions where no polymerisation was observed.

Additionally, an SEM image of the scaffolds for HB pTCDMDA has been included as Figure 4.7.

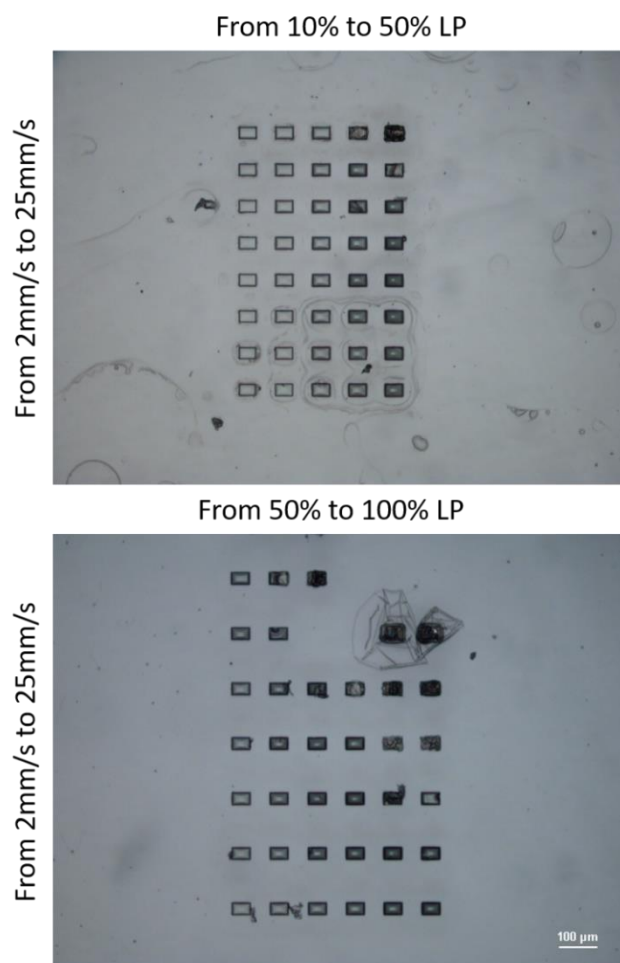


Figure 4.7. Polymerization threshold SEM images of HB pTCDMDA formulation.

Comparing the results for the commercial TCDMDA feedstock (Figure 4.6, top) and the HB pTCDMDA (Figure 4.6, bottom), it was first clear that the use of HB polymer significantly broadened the polymerisation threshold, with good scaffolds produced across a wider range of conditions, including lower laser powers and increased printing speeds. Raman spectroscopy was used to determine the average reacted vinyl group (RVP) as a percentage for each array. For the commercial TCDMDA the average RVP was 30%, while for the HB materials a RVG of 80% was achieved, indicating an increased degree of conversion of ~50% when using the HB polymer.

This suggested that the use of HB materials caused the formulation to cure more quickly and to a greater extent than with the commercial monomer, as expected

given that ~60% monomer conversion or higher was achieved during the HB polymer synthesis, prior to any printing taking place (see Table 4.5). Not only did this enable printing times to be reduced, the ability to use lower laser powers also enables higher resolution printing. Additionally, the higher average RVP ensures that less monomer must be removed to prevent toxicity of the resulting materials.

Following printing, the HB pTCMDMA scaffolds were sent to Dr Adja Toure, who conducted a Live/Dead Biocompatibility test, which is shown in Figure 4.8.

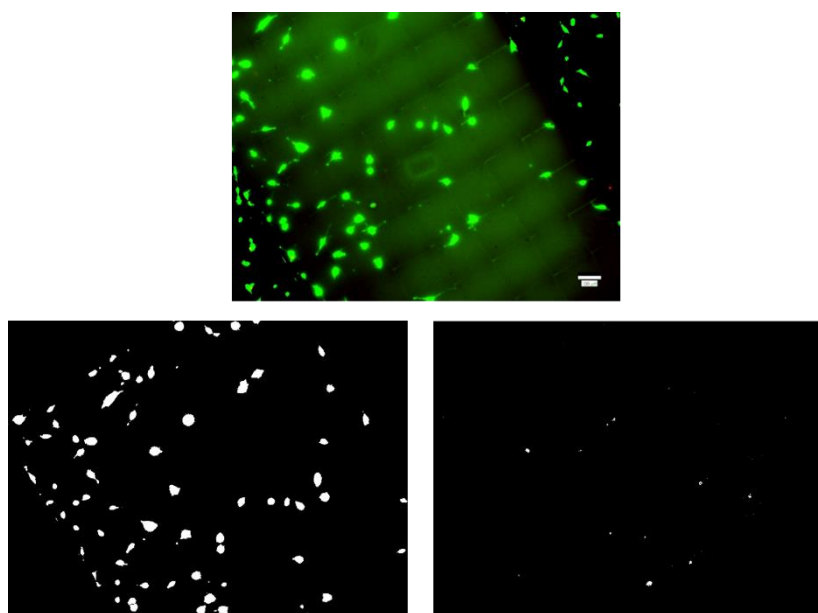


Figure 4.8. Microscope image of fluorescing fibroblast cell cultured on HB pTCMDMA scaffolds produced via 2PPs. In the composite image (top), green indicates live cells, while red indicates dead cells. In the example raw images (bottom), the white spots indicate regions of fluorescence from live cells (left) and dead cells (right).

In this test, a facile two-colour assay was used to determine the viability of fibroblast cells (see Chapter 2.3.2.5). This test indicated that the printed polymer demonstrated high biocompatibility, with 92% live cells (green fluorescence in top image, all fluorescence in bottom left image) and only 8% dead cells (red fluorescence in top image, all fluorescence in bottom right image) following staining after 1 hour.

Thus, these HB TCDMDA polymers hold promise for use in biological applications, as well as helping to combat some of the major challenges in 2PP, including reduced fabrication time and increased printing resolution.

4.3.3 Preliminary Studies of HB Copolymers *via* Macromer Controlled CTP for Stem Cell Attachment

From 2D screening in work conducted by Dr Jordan Thorpe in the School of Pharmacy, it was found that when TCDMDA monomer was mixed with butyl acrylate (BA) in a ratio 2:1 v/v in a 6-well plate and polymerised using UV polymerisation, the resulting copolymer was able to support the long-term culture of human pluripotent stem cells (hPSCs), likely due to high levels of transforming growth factor beta 1 (TGF1) absorption on the polymer surface [85]. However, the cells only survived for 2-3 days after which they were found to die. Surface analysis with atomic force microscopy (AFM) revealed a nanoscale topography in deformation and modulus images, as shown in Figure 4.9 [52], of this polymer, indicating a phase separation of the monomers prior to polymerisation.

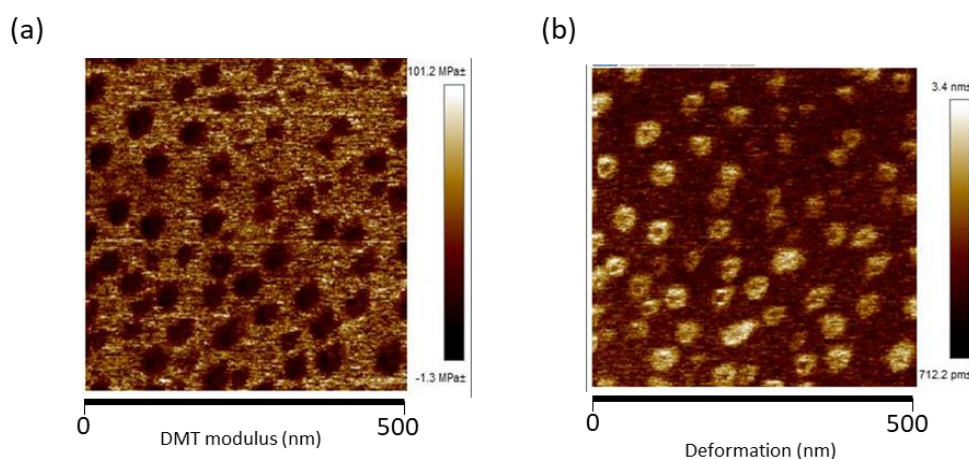


Figure 4.9. Atomic force microscopy (a) modulus and (b) deformation micrographs of poly(TCDMDA-blend-BA) surface coated on poly(styrene) six well plates shows a nanoscale blend of poly-BA (~50nm islands of minor component, 30% v/v) in poly-TCD (background, major component, 70% v/v) [52].

It was proposed that it was this phase separation which contributed to the loss of cell viability with time.

This phase separation resulted in the equivalent of a blend of pBA (minor component, 30 % v/v as \sim 50 nm islands) in a continuous phase of pTCDMDA (major component, 70% v/v) rather than a uniform surface that would be representative of a copolymer. It was therefore proposed that HB copolymers of TCDMDA and BA prepared in solution then cast to the well plates could address this phase separation issue and potentially allow for a more consistent culture surface and long-term viability of the cells in contact with this surface, thus proving the eventual viability of scaling up this material and process.

4.3.3.1 Producing Copolymers in Solution

Initially, a direct copolymerization of TCDMDA and BA monomers was attempted *via* CCTP. However, it was found that the two monomers would not easily copolymerize in solution, which was attributed to their different reactivity ratios. H^1 NMR analysis confirmed that the TCDMDA polymer was not copolymerising well with the BA monomer, with very little incorporation of BA into the copolymer, as shown in Figure 4.10.

Consequently, the polymerisation strategy was altered to the homopolymerisation of TCDMDA which was controlled using BMA macromers (BMA_2) as the CTA. This was an analogous method to that described in Chapter 3, where divinyl benzene was controlled using lauryl methacrylate macromers. BMA_2 was chosen as the macromer control agent over BA_2 for two main reasons. Firstly, it can be difficult to control the CCTP reaction of acrylate monomers sufficiently to achieve dimerization. Secondly, BMA was a more hydrophobic monomer than BA due to the presence of an extra CH_3 group, which should encourage improved mixing between it and the hydrophobic TCDMDA monomer compared to BA. The BMA macromers were synthesized *via* CCTP, using toluene as a solvent and high levels of PhCoBF, which

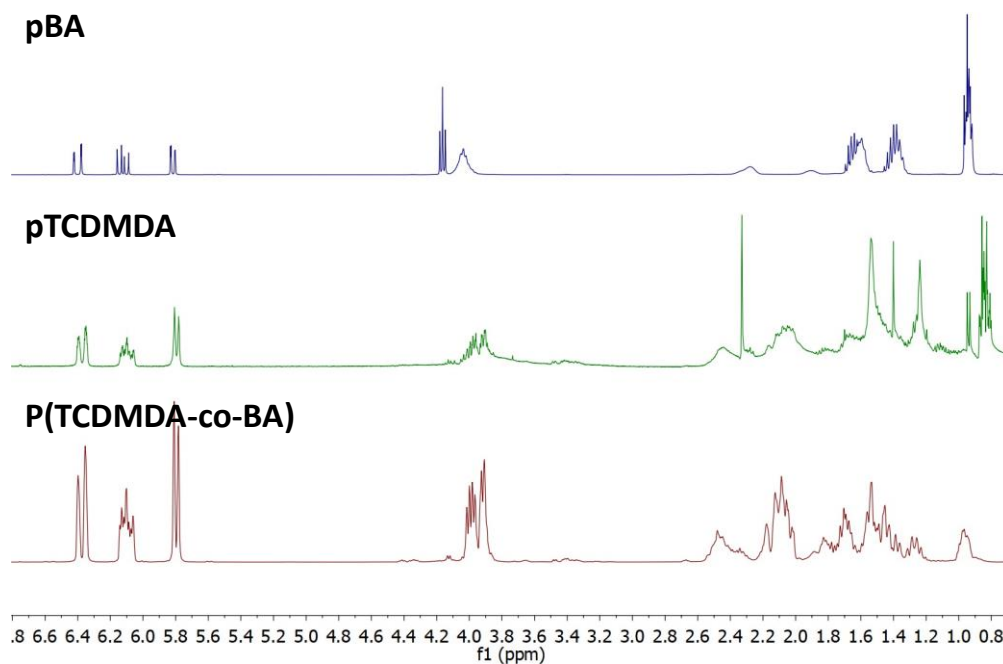


Figure 4.10. ^1H NMR of homopolymers of butyl acrylate (top, blue), TCDMDA (middle, green) and the direct CCTP copolymer HB $p(\text{TCDMDA-co-BA})$ (bottom red). By comparing the peaks in each spectrum, it is clear that the spectrum originating from the supposed HB copolymer displays no peaks which are not also observed in the TCDMDA homopolymer spectrum, indicating that the HB copolymer is in fact a homopolymer of TCDMDA, with little-to-no inclusion of the BA monomer in the structure.

resulted in an oligomeric mixture of BMA macromers with an average monomer conversion of 22.0 %, as summarised in Table 4.6, Entry 1.

Table 4.6. Summary of the reaction conditions used to synthesize BMA macromers, and for macromer controlled CTP of TCDMDA. The average yield, molecular weights and polydispersity are also quoted.

Entry	Mon: sol (v/v)	Temperature (°C)	AIBN (% wt)	PhCoBF (ppm)	Reaction Time	Yield ^a (%)	M _n ^b (kD)	M _w ^b (kD)	Đ ^b
1. BMA macromer	20:1	80	1.0	800	24 hrs	22	-	-	-
2. TCDMDA-co-BMA	1:3	65	0.5	-	2hr 18	46	15.9	211.0	13.3

^a Determined gravimetrically. ^b Determined via gel permeation chromatography.

These oligomers/macromers were then used as CTAs in their own right and reacted under conditions similar to those outlined in Table 4.2, Entry 2, as these conditions had, to this point in the study, resulted in the highest polymer yields for CCT-based polymerisations of TCDMDA. Initially, this copolymerisation was conducted on a 1 mL scale, as a proof-of-concept experiment. An increase in the

reaction time compared to the homopolymerisation was observed, from 1hr 53 min to 2 hrs 18 min as shown in Table 4.6, Entry 2. This was an expected result, as when a mono-functional methacrylate monomer was added to the polymerisation mixture, it would be expected that radical addition to methacrylate groups would slow the reaction rate, whilst producing more control. This is due to the need for the beta scission process to occur, which is a slower process than radical addition. The yield (46 %) also improved compared to the CCT TCDMDA homopolymerisation, while the dispersity (13.3) was considerably greater, indicating a higher degree of branching and monomer conversion. This suggested that the BMA macromer was a more suitable control agent for the TCDMDA monomer than PhCoBF, possibly due to its greater similarity with respect to hydrophobicity. The improved incorporation of the BMA monomer in the copolymer was confirmed by H^1NMR , which is shown in Figure 4.11

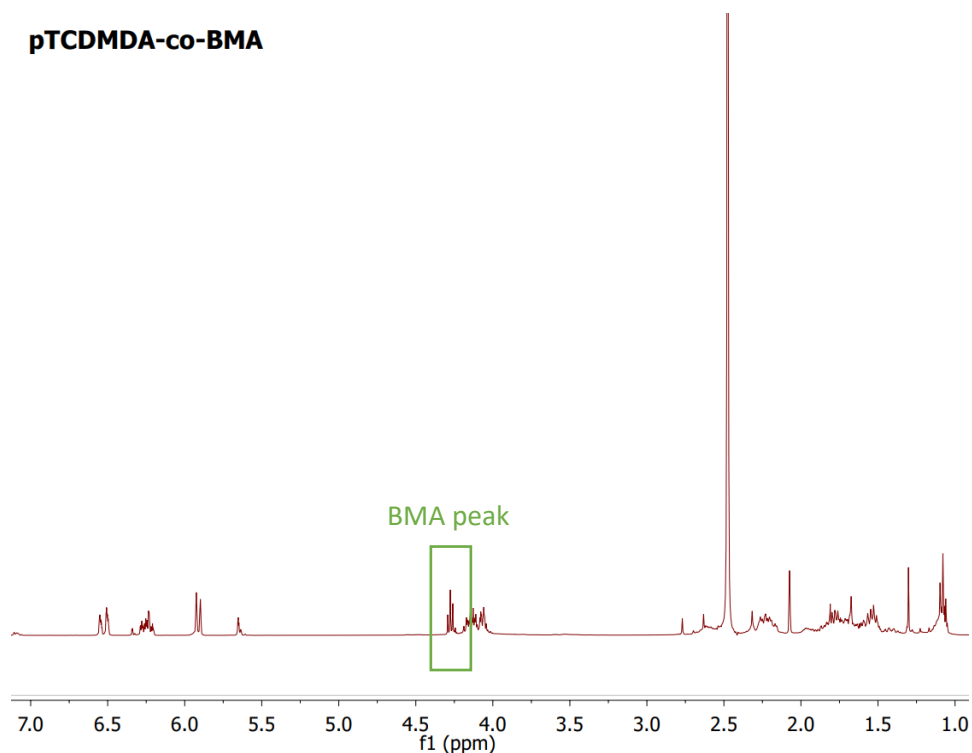


Figure 4.11. H^1NMR of the TCDMDA/BMA copolymer synthesised using BMA macromer control. A peak is seen at $\delta = 4.30$ ppm, which can be attributed to the BMA monomer. This peak was not observed previously (see Fig. 4.10) when direct CCT copolymerisation was attempted. This indicated that macromer control improved the level of BMA incorporation in the HB copolymer.

4.3.3.2 Cell Growth Studies

Following the successful synthesis of a small sample of TCDMDA/BMA copolymer, some preliminary cell growth testing was conducted by Dr Jordan Thorpe with the School of Pharmacy at the University of Nottingham on a hESC HUES7 line of stem cells, where 4 serial passages were achieved (n=1). It was observed that additional purification of the polymer (i.e. redissolution and precipitation) was required to ensure the polymer was suitable for use. This was attributed to the need to remove any residual free monomer from the system. This was not unexpected, since it was the presence of unreacted free monomer in the original TCDMDA:BA UV copolymerisation that was attributed to the onset of cell death. A solution of 42 mg of p(TCDMDA-co-BMA) was dissolved in 1200 μ L of isopropanol using a heat gun. The solution was then coated onto well-plates (100 μ L/well of 6-well plate) both with and without oxygen plasma treatment. This treatment was applied as a standard surface treatment to the glass plates produced for use in the UV polymerisation methods used in the bio instructive screening experiments.

The plates were then sterilised and cultured with human pluripotent stem cells (hPSCs), and the growth was monitored, as shown in Figure 4.12.

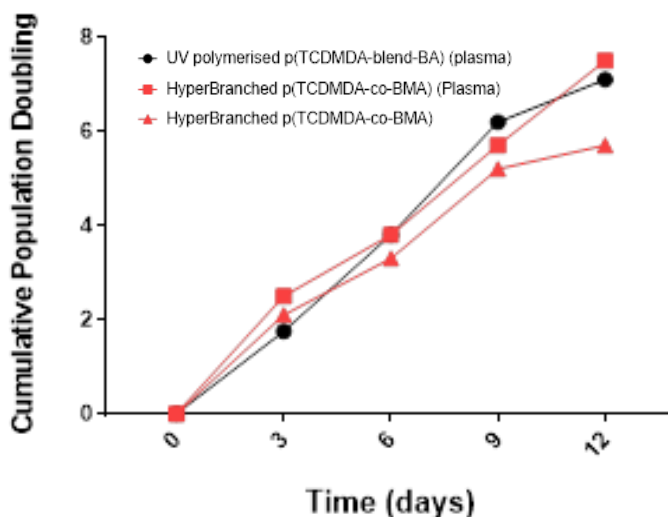


Figure 4.12. Growth comparison of HUES7 hPSCs on poly(TCDMDA-blend-BA) UV polymerized and hyperbranched poly(TCDMDA-co-BMA) 6 well-plates. Plates produced for the hyperbranched condition were prepared with and without plasma treatment, whilst all plates produced by the UV polymerization methods have been plasma treated prior to well coating.

From this brief analysis, it was concluded that comparable growth was seen when using the HB polymer solutions, relative to the UV-produced polymers. It was also noted that plasma treatment may not be necessary for the plates prepared using the HB polymers, as similar growth was seen in Figure 4.12 both with (solid squares) and without (solid triangles) plasma treatment. It was also noted that isopropanol (IPA) was not an ideal solvent for this hyperbranched polymer, and an improved one would be required for future work. It is important to note that the UV and HB tests were not conducted in parallel, and independent batches of HUES7 cells were used for the UV and HB polymers. This makes any more detailed comparison of the results difficult, as the cell cultures were not directly comparable.

4.3.4 Solution Casting Pro-Attachment Polymers on Well Plates

Following the successful synthesis and encouraging growth results for the TCDMDA/BMA CTA-functionalised polymer sample which was prepared at a small scale (see Table 4.6, Entry 2), the polymerisation was conducted at a larger scale in order to obtain sufficient material in order to enable the TCDMDA/BMA copolymer to both be tested at larger scale for pro-stem cell attachment properties and prove

industrial viability. Additionally, the HB polymer obtained was also required to be purified more thoroughly in the lubricant-based materials at this larger scale (Chapter 3). This was to remove unreacted monomer/residual solvent, to ensure cell viability. Finally, a suitable solvent needed to be identified to enable the solid HB polymer product to be easily and uniformly coated onto 6-well plates.

4.3.4.1 Polymerisation Scale-Up and Purification

Therefore, the reaction was scaled by a factor of ~30, and is summarised in

Table 4.7.

Table 4.7. Summary of the reaction conditions used to synthesize BMA macromers, and for macromer controlled CTP of TCDMDA (2:1 v/v TCDMDA:BMA) at increased scale. The average yield, molecular weights and polydispersity are also quoted.

Entry	Mon: sol (v/v)	Temperature (°C)	AIBN (% wt)	PhCoBF (ppm)	Reaction Time	Yield ^a (%)	Mn ^b (kD)	Mw ^b (kD)	Đ ^b
1. BMA macromer	20:1	80	1.0	800	24 hrs	24	-	-	-
2. TCDMDA-co-BMA	1:3	65	0.5	-	3hr 35	57.2	36.6	307.6	8.4

^a Determined gravimetrically. ^b Determined via gel permeation chromatography.

Entry 1 shows the large scale CCTP of 30 mL of BMA monomer to produce BMA macromers. The macromers were then used as the CTA to control the polymerisation of 60 mL of TCDMDA monomer, as described in Section 4.3.3, the results of which are summarised in Table 4.7, Entry 2. The yield (57.2 %) was higher than that of the small-scale reaction detailed in Table 4.6, Entry 2. While this may have been due to improved efficiency at larger scales, there may also have been residual monomer/anti-solvent present in the sample. The latter conclusion was supported by the observation that, following the first precipitation, the final form was a tacky, “putty-like” solid which could not be fully dried in a vacuum oven.

The reaction time (3hr 52 minutes) also increased at the larger scale compared to smaller scale (2 hr 18 minutes). This may have been due to decreased

heat and mass transfer efficiency at larger scale. However, it may also have been related to the earlier issues observed when polymerizing the TCDMDA monomer (Section 4.3.1). TCDMDA was found to be a difficult polymerisation to control, even at smaller scales, thus scaling up the polymerisation potentially would have only increased the variability.

The molecular weights ($M_n = 36.6$ kDa, $M_w = 307.6$ kDa) and dispersity (8.4) of the polymer produced at a larger scale were very similar to that produced on a smaller scale (Table 4.6), which indicated that the scale-up process did not significantly affect the architecture of the resulting HB polymer.

For initial biological testing to ensure the scale up process had not affected the activity of the polymer, sub-samples (~2 g) of the large-scale batch of HB pTCDMDA-co-BMA were extracted from the main batch and purified further. In this case, the polymer was precipitated twice to ensure that no unreacted monomer would be present in the final product, as this would be toxic to the stem cells: this was confirmed *via* H^1 NMR analysis, which is shown in Figure 4.13. This data showed that no further monomer was present in the supernatant following the second precipitation.

The next step in the preparation was to dry the product to constant mass to ensure no residual solvent/anti-solvent remained. For the first sample of HB pTCDMDA-co-BMA, this was attempted using a vacuum oven set at 25 °C, as this had been both the standard practice used throughout the study and had been demonstrated to be the most effective method of solvent removal. However, after 24 hours it was found that the polymer had crosslinked, forming an insoluble gel. This was confirmed when attempted dissolution in chloroform failed. This was attributed

to the slightly raised temperature inside the vac oven compared to ambient temperature (18 – 20 °C).

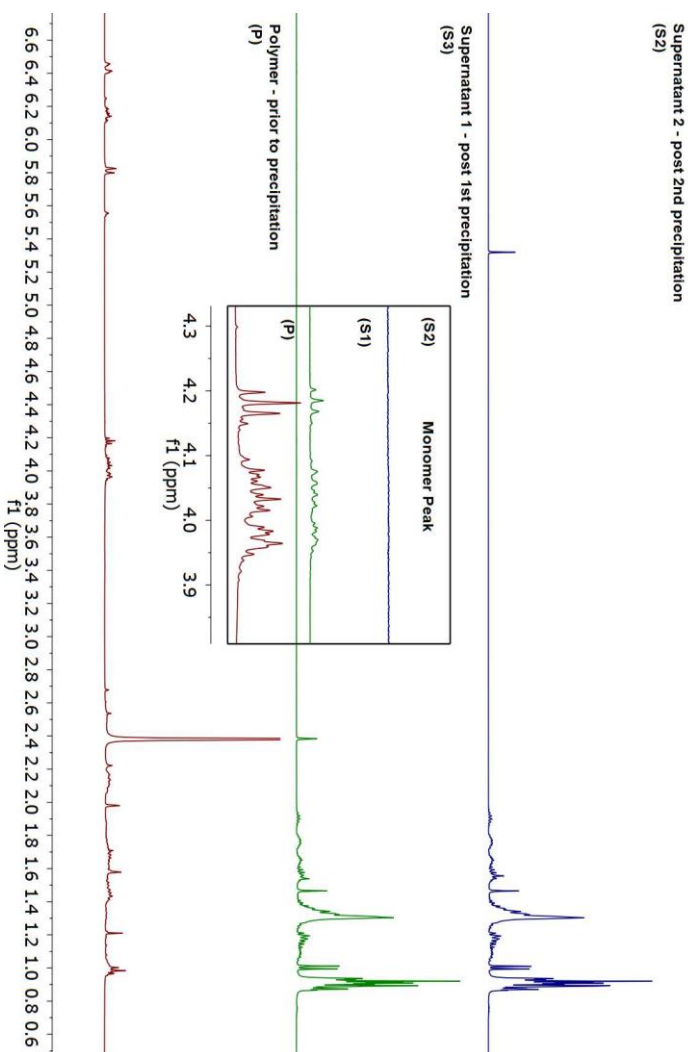


Figure 4.13. ¹H NMR analysis of TCDMDA/BMA polymerisation solution following quenching of the reaction, throughout the purification process. Spectra were acquired: before precipitation (bottom); after a first precipitation into cold hexane (middle); and following a second precipitation into cold hexane (top). In the spectrum acquired prior to precipitation (bottom), peaks which can be attributed to the monomer, rather than the polymer, can be seen at $\delta = 4.18$ ppm, 4.04 ppm and 3.97 ppm, indicating the presence of residual, unreacted monomer in the polymerisation mixture. The expansion zooms in on these peaks to help make them easier to see and compare across the spectra. In the spectrum acquired following the first precipitation of the reaction mixture into the hexane antisolvent (middle), these residual monomer peaks are seen to reduce in intensity, but are still visible, indicating that while some of the residual monomer was removed by the first precipitation, some still remained. In the spectrum acquired following the second precipitation of the reaction mixture, the intensities of these residual monomer peaks have decreased further, vanishing completely. This indicated that two purifications of the reaction mixture into antisolvent were required for to fully remove any unreacted monomer and ensure full purification of the polymer.

Consequently, a new sub-sample was prepared which was dried for 24 hours in a fume hood at ambient temperature. The resulting product was a solid, waxy powder, which was soluble in chloroform. An ^1H NMR of the dried product, shown in Figure 4.14, indicated that the hexane antisolvent, residual monomer and other impurities had been removed to a sufficient degree for use in stem cell culture applications.

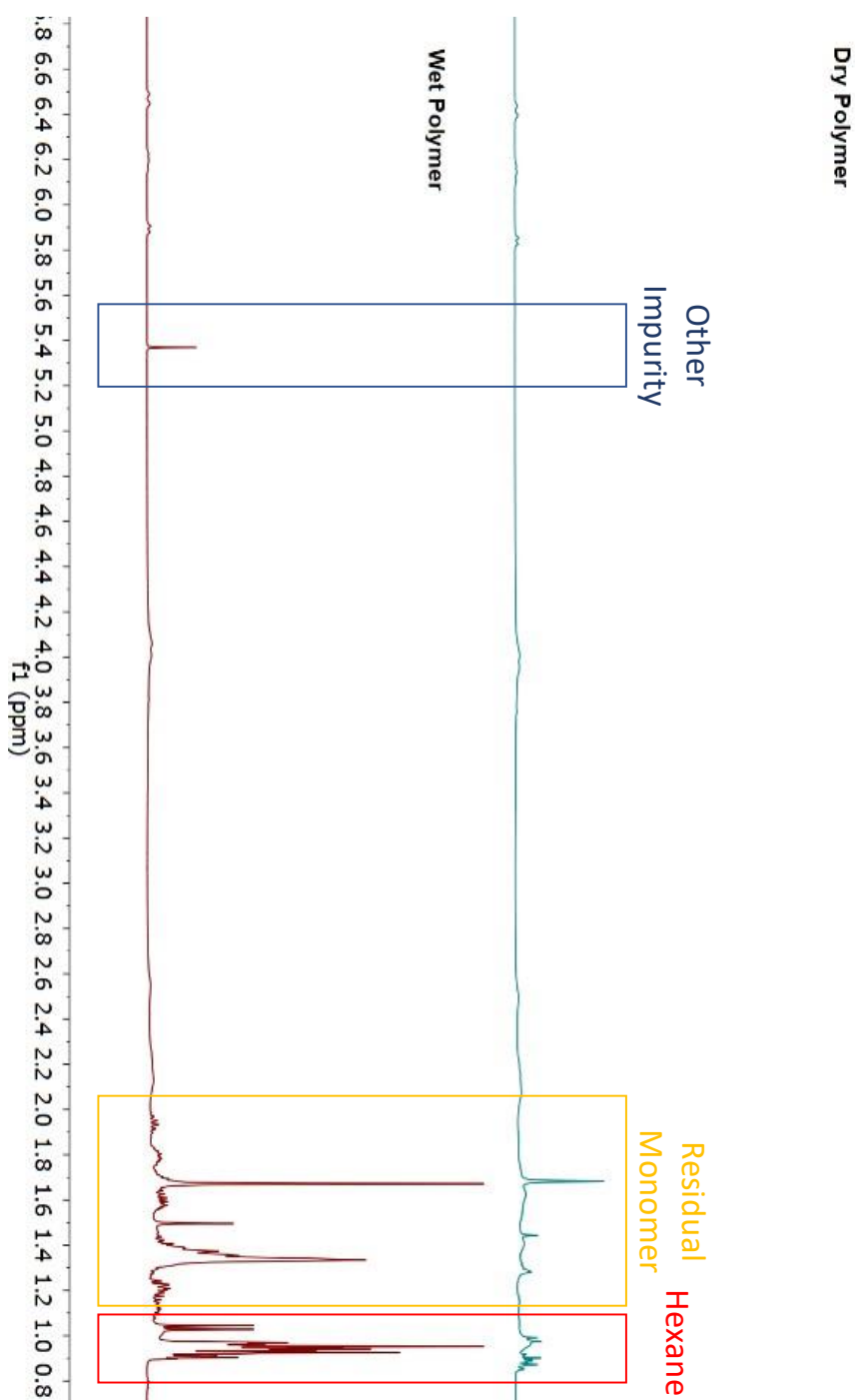
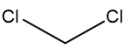
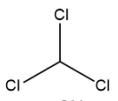
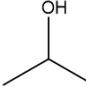
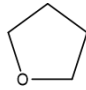
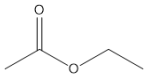
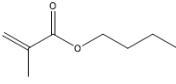
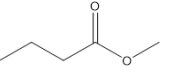


Figure 4.14. ^1H NMR spectra of a sample of p(TCDMDA-co-BMA) sample before (bottom) and after (top) drying for 24 hours in a fume hood at room temperature. In the spectrum acquired prior to drying, peaks due to residual monomer (region shown in yellow box), residual hexane antisolvent (region shown in red box) and another impurity (region shown in blue box) could be observed. Following 24 hours drying in a fume hood (top), these impurity are greatly reduced in intensity, indicating that these substances have been removed from the polymer product.

4.3.4.2 Solvent Determination and Well Plate Preparation

Thus, a sample of HB pTCDMDA-co-BMA polymer had been successfully synthesised, isolated and purified. A suitable solvent for the polymer now needed to be identified, as the solid polymer needed to be solubilized to be deposited into the well plates for biological testing. A target solution concentration of 35 g/L was chosen, as this had previously been found to result in good coverage of the bottom of the wells, with a thin, uniform film being achieved. A summary of the solvents tested during this work is shown in Table 4.8.

Table 4.8. Summary of the solubility studies conducted for HB p(TCDMDA-co-LMA). Y = polymer dissolved, N = polymer did not dissolve, P = partial dissolution and D = dispersion formed.

Solvent	Structure	Solubilises Polymer?	Non-cytotoxic?	Transparent Film?
Dichloromethane		Y	N	N/A
Chloroform		Y	N	N/A
Isopropyl Alcohol		N	Y	P
Tetrahydrofuran		Y	P	N
Ethyl Acetate		P	Y	N
Butyl Methacrylate		D	Y	P
Methyl Butyrate		P	Y	P

Solvents used in biological applications with polystyrene well plates such as those used in this work must strike a balance between solvency and toxicology/corrosivity. They must fully dissolve the polymer of interest, while both being non-toxic to cells and not degrading the polymer of the well plates. From the purification work and NMR analysis, it was shown that the HB TCDMDA/BMA copolymer was soluble in dichloromethane (DCM), deuterated chloroform (CDCl₃) and

tetrahydrofuran (THF). However, DCM and chloroform were too toxic for biological applications. Meanwhile, THF was known to dissolve and degrade styrenyl polymers, though it had been used in well-plate applications previously in the School of Pharmacy and so remained a candidate for future investigation. Isopropyl alcohol (IPA) had been identified as a preferred solvent in the UV polymerisation studies using the monomers only, as it was known to be compatible with the styrene well plates being used and non-toxic to stem cells. However, despite attempts to dissolve the polymer using a vortex mixer at the desired 35 g/L concentration and at reduced concentration (~3 g/L), and at both room temperature (18 – 20 °C) and elevated temperature (50 °C), full dissolution of the HB polymer in IPA could not be achieved.

Consequently, THF was investigated as an alternative solvent which could strike the best balance of properties. THF is a relatively non-toxic solvent, [86] which was more hydrophobic than IPA, thus potentially leading to improved dissolution of the hydrophobic HB polymer. While THF was known to degrade/dissolve styrenyl polymers, it was hoped that the effect may have been small enough to allow the plates to still be of use. Hence, a solution of HB TCDMDA/BMA polymer was prepared in THF at 35 g/L. A small quantity (300 µL per well to ensure full coverage) of the polymer/THF solution was pipetted into a selection of 6-well plates, which were sent to the School of Pharmacy (Dr Aishah Nasir) for initial biological testing. However, following preliminary washing and incubation steps, (see Chapter 2, Section 2.3.2.6), it was noted that the effect of the THF solvent on the polymeric well plate was too great to enable meaningful data on the formation of a pro-attachment film to be collected, as rippling/cracking of the surface followed by a whitening was seen. This is illustrated in the photograph in Image 4-1A.

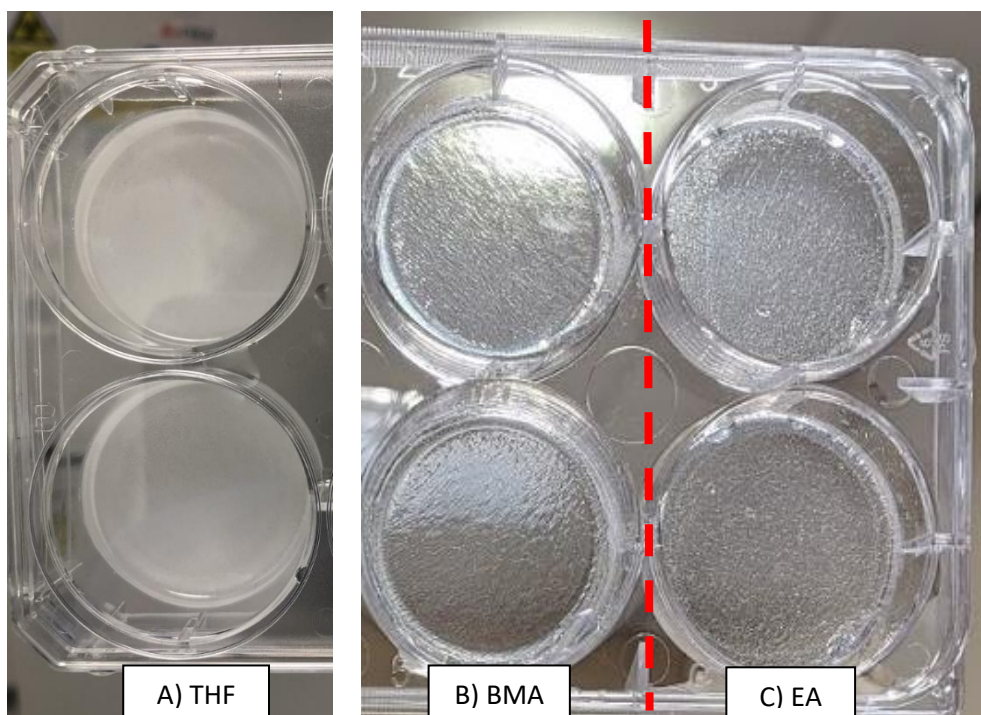


Image 4-1. A) THF, B) BMA and C) EA polymer solutions post IMS wash and soaking in DI H₂O for ~ 6 days at A) 37 °C B/C) room temperature. Cracking and whitening of the polystyrene well is highly visible where THF and EA are used.

This effect was attributed to the combination of two processes. First, solvent crazing of the polystyrene by the THF, in which THF penetrated and plasticized the polymer, allowing small cracks/pores to open up in the polymer. Next, the application of water during the washing step resulted in the formation of small water “pockets” within the surface/crazes. These water pockets scattered light when present in sufficient size and number, resulting in the polymer becoming opaque. However, it was unclear whether the whitening effect originated from the well plate surface, or from the HB TCDMDA/BMA polymer film deposited on top of the surface. It was also noted that the film thickness was slightly too great to get a clear microscope image, thus future preparations would need to use a smaller volume of polymer/solvent solution per well.

Consequently, alternative solvents for the HB pTCDMDA-co-BMA which would cause less crazing/whitening were sought. Candidates included ethyl acetate (EA), butyl methacrylate (BMA) monomer and methyl butyrate. Ethyl acetate was

investigated as a new solvent due to its prior use [87], [88] for biological applications with relatively hydrophobic polymers, while BMA monomer was known to be non-cytotoxic to stem cells from previous investigations into UV polymerisation.

Thus, the HB TCDMDA/BMA polymer was dissolved at the same concentration as previously (35 g/L) in both EA and BMA. The polymer almost fully dissolved in EA, with only very small amounts of undissolved polymer remaining after 10 minutes vortexing at room temperature. However, a cloudy dispersion was formed in BMA, likely due to the large amount of TCDMDA present in the HB polymer, compared to BMA. The two solutions were applied to a well plate. In this case, 200 μ L of solution per well was used, to decrease the thickness of the film formed. As a preliminary check for surface effects, these films were then dried, washed with methylated spirit, and soaked in deionised water (DI H₂O) at room temperature (rather than at 37 °C as used for the THF previously) for ~6 days. The results for BMA and EA are shown in Image 4-1B and Image 4-1C respectively. Compared to the THF, both BMA and EA resulted in greatly reduced cracking and whitening effects, while BMA displayed the most transparent, uniform surface. However, solvent effects could still be observed despite the reduced incubation temperature. Additionally, the transparency of the films was still too low, possibly due to the concentration of the polymer solution being too high.

Consequently, methyl butyrate was chosen as the next candidate, due to its increased hydrocarbyl character compared to EA. The HB TCDMDA/BMA polymer was dissolved at concentrations of 5 - 35 g/L in 10 g/L intervals in methyl butyrate, in order to determine a more suitable polymer concentration. Upon vortexing, increased dissolution of the polymer was observed compared to EA, though some polymer remained un-dissolved in each case. Thus, the actual concentrations achieved were

lower than the theoretical values. These polymer solutions were then coated onto a well plate, with a volume of 150 μ L used per well. Following drying, washing with IMS and soaking in DI H₂O at room temperature for \sim 6 days as previously described, no cracking or whitening of the well surfaces was observed. This indicated that the methyl butyrate solvent did not react with the polystyrene under these conditions. However, during plate preparation for stem cell attachment, the plates would need to be incubated with DI H₂O at 37 °C. Thus, to simulate these conditions, the plates were placed in a vacuum oven (no vacuum applied) and heated to 37 °C for \sim 36 hours. Following incubation, the plates were still free from surface effects, as seen in Image 4-2, suggesting methyl butyrate was a suitable choice of solvent for this system.

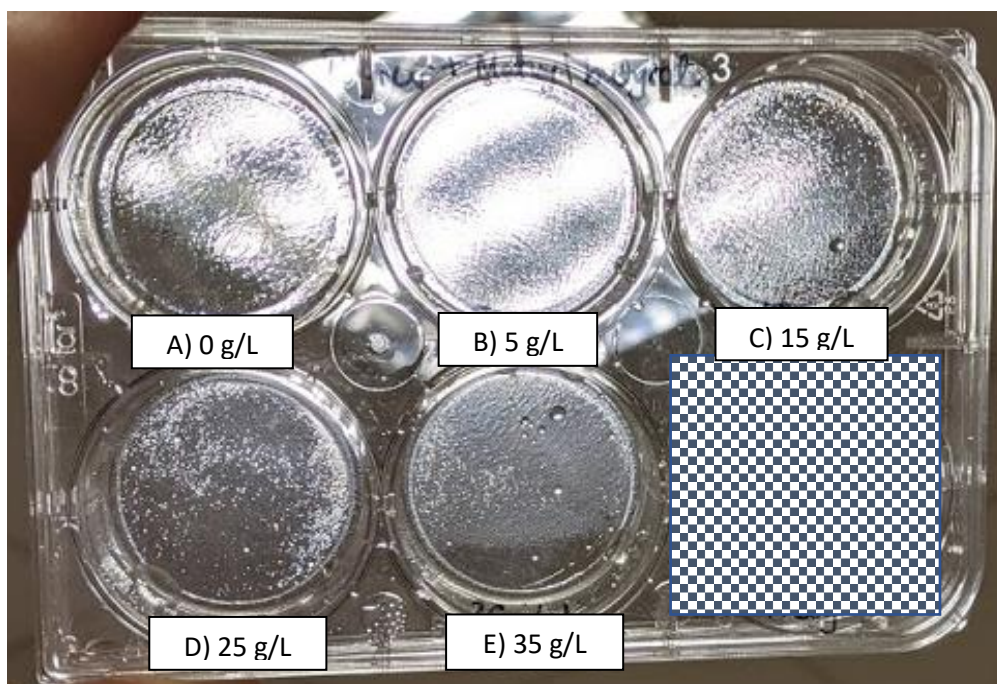


Image 4-2. Polymer/methyl butyrate solutions following soaking at 37 °C for 36 hrs, at concentrations A) 0 g/L, B) 5 g/L, C) 15 g/L, D) 25 g/L and E) 35 g/L.

4.3.5 Biological Testing – Stem Cell Attachment

To determine the correct concentration of polymer/solvent solution to use, the plate was then subject to preliminary biological testing by Dr Aishah Nasir in the School of Pharmacy. Significant levels of stem cell attachment were observed following 24 hours of incubation in all cases where polymer was present, as shown by

the pale patches in Figure 4.15. Meanwhile, the 5 g/L concentration appeared to give the best transparency, and so was chosen as the ideal concentration for further work.

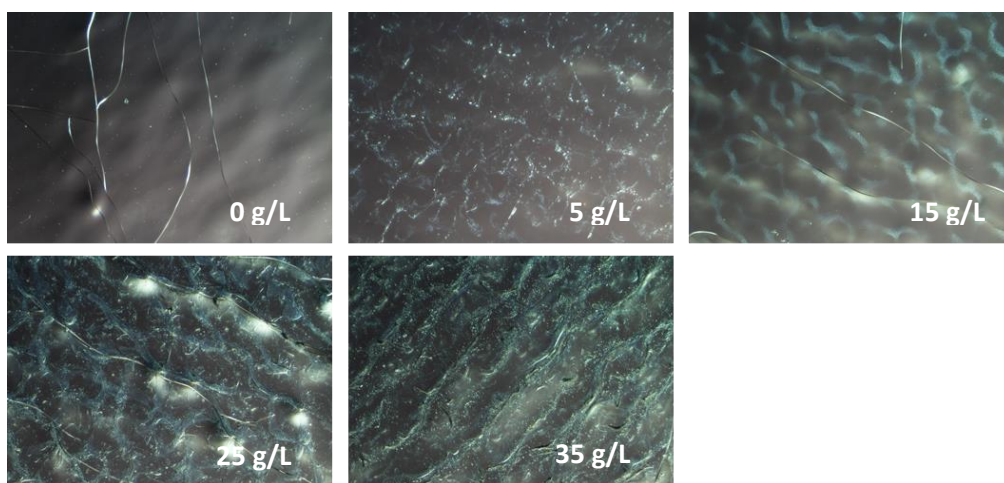


Figure 4.15. Microscope images of wells following incubation of plate with stem cells for 24 hours

Consequently, an initial batch of 6-well plates were made up, with 150 μ L of 5 g/L p(TCDMDA-co-BMA) in methyl butyrate in 5 of the wells and 150 μ L of pure methyl butyrate in one well as a control. These plates were sent to the School of Pharmacy to undergo AFM testing, in order to confirm that the use of pre-polymerised HB polymer resulting in a more uniform coating being formed than when TCDMDA and BA were copolymerised with a UV initiator (Figure 4.9). Unfortunately, due to restrictions, these tests could not be completed and are still ongoing.

4.4 Conclusions

4.4.1 Optimising TCDMDA Homopolymerisation for Anti-Bacterial-Attachment Applications:

- TCDMDA is not compatible with CCTP: PhCoBF is a poor control agent for TCDMDA, leading to low yields and non-reproducible gelation times.
- TCDMDA reactions are better controlled by thiols, and these control methods are scalable and suitable for industrial use.

- Thiol control also allows for the synthesis of tailored polymers for specific applications.
- Yields are also improved compared to CCTP of HB polymers
- HB pTCDMDA is better feedstock for two-photon polymerisation (2PP) than commercial TCDMDA, resulting in reduced printing times and increased resolution.
 - HB pTCDMDA shows high biocompatibility after printing, suggesting it may be a useful polymer for future bio-applications.

4.4.2 Macromer Control of TCDMDA for Pro-Stem Cell Attachment Surfaces

- UV initiated copolymerisation of TCDMDA and BA on mg scale produces surfaces capable of supporting stem cell growth over 24 hrs.
- However, AFM shows phase separation of the polymers, with islands of BA in 'sea' of TCDMDA – surface is not uniform and may cause problems on scale up.
- Macromer control method, using BMA macromers, produces polymers which can be coated on the surface of well plates and shows very similar results in terms of stem cell growth as the UV in preliminary testing
 - Hypothesised that the CTA mechanism will prevent phase separation due to improved incorporation of BMA into polymer structure.
- Macromer control can produce 10s of grams of polymer, so is scalable and industrially viable.
 - Macromer control is a viable control method for TCDMDA
- Scale-up does not affect bio-activity of polymer coating.
- Further application testing could not be completed due to Covid 19 restrictions.

4.5 Future Work

4.5.1 Optimising TCDMDA Homopolymerisation for Anti-Bacterial-Attachment Applications:

In future work, the application of thiol-controlled pTCDMDA as a coating for meshes/coupons in metal-working fluid systems should be further investigated. A suitable solvent should be identified, and the meshes should be dip-coated in the pTCDMDA/solvent solution. These coupons should then be returned to BP laboratories to undergo bacterial testing. This would include placing the coupons into an unprotected control fluid (no anti-microbial agent), which would be spiked with a number of bacteria and fungi once a week. The coupons would then be sequentially removed, one per week, and tested for biofouling to determine whether the pTCDMDA is effective at preventing biofilm formation.

Additionally, this control method enables the incorporation of an additional functionality into the TCDMDA polymer. In the case of the thiol 3-MPA, this would lead to the incorporation of acidic groups. Thus, in future work, the acid value of the polymer should be determined. If the polymer demonstrates sufficient amphiphilicity, it would be interesting to attempt to use the polymers as surfactants to create microparticles using microfluidics.

4.5.2 Macromer Control of TCDMDA for Pro-Stem Cell Attachment Surfaces

In future work, the planned testing of pTCDMDA-co-BMA (2:1 v/v) for use as a stem cell culture coating should be completed.

Firstly, AFM should be completed on the pre-prepared plates, along with cell distribution analysis, to determine whether the use of macromer-controlled HB polymers does improve the uniformity of the surface, and thus the uniformity of the

cell distribution when compared to that seen with the UV polymer. Additionally, Time-of-Flight Secondary Ion Mass Spectrometry (ToF-SIMS) should be conducted as a follow-up, to confirm the presence of the pTCDMDA-co-BMA coating.

Following these tests, the following biological experiments should be conducted, using three different cell lines:

- Long-term stem cell expansion (at least 5 serial passages).
- Karyotype tests, to determine whether stem cells maintain integrity after long-term culture.
- Staining for pluripotency makers, to determine whether stem cells maintain pluripotency properties.
- Integrin attachment for 2 cell lines and 12 antibodies, to investigate the mechanism of stem cell attachment.

Additionally, a wider variety of TCDMDA-based (co)polymers, such as those produced using 3-MPA or DDM (see above) or other macromers (see Chapter 5), should be tested for bioactivity with regards to stem cell culture. This would help to determine which features within the copolymers are most important in determining the polymer bioactivity, and will help to expand the library of such monomers for future use.

4.6 References

- [1] L. Pasteur, "Scientific Papers," *The Harvard Classics*, vol. 38. P.F Collier & Son 1909-14: Bartelby.com, 2001, New York.
- [2] Encyclopedia.com: FREE online dictionary, "Plankton and Planktonic Bacteria - Dictionary definition of Plankton and Planktonic Bacteria." [Online]. Available: <http://www.encyclopedia.com/science/encyclopedias-almanacs->

transcripts-and-maps/plankton-and-planktonic-bacteria. [Accessed: 24-Apr-2017].

- [3] R. M. Donlan, "Biofilms: Microbial life on surfaces," *Emerg. Infect. Dis.*, vol. 8, no. 9, pp. 881–890, 2002.
- [4] J. W. Costerton, Z. Lewandowski, D. E. Caldwell, D. R. Korber, and H. M. Lappin-Scott, "Microbial Biofilms," *Annu. Rev. Microbiol.*, vol. 49, pp. 711–745, 1995.
- [5] T. B. Rasmussen and M. Givskov, "Quorum-sensing inhibitors as anti-pathogenic drugs," *Int. J. Med. Microbiol.*, vol. 296, pp. 149–161, 2006.
- [6] C. Cattò and F. Cappitelli, "Molecular Sciences Testing Anti-Biofilm Polymeric Surfaces: Where to Start?," *Int. J. Mol. Sci. Rev.*, vol. 20, no. 15, p. 3794, 2019.
- [7] A. L. Hook *et al.*, "Combinatorial discovery of polymers resistant to bacterial attachment.," *Nat. Biotechnol.*, vol. 30, no. 9, pp. 868–75, 2012.
- [8] A. Gonzalez-Martin *et al.*, "Simultaneous TOC Reduction and Biofouling Prevention in BWP Processed Water," *SAE Int. J. Aerosp.*, vol. 1, no. 1, pp. 454–460, 2008.
- [9] R. F. Piola, C. Grandison, and DSTO Defence Science and Technology Organisation, "In-water Treatment of Biofouling in Internal Systems : Field Validation of Quaternary Ammonium Compound (QAC) Chemical Treatment Protocols," *US Nav. Inst.*, p. 38, 1952.
- [10] Woods Hole Oceanographic Institute (WHOI), "The Effects of Fouling," *Mar. Fouling its Prev.*, no. 580, pp. 3–19, 1952.
- [11] D. Davies, "Understanding biofilm resistance to antibacterial agents," *Nat.*

- Rev. Drug Discov.*, vol. 2, no. 2, pp. 114–122, 2003.
- [12] F. Costa, I. F. Carvalho, R. C. Montelaro, P. Gomes, and M. C. L. Martins, “Covalent immobilization of antimicrobial peptides (AMPs) onto biomaterial surfaces,” *Acta Biomater.*, vol. 7, no. 4, pp. 1431–1440, 2011.
- [13] P. Li *et al.*, “A polycationic antimicrobial and biocompatible hydrogel with microbe membrane suctioning ability,” *Nat. Mater.*, vol. 10, no. 2, pp. 149–156, 2011.
- [14] R. O. Darouiche, M. D. Mansouri, P. V. Gawande, and S. Madhyastha, “Efficacy of combination of chlorhexidine and protamine sulphate against device-associated pathogens,” *J. Antimicrob. Chemother.*, vol. 61, no. 3, pp. 651–657, 2008.
- [15] L. Caillier, E. T. de Givenchy, R. Levy, Y. Vandenberghe, S. G ribaldi, and F. Guittard, “Synthesis and antimicrobial properties of polymerizable quaternary ammoniums,” *Eur. J. Med. Chem.*, vol. 44, no. 8, pp. 3201–3208, 2009.
- [16] D. Guay, “An update on the role of nitrofurans in the management of urinary tract infections.,” *Drugs*, vol. 61, no. 3, pp. 353–64, 2001.
- [17] J. I. Greenfeld, L. Sampath, S. J. Popilskis, S. R. Brunnert, S. Stylianos, and S. P. Modak, “Decreased bacterial adherence and biofilm formation on chlorhexidine and silver sulfadiazine-impregnated central venous catheters implanted in swine.,” *Crit Care Med*, vol. 23, no. 5, pp. 894–900, 1995.
- [18] K. Jaeger *et al.*, “Efficacy of a benzalkonium chloride-impregnated central venous catheter to prevent catheter-associated infection in cancer patients,” *Chemotherapy*, vol. 47, no. 1, pp. 50–55, 2001.

- [19] K. Yorganci, C. Krepel, J. A. Weigelt, and C. E. Edmiston, "Activity of antibacterial impregnated central venous catheters against *Klebsiella pneumoniae*," *Intensive Care Med.*, vol. 28, no. 4, pp. 438–442, 2002.
- [20] K. Adlington *et al.*, "Application of Targeted Molecular and Material Property Optimization to Bacterial Attachment-Resistant (Meth)acrylate Polymers," *Biomacromolecules*, vol. 17, no. 9, pp. 2830–2838, 2016.
- [21] I. Francolini, C. Vuotto, A. Piozzi, and G. Donelli, "Antifouling and antimicrobial biomaterials : an overview," *APMIS*, vol. 125, no. 4, pp. 392–417, 2017.
- [22] R. D. Monds and G. A. O'Toole, "The developmental model of microbial biofilms: ten years of a paradigm up for review," *Trends Microbiol.*, vol. 17, no. 2, pp. 73–87, 2009.
- [23] M. Cloutier, D. Mantovani, and F. Rosei, "Antibacterial Coatings: Challenges, Perspectives, and Opportunities," *Trends Biotechnol.*, vol. 33, no. 11, pp. 637–652, 2015.
- [24] P. F. Holmes, E. P. K. Currie, J. C. Thies, H. C. Van Der Mei, H. J. Busscher, and W. Norde, "Surface-modified nanoparticles as a new, versatile, and mechanically robust nonadhesive coating: Suppression of protein adsorption and bacterial adhesion," *J. Biomed. Mater. Res. - Part A*, vol. 91, no. 3, pp. 824–833, 2009.
- [25] G. Cheng, Z. Zhang, S. Chen, J. D. Bryers, and S. Jiang, "Inhibition of bacterial adhesion and biofilm formation on zwitterionic surfaces," *Biomaterials*, vol. 28, no. 29, pp. 4192–4199, 2007.
- [26] G. Cheng, G. Li, H. Xue, S. Chen, J. D. Bryers, and S. Jiang, "Zwitterionic

- carboxybetaine polymer surfaces and their resistance to long-term biofilm formation," *Biomaterials*, vol. 30, no. 28, pp. 5234–5240, 2009.
- [27] S. I. Jeon, J. H. Lee, J. D. Andrade, and P. G. De Gennes, "Protein—surface interactions in the presence of polyethylene oxide: I. Simplified theory," *J. Colloid Interface Sci.*, vol. 142, no. 1, pp. 149–158, 1991.
- [28] J. B. Schlenoff, "Zwitteration: Coating Surfaces with Zwitterionic Functionality to Reduce Nonspecific Adsorption," *Langmuir*, vol. 30, no. 32, pp. 9625–9636, Aug. 2014.
- [29] S. Chen, L. Li, C. Zhao, and J. Zheng, "Surface hydration: Principles and applications toward low-fouling/nonfouling biomaterials," *Polymer (Guildf)*, vol. 51, no. 23, pp. 5283–5293, 2010.
- [30] Y.-L. Zhang, H. Xia, E. Kim, and H.-B. Sun, "Recent developments in superhydrophobic surfaces with unique structural and functional properties," *Soft Matter*, vol. 8, no. 44, pp. 11217–11231, 2012.
- [31] X. Zhang, L. Wang, and E. Levänen, "Superhydrophobic surfaces for the reduction of bacterial adhesion," *RSC Adv.*, vol. 3, no. 30, pp. 12003–12020, 2013.
- [32] L. Feng *et al.*, "Super-Hydrophobic Surfaces: From Natural to Artificial," *Adv. Mater.*, vol. 14, no. 24, pp. 1857–1860, 2002.
- [33] T. Nishino, M. Meguro, K. Nakamae, M. Matsushita, and Y. Ueda, "The Lowest Surface Free Energy Based on –CF₃ Alignment," *Langmuir*, vol. 15, no. 13, pp. 4321–4323, Jun. 1999.
- [34] R. N. Wenzel, "RESISTANCE OF SOLID SURFACES TO WETTING BY WATER," *Ind. Eng. Chem.*, vol. 28, no. 8, pp. 988–994, Aug. 1936.

- [35] A. B. D. Cassie and S. Baxter, "Wettability of porous surfaces," *Trans. Faraday Soc.*, vol. 40, no. 0, pp. 546–551, 1944.
- [36] C. McKee and G. R. Chaudhry, "Advances and challenges in stem cell culture," *Colloids Surfaces B Biointerfaces*, vol. 159, pp. 62–77, 2017.
- [37] N. Biologicals, "Stem Cells: Novus Biologicals." [Online]. Available: <https://www.novusbio.com/research-areas/stem-cells>. [Accessed: 07-Jan-2021].
- [38] S. K. Schmitt, A. W. Xie, R. M. Ghassemi, D. J. Trebatoski, W. L. Murphy, and P. Gopalan, "Polyethylene Glycol Coatings on Plastic Substrates for Chemically Defined Stem Cell Culture," *Adv. Healthc. Mater.*, vol. 4, no. 10, pp. 1555–1564, 2015.
- [39] M. D. Kurkuri, C. Driever, G. Johnson, G. McFarland, H. Thissen, and N. H. Voelcker, "Multifunctional polymer coatings for cell microarray applications," *Biomacromolecules*, vol. 10, no. 5, pp. 1163–1172, 2009.
- [40] A. H. Broderick, S. M. Azarin, M. E. Buck, S. P. Palecek, and D. M. Lynn, "Fabrication and selective functionalization of amine-reactive polymer multilayers on topographically patterned microwell cell culture arrays," *Biomacromolecules*, vol. 12, no. 6, pp. 1998–2007, 2011.
- [41] D. S. W. Benoit, M. P. Schwartz, A. R. Durney, and K. S. Anseth, "Small functional groups for controlled differentiation of hydrogel-encapsulated human mesenchymal stem cells," *Nat. Mater.*, vol. 7, no. 10, pp. 816–823, 2008.
- [42] K. A. Kilian and M. Mrksich, "Directing Stem Cell Fate by Controlling the Affinity and Density of Ligand-Receptor Interactions at the Biomaterials

- Interface," *Angew. Chemie*, vol. 124, no. 20, pp. 4975–4979, 2012.
- [43] J. T. Koepsel, P. T. Brown, S. G. Loveland, W. J. Li, and W. L. Murphy, "Combinatorial screening of chemically defined human mesenchymal stem cell culture substrates," *J. Mater. Chem.*, vol. 22, no. 37, pp. 19474–19481, 2012.
- [44] Y. Liu, T. T. Yang Tan, S. Yuan, and C. Choong, "Multifunctional P(PEGMA)-REDV conjugated titanium surfaces for improved endothelial cell selectivity and hemocompatibility," *J. Mater. Chem. B*, vol. 1, no. 2, pp. 157–167, 2013.
- [45] M. Zhang, T. Desai, and M. Ferrari, "Proteins and cells on PEG immobilized silicon surfaces," *Biomaterials*, vol. 19, no. 10, pp. 953–960, 1998.
- [46] D. J. Irvine, A. M. Mayes, and L. G. Griffith, "Nanoscale clustering of RGD peptides at surfaces using comb polymers. 1. Synthesis and characterization of comb thin films," *Biomacromolecules*, vol. 2, no. 1, pp. 85–94, 2001.
- [47] S. Tugulu and H. A. Klok, "Stability and nonfouling properties of poly(poly(ethylene glycol) methacrylate) Brushes under cell culture conditions," *Biomacromolecules*, vol. 9, no. 3, pp. 906–912, 2008.
- [48] F. M. Veronese, "Peptide and protein PEGylation: A review of problems and solutions," *Biomaterials*, vol. 22, no. 5, pp. 405–417, 2001.
- [49] J. T. Koepsel and W. L. Murphy, "Patterned Self-Assembled Monolayers: Efficient, Chemically Defined Tools for Cell Biology," *ChemBioChem*, vol. 13, no. 12, pp. 1717–1724, 2012.
- [50] G. A. Hudalla and W. L. Murphy, "Immobilization of peptides with distinct biological activities onto stem cell culture substrates using orthogonal chemistries," *Langmuir*, vol. 26, no. 9, pp. 6449–6456, 2010.

- [51] O. Sanni *et al.*, "Bacterial Attachment to Polymeric Materials Correlates with Molecular Flexibility and Hydrophilicity," *Adv. Healthc. Mater.*, vol. 4, no. 5, pp. 695–701, Apr. 2015.
- [52] A. Nasir *et al.*, "Discovery of a Novel Polymer for Xeno-Free, Long-Term Culture of Human Pluripotent Stem Cell Expansion," *Adv. Healthc. Mater.*, vol. 2001448, pp. 1–7, 2020.
- [53] E. Buhleier, W. Wehner, and F. Vogtle, "'Cascade'- and 'Nonskid-Chain-like' Syntheses of Molecular Cavity Topologies," *Synthesis (Stuttg.)*, vol. 2, pp. 155–158, 1978.
- [54] D. A. Tomalia *et al.*, "A New Class of Polymers: Starburst-Dendritic Macromolecules," *Polym. J.*, vol. 17, no. 1, pp. 117–132, 1985.
- [55] G. R. Newkome, Z. Yao, G. R. Baker, and V. K. Gupta, "Cascade Molecules: A New Approach to Micelles. A [27]-Arborol," *J. Org. Chem*, no. 3, pp. 2003–2004, 1985.
- [56] K.-M. Kim, M. Jikei, and M. Kakimoto, "Preparation and Properties of Novel Hyperbranched Poly(dimethylsiloxane)s," *Polym. J.*, vol. 34, no. 4, pp. 275–279, 2002.
- [57] R. H. Kienle, P. A. van der. Meulen, and F. E. Petke, "The Polyhydric Alcohol-Polybasic Acid Reaction. IV. Glyceryl Phthalate from Phthalic Acid," *J. Am. Chem. Soc.*, vol. 61, no. 9, pp. 2268–2271, Sep. 1939.
- [58] Y. H. Kim, "Hyperbranched polyarylene," 4,857,630, 1989.
- [59] M. Javaid and A. Haleem, "Additive manufacturing applications in medical cases: A literature based review," *Alexandria J. Med.*, vol. 54, no. 4, pp. 411–422, 2018.

- [60] N. Noor, A. Shapira, R. Edri, I. Gal, L. Wertheim, and T. Dvir, "3D Printing of Personalized Thick and Perfusible Cardiac Patches and Hearts," *Adv. Sci.*, vol. 6, no. 11, 2019.
- [61] Y. Chen *et al.*, "Noninvasive in vivo 3D bioprinting," *Sci. Adv.*, vol. 6, no. 23, pp. 1–11, 2020.
- [62] A. K. Miri, A. Khalilpour, B. Cecen, S. Maharjan, S. R. Shin, and A. Khademhosseini, "Multiscale bioprinting of vascularized models," *Biomaterials*, vol. 198, pp. 204–216, 2019.
- [63] M. Javaid and A. Haleem, "Current status and applications of additive manufacturing in dentistry: A literature-based review," *J. Oral Biol. Craniofacial Res.*, vol. 9, no. 3, pp. 179–185, 2019.
- [64] "How Much Does a 3D Printed House Cost in 2021? | All3DP." [Online]. Available: <https://all3dp.com/2/3d-printed-house-cost/>. [Accessed: 16-Feb-2021].
- [65] "NASA's Centennial Challenges: 3-D Printed Habitat Challenge | NASA." [Online]. Available: https://www.nasa.gov/directorates/spacetech/centennial_challenges/3DPHabit/index.html. [Accessed: 16-Feb-2021].
- [66] S. A. M. Tofail, E. P. Koumoulos, A. Bandyopadhyay, S. Bose, L. O'Donoghue, and C. Charitidis, "Additive manufacturing: scientific and technological challenges, market uptake and opportunities," *Mater. Today*, vol. 21, no. 1, pp. 22–37, Jan. 2018.
- [67] S. C. Ligon, R. Liska, J. Rgen Stampfl, M. Gurr, and R. Mü, "Polymers for 3D Printing and Customized Additive Manufacturing," *Chem. Rev.*, vol. 117, no.

- 15, pp. 10212–10290, 2017.
- [68] S. D. Nath and S. Nilufar, “An overview of additive manufacturing of polymers and associated composites,” *Polymers (Basel)*, vol. 12, no. 11, pp. 1–33, 2020.
- [69] I. Jasiuk, D. W. Abueidda, C. Kozuch, S. Pang, F. Y. Su, and J. McKittrick, “An Overview on Additive Manufacturing of Polymers,” *Jom*, vol. 70, no. 3, pp. 275–283, 2018.
- [70] S. Maruo, O. Nakamura, and S. Kawata, “Three-dimensional microfabrication with two-photon-absorbed photopolymerization,” vol. 22, no. 2, pp. 132–134, 1997.
- [71] “Two-photon absorption - Chemistry LibreTexts.” [Online]. Available: [https://chem.libretexts.org/Bookshelves/Physical_and_Theoretical_Chemistry_Textbook_Maps/Supplemental_Modules_\(Physical_and_Theoretical_Chemistry\)/Spectroscopy/Electronic_Spectroscopy/Two-photon_absorption](https://chem.libretexts.org/Bookshelves/Physical_and_Theoretical_Chemistry_Textbook_Maps/Supplemental_Modules_(Physical_and_Theoretical_Chemistry)/Spectroscopy/Electronic_Spectroscopy/Two-photon_absorption). [Accessed: 23-Feb-2021].
- [72] V. F. Paz *et al.*, “Development of functional sub-100 nm structures with 3D two-photon polymerization technique and optical methods for characterization,” *J. Laser Appl.*, vol. 24, no. 4, p. 042004, 2012.
- [73] A. El-Tamer, U. Hinze, and B. N. Chichkov, “Two-Photon Polymerization in Optics, Microfluidics, and Biomedicine,” in *Handbook of Laser Micro- and Nano-Engineering*, K. Sugioka, Ed. Cham: Springer International Publishing, 2020, pp. 1–44.
- [74] A. Koroleva, S. Gittard, S. Schlie, A. Deiwick, S. Jockenhoevel, and B. Chichkov, “Fabrication of fibrin scaffolds with controlled microscale architecture by a

- two-photon polymerization-micromolding technique," *Biofabrication*, vol. 4, no. 1, 2012.
- [75] D. M. Haddleton, D. R. Maloney, and K. G. Suddaby, "Competition between β -Scission of Macromonomer-Ended Radicals and Chain Transfer to Cobalt(II) in Catalytic Chain Transfer Polymerization (CCTP)," *Macromolecules*, vol. 29, no. 1, pp. 481–483, Jan. 1996.
- [76] A. Anastasaki *et al.*, "Polymerization of long chain [meth]acrylates by Cu(0)-mediated and catalytic chain transfer polymerisation (CCTP): high fidelity end group incorporation and modification," *Polym. Chem.*, vol. 4, no. 15, pp. 4113–4119, 2013.
- [77] D. M. Haddleton, D. R. Maloney, and K. G. Suddaby, "Catalytic chain transfer polymerisation (CCTP) of methyl methacrylate: Effect of catalyst structure and reaction conditions on chain transfer coefficient.," *Macromol. Symp.*, vol. 111, pp. 37–46, 1996.
- [78] D. M. Haddleton *et al.*, "(CCTP) in Water and Water / Alcohol Solution," *Polym. Sci. Part A Polym. Chem.*, vol. 39, no. 14, pp. 2378–2384, 2001.
- [79] K. Adlington *et al.*, "Mechanistic Investigation into the Accelerated Synthesis of Methacrylate Oligomers via the Application of Catalytic Chain Transfer Polymerization and Selective Microwave Heating," *Macromolecules*, vol. 46, no. 10, pp. 3922–3930, May 2013.
- [80] K. Adlington, "Microwave Assisted Controlled Polymerisation and Catalysis," University of Nottingham, 2014.
- [81] K. Adlington, R. McSweeney, G. Dimitrakis, S. W. Kingman, J. P. Robinson, and D. J. Irvine, "Enhanced 'in situ' catalysis via microwave selective heating:

- catalytic chain transfer polymerisation," *RSC Adv.*, vol. 4, no. 31, pp. 16172–16180, 2014.
- [82] M. J. Kamaruddin *et al.*, "Continuous direct on-line reaction monitoring of a controlled polymerisation via dielectric measurement," *Green Chem.*, vol. 13, pp. 1147–1151, 2011.
- [83] K. G. Suddaby, D. M. Haddleton, J. J. Hastings, S. N. Richards, and J. P. O'Donnell, "Catalytic Chain Transfer for Molecular Weight Control in the Emulsion Polymerization of Methyl Methacrylate and Methyl Methacrylate–Styrene," *Macromolecules*, vol. 29, no. 25, pp. 8083–8091, 1996.
- [84] N. M. B. Smeets, R. W. K. Lam, R. P. Moraes, and T. F. L. McKenna, "Catalytic chain transfer polymerization for molecular weight control in microemulsion polymerization," *Polym. Chem.*, vol. 3, pp. 514–524, 2012.
- [85] A. Nasir *et al.*, "Discovery of a Novel Polymer for Xeno-Free, Long-Term Culture of Human Pluripotent Stem Cell Expansion," *Adv. Healthc. Mater.*, vol. 10, no. 6, pp. 1–7, 2021.
- [86] J. Fowles *et al.*, "A review of the toxicological and environmental hazards and risks of tetrahydrofuran," *Crit. Rev. Toxicol.*, vol. 43, no. 10, pp. 811–828, 2013.
- [87] C. E. Vasey *et al.*, "Amphiphilic tri- and tetra-block co-polymers combining versatile functionality with facile assembly into cytocompatible nanoparticles," *Biomater. Sci.*, vol. 7, no. 9, pp. 3832–3845, 2019.
- [88] M. Vergaelen *et al.*, "Ethyl acetate as solvent for the synthesis of poly(2-ethyl-2-oxazoline)," *Green Chem.*, vol. 22, no. 5, pp. 1747–1753, 2020.

- [89] Whiteley, "Biofilms." [Online]. Available:
<https://www.whiteley.com.au/biofilms>. [Accessed: 07-Jan-2021].

5 Chapter 5: Synthesis and Optimisation of Clean Burn & Anti-Biofilm Copolymers

This chapter outlines the synthesis and optimisation of hyperbranched (HB) polymers of divinylbenzene (DVB), ethylene glycol dimethacrylate (EGDMA), tricyclo[5.2.1.0^{2,6}]decanedimethanol diacrylate (TCDMDA) on 5 - 50mL scales. These polymers were synthesised using the macromer control methods described in previous Chapters. The macromers used in this work were derived from lauryl methacrylate (LMA), and diethylene glycol dimethacrylate (DEGMA), which were chosen in order to optimise copolymer solubility in the target solvent. These copolymers were intended for use as anti-biofilm and clean-burn alternatives to the polymer described in Chapter 3. The polymers were analysed using H¹NMR and gel permeation chromatography (GPC).

5.1 Introduction

5.1.1 Soot Formation in Engines

Car, engine, and lubricant manufacturers are facing increasing pressure to lengthen service intervals and therefore oil life in order to reduce lifetime vehicle costs for the customer and the overall impact that the vehicles have on the environment, i.e. a reduction in the amount of engine oil that is discarded. Increasing sump drain intervals, however, means that oils are becoming increasingly contaminated with high levels of soot and increasingly more degraded [1], [2]. Soot is a microscopic carbonaceous particle that is a product of incomplete combustion of hydrocarbons (in this case, gasoline or diesel fuel). It consists of carbon, ash, and unsaturated (un-burned) hydrocarbons. The unsaturated hydrocarbons are essentially acetylene and polycyclic aromatic hydrocarbons. These components have particularly high levels of acidity and volatility. Measurements have shown that it

typically contains 90 % carbon, 4 % oxygen, and 3 % hydrogen with the remainder consisting of nitrogen, sulphur, and traces of metal [3]. Individual or primary soot particles from diesel combustion have been measured to be approximately 40 nm [3]. Because of soot's colloidal properties, the particles agglomerate up to a maximum of approximately 500 nm, with a mean soot agglomerate size of 200 nm [3]. On top of this, the use of exhaust gas recirculation (EGR) is increasing; this is where a portion of the exhaust gases are recirculated into the inlet manifold [4]. This acts to reduce the peak combustion temperature and therefore to reduce the nitrogen oxide (NO_x) emissions. EGR also causes combustion products to be recirculated, rather than to pass out of the engine in the exhaust gases, which leads to further oil contamination. This soot can thicken engine oil, increasing the viscosity and requiring the engine to use more energy to start and run during cold temperatures [2], [4]. Soot circulation also contributes to the formation of varnish and carbon deposits throughout the engine, which can wear down valves and seals, reducing efficiency and eventually causing failure. When excessive soot collects, it forms a congealed mass known as sludge, which is a leading cause of premature failure in diesel engines [1]. Wear problems are also arising from demands for improved fuel economy and performance, and lower oil consumption, which leads to many component contacts within an engine operating under higher loads with thinner lubricant films [2], [5].

The problem of increasing soot levels or particulate matter levels less than 10mm in diameter can be partially solved through further understanding of the formation of soot during fuel combustion and investigating how the amount that is produced can be reduced. This is an area of work that has already attracted much research interest [2]. The problem has also been investigated from a lubricant viewpoint, in terms of designing lubricants that will disperse particles within the lubricant and keep them in suspension. Vehicle service intervals are currently dictated

by the length of time that lubricants can maintain their physical properties, but also, and possibly more importantly, by the length of time that they can hold particles in suspension. The soot particles are contained within the lubricant by dispersant additives. Current lubricant technology, however, has reached a limit on the amount of dispersants that can be added, as adding any further quantities of the current materials will result in a corrosion problem in the engine due to the free amines associated with the dispersant [2].

Additionally, as they have to be miscible with engine oils, the current lubricants themselves generally contain large quantities of hydrocarbon character. This leads to increased levels of incomplete combustion when they are burned within an engine, and thus they can contribute to carbonaceous deposits building up within the engine. Hence, new cleaner-burning lubricant formulations would be of interest to help reduce the contribution from the oil. Furthermore, it would be ideal if these clean-burn additives could simultaneously act as soot dispersants [6]–[10].

5.1.1.1 Clean Burn Copolymers

While DVB-LMA copolymers (see Chapter 3) have proven themselves to be excellent low viscosity lubricants [11], they do have a large amount of aromatic and aliphatic hydrocarbon character. The synthesis of a cleaner-burning additive may be achieved through the use of monomers with higher oxygen contents than DVB and LMA, which would help to ensure complete combustion of the engine oil, and thus less soot formation. For example, the DVB core used previously may be substituted for one made from a less aromatic, more oxygen rich di-functional monomer. However, while this may improve the clean-burn properties of the polymer, it could also adversely affect the advantageous film-formation properties, that DVB has been

proposed to impart. One such monomer is ethylene glycol dimethacrylate (EGDMA), the structure of which is shown in Figure 5.1a

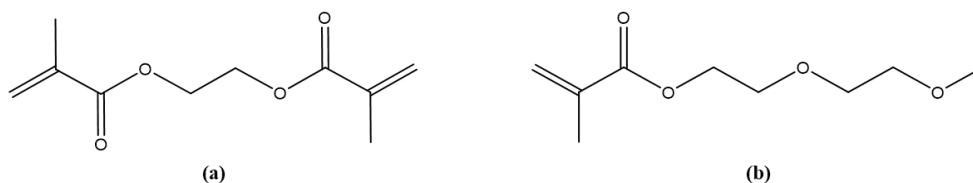


Figure 5.1. Structure of a) ethylene glycol dimethacrylate and b) diethylene glycol methyl ether methacrylate.

Alternatively, the LMA monomer may be substituted for a more oxygen rich monofunctional monomer such as diethylene glycol methyl ether methacrylate (DEGMA), the structure of which can be seen in Figure 5.1b, producing a HB copolymer with a pDVB core and a hydrophilic outer shell. Such copolymers may no longer be soluble in the base oil used in engines, though they may find application in water-based systems such as marine systems, as surfactants or eventually as drug delivery systems in the human body.

Additionally, HB polymers have previously been observed to act a transport molecules, hence these polymers may also be able to acts as soot dispersants [10], [12]–[14].

5.2 Aims and Objectives

5.2.1 Aims

- To develop new HB copolymers using the macromer control method for use as lubricant additives in engine oils and other water-borne other applications.

5.2.2 Objectives:

- Synthesise macromers of LMA and DEGMA *via* CCTP at 50 mL scales.

- Use LMA macromers to control the polymerisation of EGDMA and TCDMDA at 5 mL scales, with monomer:LMA ratios between 1:9 and 5:5 v/v, to produce oil soluble clean burn and antifouling HB copolymers respectively.
- Test the solubility of these copolymers by attempting to dissolve them in PA04 base oil at room temperature and at 56 °C, with stirring.
- Scale up synthesis of oil soluble HB polymers to 50 mL scale.
- Send soluble copolymers to BP/Castrol for further tribological testing for comparison with the DVB/LMA copolymers produced previously (as described in Chapter 3).
- Use DEGMA macromers control the polymerisation of DVB at 5 mL scales, with DVB:DEGMA ratios between 1:9 and 5:5 v/v, to synthesise polar-solvent soluble HB polymers.
- Test the solubility of the DVB/DEGMA HB polymers in polar solvents at room temperature and at 56 °C.

5.3 Results and Discussion

5.3.1 EGDMA/LMA Copolymers

5.3.1.1 Synthesis Optimisation

Lauryl methacrylate oligomers were synthesised using the procedure outlined in Chapter 2, Section 2.4.2.1, with a conversion in the range 35-40%. A toluene solvent and 2,2'-azobis(2-methylpropionitrile) (AIBN) initiator were used. EGDMA was added to the LMA oligomers and polymerised according to the procedure outlined in Chapter 2, Section 2.4.2.2, with EGDMA:LMA ratios of 1:9, 2:8, 3:7, 4:6 and 5:5 (v/v).

Initially, the LMA₂ and EGDMA monomer were reacted in a variety of ratios at 80 °C using only toluene as the solvent: these reactions are summarised in Table 5.1, Entries 1-3.

Table 5.1. Summary of the reaction conditions used in the investigation of LMA-PEG copolymers. The yields, molecular weights and polydispersities of the polymers produced are also shown.

Entry	Solvent	Sol Vol (ml)	Temperature (°C)	Monomer ratio EGDMA:LMA (V/V)	Monomer ratio EGDMA:LMA (mol/mol) ^a	Copolymer ratio (mol/mol) ^b	Reaction/Gel Time	Yield (%) ^a	M _n ^b (kDa)	M _w ^b (kDa)	D ^b
1	Toluene	2	80	1:9	1:5.7	1:20	>24 hrs	27.0%	-	-	-
2	Toluene	2	80	2:8	1:2.3	1:5.3	>24 hrs	38.0%	-	-	-
3	Toluene	2	80	3:7	1:1.5	1:5.0	>24 hrs	28.0%	-	-	-
4	Toluene & Diglyme	2,2	80	1:1	1:0.8	1:0.8	>24 hrs	35.0%	7.80	14.1	18.0
5	Toluene & Diglyme	1,1	80	1:1	1:0.7	1:0.4	>24 hrs	28.0%	23.8	315	13.3
6	Toluene & Diglyme	0.5,0.5	80	1:1	1:0.7	1:0.2	>24 hrs	14.0%	2.37	65.9	27.8
7	Diglyme	2	150	1:1	1:0.7	1:0.6	33 min	55.0%	5.76	188	32.6

^a Determined gravimetrically. ^b Determined via gel permeation chromatography.

These reactions did not gel after 24 hours, and the resulting polymer was non-viscous and transparent. NMR analysis was used to determine the actual molar ratio of pEGDMA and pLMA in the final product. In each case, the ratio of EGDMA to LMA was considerably reduced in the final copolymer compared to the monomer feed ratios of the reactants: this was attributed to poor copolymerisation. For example, despite a monomer ratio of 1:5.7 (mol/mol), the copolymer ratio for Entry 1 was only 1:20 (mol/mol) from the ^1H NMR analysis, which is shown in Figure 5.2 as an example of copolymer ratio determination.

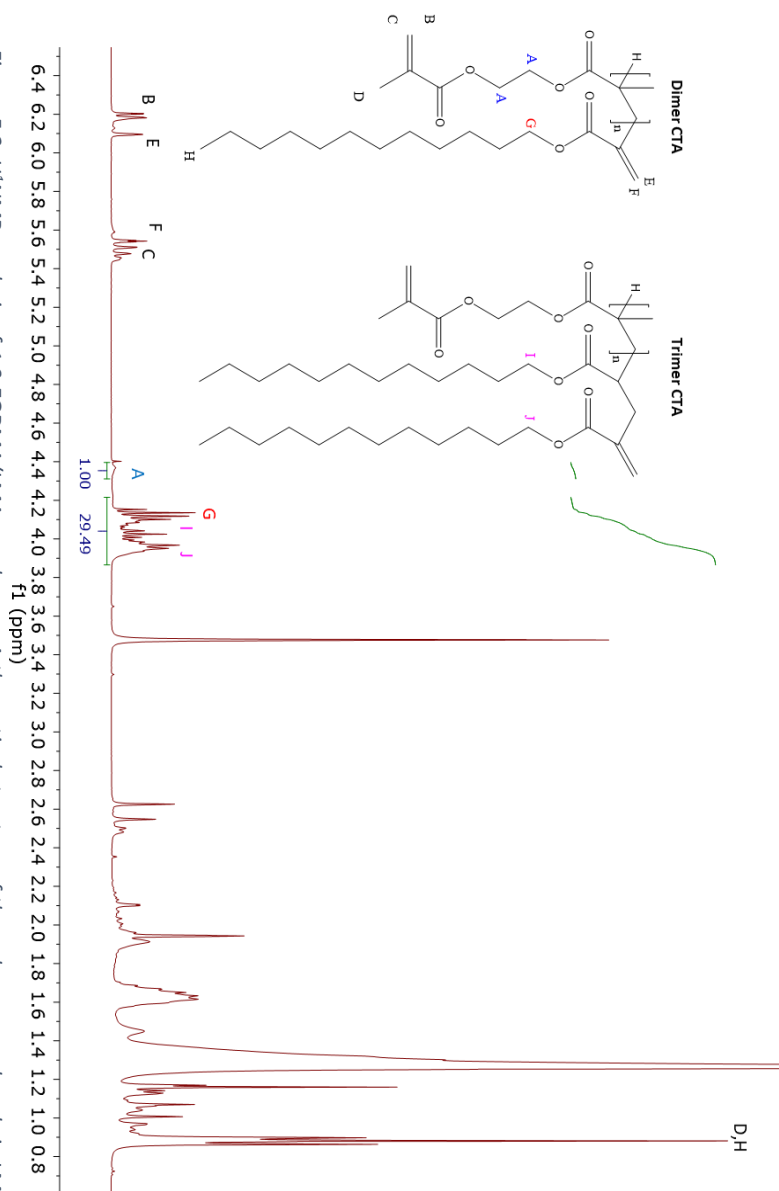


Figure 5.2. ^1H NMR analysis of 1:9 EGDMA/LMA copolymer. A theoretical structure of the polymers produced via LMA dimer and trimer control are shown. The peak at $\delta = 4.36$ ppm, labelled A, corresponds to the four H atoms in the two $-\text{CH}_2$ groups present in the EGDMA pendant groups. The peak at 4.14 ppm, labelled G, corresponds to the H atoms in the $-\text{CH}_2$ groups present in the LMA CTA fragment when the fragment originates from a dimer. The peaks at 4.2 ppm and 3.97 ppm, labelled I and J respectively, correspond to the H atoms in the $-\text{CH}_2$ groups present in the LMA CTA fragment when the fragment originates from a trimer. The relative intensities of the peaks originating from the EGDMA (1.00) and LMA (29.49) indicate that the relative amount of EGDMA included in the structure is significantly smaller than the amount of LMA.

This suggested that the polymer produced was in fact almost a homopolymer of pLMA, with little EGDMA in the structure. It was concluded that the EGDMA monomer was not copolymerising with the LMA₂, likely due to poor solubility of the EGDMA in toluene and in LMA. Both toluene and LMA have much hydrocarbon character, while EGDMA was significantly more hydrophilic, which would have resulted in poor mixing.

Hence, diethylene glycol dimethyl ether (diglyme), structure shown in Figure 5.3, was chosen to supplement the toluene, as it had regions with both hydrophilic and hydrophobic character, and thus solubilised both the EGDMA and the LMA₂.

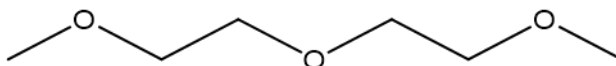


Figure 5.3. Structure of diethylene glycol dimethyl ether (diglyme).

Using a 1:1 (v/v) combination of these solvents, the 5:5 EGDMA/LMA copolymerisation (for simplicity) was attempted, using 2 mL of each solvent at 80 °C, as shown in Entry 4 of Table 5.1. The reaction did not gel, so was removed from the heat after 24 hours. The number and weight average molecular weight, (7.80 kDa and 141 kDa) respectively, and polydispersity, (18.0), indicated that a low molecular weight hyperbranched polymer was successfully synthesised. A low molecular weight was expected, as the reaction did not gel and therefore did not run to maximum conversion. Importantly, however, the copolymer ratio (1:0.8 mol/mol) obtained was the same as the monomer ratio, which indicated that the EGDMA monomer was significantly better solubilised by the addition of the diglyme.

The effect of decreasing the proportion of solvent used was then investigated, with the aim of sufficiently reducing the reaction time such that the reaction gelled in under 24 hours. The volume of each solvent was reduced from 2 mL to 1 mL to 0.5 mL, shown in Entries 5 and 6. However, whilst these changes did not lead to a gel

time under 24 hrs, each of the molecular weight, polydispersity and copolymer ratio did vary. With the initial reduction in solvent volume (Entry 5), the number average molecular weight increased to 23.8 kDa and yield decreased from 35% to 28%, while the polydispersity remained similar (given the error associated with measuring HB polymers). This was likely due to an increase in monomer conversion due to the increased monomer concentration: this increased the probability of successful molecular collisions during propagation, and thus increased the final monomer conversion achieved in the 24 hr reaction period.

However, upon further decrease of solvent volume, and thus further increase in monomer concentration, (Entry 6), the molecular weight achieved decreased ($M_n = 2.37$ kDa) while the dispersity increased (27.8). Again, the change in M_n may simply have been an artefact of the GPC measurement process, however, the change in dispersity could be explained by looking at the achieved copolymer ratios. Reducing the amount of solvent appeared to favour the EGDMA monomer over the LMA monomer, with a ratio of 1:0.2 mol/mol observed for Entry 6 compared to 1:0.8 mol/mol for Entry 4. This was attributed to the fact that LMA was only largely solubilised by one of the solvents, while EGDMA was at least partly solubilised by both. This preferential EGDMA solubility would result in a greater degree of branching within the copolymer, due to a greater density of di-functional monomer being included in the polymer structure and leading to more branching points.

The effect of reaction temperature was also investigated as another route to reducing the reaction time. Similarly to Entry 4, a 1:1 (v/v) EGDMA-LMA copolymerisation was conducted at 150 °C. In this case, the reaction was conducted using diglyme only as the solvent, as toluene boils at 110.6 °C: the results are summarised in Entry 7. A gelation time of approximately 40 minutes was observed,

hence the reaction was repeated and removed from the heat after 33 minutes. The polymer formed was a similar molecular weight ($M_n = 5.76$ kDa, $M_w = 188$ kDa) to that obtained at 80 °C, though the yield was significantly greater, indicating higher conversion. Additionally, the achieved copolymer ratio (1:0.6 mol/mol) was not significantly affected by the temperature increase when compared with Entry 4 (1:0.8 mol/mol), possibly indicating a copolymer of similar structure to that produced in Entry 4 was synthesised. Confirmation of this would require further analysis, including DSC and rheological measurements. However, these were not conducted here, as understanding the exact structures produced was secondary to developing a facile method of synthesising HB copolymers of EGDMA/LMA which were of approximately the correct copolymer ratios to enable PA04 base oil solubility. Thus, this provides a more rapid, though more energy intensive, way of producing EGDMA/LMA copolymers.

5.3.1.2 Scale Up and Extended Solubility Testing

Overall, to ensure consistency in the method applied, it was determined to use the conditions described in Entry 4 to synthesise copolymers of EGDMA and LMA in ratios from 1:9 to 5:5 v/v.

Therefore, following the synthesis optimisation, the full range of EGDMA:LMA ratios were synthesised on a 5 mL scale using a 1:1 solvent mixture at 80 °C, as summarised in Table 5.2. This enabled sufficient polymer to be synthesised for solubility testing.

It was observed that the achieved monomer ratios in these copolymers, estimated using H^1 NMR analysis, were very similar to the theoretical ones, with no obvious trend of being significantly higher or lower than expected except in the case

of 1:9 v/v. Here, there was a difference of 1.2 between the theoretical and experimental ratios, as well as a reduced yield and molecular weight compared to the other copolymers produced (Entry 2-5). This was likely because the copolymer was quenched slightly further from the gelation point than was ideal, hence the branching

Table 5.2. Summary of the volumetric ratios, monomer ratios, copolymer ratios and yields obtained for EGDMA:LMA copolymers of various ratios at 5 mL scale. The mean number average molecular weight, weight average molecular weight and polydispersity are also shown.

Entry	Monomer ratio (v:v)	Theoretical ratio (mol:mol)	Actual ratio (mol:mol)	Yield ^a (%)	M _n ^b (kDa)	M _w ^b (kDa)	D _p ^b
1	1:9	1 : 5.8	1 : 4.6	26	0.61	2.09	3.4
2	2:8	2 : 5.1	2 : 5.5	54	2.85	140.20	49.1
3	3:7	3 : 4.5	3 : 3.6	49	2.40	32.72	13.6
4	4:6	4 : 3.9	4 : 4.0	62	2.79	69.36	24.8
5	5:5	5:3.2	5 : 3.6	73	2.68	74.35	27.7

^a Determined gravimetrically. ^b Determined via gel permeation chromatography.

was not at a maximum. This was difficult to confirm given that all the copolymerisations except the 5:5 v/v had not gelled after 24 hours, and so were simply removed from the heat after this time. However, the 1:9 v/v copolymerisation was expected to be slowest, as it contained the lowest relative concentration of difunctional monomer, and therefore would have been expected to achieve the lowest conversion in the 24hr reaction time.

Nevertheless, all the copolymers produced here demonstrated polydispersities greater than those generally seen with linear polymers, indicating that all the copolymers had indeed formed hyperbranched copolymers of EGDMA/LMA. This was supported by the shape of the refractive index (RI) measurements obtained *via* GPC of the copolymers, which are shown in Figure 5.4.

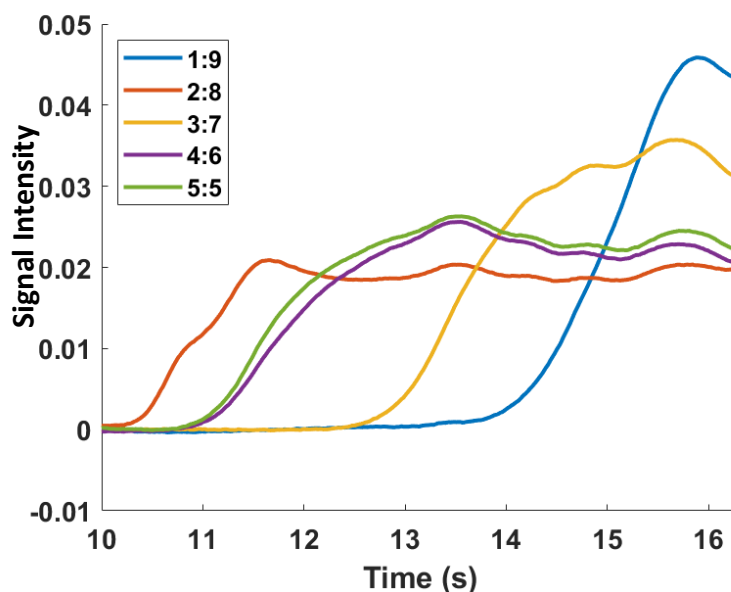


Figure 5.4. The refractive index measurements for EGDMA:LMA copolymers from 1:9 to 5:5, obtained *via* GPC measurement.

These plots showed broad, multimodal peaks for all of the copolymers from 2:8 – 5:5 v/v ratios, which was indicative of the presence of hyperbranching. The molecular weights (M_n) observed were also all below 3 kDa, indicating that the LMA provided a good level of control over the polymerisation and resulting polymer molecular weight

of EGDMA monomer. However, the trace for the 1:9 copolymer (blue) was most narrow, though the polydispersity (3.4) was larger than is generally observed for linear polymers. This indicated that a very lightly branched polymer was produced in this case, which was attributed to the relatively large concentration on LMA CTA present for this polymerisation.

These copolymers were then tested for solubility in PA04 base oil and the data collected is summarised in Table 5.3.

Table 5.3. The solubility of copolymers of EGDMA and LMA in PA04 hydrocarbon base oil at room temperature and at 56 °C. N = insoluble in PA04, Y = soluble in PA04.

Entry	Monomer ratio (v:v)	Soluble in PA04?				
		Rm Temp (24 hrs)	T = 56°C (15 min)	T = 56°C (1 hr)	T = 56°C (4 hr)	T = 56°C (24 hr)
1	1:9	Partial	Y	Y	Y	Y
2	2:8	N	N	N	N	Partial
3	3:7	N	N	N	N	N
4	4:6	N	N	N	N	N
5	5:5	N	N	N	N	N

It was clear that only the 1:9 and 2:8 (v/v) copolymers demonstrated any solubility in the base oil, and only when heated to 56 °C. This temperature was chosen as it is the standard temperature used within BP/Castrol for solubilising additives.

5.3.1.3 Scale Up of 1:9 EGDMA:LMA Polymerisation

Consequently, the 1:9 copolymer was chosen for further scale up and tribological testing at BP/Castrol. The polymerisation was conducted on a 50 mL, the results of which are shown in Table 5.4.

Table 5.4. Molar ratios, yield, molecular weight and polydispersity values obtained for scaled 1:9 v/v EGDMA/LMA copolymer.

Entry	Monomer ratio (v:v)	Theoretical ratio (mol:mol)	Actual ratio (mol:mol)	Yield ^a (%)	M _n ^b (kDa)	M _w ^b (kDa)	Đ ^b
1	1:9	1 : 5.8	1 : 6.9	63	1.78	4.04	2.3

^a Determined gravimetrically. ^b Determined *via* gel permeation chromatography.

Comparing this data to that obtained for the smaller-scale polymerisation (Table 5.2, Entry 1), firstly, it was observed that the relative incorporation of LMA was increased for the larger scale polymerisation, as the molar ratio changed from 1:4:6 (Table 5.2, Entry 1) to 1:6.9 (EGDMA:LMA). This could indicate increased levels of chain transfer, which was supported by the observation that the LMA macromer conversion (from ¹H NMR) was 39% for the smaller scale polymerisation, and was 44% for the larger scale polymerisation. This suggested that more LMA was in macromer form and thus available for chain transfer during the large-scale polymerisation. Additionally, the yield obtained at larger scale was increased from 26% to 63%, which was attributed to a reduced fraction of the resulting viscous polymer being lost due to mechanical losses during work up.

Both the number average (1.78 kDa) and weight average molecular weight (4.04 kDa) were observed to be greater for the polymer produced on the larger scale than those of the polymer produced on the smaller scale (M_n = 0.61 kDa, M_w = 2.09 kDa). However, the polydispersity of the larger-scale polymerisation (2.3) was lower than that of the smaller-scale polymerisation (3.4). This suggested that, while the overall molecular weight of the polymer increased, the level of branching decreased

slightly upon scale-up and a more linear polymer was produced. Visual inspection of the GPC trace shown in Figure 5.5 for the larger-scale polymer confirmed that some branching was still present, as the peak was not entirely mono-modal.

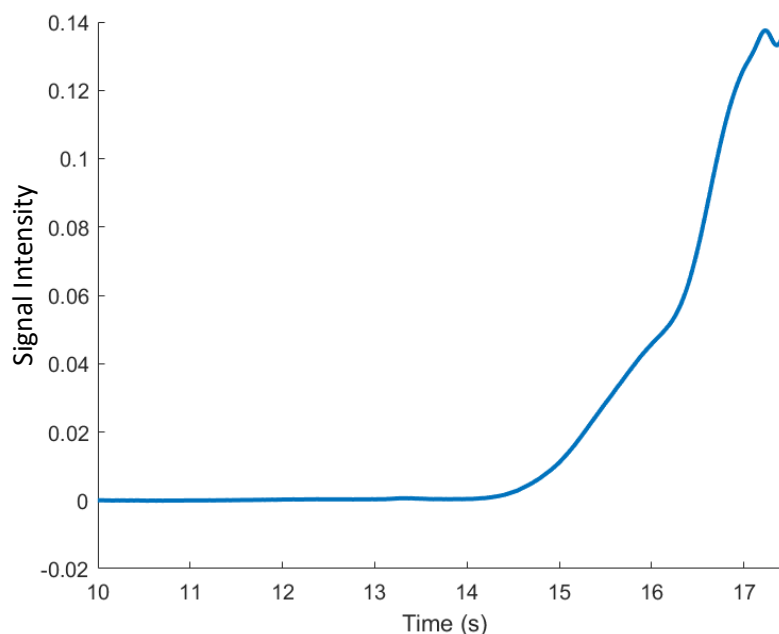


Figure 5.5. The refractive index measurements for large scale 1:9 EGDMA:LMA copolymer obtained via GPC measurement.

This suggested that the observed increase in LMA incorporation discussed in the paragraph above may not have been due to increased levels of chain transfer, but to the incorporation of larger numbers of unconverted LMA monomer into the backbone of the polymer.

Despite this slightly reduced branching, the large-scale polymer batch then underwent solubility testing. The polymer was dissolved in PA04 base oil at 1.0 wt % loading, and full solubility was achieved at room temperature, as was observed for the smaller-scale batch of polymer. This indicated that the change in polymer architecture observed upon scale up did not prevent the polymer from dissolving in the base oil. The reduction in the level of branching observed would have been expected to cause the polymer solubility to decrease, due to the reduced number of LMA-functionalised end groups. However, this was likely offset by the increased LMA

incorporation into the backbone, which would have increased the hydrocarbyl character of the backbone polymer.

5.3.2 DVB/DEGMA Copolymers

5.3.2.1 Synthesis Optimisation

Diethylene glycol methyl ether methacrylate (DEGMA) oligomers were synthesised using the procedure outlined in Chapter 2, Section 2.4.2.1, with an average conversion of 35% achieved (from H^1 NMR). DVB was then polymerised using the DEGMA macromers as CTAs, according to the procedure outlined in Chapter 2, Section 2.4.2.2, at 150 °C with DVB:DEGMA ratios of 1:9, 2:8, 3:7, 4:6, 5:5 (v/v).

DEGMA and DVB were found to not be copolymerizing well without the addition of the diglyme solvent, as for the EGDMA/LMA polymer in the Section above. Upon the addition of an equal volume of diglyme, the DEGMA oligomeric mixture was successfully used to control the polymerisation of DVB in various volume ratios: the data for these reactions are shown in Table 5.5.

This data indicated that the final copolymer ratios obtained (via H^1 NMR analysis) were significantly reduced compared to the theoretical monomer molar ratios, though the difference decreased as the concentration of DEGMA decreased. This may have been due to the fact that there was residual PhCoBF catalyst present in the DEGMA oligomer mixture when the DVB polymerization was conducted. This may have caused some chains to be controlled with the cobalt CTA rather than the oligomeric CTA, and thus be terminated with double bonds via CCTP rather than with DEGMA fragments. This would reduce the relative amount of DEGMA in the copolymer.

Table 5.5: Summary of the volumetric ratios, monomer ratios, copolymer ratios and yields obtained for DVB:DEGMA copolymers of various ratios at 5 mL scale. The mean number average molecular weight, weight average molecular weight and polydispersity are also shown.

Entry	DVB:DEGMA (v/v)	DVB:DEGMA (mol/mol theoretical)	DVB:DEGMA (mol/mol experimental)	Reaction/Gel Time (min)	Yield ^a (%)	M _n ^b (kDa)	M _w ^b (kDa)	P _n ^b
1	1:9	1 : 6.9	1 : 3.9	90	35	1.13	56.5	59.9
2	2:8	2 : 6.2	2 : 3.5	44	53	1.76	84.8	48.2
3	3:7	3 : 5.4	3 : 2.6	25	37	1.54	26.1	17.1
4	4:6	4 : 4.6	4 : 3.0	18	41	1.63	44.8	27.4
5	5:5	5 : 3.9	5 : 2.1	10	39	2.41	75.7	31.4

^a Determined gravimetrically; ^b Determined *via* gel permeation chromatography.

Additionally, the polydispersities obtained were sufficiently large to be indicative of HB polymers having been formed, which was supported by the refractive index (RI) plots seen in Figure 5.6: the broad, multimodal peak seen in these plots are characteristic of HB polymers.

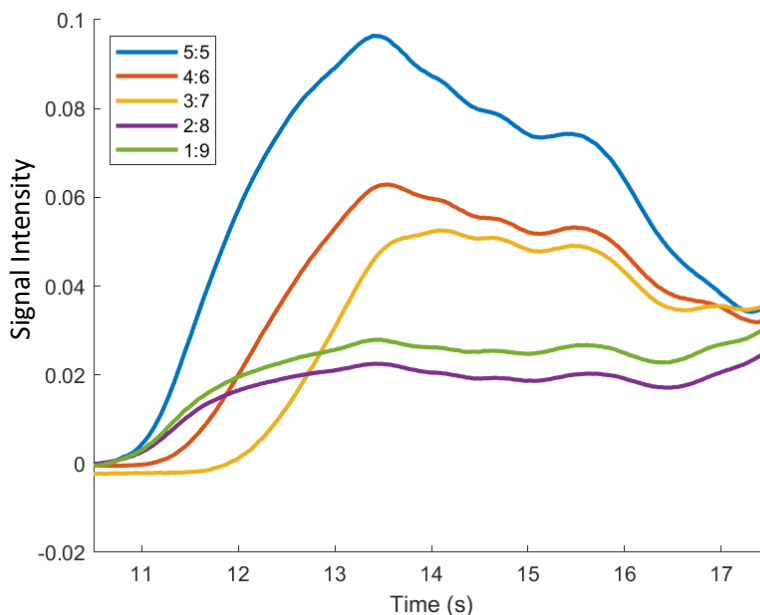


Figure 5.6. The refractive index measurements for DVB/DEGMA copolymers obtained via GPC measurement.

Similarly to the EGDMA/LMA copolymers discussed above, the molecular weights obtained for these polymers were all lower than 2.5 kDa, which suggested that the DVB polymer was effectively controlled by the DEGMA oligomer.

There was no obvious trend in the molecular weight values obtained for these copolymers. However, visually inspecting the RI measurements obtained via GPC in Figure 5.8, it was clear that there were two different general shapes: the copolymers with relatively more DVB than DEGMA (mol:mol) appeared to have a pronounced peak in intensity between 13 and 14 seconds, while the copolymers with relatively more DEGMA than DVB did not display a pronounced peak. As retention time correlated inversely with molecular weight, this indicated that the latter copolymers were more uniformly dispersed in molecular weight, while those with a greater proportion of DVB also tended to have more, higher molecular weight, polymer. This could have been due to the effect of the DEGMA. DEGMA was used as the CTA, which had the effect of reducing the average molecular weight. Hence, where less CTA was used, higher molecular weight polymers were more likely to form.

The DVB/DEGMA polymers produced above then underwent preliminary solubility testing in PA04 base oil using 1 wt% polymer/oil solutions, as summarized in Table 5.6. It was clear that all the copolymers synthesized were insoluble in the PA04 base oil, even after 24 hours at 56 °C. Both DVB and DEGMA monomer/homopolymer are known to be insoluble in PA04, so the lack of solubility of these copolymers in PA04 was not unexpected. In future work, solubility testing in other base oils may be completed, to see if these copolymers may be suitable for different applications.

Table 5.6. The solubility of copolymers of DVB and DEGMA in PA04 hydrocarbon base oil at room temperature and at 56 °C. N = insoluble in PA04, Y = soluble in PA04.

Entry	Monomer ratio (v:v)	Soluble in PA04?	
		Rm Temp (24 hrs)	T = 56°C (24 hr)
1	1:9	N	N
2	2:8	N	N
3	3:7	N	N
4	4:6	N	N
5	5:5	N	N

It was hoped that the inclusion of the glycol groups in DEGMA may have enabled the copolymer to dissolve in more polar, hydrophilic systems. Hence, the solubility of the 1:9 and 1:1 (v/v) DVB/DEGMA copolymers in methanol, acetone and water, which are a mixture of protic and aprotic solvents, was also investigated, as shown in Table 5.7.

Table 5.7. The solubility of copolymers of DVB and DEGMA in acetone, methanol and water, initially at room temperature, then at 56 °C for up to 24 hours.

Entry	Solvent	Copolymer Ratio (DVB:DEGMA, v/v)	Soluble in PA04?		
			15 min (Rm Temp)	15 min (T = 56°C)	24 hr (T = 56°C)
1	Acetone	1:9	Y	Y	Y
		1:1	Y	Y	Y
2	Methanol	1:9	Y	Y	Y
		1:1	N	N	N
3	Water	1:9	N	Y	Y
		1:1	N	N	N

It was found that the 1:9 copolymer was soluble in all the solvents (subject to heating for water), while the 1:1 copolymer was only soluble in acetone. This suggested that greater incorporation of DEGMA did lead to improved solubility in polar and hydrophilic solvents, as expected. As DVB was insoluble in methanol and water, the insolubility of the 1:1 copolymer, which had a much greater relative DVB content compared to the 1:9 polymer was an expected result.

In future work, the polymerisation should be demonstrated and optimised at larger scale, to enable sufficient polymer to be produced for application testing. One such application may be as a mega-surfactant, due to the potential amphiphilicity of the polymer (see Chapter 1, Section 1.8). This may also enable these polymers to be used as surfactants for microparticle formulation *via* microfluidic techniques [15].

5.3.3 TCDMDA/LMA Copolymers

5.3.3.1 Synthesis and Solubility Testing

Due to the prior successful use of LMA macromer control in a 2:8 di-functional monomer:LMA (v/v) ratio to produce PA04 base oil-soluble polymers, (see Chapter 3 and Chapter 5 Section 5.3.1.2)), it was decided to synthesise and test a TCDMDA/LMA polymer using a 2:8 (v/v) monomer ratio on a 50 mL scale. The LMA monomer

displayed 37.5 % conversion to LMA macromer (from $^1\text{H NMR}$). The data for the copolymer produced is shown in Table 5.8.

Table 5.8. Summary of the data obtained for 2:8 v/v copolymer of TCDMDA and LMA. The monomer ratios, gravimetric yield, molecular weights and polydispersity are included.

Entry	Monomer ratio (v:v)	Theoretical ratio (mol:mol)	Actual ratio (mol:mol)	Yield ^a (%)	M _n ^b (kDa)	M _w ^b (kDa)	D ^b
1	2 : 8	2 : 7.6	2 : 2.3	74	5.73	19.53	3.4

^a Determined gravimetrically. ^b Determined *via* gel permeation chromatography.

Firstly, the achieved molar ratio (2:2.3) was observed to be considerably different from the theoretical ratio (2:7.6) for the TCDMDA:LMA polymer, which demonstrated that less LMA was incorporated into the structure than expected. This was attributed to the problems previously observed when attempting to copolymerise this monomer (see Chapter 4, Sections 4.3.1 and 4.3.2). It was observed that TCDMDA was a difficult monomer to control, irrespective of the control method, with poor copolymerisation observed in many instances. In this work, it was likely that the LMA content of the final polymer was reduced because the TCDMDA did not copolymerise readily with the residual monomer present in the LMA macromer mixture. Thus, while some LMA content would have been incorporated *via* the control method, relatively little was incorporated into the polymer backbone. This hypothesis was supported by the molecular weight ($M_n = 5.73$ kDa, $M_w = 19.53$ kDa) and dispersity values (3.4) observed for this polymer. These values were very similar to those obtained previously in this work for similar polymerisations, and indicated both that a hyperbranched polymer was produced and that the polymerisation was well controlled by the LMA oligomers. This was confirmed by inspecting the GPC RI trace, which is shown in Figure 5.7, where a multimodal peak can be observed.

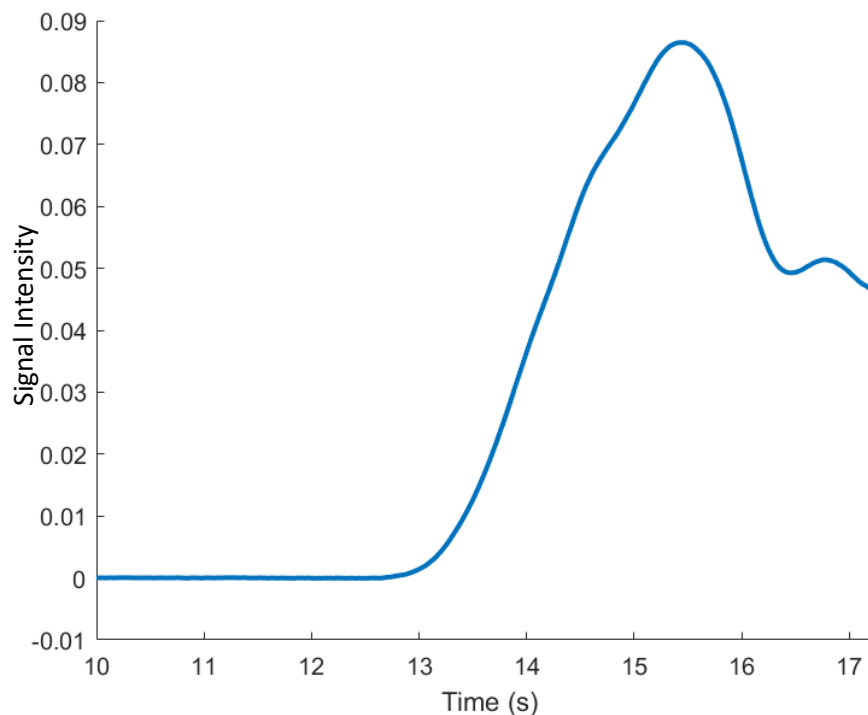


Figure 5.7. The refractive index measurement for TCDMDA/LMA copolymer obtained via GPC measurement.

Furthermore, due to time constraints, no solvent optimisation work could be conducted for this polymerisation. Thus, as was observed for the EGDMA/LMA polymer (see Section 5.3.1 above), the poor LMA incorporation could have been due to unresolved issues with solvent/monomer compatibility.

The solubility of this copolymer in PA04 base-oil was then tested at both room temperature and at 56 °C, the data for which is shown in Table 5.9.

Table 5.9. Solubility of 2:8 TCDMDA/LMA copolymer in PA04 base oil at room temperature and at 56 °C with agitation.

		Soluble in PA04?		
Entry	Monomer ratio (v:v)	Rm Temp (24 hrs)	T = 56°C (15 min)	T = 56°C (24 hr)
1	2:8	N	Y	Y

The TCDMDA/LMA polymer was found to be insoluble in PA04 at room temperature, but was soluble upon heating to 56 °C.

5.3.4 Tribological Testing

Due to the PA04 base oil solubility demonstrated by both the 2:8 (v/v) TCDMDA/LMA and the 1:9 (v/v) EGDMA/LMA polymers above, samples of both polymers were subjected to tribological testing at BP/Castrol laboratories. This was to be analogous to the testing conducted with the 2:8 (v/v) DVB/LMA polymer, as described in Chapter 3, Sections 3.3.1 – 3.3.4. Unfortunately, due to government restrictions, this testing was unable to be conducted in the required time frame, thus we do not have confirmation of the effectiveness of these two polymers as lubricant additives.

5.4 Conclusions

5.4.1 EGDMA/LMA Polymers

- Successfully synthesised HB polymers of EGDMA controlled using LMA macromers, with copolymer ratios 1:9 – 5:5 v/v on 5 mL scale.
 - Optimised reaction conditions to produce HB polymers.
 - Actual monomer ratios achieved very similar to theoretical monomer ratios.
 - LMA macromer is effective control agent for EGDMA, good molecular weight control observed.
- The 1:9 copolymer demonstrated good solubility in PA04 base oil, so was chosen for scale up.
- 1:9 copolymer successfully produced on 50 mL scale.
 - Lower level of branching observed, polymer was more linear.

- Polymer still soluble in base oil, good candidate for clean burn polymer additive.
- LMA macromer is effective control agent for EGDMA, good molecular weight control observed.

5.4.2 DVB/DEGMA Polymers

- Successfully synthesised HB polymers of DVB controlled using DEGMA macromers, with copolymer ratios 1:9 – 5:5 v/v on 5 mL scale.
 - Final copolymer ratios obtained (via H^1 NMR analysis) were significantly reduced compared to the theoretical monomer molar ratios, though the difference decreased as the concentration of DEGMA decreased.
 - DEGMA macromer is effective control agent for DVB, good molecular weight control observed.
- DVB/DEGMA copolymers not soluble in PA04 base oil.
- Tested more hydrophilic/polar solvents.
 - 1:9 copolymer soluble in all three (acetone, methanol, water).
 - 1:1 copolymer soluble only in acetone.
 - Greater incorporation of DEGMA did lead to improved solubility in polar and hydrophobic solvents.

5.4.3 TCDMDA/LMA Polymers

- Successfully synthesised HB polymers of TCDMDA controlled using LMA macromers, with copolymer ratio 2:8 v/v on 5 mL scale.
 - Achieved molar ratio considerably different than theoretical, much less LMA incorporated than expected.

- Due to problems with TCDMDA and LMA monomer copolymerising.
 - LMA macromer is effective control agent for TCDMDA, good molecular weight control observed.
- 2:8 v/v TCDMDA/LMA copolymer soluble in PA04 base oil.
- Good candidate for dispersant additive with cleaner burning properties.
- Tribological testing could not be completed due to government restrictions.

5.5 Future Work

For the polymers which have demonstrated solubility in the PA04 base oil (pEGDMA-co-LMA 1:9 v/v and pTCDMDA-co-LMA 2:8 v/v), the next step will be for them to undergo tribological testing at the BP/Castrol laboratories, analogous to that conducted for the pDVB-co-LMA 2:8 v/v copolymers discussed in Chapter 3, to investigate their suitability as lubricant additives. Additional testing to determine whether these polymers may act as soot dispersants should also be conducted. Further solubility testing is needed for the DVB/DEGMA polymers, in order to find suitable solvents for new applications, e.g. metal-working fluids

Additionally, further optimisation of TCDMDA/LMA polymerisation is needed. Specifically, the use of different solvents/combinations of solvents to improve the incorporation of the LMA macromer into the HB polymer structure should be investigated. This may help to improve the solubility of the polymer in PA04.

Finally, it would be of value to investigate the surfactancy properties of these polymers. It is possible, due to the combination of hydrophobic and hydrophilic monomers used in the DVB/DEGMA and EGDMA/LMA, that these HB polymers may be amphiphilic structures. Additionally, due to the proposed core-shell architecture that this macromer-control method should result in and the high density of end

groups inherent to HB polymers, they may display “megasurfactancy” behaviour. Thus, they may find application in microfluidics for production of microparticles.

5.6 References

- [1] “How to Prevent Soot Buildup in Your Car’s Engine | HowStuffWorks.” [Online]. Available: <https://auto.howstuffworks.com/how-to-prevent-soot-buildup-in-your-cars-engine.htm>. [Accessed: 20-Dec-2018].
- [2] D. A. Green and R. Lewis, “The effects of soot-contaminated engine oil on wear and friction: A review,” *Proc. Inst. Mech. Eng. Part D J. Automob. Eng.*, vol. 222, no. 9, pp. 1669–1689, 2008.
- [3] A. D. H. Clague, J. B. Donnet, T. K. Wang, and J. C. M. Peng, “A comparison of diesel engine soot with carbon black,” *Carbon N. Y.*, vol. 37, no. 10, pp. 1553–1565, 1999.
- [4] A. A. J. Dennis, C. P. Garner, D. H. C. Taylor, and A. J. Dennis, “Effect of EGR on Diesel Engine Wear,” *J. Engines*, vol. 108, pp. 1185–1197, 1999.
- [5] S. Li, A. A. Csontos, B. M. Gable, C. A. Passut, and E. P. Additives, “Wear in Cummins M-1 1 / EGR Test Engin,” *J. Engines*, vol. 111, no. May, pp. 2258–2271, 2002.
- [6] F. K. L. Huang, C.-J. Yoo, C. Okonkwo, D.-J. Tao, C. W. Jones, and S. Dai, “Facilely Synthesized Meso-Macroporous Polymer as Support of Poly(ethyleneimine) for Highly Efficient and Selective Capture of {CO₂},” *Chem. Eng. J.*, vol. 314, p. , 2016.
- [7] Z. Yang, Q. Wang, and T. Wang, “Engineering a hyperbranched polyimide membrane for shape memory and CO₂ capture,” *J. Mater. Chem. A*, vol. 5, no. 26, pp. 13823–13833, 2017.

- [8] K. Adlington, D. J. Irvine, I. Barker, and L. Stevens, “Accelerated Synthesis of Hyperbranched Divinylbenzene Polymers via Catalytic Chain Transfer Polymerisation and their Use as Gas Capture Agents - Manuscript in preparation,” Nottingham, 2017.
- [9] Y. Zheng, S. Li, Z. Weng, and C. Gao, “Hyperbranched polymers: advances from synthesis to applications,” *Chem. Soc. Rev.*, vol. 44, no. 12, pp. 4091–4130, 2015.
- [10] K. Inoue, “Functional dendrimers, hyperbranched and star polymers,” *Prog. Polym. Sci.*, vol. 25, no. 4, pp. 453–571, 2000.
- [11] S. R. Goodwin *et al.*, “Novel, Low Viscosity Lubricants via Facile Synthesis of Functionalised Hyperbranched Polymers: Formulation and Testing,” Nottingham, 1, 2021.
- [12] S. A. Didas, S. Choi, W. Chaikittisilp, and C. W. Jones, “Amine-Oxide Hybrid Materials for CO₂ Capture from Ambient Air,” *Acc. Chem. Res.*, vol. 48, no. 10, pp. 2680–2687, 2015.
- [13] O. Wagner, M. Zieringer, W. J. Duncanson, D. A. Weitz, and R. Haag, “Perfluoroalkyl-functionalized hyperbranched polyglycerol as pore forming agents and supramolecular hosts in polymer microspheres,” *Int. J. Mol. Sci.*, vol. 16, no. 9, pp. 20183–20194, 2015.
- [14] W. Daniel, S. E. Stiriba, and F. Holger, “Hyperbranched polyglycerols: From the controlled synthesis of biocompatible polyether polyols to multipurpose applications,” *Acc. Chem. Res.*, vol. 43, no. 1, pp. 129–141, 2010.
- [15] A. A. Dundas *et al.*, “Achieving Microparticles with Cell-Instructive Surface Chemistry by Using Tunable Co-Polymer Surfactants,” *Adv. Funct. Mater.*, vol.

30, no. 36, 2020.